Impact of Test Setup on Tensile Behavior of Adhesive Anchors

Final Report

Prepared by

Da Luo
BS, Central South University, 2013
MS, Guangxi University, 2015
PhD, Guangxi University, 2020
Visiting Scholar, UW-Milwaukee, 2019

Hua Liu
BS, Fuzhou University, 2004
MS, East Carolina University, 2013
PhD, University of Wisconsin, Milwaukee, 2020

and

Jian Zhao

Department of Civil & Environmental Engineering
University of Wisconsin-Milwaukee

August 2020

This page is blank

Technical Report Documentation Page

1. Report No. SERZ-2020-1	2. Government Accession No.	3. Recipient's Catalog No.	
4. Title and Subtitle Impact of Test Setup on Tensile Behavior of Adhesive Anchors		5. Report Date **August 2020** 6. Performing Organization Code	
7. Author(s) **Da Luo, Hua Liu, and Jian Zhao**		8. Performing Organization Report No.	
9. Performing Organization Name and Address Department of Civil & Environmental Engineering University of Wisconsin at Milwaukee 3200 N. Cramer Street Milwaukee, WI 53211		10. Work Unit No. 11. Contract or Grant No.	
12. Sponsoring Agency Name and Address		13. Type of Report and Period Covered Final Report (04/2019-08/2020) 14. Sponsoring Agency Code	
15. Supplementary Notes			

16. Abstract

This report describes a study of adhesive anchors in two types of tension tests. Confined tension (CT) tests are relatively easy to implement; however, the closely placed reaction may create undesirable and unrealistic confining condition to test anchor. Unconfined tension (UCT) tests are then needed to verify the tensile capacities, which usually correspond to lower bond strength than those from CT tests. Therefore, bond strengths obtained from CT tests must be reduced, and a reduction factor of 0.75 has been stipulated in ACI 355.4 document. This reduction factor (α_{setup}) is currently being challenged.

In this study, we attempt to explore the impact of test setup on behavior of adhesive anchors using laboratory tests and finite element (FE) analyses. A total of 28 CT tests and 44 UCT tests were conducted. The measured capacities were found proportional to the embedment depths, indicating that the current uniform bond stress model in ACI 318-19 is reasonable. The tests indicated that the current reduction factor is reasonable when the bond strength is determined as the 5%-fractile from CT tests. The reduction factor (0.75) is unconservative if the bond strength is determined as the average strength from CT tests and a reduction factor of 0.5 is reasonable. The FE analyses indicate the the impact of lateral confining pressure from closely placed reaction in CT tests is reasonably negligible. Instead, the concrete surrounding adhesive anchors in UCT tests may develop dilation/splitting cracks near the top portion of concrete, leading to partial disengagement of adhesive from concrete and thus reduced bond resistance. Finally, concrete breakout may occur at top simultaneously with bond failure. This behavior, widely observed only in UCT tests, may also be responsible for the calculated capacity reduction.

The above conclusion is limited by the fact that the vinylester adhesive used in this study had a low-medium bond strength as the average bond strength with ½-in. diameter anchors was about 2800 psi.

17. Key Words adhesive anchor; concrete anchor; tension; adhesive; chemical anchor; laboratory tests; building codes		18. Distribution Statement No restrictions.	
19. Security Classification (of this report) Unclassified	20. Security Classification (of this page) Unclassified	21. No. of pages 173	22. Price

Disclaimers

Authors' disclaimer: The contents of this report reflect the views of the authors, who are responsible for the facts and the accuracy of the data presented herein. This report does not constitute a standard, specification, or regulation.

Patent disclaimer: There was no invention or discovery conceived or first actually reduced to practice in the course of or under this contract, including any art, method, process, machine manufacture, design or composition of matter, or any new useful improvement thereof, or any variety of plant, which is or may be patentable under the patent laws of the United States of America or any foreign country.

Acknowledgments

The authors would like to acknowledge the support from the Department of Civil and Environmental Engineering (CEE) at the University of Wisconsin, Milwaukee (UWM). Mr. Da Luo is grateful to the CEE department at UWM for hosting Mr. Da Luo during October 2018 through October 2019. The authors also thank the colleagues in American Concrete Institute (ACI) Committee 355 for their valuable inputs.

We are grateful to China Scholarship Council. The provided funding made it possible for Mr. Da Luo to visit UWM in 2018-19 and work with Mr. Hua Liu and Dr. Zhao on this topic.

Mr. Jerry King from Precast Engineering Company and Mr. Brian Lederman from Illini Precast donated labor and some materials for the reinforcing bars. We are grateful to the support from the local industry.

We are grateful to Farzaneh Elyasigorji, Rong Xu, and Qian Lin, graduate students at the UWM CEE department for their help during the tests.

Executive Summary

This report describes a study of adhesive anchors in tension focusing on the behavioral difference of the anchors in confined and unconfined tension tests. The bond strength of adhesive anchors is obtained from pullout tests, as bond failure at the adhesive-concrete interface is one of the controlling failure modes. Two test methods are usually used: 1) confined tension (CT) tests to evaluate the bond strength of adhesive and 2) unconfined tension (UCT) tests to evaluate the tensile capacity of adhesive anchors. The setup for the tension tests is a self-balanced loading system: the tensile loading applied to the test anchor is balanced by the reaction applied to the concrete. The reaction in CT setup is placed very close to the test anchors, leading to convenient and material-saving tests. However, the closely placed reactions may create undesirable and unrealistic confining conditions to the specimen. Therefore, bond strengths obtained from confined tension tests must be reduced.

Section 10.4.5.1 of ACI 355.4-11 indicates that α_{setup} shall be 1.0 if service-condition tests are performed as unconfined tests, 0.75 if service-condition tests are performed as confined tests, and 0.70 if service-condition tests in cracked concrete are performed as confined tests. Based on the tests by Davis (2012), Cook (2018) suggested that if α_{setup} is not determined by unconfined tension tests, the reduction factor should be taken as 0.5 instead of 0.75 currently stipulated in ACI 355.4-11. Committee 355 discussion in 2018 indicated that this is a critical issue for the committee, and a task group (TG9) was formed in 2019 to investigate the reduction factor.

In this study, we attempted to explore the impact of test setup on behavior of adhesive anchors. One adhesive and one concrete strength (6200 psi) were used while multiple anchor diameters (that is 1/2, 5/8, and 3/4 in.) and multiple embedment depths were used. Tests were conducted under indoor temperature, which is different from that in Davis (2012). Bond failure, especially along the adhesive-concrete interface was the targeted failure mode following the suggestion by Wall (2109). Test design indicated that concrete breakout may be a controlling failure mode; hence specimens were included, in which anchor reinforcement was used to force bond failure. A standard installation procedure was strictly followed to ensure the quality of the tests.

A total of 28 confined tension tests and 44 unconfined tension tests were conducted. The specimens in confined tension tests had an embedment of $4d_a$ or $6d_a$ while those in unconfined tension tests had an embedment of $4d_a$, $6d_a$, $8d_a$, and $10d_a$ (only for ½-in. anchors). The measured capacities in both confined and unconfined tension tests were reasonably proportional to the embedment depths though more than half of the specimens in unconfined tension tests were controlled by combined breakout-pullout failure, indicating that the current uniform bond stress model in ACI 318-19 is reasonable. The tests also indicated that α_{setup}=0.75 is unconservative if bond strength is determined as the average measured bond from confined tension tests and a reduction factor of 0.5 seems reasonable; however, α_{setup}=0.75 is appropriate if bond strength is determined as the 5%-fractile of measured bond from confined tension tests.

We envisioned the following difference between confined and unconfined tension tests:

- Closely placed reaction may cause lateral pressure on adhesive-concrete interface in confined tension tests, leading to increased bond strength.
- Closely placed reaction may also change the stress field in concrete such that splitting cracks is restrained in confined tension tests while such restrain does not exist in unconfined tension tests. The splitting cracks, though not through the entire embedment depth, may disengage the

microscopic interlock between hardened adhesive and concrete, leading to reduced bond strength, especially near the concrete surface.

- Closely placed reaction prohibits the formation of concrete breakout cones, which often occurs in unconfined tension tests along with bond failure. The mixed failure mode may occur under a lower tensile load than the individual failure modes.

Nonlinear finite element analyses were conducted to explore the impact of these factors. We believe the bond along adhesive-concrete (A-C) interface is established through hardened adhesive in micro-indents, randomly generated in concrete during hole drilling and proper hole cleaning, along the entire embedded depth; hence nonlinear interface models were created in this study. The FE analyses indicated that 1) the impact of lateral confining pressure from closely placed reaction is reasonably negligible; 2) the concrete surrounding adhesive anchors in unconfined tension tests may develop splitting in unconfined tension tests, especially near the top portion of concrete, leading to partial disengagement of adhesive and concrete and reduced bond resistance. Such splitting cracks are not permitted in confined tension tests; hence, we believe the main difference of the two tests and the reason for the reduction factor is that closely placed reaction in confined tension tests restrains tensile strain/splitting near concrete top, which disengage top part of A-C interface. Meanwhile, concrete breakout may occur at top simultaneously with bond failure. This widely observed behavior only in unconfined tension tests may also be responsible for the reduction factor.

Interpretation of the conclusion of this study should consider the fact that the adhesive used in this study had a low-medium bond strength (the measured average bond strength from confined tension tests with ½-in. diameter threaded rods was about 2800 psi). The reduction factor from test setup is expected to be lower than the current code recommendation (that is 0.75) mainly for adhesives with relatively high bond strength; therefore, the tests should be repeated using a different adhesive, such as a high-strength epoxy.

Finally, it was interesting to notice that with the same adhesive, confined tension tests with larger-size anchors showed a lower average bond strength (the measured average bond strength from confined tension tests with 3/4-in. diameter threaded rods was only about 1800 psi). This may have been attributed to poor hole cleaning even with the same standard installation (hole cleaning) procedure. Further research should be conducted to investigate this reduction as it is reported in the literature.

Table of Content

Disclaimers ii
Acknowledgments iii
Executive Summary iv
Table of Content vi
List of Figures x
List of Tables xiii
Nomenclature xiv
Chapter 1. Introduction 1
1.1 Introduction 1
1.2 Definition of Problem 2
1.3 Organization of Report 3
Chapter 2. Literature Review 5
2.1 Research by Davis (2012) 5
2.2 Research by Appl (2009) 6
2.3 Discussion by Eligehausen and Asmus (2019) 6
Chapter 3 Experimental Investigation 12
3.1 Introduction 12
3.2 Experimental program 12
3.3 Specimen Design 13
Specimen dimensions 13
Material properties 14
Test setup 14
Instrumentation and data acquisition 15
3.4 Installation Procedure 15
Chapter 4. Results of Experiments 27
4.1. Confined Tension Tests 27
4.2. Unconfined Tension Tests 28
4.3. Observed Reduction Factor α_{setup} 28
4.4 Analyses of Combined Breakout-Pullout Failure 29
4.5 Comparison of Anchors in Plain and Reinforced Concrete 30
4.6 Summary 30
Chapter 5. Finite Element Analyses 41

5.1. Introduction 41
5.2 Brief Literature Review 41
Research by McVay et al. (1996) 42
Research by Davis (2012) 42
Research by Appl (2009) 43
Research by Delhomme and Brun (2018) 43
5.3 Finite Element Analyses 44
Model geometry and boundary conditions 44
Element selection 45
Material properties 45
FE analysis results 46
5.4 Summary 47
Chapter 6. Summary 60
6.1 Summary of Research Activities 60
6.2 Conclusions 60
6.3 Suggested Future Studies 61
References 62
Appendix I: Summary of specimen preparation and tests 64
Appendix II: Details of confined tension tests 71
1. C-0.5-2.0-#1 71
2. C-0.5-2.0-#2 72
3. C-0.5-2.0-#3 73
4. C-0.5-2.5-#1 74
5. C-0.5-2.5-#2 75
6. C-0.5-2.5-#3 76
7. C-0.5-3.0-#1 77
8. C-0.5-3.0-#2 78
9. C-0.5-3.0-#3 79
10. C-0.625-2.0-#1 80
11. C-0.625-2.5-#1 81
12. C-0.625-2.5-#2 82
13. C-0.625-2.5-#3 83
14. C-0.625-3.0-#1 84
15. C-0.625-3.0-#2 85
16. C-0.625-3.0-#3 86

17. C-0.625-3.75-#2 87
18. C-0.625-3.75-#3 88
19. C-0.75-2.0-#1 89
20. C-0.75-2.5-#1 90
21. C-0.75-2.5-#2 91
22. C-0.75-2.5-#3 92
23. C-0.75-3.0-#1 93
24. C-0.75-3.0-#2 94
25. C-0.75-3.0-#3 95
26. C-0.75-4.5-#2 96
27. C-0.75-4.5-#3 97
28. C-0.75-6.0-#4 98
Appendix III: Details of unconfined tension tests 99
1. UC-0.5-2.0-#1 99
2. UC-0.5-2.0-#4 101
3. UC-0.5-2.5-#3 103
4. UC-0.5-3.0-#1 105
5. UC-0.5-3.0-#2 106
6. UC-0.5-3.0-#3 106
7. UC-0.5-3.0-#4 106
8. UC#R-0.5-3.0-#4 107
9. UC-0.5-3.75-#2 109
10. UC-0.5-4.0-#1 111
11. UC-0.5-4.0-#2 113
12. UC-0.5-4.0-#3 115
13. UC-0.5-4.0-#4 117
14. UC#R-0.5-4.0-#1 119
15. UC#R-0.5-4.0-#2 121
16. UC#R-0.5-4.0-#3 123
17. UC#R-0.5-4.0-#4 125
18. UC#R-0.5-4.5-#3 127
19. UC#R-0.5-5.0-#1 128
20. UC#R-0.5-5.0-#2 129

21. UC-0.625-2.5-#1 130
22. UC-0.625-2.5-#2 132
23. UC-0.625-2.5-#3 134
24. UC-0.625-2.5-#4 135
25. UC-0.625-3.75-#1 135
26. UC-0.625-3.75-#2 136
27. UC-0.625-3.75-#3 137
28. UC-0.625-3.75-#4 138
29. UC-0.625-5.0-#1 139
30. UC-0.625-5.0-#2 141
31. UC-0.625-5.0-#3 143
32. UC-0.625-5.0-#4 145
33. UC#R-0.625-5.0-#1 147
34. UC#R-0.625-5.0-#2 148
35. UC#R-0.625-5.0-#3 150
36. UC#R-0.625-5.0-#4 152
37. UC-0.75-3.0-#1 154
38. UC-0.75-3.0-#2 155
39. UC-0.75-3.0-#3 156
40. UC-0.75-3.0-#4 157
41. UC#R-0.75-4.5-#1 158
42. UC#R-0.75-4.5-#2 160
43. UC#R-0.75-4.5-#3 162
44. UC#R-0.75-4.5-#4 163
45. UC#R-0.75-6.0-#1 165
46. UC#R-0.75-6.0-#2 167
47. UC#R-0.75-6.0-#3 169
48. UC#R-0.75-6.0-#4 171
Appendix IV: Percentiles of the Student's t Distribution 173

List of Figures

Figure 1.1 The capacity reduction factor proposed by Cook (2018): (τu=2000psi) 4
Figure 1.2 The capacity reduction factor proposed by Cook (2018): (τu=4000psi) 4
Figure 2.1 Concrete specimen (Figure 4-6 in Davis (2012)) 7
Figure 2.2 Embedment depth chair (Figure 4-21 in Davis (2012)) 7
Figure 2.3 Confined tension test setup in (Fig. 4-1 in Davis (2012)) 8
Figure 2.4 Unconfined tension test setup (Fig. 4-2 in Davis (2012)) 8
Figure 2.5 Short-term tension tests of adhesive anchors by Davis (Cook 2019) 9
Figure 2.6 Unconfined tension tests of adhesive anchors by Davis (Cook 2019) 9
Figure 2.7 Alpha Setup summarized by Appl (Figure 10.9 in Appl (2009)) 10
Figure 2.8 Example of test setup for adhesive anchors in ACI 355.4-19 11
Figure 3.1 Determination of anchor embedment based on predicted capacities 20
Figure 3.2 Schematics of plain concrete blocks 20
Figure 3.3 Schematics of reinforced concrete blocks 21
Figure 3.4 Measured compressive strengths of concrete using 4x8 cylinders 21
Figure 3.5 Stress-strain relationship of ASTM A193 Grade B7 threaded rods. 22
Figure 3.6 Stress-strain relationship of the vinylester adhesive. 22
Figure 3.7 Test setup for confined tension tests 23
Figure 3.8 Test setup for unconfined tension tests 24
Figure 3.9 Drilled holes in concrete to demonstrate the installation procedure 25
Figure 4.4 Bond strength from confined tension tests with three adhesives (Figure 5.5 of Meszaros (2002)) 33
Figure 4.7 Failure of debonded anchors in confined tension tests 35
Figure 4.12 Multiple breakout cracks in Specimen UC-0.625-5.0-#1 38
Figure 4.13 Comparison of measured capacity of specimens with measured breakout depth and prediction. 38
Figure 4.14 Monte Carlo simulation of combined breakout-pullout failure 39
Figure 4.15 Impact of anchor reinforcement 39
Figure 5.1 Load transfer model in adhesive anchors by Cook et al. (1993) 49
Figure 5.2 Finite element model for anchor bolt pullout simulation (Fig. 6 from McVay et al. (1996)) 49
Figure 5.3 Simulated breakout-pullout failure of a 4-in. anchor (Fig. 8c from McVay et al. (1996)) 50
Figure 5.4 Shear (bond) stresses along concrete-adhesive layer interface in McVay et al. (1996) 50
Figure 5.5 2D finite element model of adhesive anchors (Figure 7-4 in Davis (2012)) 51
Figure 5.6 shear stress at interface at various load levels (Figure 7-5 in Davis (2012)) 51
Figure 5.7 Finite element model in FEMAP by Appl (2009) 52
Figure 5.8 Anchor-adhesive-concrete interface in Appl (2009) 53
Figure 5.9 Principal tensile strains in concrete (M12, h_{ef}/d = 10, fcc = 25 MPa, Adhesive C) 53
Figure 5.10 Axisymmetric model and anchor-concrete interface model by Delhomme and Brun (2018) 54
Figure 5.11 Analysis results by Delhomme and Brun (2018) 54
Figure 5.12 Finite element model of Specimen UC-0.5-4.0. 55
Figure 5.13 Material model for nonlinear springs representing A-C interface bond 55
Figure 5.14 Comparison of FE analysis with tests of Specimens UC-0.5-4.0 55

Figure 5.15 Comparison of spring forces in Specimens UC-0.5-4.0. a) in confined tension test; and b) in unconfined tension test 56
Figure 5.16 Misses stresses in concrete developed in Specimen UC-0.5-4.0 at peak loads..... 57
Figure 5.17 Pressure generated on adhesive-concrete interface in Specimen UC-0.5-4.0 at peak loads. 57
Figure 5.18 Comparison of the maximum principal stress in concrete in Specimen UC-0.5-4.0 at peak loads..... 57
Figure 5.19 Comparison of the X-direction strain in concrete in Specimen UC-0.5-4.0 at peak loads. 58
Figure 5.20 Comparison of the Y-direction strain in concrete in Specimen UC-0.5-4.0 at peak loads. 58
Figure 5.21 Comparison of bond failure at A-C interface. 58
Figure 5.22 Bond failure observed by Barnat and Bajer (2011) 59
Figure I.1 Casting position of concrete blocks 67
Figure II.1. Observed behavior of Specimen C-0.5-2.0-#1 71
Figure II.2. Observed behavior of Specimen C-0.5-2.0-#2 72
Figure II.3. Observed behavior of Specimen C-0.5-2.0-#3 73
Figure II.4. Observed behavior of Specimen C-0.5-2.5-#1 74
Figure II.5. Observed behavior of Specimen C-0.5-2.5-#2 75
Figure II.6. Observed behavior of Specimen C-0.5-2.5-#3 76
Figure II.7. Observed behavior of Specimen C-0.5-3.0-#1 77
Figure II.8. Observed behavior of Specimen C-0.5-3.0-#2 78
Figure II.9. Observed behavior of Specimen C-0.5-3.0-#3 79
Figure II.10. Observed behavior of Specimen C-0.625-2.0-#1 80
Figure II.11. Observed behavior of Specimen C-0.625-2.5-#1 81
Figure II.12. Observed behavior of Specimen C-0.625-2.5-#2 82
Figure II.13. Observed behavior of Specimen C-0.625-2.5-#3 83
Figure II.14. Observed behavior of Specimen C-0.625-3.0-#1 84
Figure II.15. Observed behavior of Specimen C-0.625-3.0-#2 85
Figure II.16. Observed behavior of Specimen C-0.625-3.0-#3 86
Figure II.17. Observed behavior of Specimen C-0.625-3.75-#2 87
Figure II.18. Observed behavior of Specimen C-0.625-3.75-#3 88
Figure II.19. Observed behavior of Specimen C-0.75-2.0-#1 89
Figure II.20. Observed behavior of Specimen C-0.75-2.5-#1 90
Figure II.21. Observed behavior of Specimen C-0.75-2.5-#2 91
Figure II.22. Observed behavior of Specimen C-0.75-2.5-#3 92
Figure II.23. Observed behavior of Specimen C-0.75-3.0-#1 93
Figure II.24. Observed behavior of Specimen C-0.75-3.0-#2 94
Figure II.25. Observed behavior of Specimen C-0.75-3.0-#3 95
Figure II.26. Observed behavior of Specimen C-0.75-4.5-#2 96
Figure II.27. Observed behavior of Specimen C-0.75-4.5-#3 97
Figure II.28. Observed behavior of Specimen C-0.75-6.0-#4 98
Figure III.1. Observed behavior of Specimen UC-0.5-2.0-#1 100
Figure III.2. Observed behavior of Specimen UC-0.5-2.0-#4 102
Figure III.3. Observed behavior of Specimen UC-0.5-2.5-#3 104
Figure III.4. Observed behavior of Specimen UC-0.5-3.0-#1 105

Figure III.8. Observed behavior of Specimen UC#R-0.5-3.0-#4 108
Figure III.9. Observed behavior of Specimen UC-0.5-3.75-#2 110
Figure III.10. Observed behavior of Specimen UC-0.5-4.0-#1 112
Figure III.11. Observed behavior of Specimen UC-0.5-4.0-#2 114
Figure III.12. Observed behavior of Specimen UC-0.5-4.0-#3 116
Figure III.13. Observed behavior of Specimen UC-0.5-4.0-#4 118
Figure III.14. Observed behavior of Specimen UC#R-0.5-4.0-#1 120
Figure III.15. Observed behavior of Specimen UC#R-0.5-4.0-#2 122
Figure III.16. Observed behavior of Specimen UC#R-0.5-4.0-#3 124
Figure III.17. Observed behavior of Specimen UC#R-0.5-4.0-#4 126
Figure III.18. Observed behavior of Specimen UC#R-0.5-4.5-#3 127
Figure III.19. Observed behavior of Specimen UC#R-0.5-5.0-#1 128
Figure III.20. Observed behavior of Specimen UC#R-0.5-5.0-#2 129
Figure III.21. Observed behavior of Specimen UC -0.625-2.5-#1 131
Figure III.22. Observed behavior of Specimen UC -0.625-2.5-#2 133
Figure III.23. Observed behavior of Specimen UC -0.625-2.5-#3 134
Figure III.25. Observed behavior of Specimen UC -0.625-3.75-#1 135
Figure III.26. Observed behavior of Specimen UC -0.625-3.75-#2 136
Figure III.27. Observed behavior of Specimen UC -0.625-3.75-#3 137
Figure III.28. Observed behavior of Specimen UC -0.625-3.75-#4 138
Figure III.29. Observed behavior of Specimen UC-0.625-5.0-#1 140
Figure III.30. Observed behavior of Specimen UC-0.625-5.0-#2 142
Figure III.31. Observed behavior of Specimen UC-0.625-5.0-#3 144
Figure III.32. Observed behavior of Specimen UC-0.625-5.0-#4 146
Figure III.33. Observed behavior of Specimen UC#R-0.625-5.0-#1 147
Figure III.34. Observed behavior of Specimen UC#R-0.625-5.0-#2 149
Figure VI.36. Observed behavior of Specimen UC#R-0.625-5.0-#3 151
Figure III.36. Observed behavior of Specimen UC#R-0.625-5.0-#4 153
Figure III.37. Observed behavior of Specimen UC-0.75-3.0-#1 154
Figure III.38. Observed behavior of Specimen UC-0.75-3.0-#2 155
Figure III.39. Observed behavior of Specimen UC-0.75-3.0-#3 156
Figure III.40. Observed behavior of Specimen UC-0.75-3.0-#4 157
Figure III.41. Observed behavior of Specimen UC#R-0.75-4.5-#1 159
Figure III.42. Observed behavior of Specimen UC#R-0.75-4.5-#2 161
Figure III.43. Observed behavior of Specimen UC#R-0.75-4.5-#3 162
Figure III.44. Observed behavior of Specimen UC#R-0.75-4.5-#4 164
Figure III.45. Observed behavior of Specimen UC#R-0.75-6.0-#1 166
Figure III.46. Observed behavior of Specimen UC#R-0.75-6.0-#2 168
Figure III.47. Observed behavior of Specimen UC#R-0.75-6.0-#3 170
Figure III.48. Observed behavior of Specimen UC#R-0.75-6.0-#4 172

List of Tables

Table 3.1 Specimen design of adhesive anchor tests 26
Table 4.1 Specimen with combined breakout-pullout failure 40
Table I.1 Summary of specimen preparation 64
Table I.2 Summary of test results 68

Nomenclature

$A_{se,V}$ = effective cross-sectional area of single anchor in shear

A_s = area of anchor reinforcement

d_a = anchor diameter

E_c = Young's modulus of concrete

E_a = Young's modulus of adhesive

f_{ac} = compressive strength of adhesive from test of 2:1 prism

f_{at} = tensile strength of adhesive from test of coupon

f_c' = concrete strength

f_{cc} = cube compressive strength

f_{ct} = tensile strength of concrete

f_{uta} = ultimate tensile strength of anchor steel

f_{va} = yield strength of anchor steel

f_y = yield strength of steel reinforcement

h_{ef} = embedment depth of adhesive anchor

h_b = length of bond failure at bottom of specimen, measured or assumed

h_{cb} = length of breakout cone depth in combined failure, $=h_{ef}-h_b$

k_{nc} = factor of concrete breakout strength

N = total anchor capacity in unconfined tension tests

N_{cb} = breakout capacity of anchor corresponding to the partial breakout cone

N_p = pullout capacity of anchor in combined failure

t = calculated bond strength from measured/calculated tensile capacity of anchor

α_{setup} = reduction factor of adhesive anchors in unconfined tension tests

$\tau_{confined}$ = bond strength from confined tension (CT) tests

$\tau_{unconfined}$ = bond strength from unconfined tension (UCT) tests

τ_u = bond strength from confined tension tests, in Eq. 1.1

Chapter 1. Introduction

1.1 Introduction

The bond strength of adhesive anchors is obtained from pullout tests, as illustrated in Figure 1. Bond failure at the adhesive-concrete interface is expected during pullout tests. Two test methods are usually used: 1) confined tension (CT) tests to evaluate the bond strength of adhesive and 2) unconfined tension (UCT) tests to evaluate the tensile capacity of adhesive anchors. The setup for the tension tests is a self-balanced loading system: the tensile loading applied to the test anchor is balanced by the reaction applied to the concrete. The reaction in CT setup is placed very close to the test anchors, leading to convenient and material-saving tests. However, the closely placed reactions may create undesirable and unrealistic confining conditions to the specimen. Therefore, the bond strength obtained from confined tension tests, according to ACI 355.4 (2011), must be reduced by a factor α_{setup} = 0.75.

This reduction factor is challenged by observations of the tension tests conducted by Davis (2012). The author concluded that

1. The results from the unconfined short-term tests seem to indicate that the 0.75 ratio of unconfined bond strength to confined bond strength in ACI 355.4-11 and ACI 318-11 to determine the unconfined bond strength from a series of confined tests might be a significant overestimate of unconfined bond strength. Tests on the three adhesives in this research project produced factors of 0.53, 0.43, and 0.37. Additional verification tests in higher strength concrete were conducted to verify the reduction factors. These verification tests at 80°F and 110°F resulted in alpha factors of 0.40 and 0.41 respectively.
2. The alpha setup factor for the relationship between unconfined to confined bond strength in ACI 355.4-11 should be adjusted or a test series added to determine this relationship for individual products. The results of this research showed that this value can be in the range of 0.35 to 0.55 and is significantly less than the value of 0.75 currently assumed in ACI 355.4-11.

This issue was discussed by Committee 355 in ACI fall 2018 convention, Las Vegas, NV. Cook (2018) proposed that the test setup factor should be revised as

$$\alpha_{setup} = 1 - 0.3\frac{\tau_u}{35\sqrt{f_c'}h_{ef}^{1.5}} \leq 0.75, \quad (1.1)$$

where τ_u is mean bond strength measured in confined service condition tests in low and high strength concrete normalized to f_c' = 2,500 psi according to ACI 355.4-11, Section 10.2.3; f_c' is the specified compressive strength of concrete, and h_{ef} is the embedded depth of anchor. The proposed test setup factor was to limit the bond strength such that concrete breakout failure, observed in many unconfined tension tests, would not cause unconservative estimation of bond strength. A close look at Eq. 1.1 indicates that the proposed changes only apply to anchors with small embedded depths (h_{ef}< 2 in.) as illustrated in Figures 1.1 and 1.2.

The committee discussion indicated that this is a critical item for the committee. The committee noted that "*New tests with new products (over last 10 years) have higher bond stresses. The new data was much lower than the current ACI 0.75 factor. Study recommended to AASHTO to use 0.5 factor instead of 0.75. It's a big change. The alpha-setup factor affects the design values that come out of the qualification testing. This only affects the anchors tested by confined testing*."

1.2 Definition of Problem

The test setup factor for adhesive anchors in tension is defined as

$$\alpha_{setup} = \frac{\tau_{unconfined}}{\tau_{confined}}, \tag{1.2}$$

where $\tau_{unconfined}$ is the bond strength from unconfined tension tests while $\tau_{confined}$ is the bond strength from confined tension tests. Section 10.4.5.1 of ACI 355.4-11 indicates that α_{setup} shall be 1.0 if service-condition tests are performed as unconfined tests, 0.75 if service-condition tests are performed as confined tests, and 0.70 if service-condition tests in cracked concrete are performed as confined tests.

Based on the tests by Davis (2012), Cook concluded that α_{setup} must be determined by tension tests. If not, use 0.5 and not 0.75 in ACI355.4-11. Details of the confined (Series 1) and unconfined (Series 16) tension tests by Davis (2012) are shown in Chapter 2. Installation anomalies were recorded for Series 16 tests as "*During installation of the above two series of five anchors (series 7 and 16) there were times at which the installer stopped the continuous injection and set the cartridge gun down for a few minutes. During this set-down period it appears that some unequal mixing of components occurred in the mixing nozzle. Adhesive C was significantly more difficult to dispense by hand during installation, compared to the other adhesives. The difficulty in dispensing indicated that at least one of the components was very viscous. If one component was significantly more viscous than the other, it is possible that during the set-down period there could have been an abundance of the other component (which flowed more easily) in the mixing nozzle. When the cartridge gun was picked back up and the installation resumed, the adhesive in the nozzle had an improper ratio of adhesive components. This resulted in the following repetition being poorly mixed and at low strength*."

Wall (2019) pointed out that "*Since the number of tests carried out in the project investigating this aspect and shown in the figure is very small (n = 3), the comparison with the calculated concrete breakout strength should not only include the mean value but also the characteristic value (meaning the basic concrete breakout strength)*." In addition, the reported tests by Davis (2012) showed interesting behavior that "*The results of these tests show similar mean maximum load levels for the various investigated adhesives, even though confined bond strength of the adhesives show a considerable difference. The results of the unconfined testing are all at or above the calculated basic concrete breakout strength for the specified concrete*." Wall finally remined the committee that "*The alpha setup factor determines the unconfined bond strength from tests with confined test setup within the same failure mode, i.e. bond failure*."

In this study, we attempted to explore the impact of test setup on observed behavior of adhesive anchors. One adhesive and one concrete strength were used while multiple anchor diameters and multiple embedment depths were used. Tests were conducted under indoor temperature, which is different from that in Davis (2012). Bond failure, especially along the adhesive-concrete interface was the targeted failure mode following the suggestion by Wall (2109). Test design indicated that concrete breakout may controlled the failure; hence specimens were included, in which anchor reinforcement was used to force bond failure. Note that the anchors in reinforced concrete does not have practical applications for post-installed anchors although the anchor reinforcement was designed according to ACI 318 (2019).

1.3 Organization of Report

In this report, the details of the findings by Davis (2012) and the disscussion by ACI Committee 355 are described in Chapter 2; our experimental program is described in Chapter 3, inclduing a detailed description of our installation procedure; the results of the tests are discussed in Chapter 4. Finite element analyses were used to explain the potential impact of closely placed reaction in Chapter 5. The study is summarized in Chapter 6, which also includes a list of suggested future research topics.

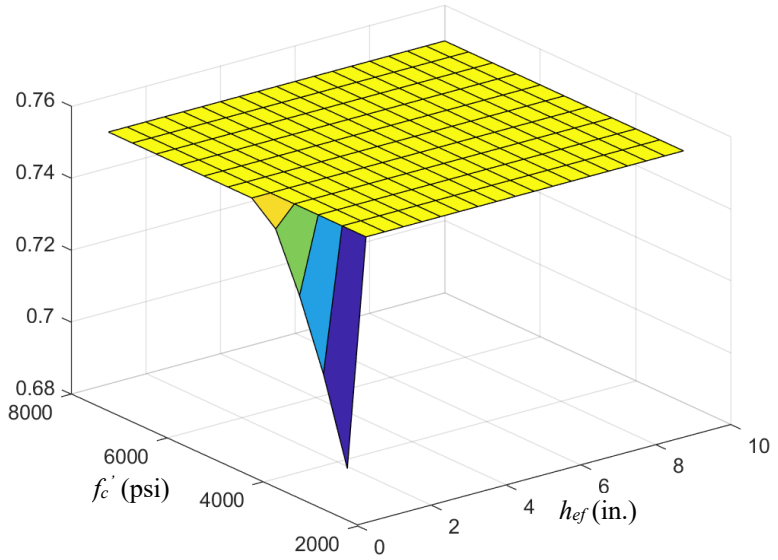

Figure 1.1 The capacity reduction factor proposed by Cook (2018): (τ_u=2000psi)

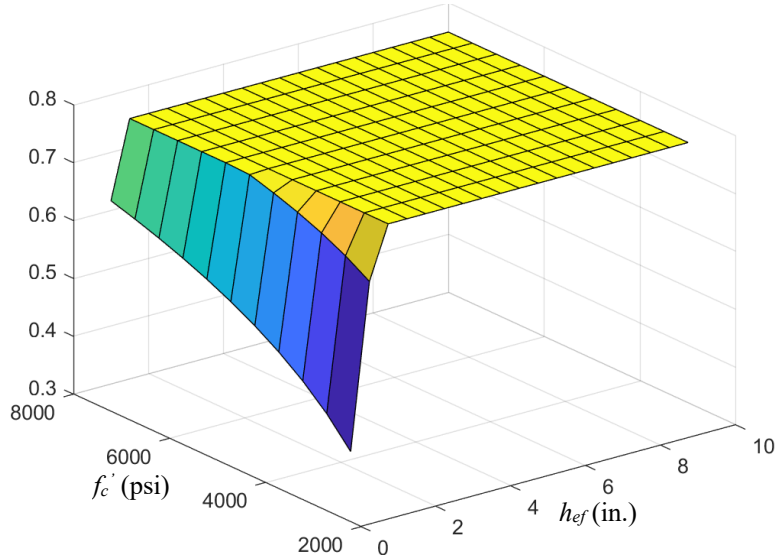

Figure 1.2 The capacity reduction factor proposed by Cook (2018): (τ_u=4000psi)

Chapter 2. Literature Review

The literature review does not include the vast available information on adhesive anchors. The readers are referred to publications by Prof. Cook and Prof. Eligehausen.

2.1 Research by Davis (2012)

Davis (2012) investigated the performance of adhesive anchors in concrete under sustained loads, which was motivated by a influential accident from adhesive anchor failure in 2006 (NTSB 2006). While the majority of the tension testes were conducted with confined tension test setup, Series 16 had a total of five tests with unconfined tension setup under short-term loading. Three types of adhesive were used in the study, inclduing Type A: a vinylester with acrylic monomers, a peroxide hardener and quartz filler; Type B: an epoxy resin with amine hardeners and quartz filler; and Type C: an epoxy resin with an amine blend. The concrete strength was between 4000 and 6000 psi. The anchors were made of 5/8-in. diameter ASTM A354 Grade BD threaded rods with a yield strength of 130 ksi and a ultimate strength of 150 ksi. Type C adhesive was used in Series 16 tests with unconfined tension setup. These tests were compared with Series 1 tests with the same adhesives.

The acnhors were installed in concrete blocks with a dimension of 60×16×12 in. as illustrated in Figure 2.1. Two No.3 60 ksi rebars were placed in longitudinal direction 5 in. from the bottom of the slab. The embedment depth for all the tests was 3-1/8 inches. The embedment depth was chosen to ensure bond (pullout) failure based on the recommendations from AASHTO (2010).

The installation procedure followed the manufacturer's printed installation instructions (MPII). Specifically,

- The holes were created with a ¾-in. carbide tipped concrete bit using a Hilti^{TM} model TE52 hammer drill.
- For Type C adhesive, the hole cleaning procidure included blow with compressed air (4x); brush with drill (1x); blow with compressed air (4x), brush with drill (1x); blow with compressed air (4x); brush with drill (1x); blow with compressed air (4x); brush with drill (1x); blow with compressed air (4x).
- According to the manufacturer's printed installation instructions (MPII), several strokes of adhesive were discharged before dispensing adhesive into the holes to ensure that the adhesive was properly mixed.
- The anchors were wiped clean with acetone and allowed to air dry. The anchors were then attached to an "embedment depth chair" for the appropriate embedment depth (Figure 2.2).
- The anchor rod was rotated counterclockwise and jiggled while it was installed in the hole. The anchors were left undisturbed during the specified gel/working time and the adhesive was allowed to cure for seven days.
- Excess adhesive was carefully chipped away from around the anchor after curing. The masking tape left around the hole prevented the concrete from being removed during chipping.
- Most of tests were conducted at 110 degrees Farenheit; hence, the specimens were kept in an environmental chamber maintaining 110ºF and 35% humidity for 24 hours (conditioning).

The short-term confined and unconfined testing setups according to ASTM E488 and are shown in Figures 2.3 and 2.4. The testing apparatus for the confined tension tests (Series 1) used a

6×6×0.03 in. Teflon® PTFE (Polytetrafluoroethylene) sheet placed beneath a 8×8×5/8 in. steel confining plate. The confining PTFE sheet was used to correct for irregularities on the surface concrete. A 1.25-in. hole was drilled though the center of the confining sheet and confining plate to fit around the anchor. In the testing apparatus for the unconfined tension tests (Series 16), the reaction wa sprovided by two 3×5×1/4 in. rectangular steel tubes, placed parallel to each other on either side of the anchor no closer than two times the embedment depth. The Teflon® PTFE sheet was not used in the unconfined tension tests. This is different from the test setup in this study.

The confined tesion tests in Series 1 using Type C adhesive showed an average capacity of 26.3 kips and a standard deviation of 1.7 kips. These ultimate loads occurred at a displacement about 0.04 in., as shown in Figure 2.5. The calculated average bond strength is about 4.3 ksi, which is close to a separate test conducted by researchers at the Unviersity of Stuttgart (3.95 ksi) for the same adhesive. The unconfined tension tests in Series 16 using Type C adhesive showed an average capacity of 9.8 kips and a standard deviation of 0.9 kips. These ultimate loads occurred at a displacement about 0.05 in. (Figure 2.5), which is only slightly larger than that of confined tension tests. The specimens were largely controlled by concrete breakout failure as shown in Figure 2.6. The equivalent bond strenght was about 1.6 ksi, leading to an observed α_{setup} of 0.37.

2.2 Research by Appl (2009)

The current α_{setup} factor in ACI 355.4, 0.75 for anchors in uncracked concrete is based on the work of Appl (2009). The author evaluated the tests of adhesive anchors in Germany between about 1995 to 2005. As illustrated in Figure 2.7, the mean bond strength of these anchors (measured in confined tests) was only between 1700 psi to 2500 psi, significantly lower than that observed in Davis (2012). Therefore, it is deemed that the test setup factor (α_{setup}) needs to be updated for mordern adhesives, likely with higher bond strengths (from confined tension tests).

2.3 Discussion by Eligehausen and Asmus (2019)

Eligehausen and Asmus (2019) concluded that $\alpha_{setup} = 0.75$ is too high from the data presented in Davis (2012). Instead of using average bond strengths, the discussion was based on 5%-fractile values from the same data (five confined tension tests and three unconfined tension tests). The authors suggested that "*if in high strength concrete the bond strength is measured in confined tension tests, the current approach in ACI 355.4 significantly overestimates the strength of the tested bonded anchor. To avoid this, the factor αsetup must be reduced to about 0.5*."

The authors recommended that "*new tests with products currently on the market should be performed and numerical investigations are recommended to understand better the behavior of bonded anchors with a low and high bond strength in confined and unconfined tests in low and high strength concrete*."



Figure 2.1 Concrete specimen (Figure 4-6 in Davis (2012))

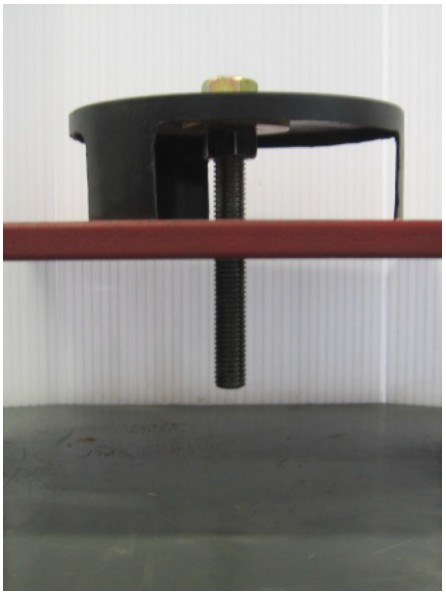

Figure 2.2 Embedment depth chair (Figure 4-21 in Davis (2012))

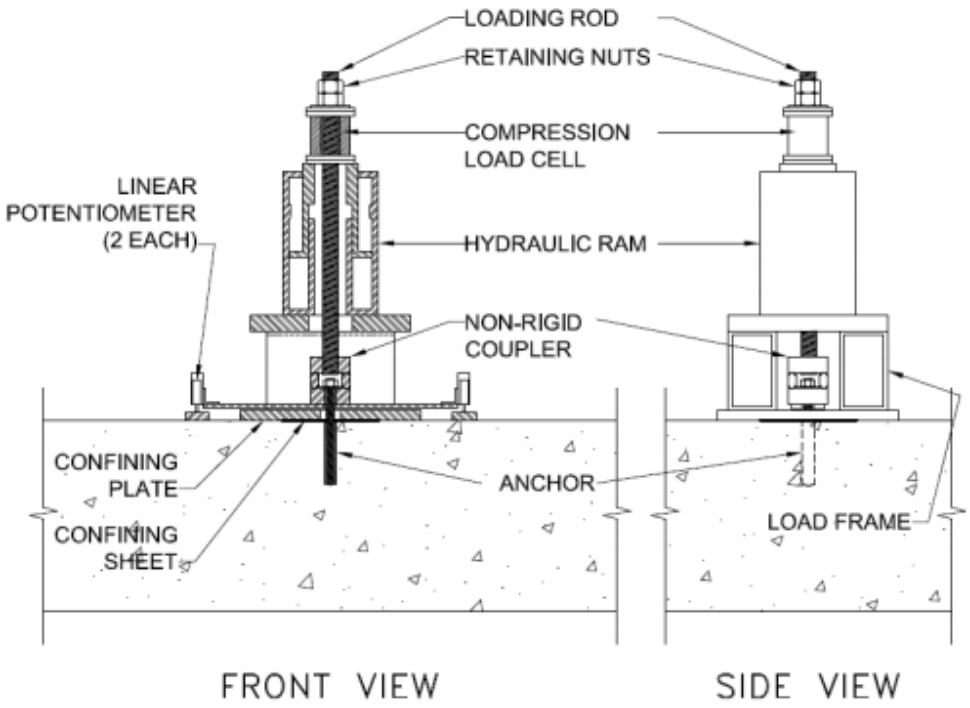

Figure 2.3 Confined tension test setup in (Fig. 4-1 in Davis (2012))

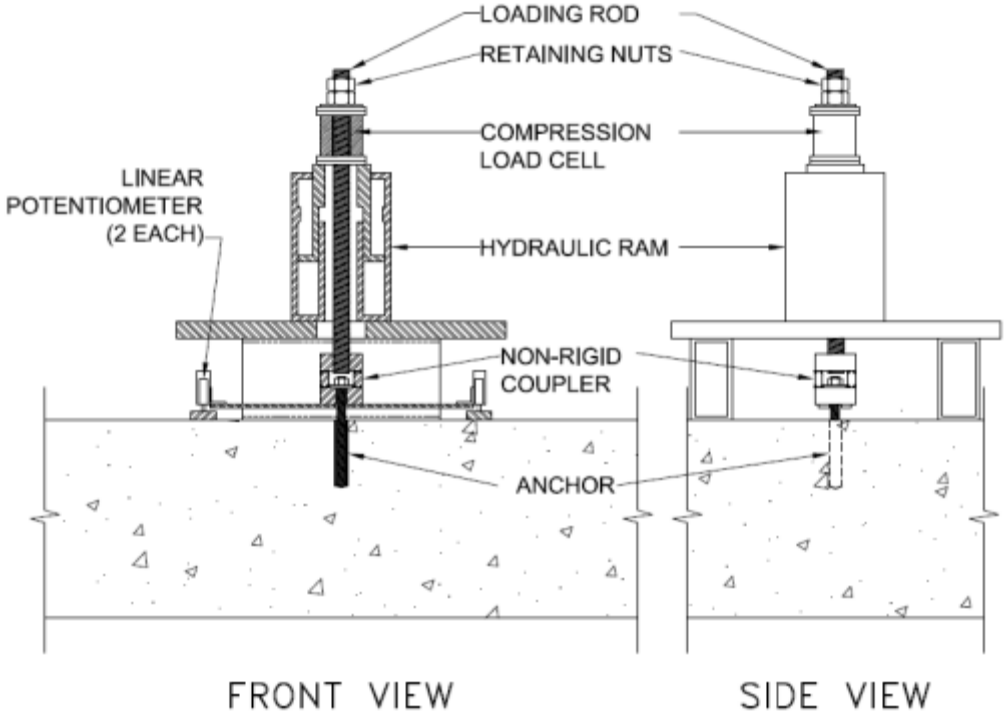

Figure 2.4 Unconfined tension test setup (Fig. 4-2 in Davis (2012))

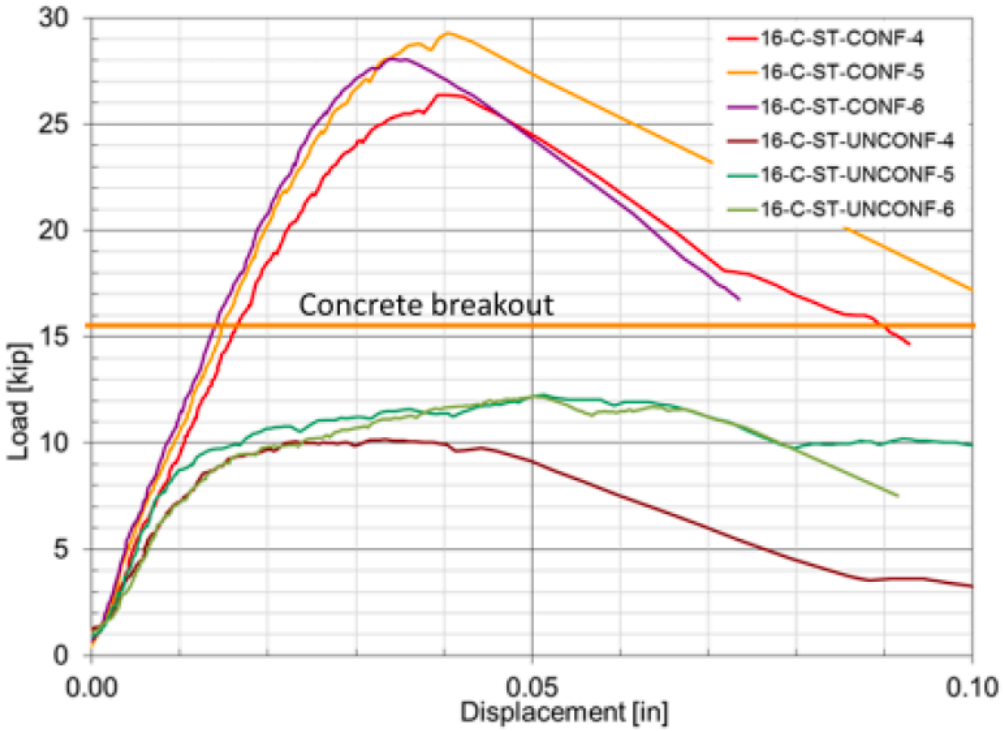

Figure 2.5 Short-term tension tests of adhesive anchors by Davis (Cook 2019)



Figure 2.6 Unconfined tension tests of adhesive anchors by Davis (Cook 2019)

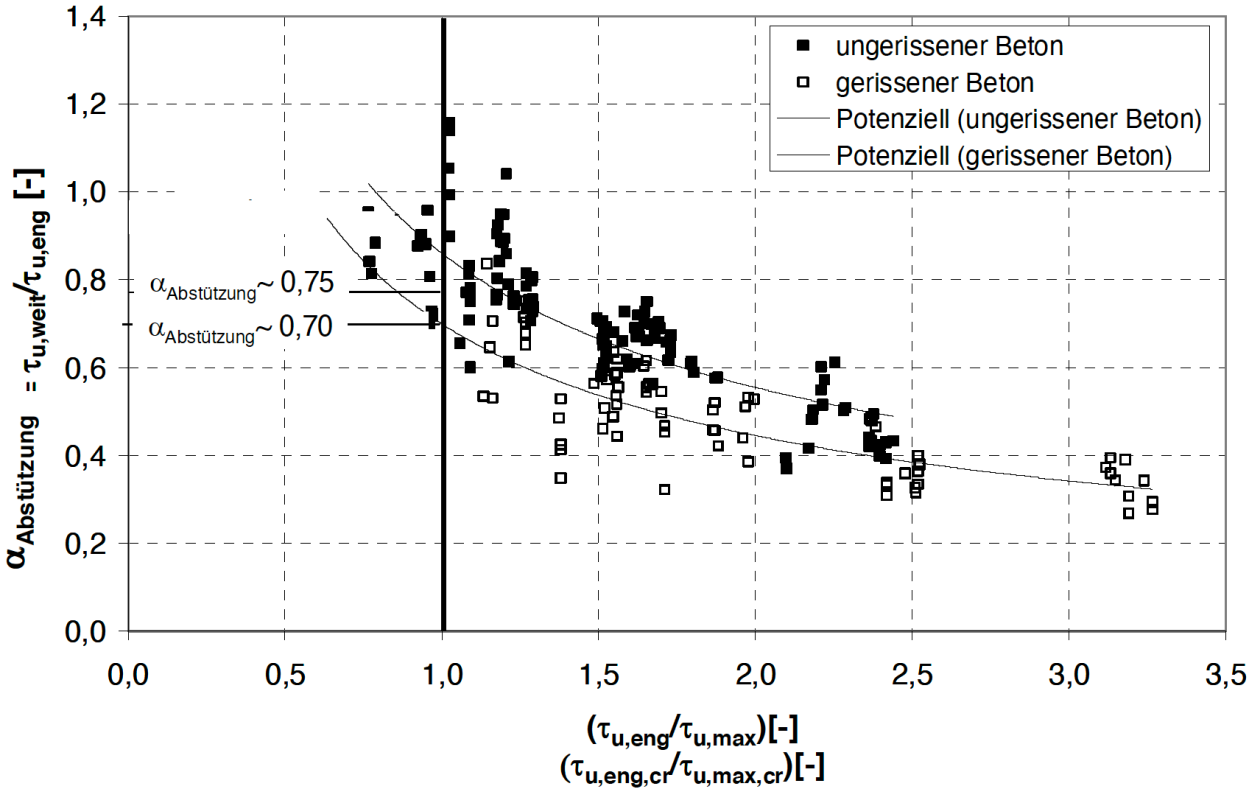

Figure 2.7 Alpha Setup summarized by Appl (Figure 10.9 in Appl (2009))

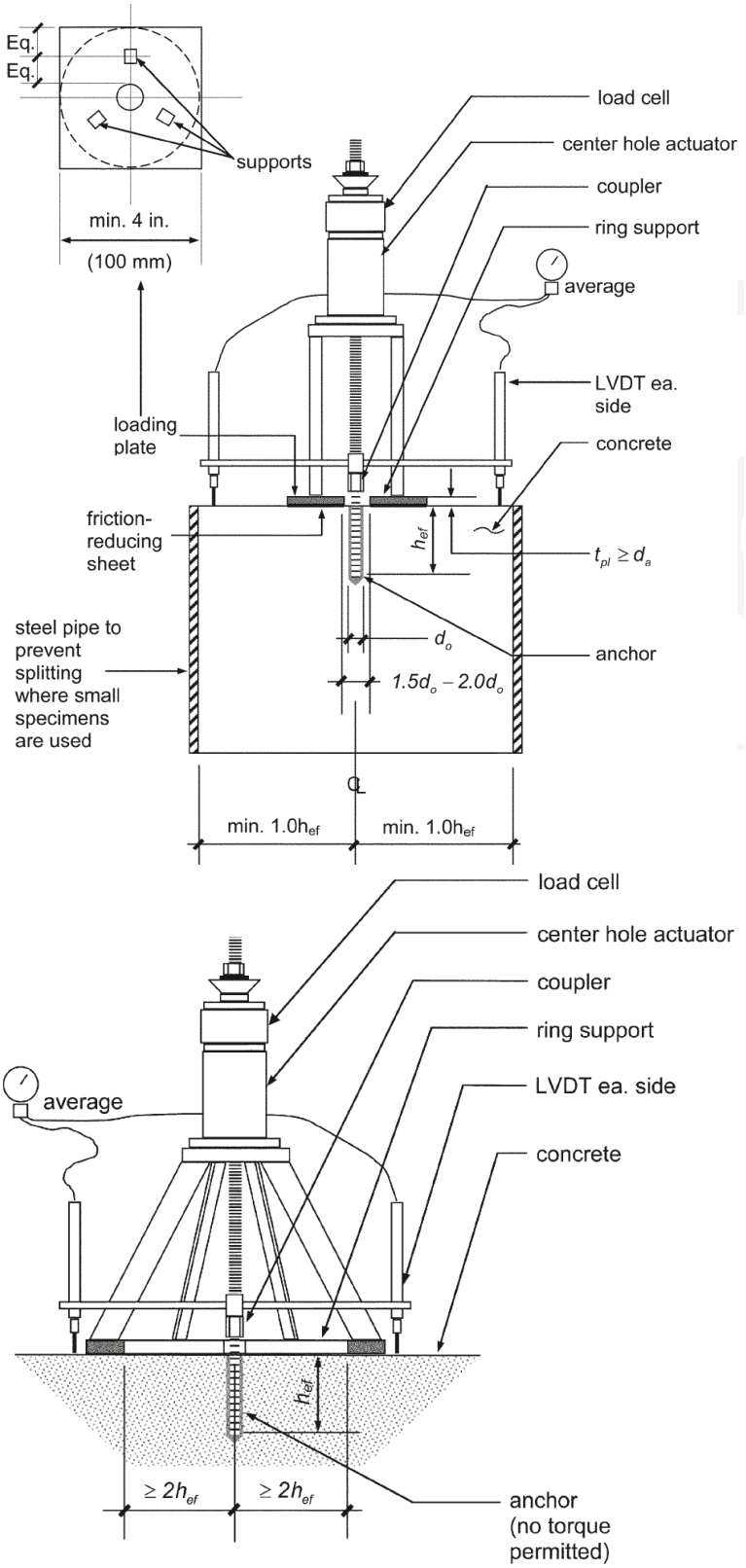

Figure 2.8 Example of test setup for adhesive anchors in ACI 355.4-19

Chapter 3 Experimental Investigation

3.1 Introduction

We conducted a total of 74 tests, including 28 confined tension tests and 46 unconfined tension tests. The installation details are shown in Appendix I. The additional tests were expected to provide information for ACI Committee 355 to update α_{setup} in the future recommendations.

3.2 Experimental program

Adhesive anchors were expected to develop bond failure at adhesive-concrete (A-C) interface in this study. Hence, the embedded depth of the test anchors must be properly chosen. Adhesive anchors in tension may fail in steel fracture, concrete breakout, and pullout (ACI 318-19). The capacities of the selected anchors (made of 1/2-in., 5/8-in., and 3/4-in. diameter threaded rods) are compared in Figures 4.1 for a range of embedded depths. The concrete breakout capacities were calculated assuming a compressive strength of 6000 psi. The concrete capacity design (CCD) method was used with a constant (k_{nc}) of 35. Note that this constant represents the upper limit of concrete breakout capacities; Hence, for comparison purposes, Figure 3.1 also include capacities calculated with a constant (k_{nc}=24) stipulated in ACI 318-19 for adhesive anchors in uncracked concrete. The capacities corresponding to steel fracture were calculated assuming an ultimate tensile strength (f_{uta}) of 125 ksi in the experiment planning phase, which is the minimum required tensile strength in ASTM A193 (2000). However, the actual ultimate tensile strength of the threaded rods in this study, measured using threaded rod specimens, showed two different ultimate strength 110 ksi and 128 ksi. The capacities calculated from the lower ultimate strength are shown in Figure 3.1 for comparison purposes. The capacities corresponding to pullout failure were calculated using the uniform bond stress model in ACI 318-19 with a bond strength (τ) of 2000 psi. This bond strength was obtained from trial pullout tests with the same adhesive (Liu 2020).

The comparison of adhesive anchors in confined and unconfined tension tests considered the following parameters:

- Anchor diameters (d_a): 1/2 in., 5/8 in., and 3/4 in.;
- Embedment depths (h_{ef}): $4d_a$ and $6d_a$ for confined tension tests;[1]

  $4d_a$, $6d_a$, $8d_a$, and $10d_a$ for unconfined tension tests[2]
- Reinforcement in concrete: no reinforcement and code-conforming anchor reinforcement.

These specimens are listed in Table 3.1. It was expected that anchors with an embedment of $4d_a$ would likely be controlled by concrete breakout; anchors with an embedment of $6d_a$ would likely be controlled by concrete breakout or anchor pullout; anchors with an embedment of $8d_a$ would likely be controlled by anchor pullout; and anchors with an embedment of $10d_a$ would likely be controlled by steel fracture. Reinforcement was used for anchors with an embedment of $8d_a$, that is UC-0.5-4.0 and UC-0.625-5.0, to increase the likelihood of anchor pullout because the concrete breakout capacity could be reduced when splitting cracks form during testing. Although code-conforming anchor reinforcement makes no practical indication for post-installed anchors as post-

[1] A total of two tests with an embedment of $3d_a$ and $8d_a$ were conducted for ¾-in. diameter specimens.
[2] Only for ½-in. diameter anchors.

installed anchors are not usually installed in concrete with proper anchor reinforcement, it was used in some specimens to delay concrete breakout failure.

3.3 Specimen Design

Specimen dimensions

The sizes of the concrete block, as schematically shown in Figure 3.2, are listed in Table 3.1. The reaction supports need to be placed $2h_{ef}$ away from the test anchor typical unconfined tension tests in ACI 355.4 (2011). Hence, the block length was determined as $2\left(2h_{ef} + 4"\right)$, where the additional 4 inches was the width of reaction supports. This resulted in a block length of 24 in. for ½-in. anchors, 28 in. for 5/8-in. anchors, and 32 in. for 3/4-in. anchors. The block widths were determined based on the minimum edge distance required for unconfined tension tests in ACI 355.4 (2011). Also, anchors were installed on four sides to provide repeated tests; hence the block widths were also determined based on the minimum depth of concrete specimens in ACI 355.4. The width/thickness of blocks was also checked to avoid flexural cracks under the maximum possible tensile loads to be developed in the test anchors. Based on the calculation, there was no need for longitudinal reinforcement. Four No. 4 bars and two stirrups were provided for all plain concrete blocks to facilitate specimen handling.

The anchor reinforcement was used for anchors with an embedment higher than $8d_a$ (that is UC#R-0.5-4.0 UC#R-0.5-5.0, UC#R-0.625-5.0 and UC#R-0.75-6.0). The reinforcement was expected to delay concrete breakout such that anchor pullout failure may control the unconfined tension tests such that the impact of reaction locations could be examined. The anchor reinforcement for cast-in anchors in tension in ACI 318 (2019) consists of U-shaped hairpins with legs parallel to the anchors located within $0.5d_a$ from the anchors. Petersen et al. (2018) indicated that anchor reinforcement can be closed stirrups, two next to the anchors and others spaced in 2 to 3 inches. This recommendation (two bars next to anchors) was not followed because the anchor reinforcement may be shifted from the designated location to interfere with the adhesive anchor installation, which may have reduced the efficiency of anchor reinforcement as explained later in Chapter 4.

The reinforced concrete block is schematically shown in Figure 3.3. The anchor reinforcement was calculated as 4 No. 3's for ½-in. anchors based on an ultimate load of 18 kips, 2 No. 3's plus 2 No. 4's for 5/8-in. anchors based on an ultimate load of 28 kips, and 4 No. 4's for 3/4-in. anchors based on an ultimate load of 42 kips. These reinforcing bars cannot be placed next to the test anchors as suggested by Petersen et al. (2018) because the anchors would be installed after concrete was placed. In addition, U-shaped hairpins as recommended by ACI 318-14 were not used because anchors were to be installed on all four faces; hence two pairs of C-shaped hooks (tied together to form two closed stirrups) were used for anchors installed on two opposite faces, as shown in Figures 3.3. The center-on-center spacing of the closed stirrups was 3 in. in one direction and 3.5 in the perpendicular direction. On average the stirrup legs that serve as anchor reinforcement were expected to be roughly $0.5h_{ef}$ away from the test anchor.

In addition to the legs parallel to the anchors serving as anchor reinforcement, Petersen et al. (2018) requires sufficient corner reinforcement on all concrete faces to control splitting cracks. Design equations were provided to determine the crack-controlling reinforcement. In the block width direction, two No. 3 closed stirrups were used not only to fix the anchor reinforcement but also to

delay splitting cracks in the longitudinal direction. In the block length direction, the short legs of the C-shaped hooks were tied together to delay splitting cracks in the transverse direction.

Material properties

Concrete used in this study was ordered from a local ready-mix batching plant. The specified concrete strength was 4000 psi. Considering the past experience with the concrete provided by the batching plant, a slump of 5 in. was specified. The concrete had a measured slump of 7.25 inches. The concrete blocks were covered with plastic sheets in an indoor environment and the cylinders were kept in their plastic molds. The 7-day strength of the concrete using three 4×8 in cylinders was 4520 psi. The formwork of the concrete blocks was thus removed at this age and the cylinders were demolded. Both the concrete blocks and the concrete were kept at the same indoor condition (roughly with a consistent temperature of 70 degrees Fahrenheit). The average compressive strength was 6200 psi at 28 days and 6280 psi at 90 days, during which the majority of tension tests were conducted. The strength development of the concrete is shown in Figure 3.4.

The ASTM A193 Grade B7 threaded rods for the tests in this study were purchased from Grainger Industrial Supply. Tensile tests conducted using threaded rods indicated two different properties of the threaded rods from the same source. The measured stress-strain curves for the threshed rods are shown in Figure 3.5.

The adhesive used in this study was a two-component vinylester adhesive. The working time is 6 minute and full curing time is 45 minutes under a temperature of 68 Fahrenheit (20 Celsius). Tests were conducted for the adhesive material in both tension and compression. The measured stress-strain relationships are shown in Figure 3.6. The modulus of Elasticity (E_a) was 315.4 ksi. The Poisson's ratio was between 0.375 and 0.4. The compressive strength (f_{ac}) was 11 ksi at a corresponding strain of 0.0668. The tensile strength (f_{at}) was 2.31 ksi at a strain of 0.0073.

Test setup

The test setup for the confined tension tests is shown in a schematic in Figure 3.7a and a picture in Figure 3.7b. The reaction was directly applied to concrete though a steel plate with a dimension of 5×5 inches. The center hole in the plate is 1.25 in. and the thickness of the plate is 0.5 in. for the 1/2-in. and 5/8-in. diameter anchors as required by Section 4.7.3.2 of ACI 355.4 (2011). The reaction plate had a 1.5-in. center hole and a thickness of 1.0 in. for 3/4-in. diameter anchors. To minimize the friction between the plate and concrete, a 1/8-in. thick plastic sheet with the same dimension of the plate was placed between the reaction plate and the concrete. The plastic sheet was called "confining sheet" in Davis (2012) (Figure 2.3) and "friction-reducing sheet" in ACI 355.4-19 (Figure 2.8a). Trial tests were first conducted without the plastic sheet, and the tests indicated that the bond failure was mostly on adhesive-steel (A-S) interface. It was later revealed that the plastic sheet between the concrete and the steel reaction plate was needed not to reduce friction because there was no apparent relative motion between concrete and the reaction plate in confined tension tests. Rather the plastic sheet between the steel reaction plate and concrete allowed dilation of concrete near surface during the pullout tests. The plastic sheet was later cut in 4 pieces to further minimize the confining effects of the reaction plate to the dilation of concrete in the confined tension tests in this study.

The test setup for the unconfined tension tests is shown in a schematic in Figure 3.8a and a picture in Figure 3.8b. The tested anchor was connected with the loading rod using a high-strength transition nut. The diameter of the loading rod was ¾ in. for both ½ in. and 5/8 in. diameter anchors

while the loading rod was 1.0 in. for ¾-in. specimens. A 2-in. diameter hole was cut in the center of the loading beam to allow the loading rod to go through. A loading beam was used to transfer the load from the loading rod to the concrete surface through two 4×4×¼ in. HSS tubes. The HSS tubes was on base plates with a dimension of 11×4×3/8 in. to distribute the even load to the concrete surface. No rigid connection was used between the HSS tubes and the loading beam. Again, a 1/8-in. thick plastic sheet was placed below the base plates to be consistent with the confined tension tests. This plastic sheet was not presented in the example test setup for unconfined tension tests in ACI 355.4-19 (Figure 2.8b). It was deemed that the steel ring support in the example test setup in ACI 355.4-19 may confine concrete and the confinement could be unrealistic, especially for anchors installed close to an edge (though still within the code-stipulated range). A plastic sheet may also be needed to account for uneven concrete surfaces. For example, Epackachi et al. (2015) used a thin layer of gypsum between the steel reaction ring and concrete. The gypsum layer, having a low Young's modulus, was deem equivalent to the plastic sheets used in this study. The HSS tubes were placed $2h_{ef}$ away in all tests, which required the position adjustments for anchors with various embedment depths.

Instrumentation and data acquisition

The loads applied to the anchors was measured by a load cell (Model THD-50K-Y) that was on top of a hydraulic jack. Two Model 0345 linear variable differential transformers (LVDTs) were fixed at each end of a steel flat bar locked between a hex nut and a coupling nut to directly measure axial displacement of an anchor. The test anchors had a length of 3 in. above the concrete surface as the operation length, which allowed the linear variable differential transformers (LVDTs) to be mounted properly.

An IO Tech DaqBook 2000 was used to collect data from the LVDTs and the load cell with a sampling rate of 10 Hz. A preload was applied about 200 lb [0.89 kN]. A wrench was used to tighten the retaining nut on the top plate until the reading of the load cell was about 0.04 volts from the data acquisition.

3.4 Installation Procedure

The following installation procedure was customized based on the manufacturer's printed installation instructions (MPII). The procedure can be divided into four major steps: 1) material preparation/handling; 2) hole drilling and cleaning; 3) adhesive placement; and 4) anchor installation and post-installation care (Liu 2020).

1. Select proper tools. Proper drill bits and hole-cleaning brushes were used following the MPII. The diameter of holes may impact the pullout capacity of adhesive anchors and likely the failure interface, that is adhesive-steel (A-S) interface and/or adhesive-concrete (A-C) interface.
2. Prepare threaded rods. After cutting anchors into desired lengths, we used masking tape to mark the embedment depth on the anchor. Saw-cutting may leave bent threads, which may cause stress concentration at anchor-adhesive interface; hence bent threads at the end of anchor or along the embedded depth were removed using a file and an angle grinder. Debris and dusts were removed from the anchor rods using a metal wire brush. A paper/fabric towel was used to remove dust, oil, grease, or water if needed.
3. Drill holes in concrete. The anchors must be perpendicular to the concrete surface in this study; hence the impact hammer drill was fixed to a drill jig. The desired drilling depth is measured

from the base plate and marked on the drill bit using a masking tape. The hole location was pre-marked on the concrete surface and dented using a metal center spot punch. Before placing the drill jig, debris were removed from the concrete surface and the bottom of the drill jig plate to ensure the concrete surface was flat and the base plate did not have a gap from the concrete surface. This was particularly important for anchors in confined tension tests. After the bit was placed at the location, the operator stood on the base plate of the drill jig such that the drilling was straight downward. Drilling started with a partial body weight downwards and completed without stop-and-check. Intermittent stops during drilling may create slightly curved vertical hole profile instead of a desired straight hole. The curved hole profile may prevent adhesive-concrete bond failure, which is critical to this study. The hammer drill was stopped during the bit retraction. This step may be important to this study because leaving the hammer drill on during bit retraction may create extra dents on the hole wall, which in turn may prevent the desired adhesive-concrete bond failure. Drilled holes are show in Figure 3.9a on a cut and split concrete block.

4. Clean drilled holes. Drilled holes must be cleaned for adhesive to form bond with based concrete. The hole cleaning included blowing dusts followed by brushing and additional blowing. The anchors were less than or equal to ¾ inches in this study; hence a hand pump was allowed, and a 25 fl. oz. hand pump was used. The cleaning process is shown below:
    - Use a vacuum with a nozzle to remove the dust and concrete debris left at the bottom of holes. This step replaced the first dust-blowing step documented in MPII because air blowing cannot completely remove dust left at the bottom of holes during the drilling process (Figure 3.9a), which may impact the final anchor embedment depths.
    - Use proper brushes to clean the holes. Install the brush to a power drill, insert a brush shallow into to the drilled hole, and start with full high-speed rotation. Push the brush to the back of the hole and pull it out immediately. Repeat the brushing process four times according to MPII. The brush wire stiffness is found critical to the cleaning results.
    - Extended the nozzle of a hand pump all the way to the back of a drilled hole and blow dusts out. Repeat this step four times. Compressed air can also be used in this step provided that the air nozzle is extended to the back of a drilled hole. Cover cleaned holes with a masking tape. The cleaned holes are shown in Figure 3.9b.
5. Inject adhesive into drilled holes. This study uses a two-component vinylester adhesive anchoring system. Two-component adhesives start curing when the resin component and the hardener component are mixed together. The viscosity of the mixed system increases as time goes by while cross-links form within the material. Hence the installation was strictly controlled to make sure Steps 5 and 6 were completed within the gel time as shown in Appendix I. Gel time is defined as the time it takes for a mixed resin system become so highly viscous that it can no longer be considered workable. The gel time is also the time for the polymer formation from starting of cross-linking to the point that if the polymer gel state is disturbed then the final polymer will not have well-established properties, such as adequate bonding strength or adhesion. Note that the cross-links form at a much faster speed in adhesive towards the end of the gel time. Hence, the working time for both anchor installation and the use of mixing nozzle is set at 5 minutes under indoor room temperature in this study. In addition, mixed adhesive left within the mixing tube must be discarded by dispensing one full stroke within this working time before injecting adhesive for a new anchor installation. The adhesive injection process is shown below:

- Mark the location of an anchor and the assisting lines. The assisting lines are created from the center of the drill holes with a theoretical offset of a half anchor diameter. Mark the position of the level along two sides while a centered threaded rod rest on the corner of the level. Put masking tape on the surface of concrete such that excessive adhesive can be easily cleaned later before testing.
- Prior to injecting adhesive into a drilled hole for the first time through a new mixing nozzle, dispense at least THREE strokes of adhesive through the mixing nozzle till the adhesive is in consistent gray color. Start the clock for the 5-minute working time. Tests have shown that the two components mix gradually in the mixing tube. Specifically, the adhesive further into the mixing tube is fully mixed and the curing process progressed during Step 7. This part of adhesive thus should be discarded for new anchor installation to ensure consistent adhesive quality among all anchor specimens. Therefore, when working in between anchors, discard at least ONE stroke of adhesive through the mixing nozzle prior to injecting adhesive into a second drilled hole, after which, restart the clock for the 5-minute working time.
- Fill the hole half to two-thirds full. The mixing nozzle must start at the bottom of the drilled hole. Slowly withdraw the mixing nozzle during injection. Although all installation in this study is downward, operator still must avoid creating air pockets or voids during injection.

6. Install threaded rods. The anchor placement process is shown below:
   - Place the assistant post level at the location marked previously and drop the rod in the hole against the right-angle corner of the post level. Push the rod in while turning it clockwise slightly to ensure positive distribution of the adhesive. Make sure the anchor rod is fully seated on the bottom of the hole. Adhesive must completely fill the annular gap at the concrete surface. Some adhesive should flow out of the hole ALL around the anchor. Do NOT pull out an inserted anchor and replace it in any case.
   - Perform minor adjustment of the anchor rod if absolutely necessary to ensure the anchor rod is centered and perpendicular to the concrete surface. The viscosity of the adhesive is high, especially with the quartz fillers; hence, slightly twist the anchor during the adjustment process to ensure good adhesive compaction around the anchor rod. Note that the adjustment should be minimized if not avoided because any gap between the anchor rod and the adhesive may weaken the A-S interface, which is detrimental to the tests in this study.
   - Briefly wipe most of the excessive adhesive on the concrete surface around the anchor rod. No need to completely clean the rod as this will be done before testing by peeling off the masking tape installed on the anchor rod if needed.
7. Cure adhesive. For all installations the anchor element was fully restrained from movement throughout the specified full cure time, where necessary through the use of temporary wedges, external supports, or other methods. Minor adjustments to the position of the anchor element may be performed during the 5-minute working time only. ACI 355.4 stipulates a minimum of 24 hours curing after the installation. The anchors in this study are allowed a minimum of 24 hours indoor curing before fixtures for testing are installed.
8. Handle specimens. Move concrete specimens with care. The anchor shall not be hit by tools and/or components during the installation of test equipment. To lock the aluminum beam that holds two LVDT's on to the test anchors, use two wrenches to tighten the nut with a transition coupler. A transition coupler must be firmly attached to the testing anchor such that a loading

rod can be used to apply tensile force to the anchor through a hydraulic jack. In addition, a small pre-load (arbitrarily 200 lbs. in this study) was applied before testing to minimize the initial slag in the testing system. The nut on the top of the plate washer was tightened by an additional 1/6 turn from the snug tight position for this purpose.

Loads were applied using a hand pump and an Enerpac hydraulic jack. The loading rate was roughly 200 lb/sec. The test results are analyzed in Chapter 4.

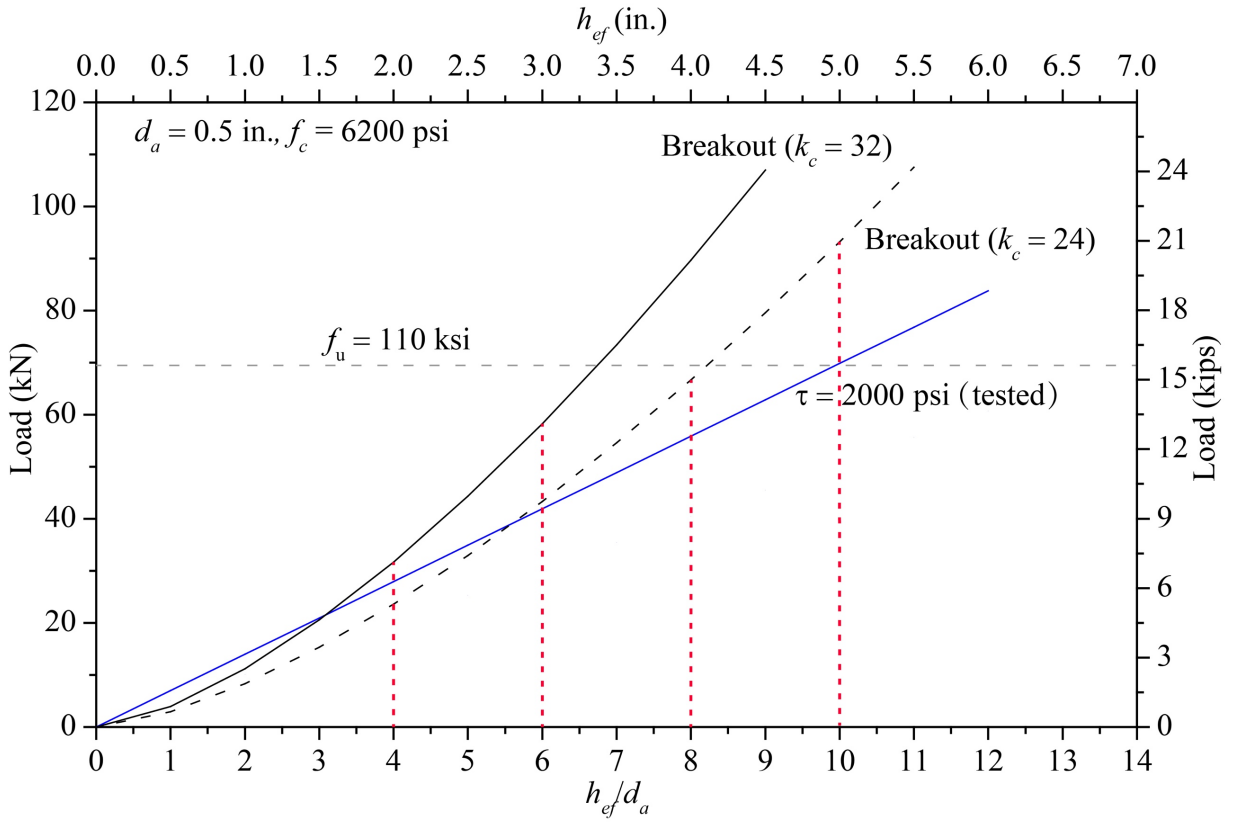
h_{ef} (in.)
0.0 0.5 1.0 1.5 2.0 2.5 3.0 3.5 4.0 4.5 5.0 5.5 6.0 6.5 7.0
d_a = 0.5 in., f_c = 6200 psi
Breakout (k_c = 32)
Breakout (k_c = 24)
f_u = 110 ksi
τ = 2000 psi (tested)
Load (kN)
Load (kips)
0 20 40 60 80 100 120
0 3 6 9 12 15 18 21 24
0 1 2 3 4 5 6 7 8 9 10 11 12 13 14
h_{ef}/d_a

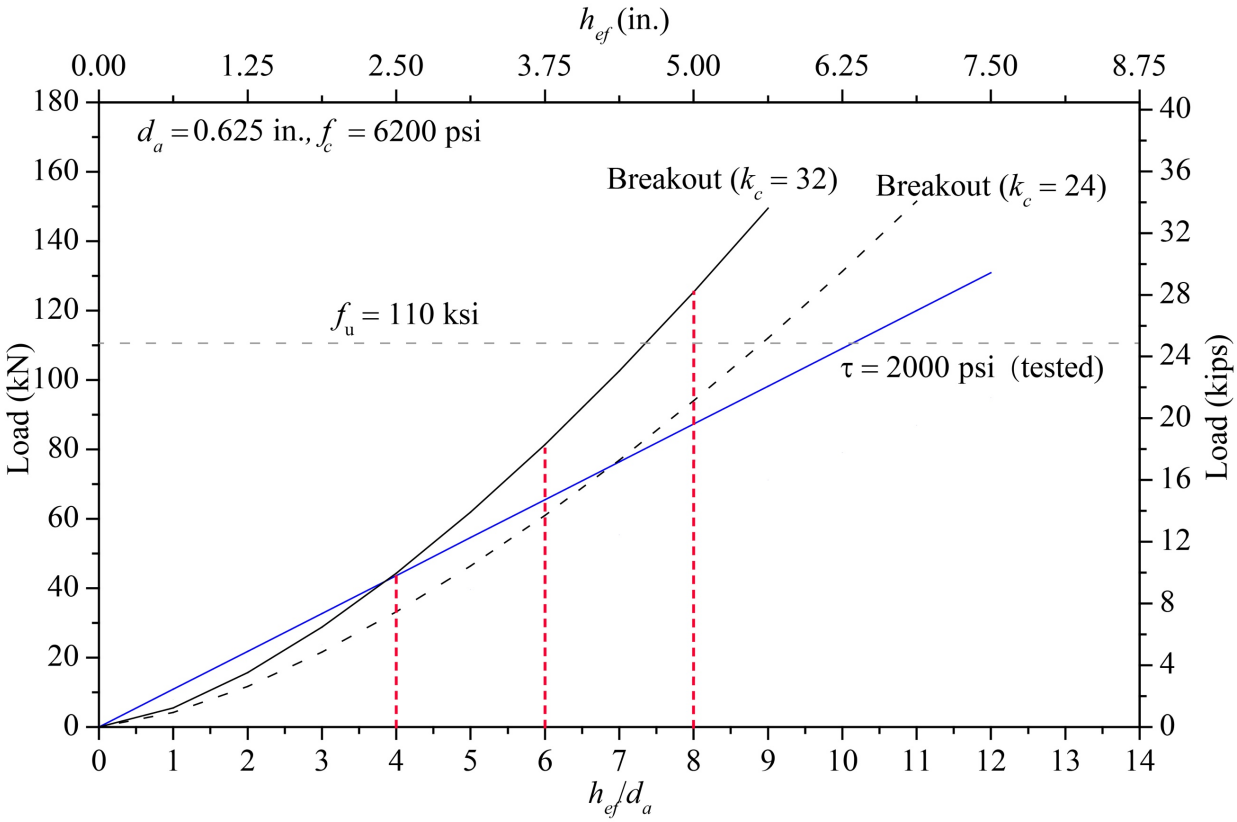
h_{ef} (in.)
0.00 1.25 2.50 3.75 5.00 6.25 7.50 8.75
d_a = 0.625 in., f_c = 6200 psi
Breakout (k_c = 32)
Breakout (k_c = 24)
f_u = 110 ksi
τ = 2000 psi (tested)
Load (kN)
Load (kips)
0 20 40 60 80 100 120 140 160 180
0 4 8 12 16 20 24 28 32 36 40
0 1 2 3 4 5 6 7 8 9 10 11 12 13 14
h_{ef}/d_a

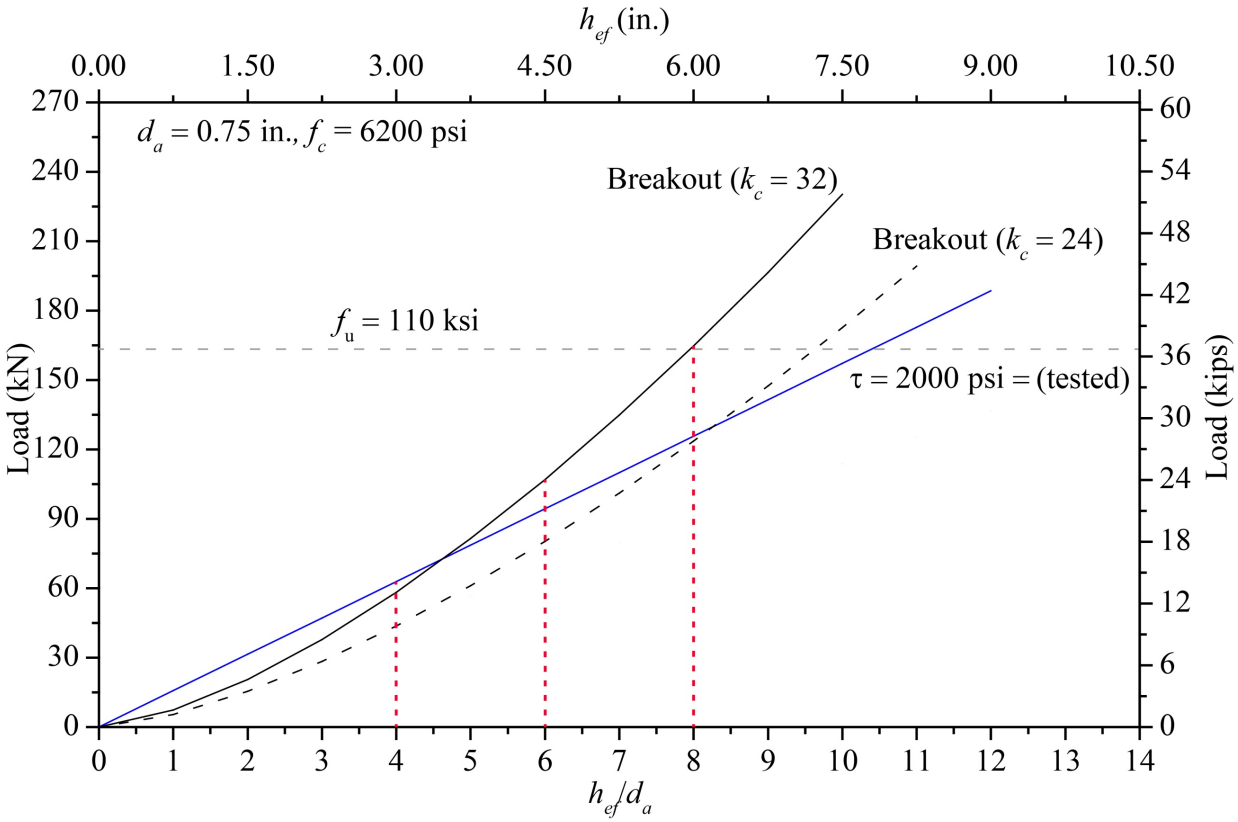

Figure 3.1 Determination of anchor embedment based on predicted capacities

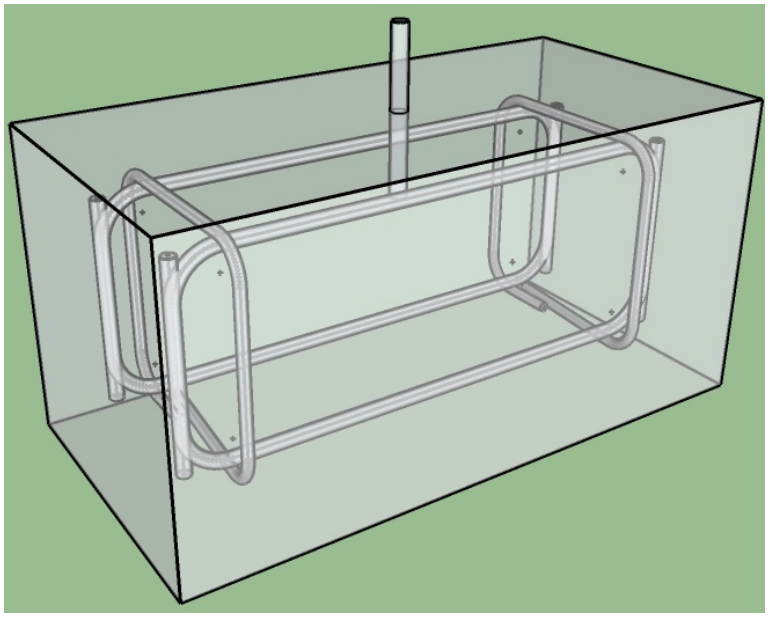

Figure 3.2 Schematics of plain concrete blocks

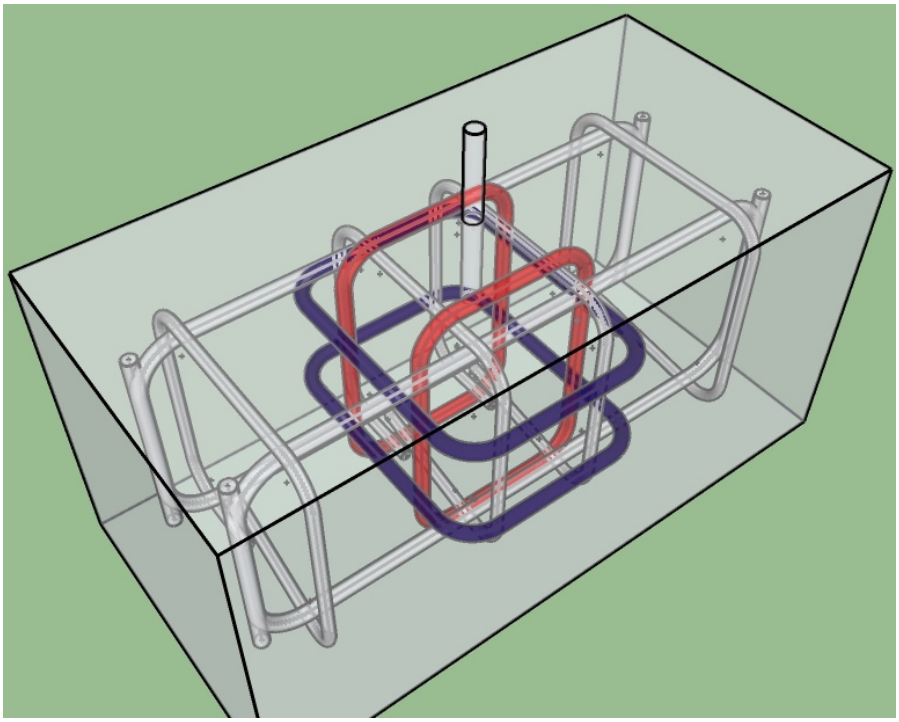

Figure 3.3 Schematics of reinforced concrete blocks

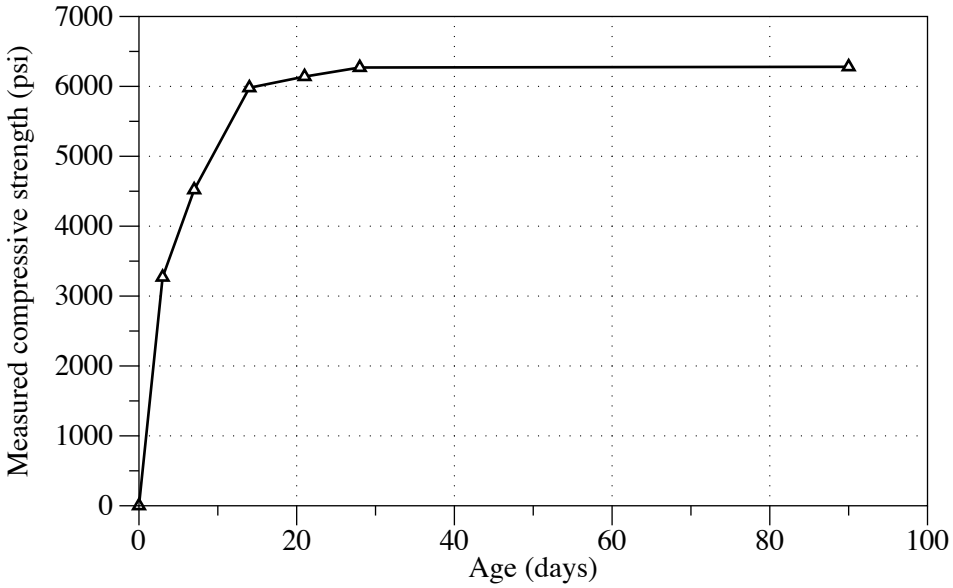

Figure 3.4 Measured compressive strengths of concrete using 4x8 cylinders

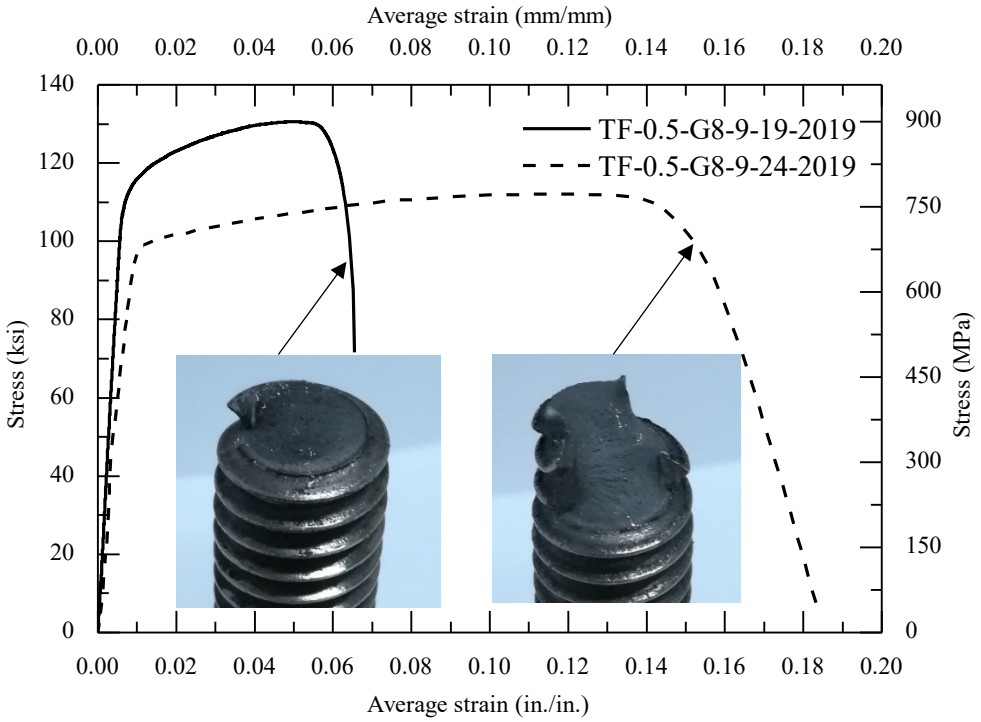

Figure 3.5 Stress-strain relationship of ASTM A193 Grade B7 threaded rods.

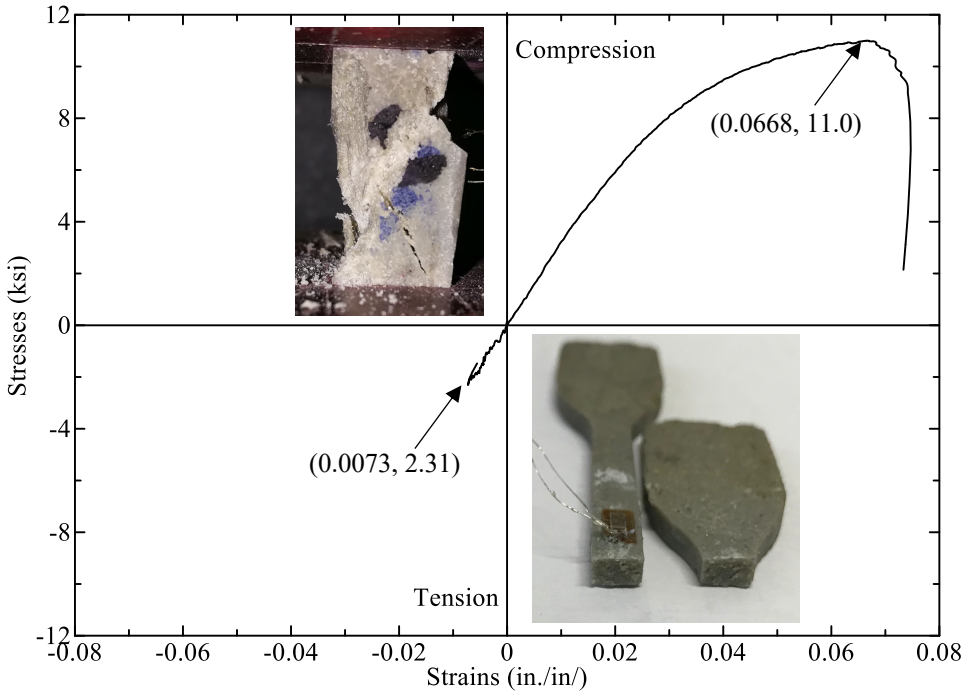

Figure 3.6 Stress-strain relationship of the vinylester adhesive.

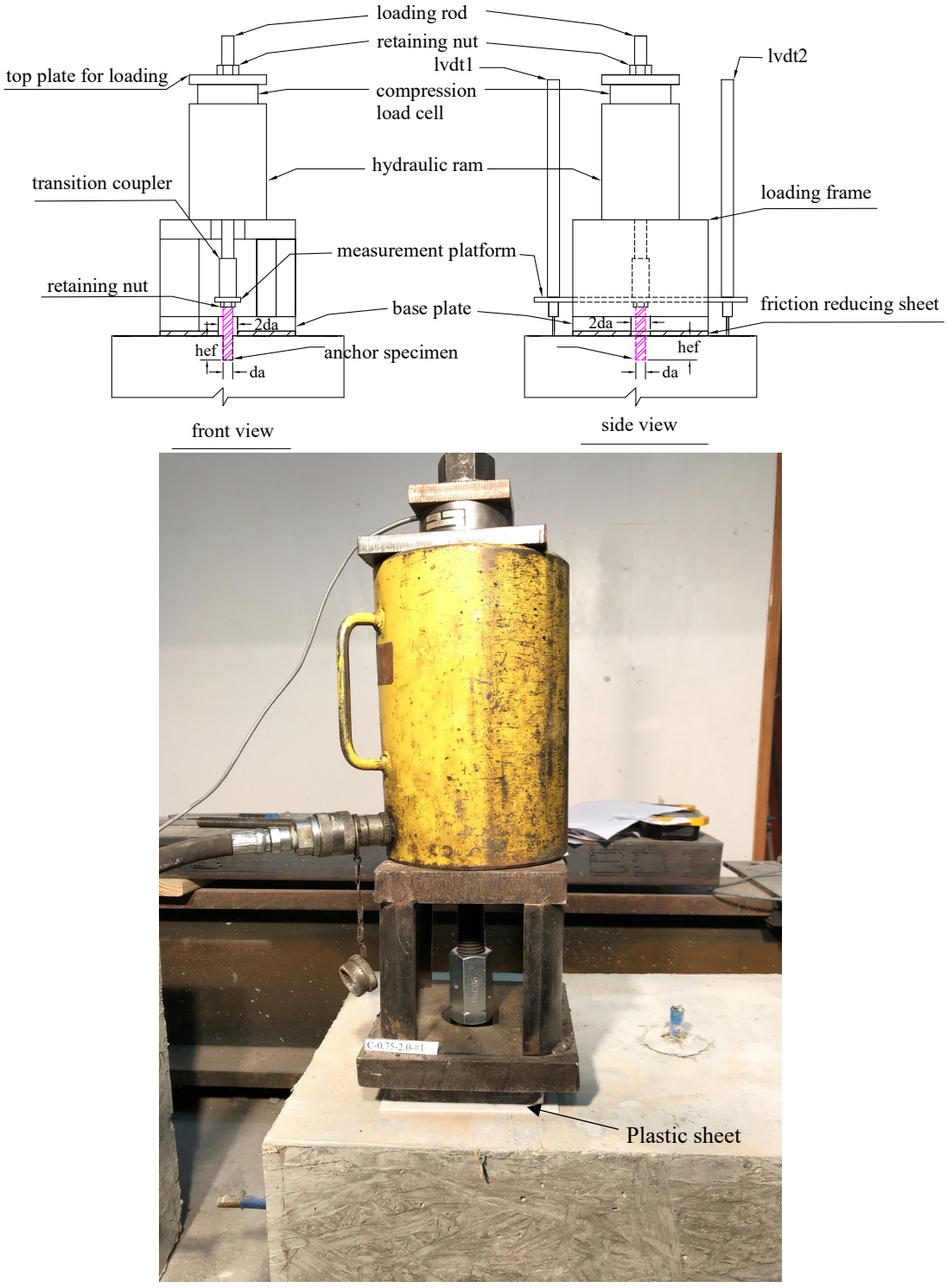

Figure 3.7 Test setup for confined tension tests

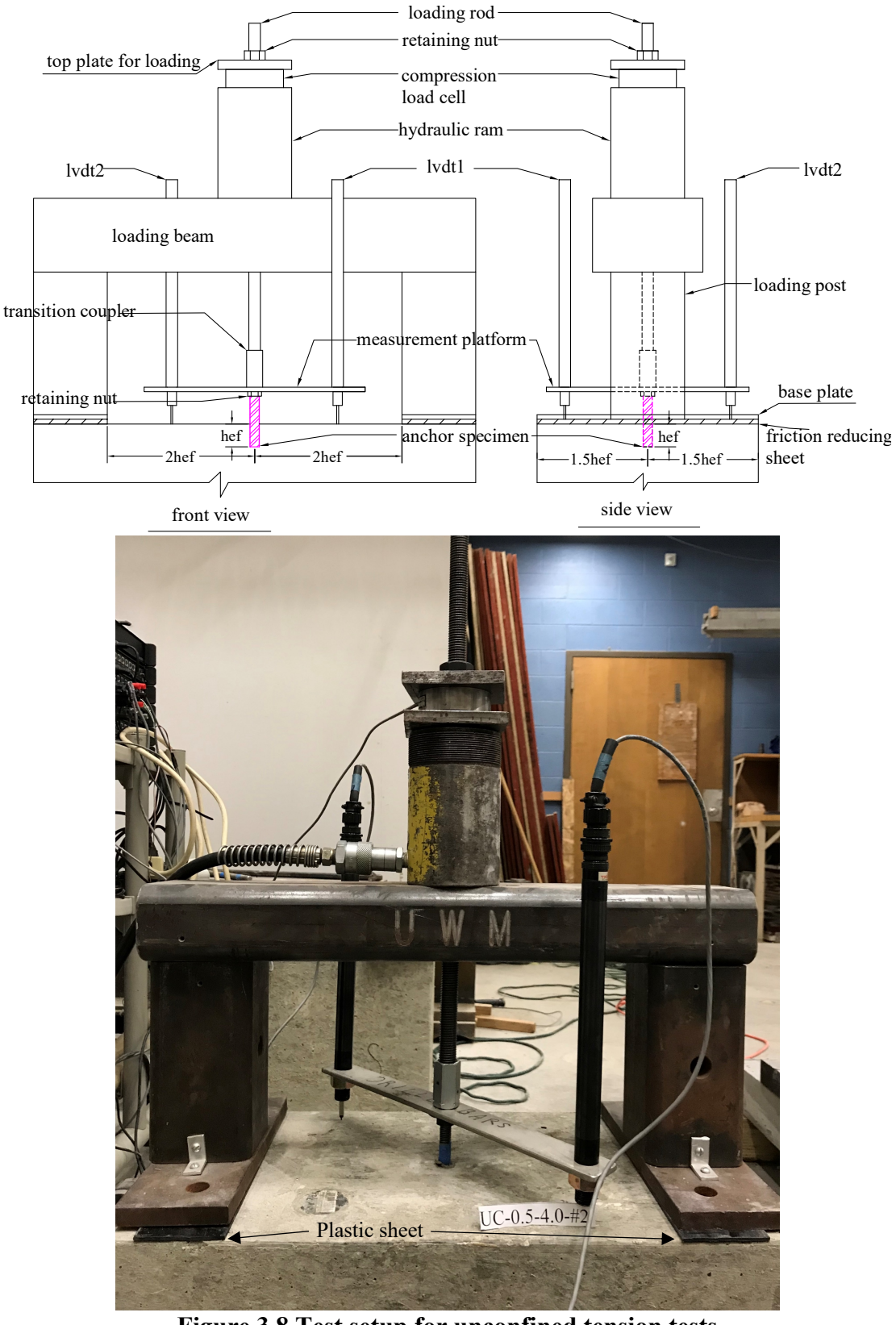

Figure 3.8 Test setup for unconfined tension tests



Figure 3.9 Drilled holes in concrete to demonstrate the installation procedure

Table 3.1 Specimen design of adhesive anchor tests

d_a (in.)	h_{ef} (in.)	h_{ef}/d_a	Block size (in.)	Note	Expected failure mode
0.5	2	4	12 × 12 × 24	Plain Concrete	breakout
0.5	3	6	12 × 12 × 24	Plain Concrete	breakout/pullout
0.5	4	8	12 × 12 × 24	Plain Concrete	pullout
0.5	4	8	12 × 12 × 24	Reinforced Concrete	pullout
0.5	5	10	15 × 15 × 28	Reinforced Concrete	pullout
0.625	2.5	4	12 × 12 × 24	Plain Concrete	breakout
0.625	3.75	6	12 × 12 × 24	Plain Concrete	breakout
0.625	5	8	15 × 15 × 28	Plain Concrete	pullout
0.625	5	8	15 × 15 × 28	Reinforced Concrete	pullout
0.75	3	4	12 × 12 × 24	Plain Concrete	breakout
0.75	4.5	6	15 × 15 × 28	Reinforced Concrete	pullout
0.75	6	8	18 × 18 × 32	Reinforced Concrete	pullout

Chapter 4. Results of Experiments

The test results are summarized in Table I.2. The confined tension tests are summarized in Appendix II while the details of unconfined tension tests are recorded in Appendix III.

4.1. Confined Tension Tests

The results of 28 confined tension (CT) tests is summarized in Figures 4.1 through 4.3, with nine tests for each anchor size. Almost all tests had an embedment of $4d_a$ or $6d_a$ except for the ¾-in. diameter anchors: one was installed with a smaller embedment and one additional test was conducted for an embedment of $8d_a$ to explore the potential relationship between the ultimate loads and embedment depths.

The test results were plotted and discussed for each anchor diameter individually though the same adhesive was used for all specimens in this study. The confined tension tests in Figures 4.1 through 4.3 indicated that the mean bond strength decreased for anchors with a larger diameter. This was similar to the observation by Meszaros (2002) using three adhesives in both low- and high-strength concrete that the mean bond strength decreases as the anchor diameter increases. The same general observation was also made by the author using finite element analyses. However, it was not clear if the finite element models were able to capture the physical behavior. The decrease of bond strength with an increase in anchor diameter was attributed to generally poorer cleaning of larger-size holes as shown in Figure 3.9 (Liu 2020). Consequently, the decrease in bond strength can be a bit random, which may have been the reason for the observed variation in the measured bond strength by Meszaros (2002) in Figure 4.4.

The results in Figures 4.1 and 4.3 indicate that uniform bond stress model is valid as the tensile capacities of the anchors (N_p) in confined tension tests are proportional to their embedment depths (h_{ef}). In addition, the linear relationship for ¾-in. anchors in Figure 4.3 existed for a wide range of embedment depths: $3d_a$ (2.25 in.) to $8d_a$ (6 in.). Knowing that the reaction plate in the confined tension tests was 5×5 in., one may recognize that the lateral confining pressure from the reaction plate would be about 2.5 in. deep. The linear N_p vs h_{ef} relationship indicated that the impact of lateral confining pressure in confined tension tests is negligible. This observation seems reasonable given the fact that the adhesive had a very small Young's modulus, only 7% of the concrete modulus. This theory was also confirmed using finite element analyses in Chapter 5.

Two additional confined tension tests were performed with bond breakers in order to isolate the specimens from lateral confining pressure at the top. Note that Cook et al. (1993) hypothesized that "*Pullout of an adhesive core can occur when the top portion of the embedment length is debonded*" after shallow breakout cones were observed in many unconfined tension tests. Debonding was achieved at the top 2 in. of the hole and anchor using silicone sealant. No image of partially debonded specimens after their tests was available in the report; however, the measured capacities of partially debonded specimens indicated that the top portion of the anchor could be important.

In this study, debonding was achieved using aluminum foil tape as shown in Figure 4.5. The tape, cut into 0.2 in. wide strips, was attached to the drilled holes at bottom (about 0.2 in.) and the concrete surface. Specimen CSD-C-0.5-2 had an embedment about 2 in. without any bond breaker while Specimen CSD-C-0.5-4.25-2.25 had a bond breaker at the top 2.25 in. such that the bonded 2 in. at the bottom was isolated from potential lateral confining pressure. The 2-in. bond length in Specimen CSD-C-0.5-6-4 was deeper to further reduce the impact of potential confining pressure.

It was expected that the measured tensile capacity would be lower for anchors with a lower bonded portion. The measured load-displacement behavior shown in Figure 4.6 does not support the hypothesis. The anchors with bond breakers, though with the same bonded length, developed higher capacities. It should be noted that the tests were conducted without a plastic sheet below the steel reaction plate; hence the bond failure occurred to the adhesive-steel (A-S) interface, as shown in Figure 4.7. Position adjustment after anchor installation as described in Step 6 in Section 3.4 was later found critical to the bond failure at A-S interfaces. Therefore, no further investigation was performed for this group of specimens and the standard installation was updated with a note to prohibit such adjustments. Nevertheless, this group of tests seemed to indicate that lateral confining pressure was not significant to the behavior of anchors in confined tension tests.

The average bond strength was smaller from the tests of anchors with a larger diameter even though the same materials were used, and the same installation procedure was implemented. Specifically, the calculated bond strengths were 2821 psi, 2011 psi, and 1766 psi for 1/2, 5/8, and 3/4 in. anchors, respectively. This may have been due to the different hole cleaning results as revealed in Figure 3.9, using strictly the same procedure: white colored dusts can be seen in larger size holes. Note that this theory needs further verification and may not be generalized to other products. Meanwhile, a practical implication is that larger size holes may need a bit longer brushing time or new hole cleaning tools must be invented/used.

4.2. Unconfined Tension Tests

The results of 44 unconfined tension tests is summarized in Figures 4.8 through 4.10. Four tests were not performed because concrete breakout failure in some specimens caused significant damage to their concrete blocks, which rendered repeated tests unviable as documented in Appendix III. The calculated bond strengths of all tested specimens were higher than code-stipulated values (that is 1000 psi in ACI 318-19). In addition, the measured capacities were reasonably proportional to the embedment depths though more than half of the specimens were controlled by combined breakout-pullout failure.

Nine tests were controlled by concrete breakout. Note that many specimens in this group, especially those with a large embedment, had a small portion of bond failure at the bottom. A test was designated as concrete breakout in this study when the breakout cone depth was larger than 80 percent of the embedment. The measured breakout capacities are compared with the code-stipulated values with a constant (k_{nc}) of 24 in Figure 4.10. The code equation is fairly reasonable from the tests in this study. The overprediction of Specimen UC-0.625-5.0-#3 may have been attributed to damaged concrete before testing as the concrete was cracked and volume reduced from the first two test repeats, a s illustrated by the inserted picture in the figure.

4.3. Observed Reduction Factor α_{setup}

The observed behavior of adhesive anchors in unconfined tension tests indicates that the uniform bond stress model in ACI 318-19 is reasonable. In addition, the design bond strength of 1000 psi is conservative. It is also reasonable for a higher bond strength to be used provided that the bond strength can be determined properly. When the bond strength is measured with confined tension tests, a reduction factor is necessary.

The data analyses in Figures 4.7 through 4.9 indicates that on average, the reduction factor was 0.758, 0.790, and 0.950 for 1/2, 5/8, and 3/4 in. anchors, respectively. The average reduction factor was determined by the average bond strengths calculated from the unconfined tension tests divided by the average bond strength from the confined tension tests. These average reduction factors indicate that the current code-stipulated factor of 0.75 is safe.

The tests do have variations; hence individual reduction factors can be computed by dividing the bond strengths from the individual unconfined tension tests by the average bond strength calculated from the confined tension tests for each anchor size. With the number of available unconfined tension tests (degrees of freedom), and the percentiles of the Student's t-distribution (Appendix IV), the 5% fractile values for the reduction factors are 0.5654, 0.5141, and 0.7039 for 1/2, 5/8, and 3/4 in. anchors, respectively. This indicates that the current code-stipulated factor of 0.75 is unconservative. A reduction factor of 0.5 is instead reasonable.

Eligehausen and Asmus (2019) indicated that the bond strengths from confined tension tests should also be 5% fractile values rather than the average strengths in the determination of reduction factors. The corresponding bond strengths at 5% fractile are shown in Figures 4.1 through 4.3. Using the reduced bond strengths in confined tension tests, the reduction factors are 0.8516, 0.8547, and 1.0233 for 1/2, 5/8, and 3/4 in. anchors, respectively. This indicates that the current code-stipulated factor of 0.75 is safe. Note that when 5% fractile bond strengths are considered, the adhesive used in this study had a small to medium bond strength. Additional tests are needed with higher strength adhesives.

4.4 Analyses of Combined Breakout-Pullout Failure

It is envisioned that combined breakout-pullout failure may become significant for anchors with high strength adhesives (e.g., an average bond strength of 4000 psi or higher). Cook et al. (1993) pointed out that combined breakout-pullout failure is likely for adhesive anchors with an embedment greater than 2-4 in. Cook et al. (1993) also noted that Cannon et al. (1981) suggested that a shallow cone forms prior to pullout of the anchor while Luke et al. (1985) suggested that the bond failure occurs first, followed by cone failure. The results of Collins et al. (1989) and Cook et al. (1993) suggested that a shallow breakout cone occurs simultaneously with bond failure along the rest of anchor. Knowing that breakout failure is prohibited by confined pullout test setup; hence combined breakout-pullout failure may be partly responsible for the capacity difference between confined and unconfined tension tests.

More than half of unconfined tension tests in this study were controlled by combined breakout-pullout failure. In addition, the depth of breakout cones varied rather randomly as shown in Appendix II. It is rather difficult to determine the time of concrete breakout relative to pullout of an anchor. Figure 4.11 shows the combined failure of Specimen UC-0.625-5.0-#1. A close look at the specimen indicates that multiple breakout cracks may have formed at different stages of loading; however, it seems that pullout failure was required to allow sufficient anchor displacement such that a breakout cone could form completely and separated from the concrete base. It is thus reasonable to assume concrete breakout occurs simultaneously with anchor pullout.

A Monte Carlo simulation was conducted to explore the impact of higher-strength adhesive on the capacity of adhesive anchors controlled by combined breakout-pullout failure. The simulation assumed a uniform distribution of the following parameters within the given range:

- Anchor diameter (d_a)=0.5:0.125:1.0 (in.);
- Concrete compressive strength (f_c')=3000:500:8000 (psi);
- Bond strength (τ)=1000:250:6000 (psi); and
- Embedment depth (h_{ef})=4:0.5:10 (in.).

In each permutated case, the depth of concrete breakout cone (h_{cb}) varied from zero to the total embedment depth; the breakout capacity was calculated as $N_{br} = 24h_{cb}^{1.5}\sqrt{f_c'}$ and the pullout capacity was $N_p = \tau\pi d_a\left(h_{ef} - h_{cb}\right)$; the simulated capacity of the anchor was the minimum of the total capacity ($N = N_{br} + N_p$); the equivalent bond strength was back calculated by $\tau_e = \frac{N}{\pi d_a h_{ef}}$; and the reduction factor was simply $\alpha_{setup} = \frac{\tau_e}{\tau}$. The result of the Monte Carlo simulation is shown in Figure 4.12. The current reduction factor (0.75) corresponded to the 58th percentile value while the smallest reduction factor from this study using average bond strength form confined tension tests (0.50) corresponded to the 33rd percentile. Another simulation with bond strength ranging up to 4000 psi indicated that the 0.5-reduction factor corresponds to the 5th percentile. Tests with high bond strengths are needed before a recommendation can be made.

4.5 Comparison of Anchors in Plain and Reinforced Concrete

Two groups of unconfined tests, one for ½-in. diameter anchors (UC-0.5-4.0 vs UC#R-0.5-4.0) and the other for 5/8-in. diameter anchors (UC-0.625-5.0 vs UC#R-0.625-5.0), may be used to demonstrate the impact of code-conforming anchor reinforcement. First of all, Table I.2 shows that without anchor reinforcement, one out of four ½-in. specimens and three out of four 5/8-in. specimens were controlled by concrete breakout while with anchor reinforcement, none of eight specimens were controlled concrete breakout. This indicates that the anchor reinforcement was able to delay concrete breakout as expected, however; the code-conforming anchor reinforcement was not able bring additional benefit, such as confining concrete near top or significantly improve the anchor capacities. Note that the last test of 5/8-in. diameter anchor (UC-0.625-5.0-#4) was significantly affected by the first three tests, which were controlled by concrete breakout, cause significant damage to the concrete block. The average capacity of the first three tests was nearly 16 kips, which is closer to the average capacity of four tests in reinforced concrete.

The anchor reinforcement was not able to restrain concrete from dilating/splitting near top because the reinforcement had an average cover of 1.5 in. whereas the large tensile strains in concrete is expected to occur near the top surface as demonstrated in Chapter 5. The majority of the anchors in reinforced concrete were controlled by combined breakout-pullout failure, and a close look at the failed pictures indicates that the breakout cracks often avoided the anchor reinforcement, which is similar to the observations documented in Petersen et al (2018) for the headed anchors in concrete with code-conforming reinforcement. Section 17.4.5 of ACI 318-19 indicates that supplementary reinforcement is expected to control splitting cracks. This may need support from further experimental tests.

4.6 Summary

A total of 28 CT tests and 44 UCT tests were conducted. The measured capacities were found proportional to the embedment depths, indicating that the current uniform bond stress model in

ACI 318-19 is reasonable. Secondly, the tests indicated that the current reduction factor is reasonable when the bond strength is determined as the 5%-fractile from CT tests. The reduction factor (0.75) is unconservative if the bond strength is determined as the average strength from CT tests and a reduction factor of 0.5 is reasonable. Finally, tests in this study indicated that adhesive at the top could be disengaged from the surrounding concrete in unconfined tension tests, which may be an important contributing factor for the reduction factor (α_{setup}). This was investigated using finite element analyses in Chapter 5.

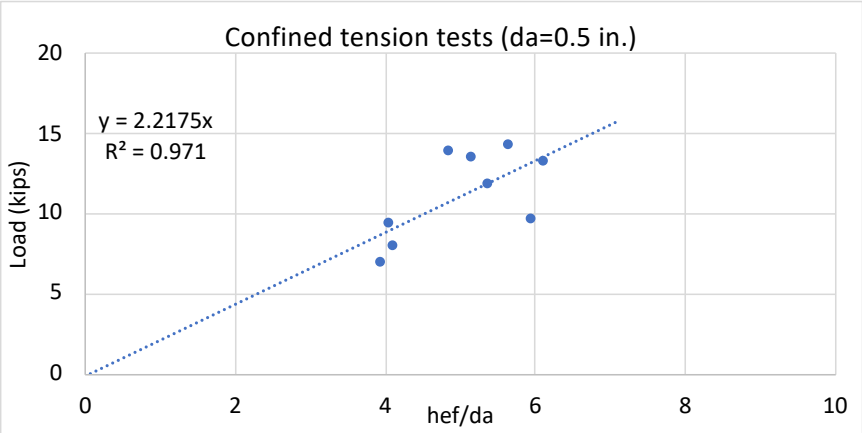

t average	2821	psi	average from data
t std.	517.3	psi	standard deviation from data
n	9		number of tests
Coefficient	1.833		5% fractile coefficient
t 5% fractile	1873.1	psi	5% fractile bond strength

Figure 4.1 Results of confined tension tests on ½-in. anchors

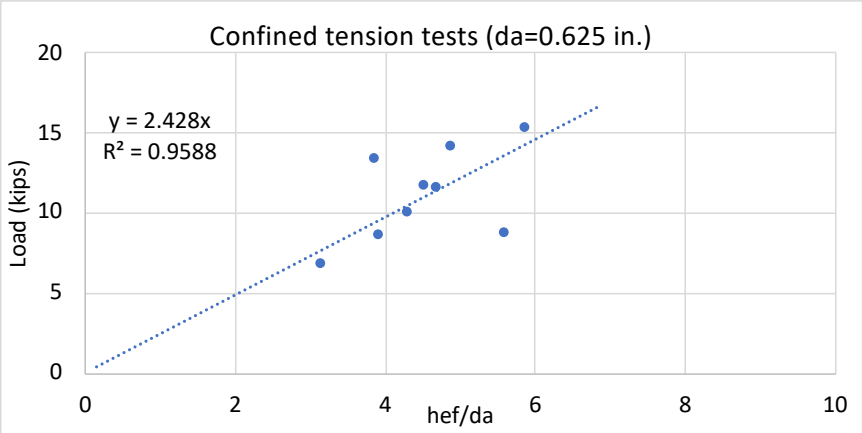

t average	2011	psi	average from data
t std.	430.3	psi	standard deviation from data
n	9		number of tests
Coefficient	1.833		5% fractile coefficient
t 5% fractile	1222.6	psi	5% fractile bond strength

Figure 4.2 Results of confined tension tests on 5/8-in. anchors

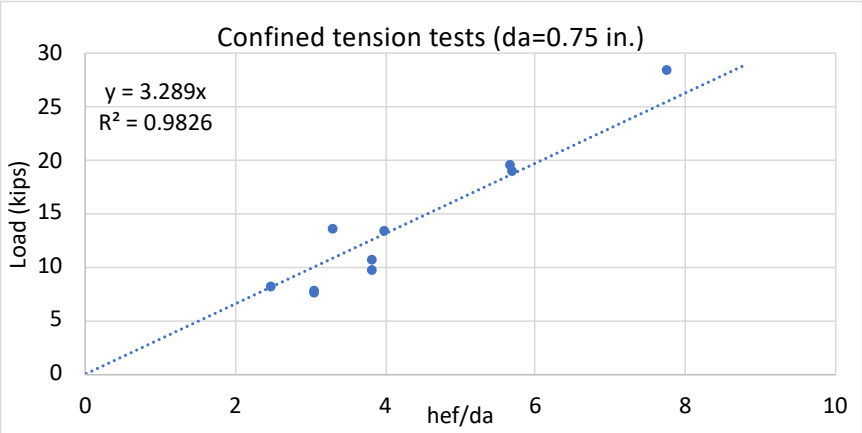

t average	1766	psi	average from data
t std.	304.1	psi	standard deviation from data
n	10		number of tests
Coefficient	1.812		5% fractile coefficient
t 5% fractile	1214.6	psi	5% fractile bond strength

Figure 4.3 Results of confined tension tests on 3/4-in. anchors

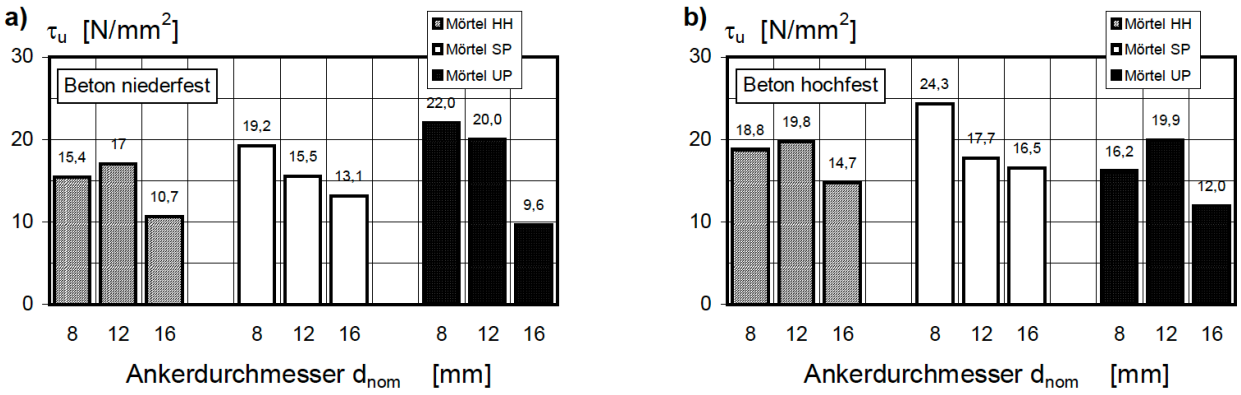

Figure 4.4 Bond strength from confined tension tests with three adhesives (Figure 5.5 of Meszaros (2002))

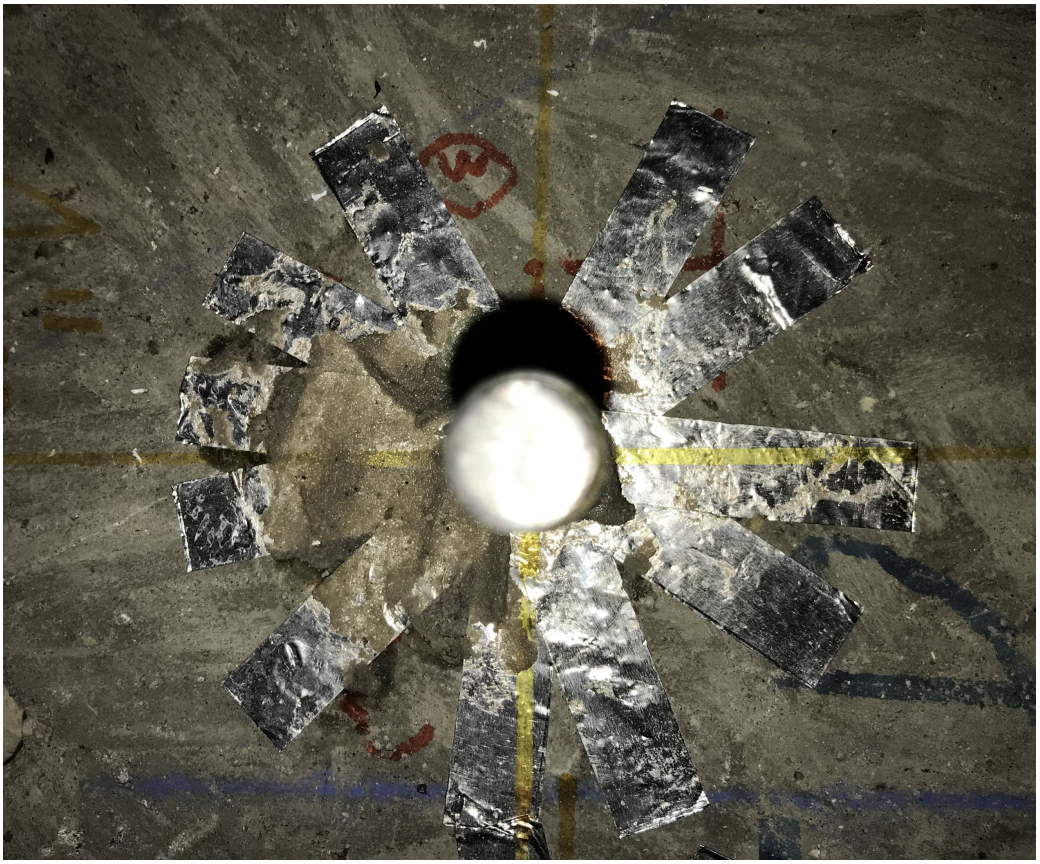

Figure 4.5 Bond breaker for debonded anchors

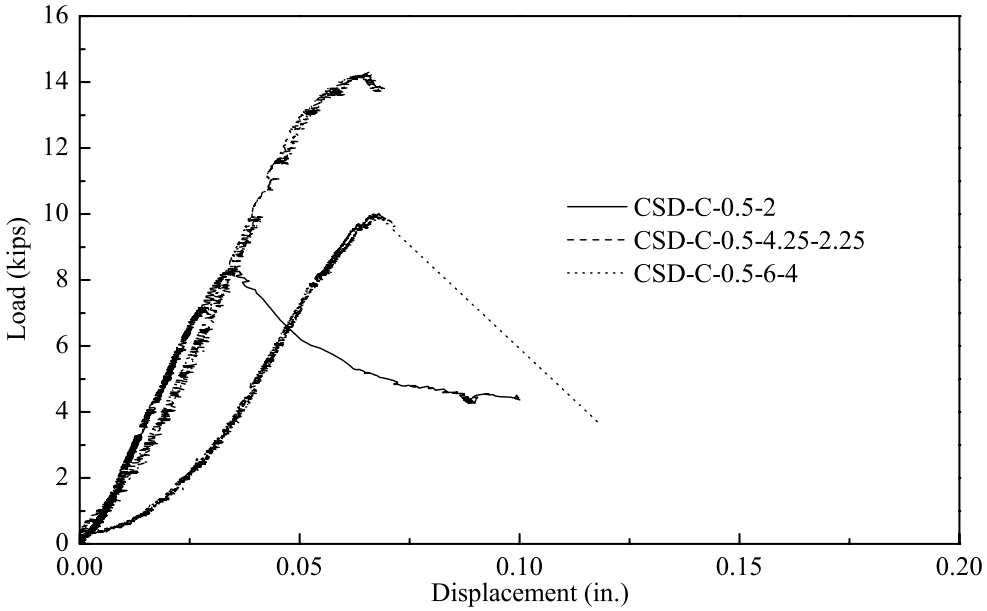

Figure 4.6 Behavior of debonded anchors in confined tension tests



Figure 4.7 Failure of debonded anchors in confined tension tests

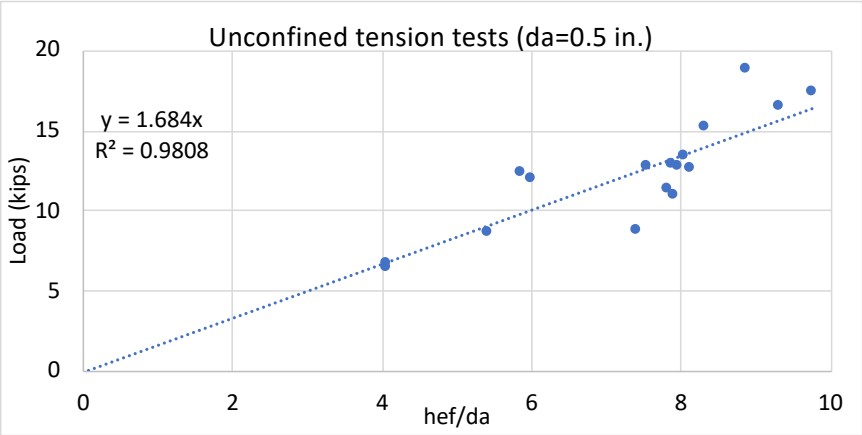

a average (5% bond)	1.142		average a from 5% fractile bond strength
a std.	0.167		standard deviation from data
n	17		number of tests
Coefficient	1.74		5% fractile coefficient
a 5% fractile	0.8516		5% fractile alpha setup
a average (ave. bond)	0.758		average a from average bond strength
a std.	0.111		standard deviation from data
a 5% fractile	0.5654		5% fractile alpha setup from ave. bond

Figure 4.8 Results of unconfined tension tests on 1/2-in. anchors

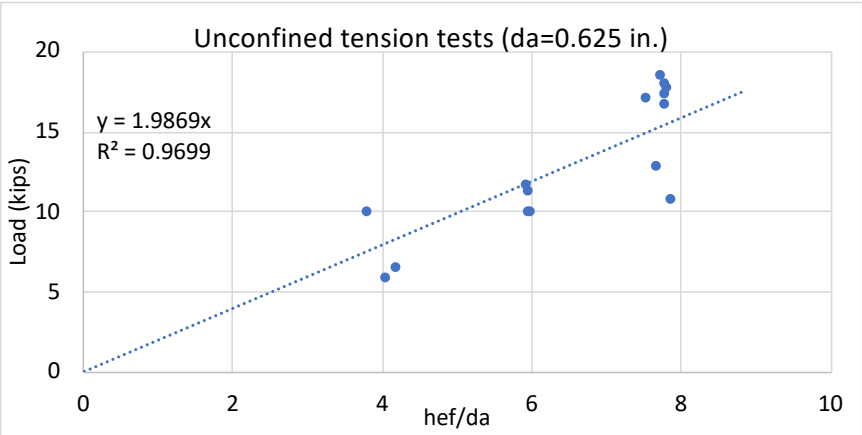

a average (5% bond)	1.299		average a from 5% fractile bond strength
a std.	0.259		standard deviation from data
n	15		number of tests
Coefficient	1.753		5% fractile coefficient
a 5% fractile	0.8457		5% fractile alpha setup
a average (ave. bond)	0.790		average a from average bond strength
a std.	0.157		standard deviation from data
a 5% fractile	0.5141		5% fractile alpha setup from ave. bond

Figure 4.9 Results of unconfined tension tests on 5/8-in. anchors

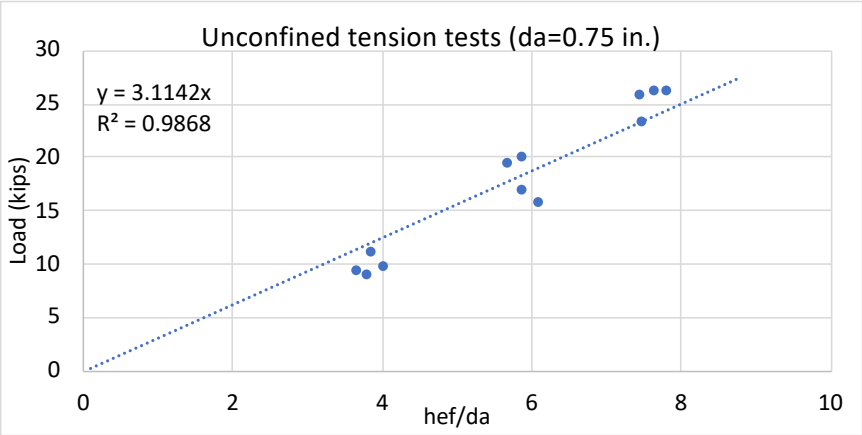

a average (5% bond)	1.380		average a from 5% fractile bond strength
a std.	0.200		standard deviation from data
n	12		number of tests
Coefficient	1.782		5% fractile coefficient
a 5% fractile	1.0233		5% fractile alpha setup
a average (ave. bond)	0.950		average a from average bond strength
a std.	0.138		standard deviation from data
a 5% fractile	0.7039		5% fractile alpha setup from ave. bond

Figure 4.10 Results of unconfined tension tests on 3/4-in. anchors

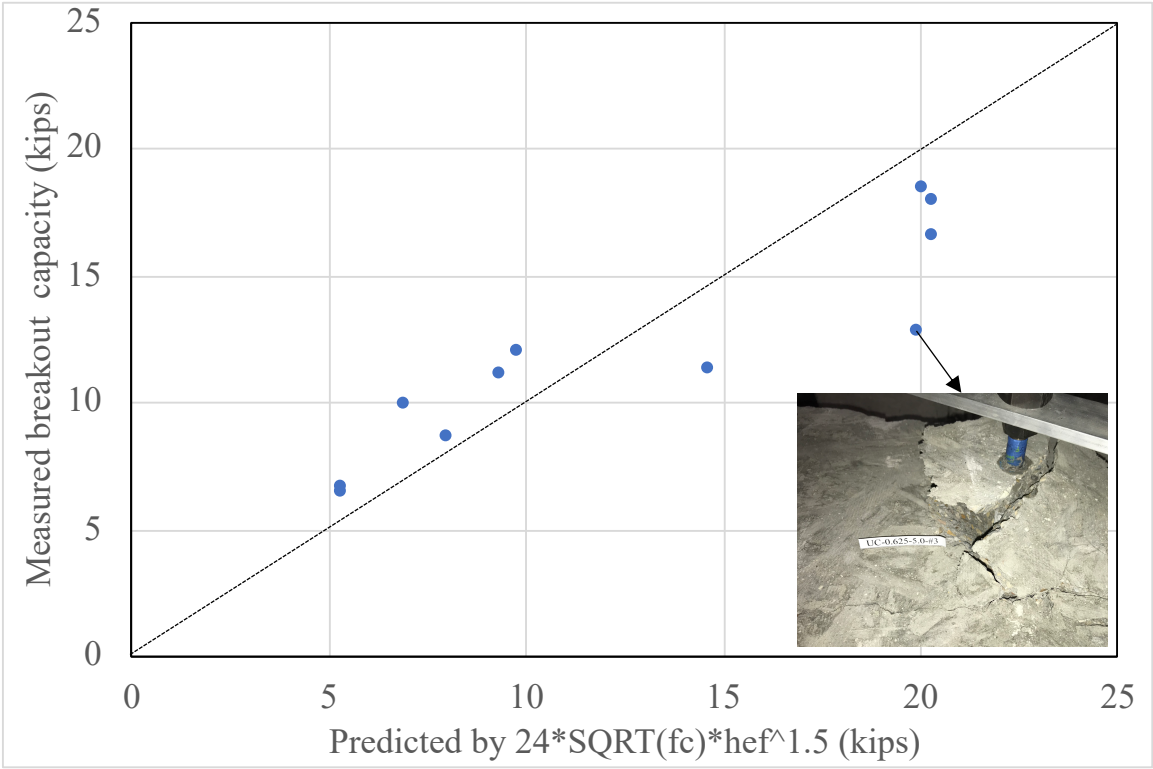

Figure 4.11 Comparison of measured breakout capacity with code equation

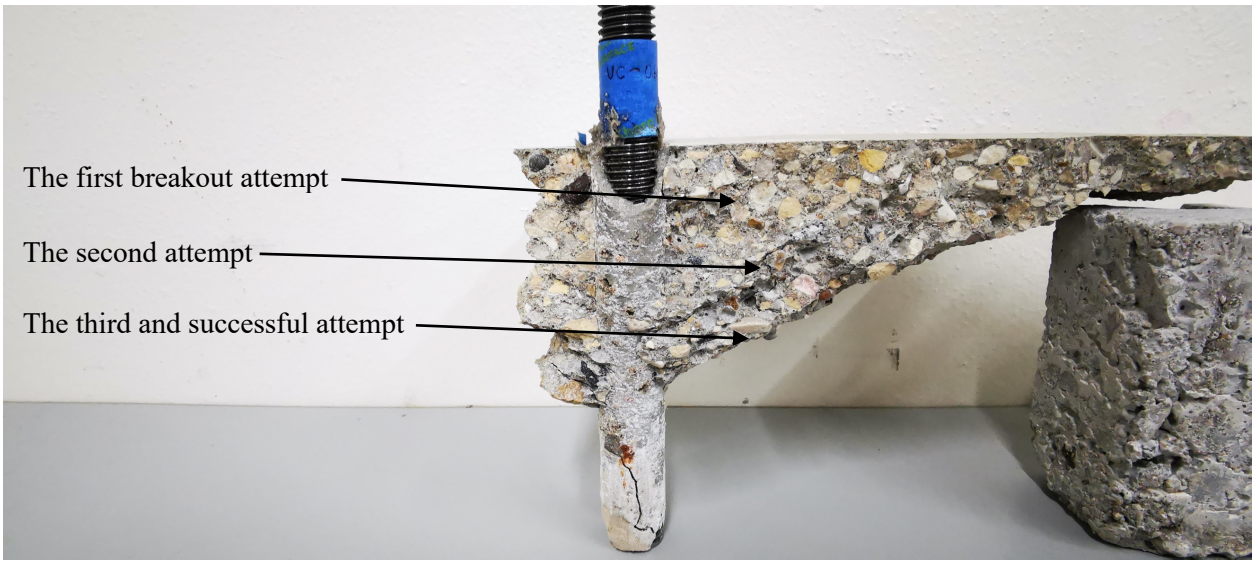

Figure 4.12 Multiple breakout cracks in Specimen UC-0.625-5.0-#1.

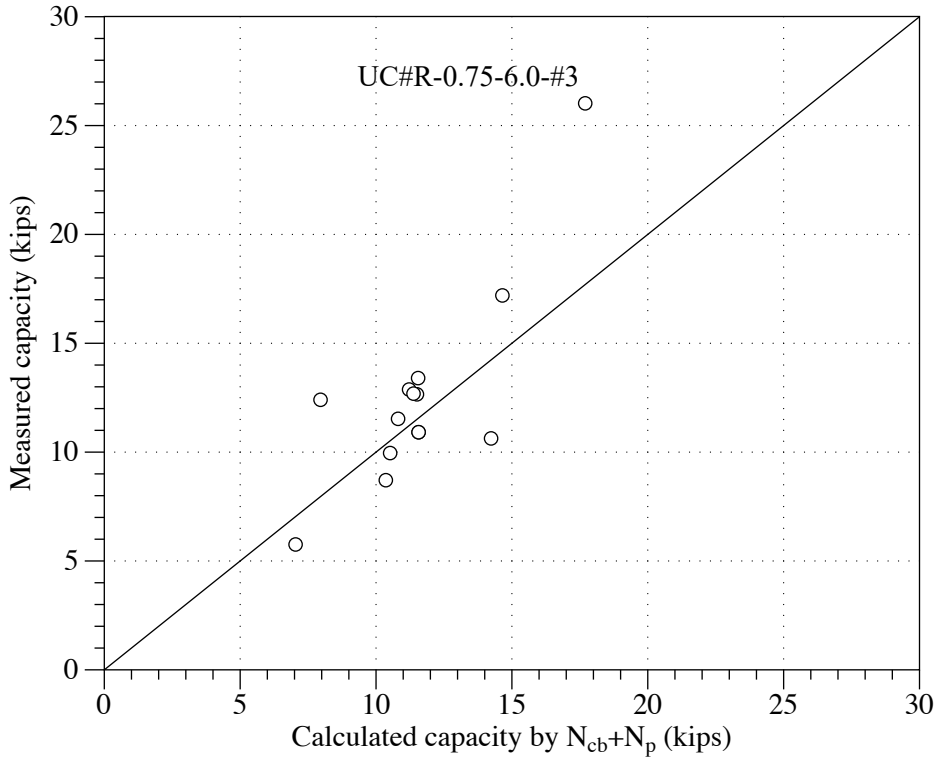

Figure 4.13 Comparison of measured capacity of specimens with measured breakout depth and prediction.

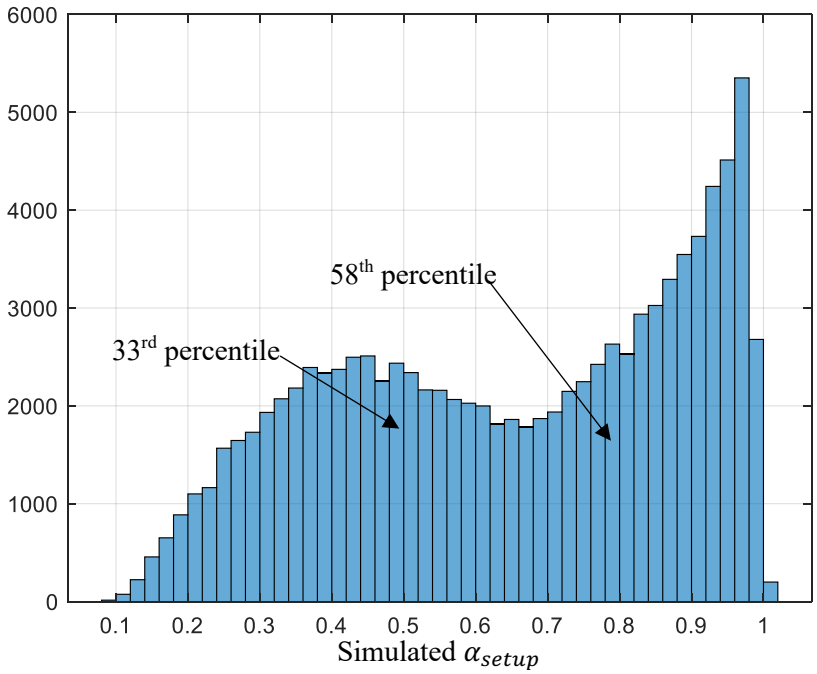

Figure 4.14 Monte Carlo simulation of combined breakout-pullout failure

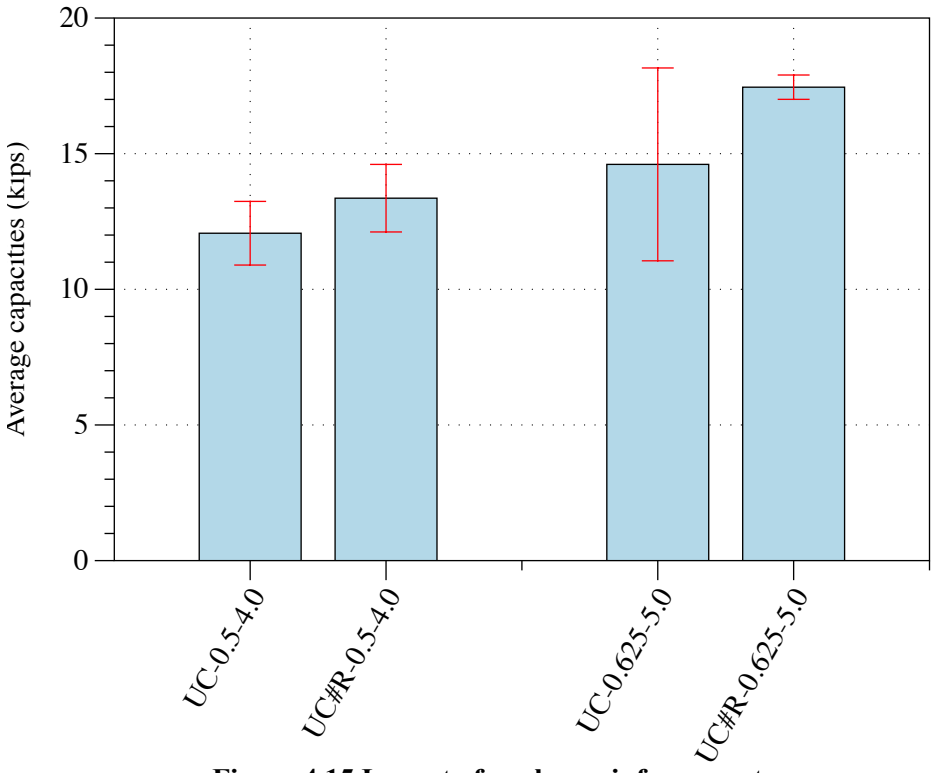

Figure 4.15 Impact of anchor reinforcement

Table 4.1 Specimen with combined breakout-pullout failure

Name	d_a	h_{ef}	h_{cb}	N_{cb}	h_b	N_p	N_{total}	t	a_{setup}	$N_{measured}$
UC-0.5-4.0-#1	0.5	3.95	0.45	0.570	3.5	10.996	11.566	1.473	0.736	10.914
UC#R-0.5-3.0-#4	0.5	2.934	1.434	3.245	1.5	4.712	7.958	1.013	0.507	12.404
UC-0.625-2.5-#2	0.625	2.543	0.543	0.756	2	6.283	7.039	0.896	0.448	5.758
UC-0.5-4.0-#3	0.5	4.028	1.778	4.480	2.25	7.069	11.549	1.470	0.735	13.400
UC#R-0.5-4.0-#4	0.5	3.939	1.689	4.148	2.25	7.069	11.217	1.428	0.714	12.875
UC-0.625-3.75-#4	0.625	3.744	1.494	3.451	2.25	7.069	10.519	1.339	0.670	9.957
UC-0.5-3.75-#2	0.5	3.707	1.207	2.506	2.5	7.854	10.360	1.319	0.660	8.710
UC#R-0.625-5.0-#2	0.625	4.881	2.256	6.403	2.625	8.247	14.650	1.865	0.933	17.197
UC#R-0.5-4.0-#2	0.5	4.07	1.32	2.866	2.75	8.639	11.505	1.465	0.732	12.654
UC-0.5-4.0-#2	0.5	3.976	0.726	1.169	3.25	10.210	11.379	1.449	0.724	12.687
UC-0.625-3.75-#2	0.625	3.716	0.466	0.601	3.25	10.210	10.811	1.377	0.688	11.529
UC#R-0.75-6.0-#3	0.75	5.754	2.504	7.488	3.25	10.210	17.698	2.253	1.127	26.020
UC-0.5-4.0-#1	0.5	3.95	0.45	0.570	3.5	10.996	11.566	1.473	0.736	10.914
UC-0.625-5.0-#4	0.625	4.92	0.92	1.668	4	12.566	14.234	1.812	0.906	10.629

Note: A total of 24 specimens in UCT tests showed combined failure as shown in Appendix III; however, only the listed specimens had a measured bond failure length (h_b)

Chapter 5. Finite Element Analyses

5.1. Introduction

We envisioned the following difference between confined and unconfined tension tests:

- Closely placed reaction may cause lateral pressure on adhesive-concrete interface in confined tension tests, leading to increased bond strength.
- Closely placed reaction may also change the stress field in concrete such that splitting cracks is restrained in confined tension tests while such restrain does not exist in unconfined tension tests. The splitting cracks, though not through the entire embedment depth, may disengage the microscopic interlock between hardened adhesive and concrete, leading to reduced bond strength, especially near the concrete surface.
- Closely placed reaction prohibits the formation of concrete breakout cones, which often occurs in unconfined tension tests along with bond failure. The mixed failure mode may occur under a lower tensile load than the individual failure modes.

Finite element (FE) analyses were conducted to examine these theories. The details of the FE analyses are shown below following a brief literature review.

5.2 Brief Literature Review

Cook et al. (1993) created an elastic continuum mechanics model to explore the distribution of bond stresses along the embedded depth of adhesive anchors. A differential equation was derived for the longitudinal displacement ($w(z)$)of the anchor shaft, and a concept of bond link was used to explain the bond stresses ($u(z)$) reacting to the applied tensile load (Figure 5.1a). The distributed reaction (bond stress) corresponded to the shear deformation of the thin adhesive between the steel anchor rod and concrete, which was assumed to develop zero deformation (Figure 5.1b); hence the stiffness, defined by the ratio of bond stress and shear strain ($u(z) = kw(z)$), was $k = \frac{G\pi d}{t}$, where G is the shear modulus of the adhesive, d is the diameter of hole; and t is the bond line thickness, usually 1/16 in. as the hole diameter is usually 1/8 in. larger than the anchor diameter. The derived bond stress distribution was a hyperbolic cosine function as illustrated in Figure 5.1c ($u(z) = P\lambda\frac{\cosh(\lambda z)}{\sinh(\lambda l)}$, where $\lambda = \sqrt{\frac{G\pi d}{tEA}}$, and E is Young's modulus of the anchor, and A is the cross sectional area of the anchor, respectively.

A closer look at the derivation (Eqs. 5 and 6) in Cook et al. (1993) indicates that governing differential equation might have been $w" + \frac{k}{EA}w = 0$, leading to solutions in terms of a cosine function rather than the hyperbolic cosine function ($u(z) = P\lambda\frac{\cos(\lambda z)}{\sin(\lambda l)}$). This indicates that the bond stress near the concrete top should be smaller than the rest, contrary to Figure 5.1c.

The model by Cook (1993) assumed perfect bond between adhesive and concrete and the displacement of an adhesive anchor is allowed by shear deformation of adhesive, as illustrated in Figure 5.1b. The material tests of a vinylester adhesive by Liu (2020) indicates that the adhesive is a brittle material (See the measured stress-strain curves in Fig. 3.6) and does not allow large tensile/compressive deformation; hence the shear deformability of the adhesive unlikely explain large displacements observed in tension tests of adhesive anchors. Instead, adhesive-concrete bond

is provided by hardened adhesive occupying the micro-indents in the wall of drilled and properly cleaned holes in concrete. The anchor displacement is thus the slip of the adhesive core (and the anchor shaft) after the adhesive in the micro-indents crushes during the tests.

Research by McVay et al. (1996)

McVay et al. (1996) used 2D elastoplastic finite element model to study the combined breakout-pullout failure of adhesive anchors. Pullout of adhesive anchors was simulated using PLASFEM, an elastoplastic finite-element code then under development at the University of Florida. The simulation revealed that the concrete-failure cone was found to initiate at the concrete-adhesive-bond interface and progress towards the surface as a tension zone. It was found that a uniform bond stress model over the entire embedded length could be sufficient in predicting pullout capacity of adhesive anchors.

The 2D finite element model used to model the unconfined tension tests is shown in Figure 5.2. Similar to Cook et al (1993), the adhesive layer in between the steel anchor and the surrounding concrete was the critical component. Eight-node, isoparametric axisymmetric elements were used for all components. Different from Cook et al (1993), the shear deformation of the adhesive elements considered the deformation of concrete. An elastoplastic material model developed by Sandler et al. (1976) was used for both the concrete and the adhesive while the anchor was modeled as an elastic material. The elastoplastic material model has a cap in the two-dimensional tension yield surface; hence, crack zones in concrete may be captured. The analysis results for an anchor with 4 in. embedment shown in Figure 5.3 indicates that concrete breakout failure may occur from 1.25 or 2.5 in. below the concrete surface. In addition, shear failure, representing bond failure, may occur below the breakout cone.

The shear stresses along the 4-in. long anchor are shown in Figure 5.4 at a variety of load levels. Under small loads, the shear stress distributions seem in agreement with the hyperbolic cosine function as revealed by Cook et al (1993). As the load increases, a more uniformed shear stress distribution could be observed, providing supportive evidence to the authors' uniform bond stress model. The uniform bond stress distribution was partly attributed to the cap set in the tensile strength of the elastoplastic material model. Meanwhile, the concrete expanded as the applied load increased and the expansion is not restrained by surrounding concrete, leading to tensile stresses in the adhesive layer in the lateral direction, which in turn caused increased shear capacities of the adhesive layer. This unrealistic increase is allowed by the elastoplastic material models.

Research by Davis (2012)

A similar modeling technique was used by Davis (2012) to investigate the viscoelastic time-dependent effects on the stress distribution of adhesive anchors in confined tension tests. A 2D finite element using isoparametric axisymmetric elements in a commercial FE package, ADINA®, is shown in Figure 5.5. The model was restrained in the vertical direction along the top of the confining plate and bottom of the model and in the radial direction along and sides to eliminate the expansion observed by McVay (1996). The adhesive in between concrete and anchor contained two layers similar to the models in Appl (2009): an outer layer with a width of one element at the interface with the concrete and an inner layer three elements wide. The anchor threads were explicitly modeled though the elements representing different materials were perfectly bonded. Elastic material models were used for both concrete and steel and an elastoplastic model was used for the adhesive elements for the analyses without time-dependent behavior.

Figure 5.6 presents the shear stress distribution near the adhesive-concrete interface at various load levels. STL in the figure represents the total measured load sustained by the anchor. The stress distribution approximated a hyperbolic cosine function when the load is below 40%STL, the shear stress was redistributed as the load increased and approached a uniform distribution at 100%STL. Note that the material models available in ADINA did not have a failure criterion; hence an arbitrary plastic strain limit of 0.2 in./in. was incorporated. The author noted that a plastic adhesive model with failure criteria is needed to better understand the behavior and shear stress distribution at failure.

Research by Appl (2009)

Appl (2009) a finite element program, MASA®, developed at the Institute for Building Materials at the University of Stuttgart for the numerical investigations of adhesive anchors. The FE program has also been previously used in Meszaros (2002) and others (Cook et al. 2007). An interface model was used in earlier studies that only transfers shear stresses between steel and concrete, and the shear strength was capped by stresses in surrounding concrete perpendicular to the anchor. In this study, the adhesive was modeled in using solid elements for both threads of the threaded rod and the adhesive. Note that the adhesive behavior was simulated using a microplane model similar to the concrete. Figure 5.7 shows the 3D model of anchors in confined and unconfined tension tests. The concrete was modeled using a microplane constitutive model for to account for the damage in concrete. The force the adhesive in between the threaded rod and concrete was again modeled in two layers, as illustrated in Figure 5.8. The layer close to the threaded rod mainly transfer the load through mechanical interlocking between the threads and adhesive tooth such that failure along adhesive-anchor interface can take place by shearing off the adhesive teeth. A second adhesive layer was used outside the first layer to account for the rest of the adhesive material. The second layer was essentially contact elements representing the adhesive-concrete (A-C) interface. The material properties of contact elements corresponded to the properties of concrete in terms of compressive strength, tensile strength and elastic modulus. Meanwhile, the shear strength of the contact elements varied to represent both high and low bond strengths. This is an advancement compared with previous modeling techniques, in which the A-C interface has been modeled using a layer of solid elements. One must note that general contact elements usually do not allow nodal separation that is critical to model shear slip at the A-C interface.

Figure 5.9 shows the simulation results of both a confined tension test and an unconfined tension test. For a 12-mm anchor with an embedment of 120 mm in 25-MPa concrete, the principal tensile strains in concrete indicates that concrete will fail near the anchor shaft in confined tension test (Figure 5.9a), indicating a pullout failure. Note that the reaction plate (or confining plate) in a confined tension test usually have a center hole that is about 2-3 times the anchor diameter, which was not accounted for in the analyses. The principal tensile strains corresponding to 50% of peak load in Figure 5.9b indicate that concrete would develop splitting cracks and breakout cracks. In addition to a breakout crack initiated at the bottom of the anchor, multiple shallow breakout cracks may also develop along with pullout failure.

Research by Delhomme and Brun (2018)

Delhomme and Brun (2018) used an axisymmetric model in ABAQUS®, shown in Figure 5.10, to simulate the pullout behavior of adhesive anchors in super high-performance fiber reinforced concrete. The adhesive layer was not explicitly modeled; instead surface-surface contact elements (represented by the interface lines in the 2D models) with a cohesive traction-separation model

were used. The cohesive traction-separation model in ABAQUS requires three sets of parameters corresponding to three modes of fracture. The parameters for in-plane shear fracture (Mode II) was provided: The peak bond strength (t_s^0) was 5366 psi, which was based on unconfined tension tests of three ½-in. diameter HIT-Z threaded steel rods with an embedment of 1.6 in. (Specimen h40 in Figure 5.11). The specimen failed in combined breakout-pullout failure, and the equivalent bond strength was 4714 psi and the failure occurred at a pullout displacement of 0.056 in. The bond stress was assumed to drop to zero at a slip of 0.27 in. (δ_s^t). The peak bond strength (t_s^0) and the corresponding slip (δ_s^0) was adjusted such that the simulated load-displacement behavior for Specimen h40 was close to the experimental results. The same parameters were then used in the analyses of other specimens with deeper embedment. The parameters corresponding to opening and out-of-plane shear fracture were not reported except that the slope of ascending branch of Mode I fracture (k_{nn}) was 1000 times of the slope for Model II fracture (k_{tt}, and the reported parameters (45.5 Nm^{-2}) had a questionable unit). The anchor was models as an elastic material while the damage plasticity model was used for the concrete with mostly default parameters.

Comparison with test results (Figure 5.11) indicated that the FE analyses were able to fit the experiments. Note that the cohesive traction-separation model did not allow separation of steel anchor from surrounding concrete as shown in Figure 5.11 for Specimen h40. The concrete, especially at the top, developed large plastic deformation along with the anchor displacement. This could have partly attributed to the shear softening of plasticity-based models. The tensile damage variable (DAMAGET) shown in Figure 5.11 indicated that at the ultimate displacement of 0.31 in., the concrete next to the anchor had entered the post-peak softening range of behavior, and the crack depth was deeper than 1.0 in. Note that the tensile damage shown in Figure 5.11 may have indicated both splitting cracks and/or breakout cracks in the axisymmetric model.

5.3 Finite Element Analyses

Model geometry and boundary conditions

The unconfined pullout test on Specimen UC-0.5-4.0 was modeled in ABAQUS® as shown in Figure 5.10a. For comparison purposes, the reaction plate for the confined pullout tests shown in Chapter 3 was placed next to the anchor to simulate the corresponding confined pullout test in Figure 5.10b. The specimens had two symmetric planes; hence, only quarter of the specimen was modeled. Specifically, the concrete block for was 12 in. wide, 24 in. long, and 12 in. deep. The concrete block is divided into two parts in the height direction: the top 4 in. had an unstructured mesh to accommodate the drilled hole while the bottom 8 in. had a structured mesh to reduce the total number of solid elements. The 0.5 in. diameter anchor was made from an ASTM A193 Grade B7 threaded rod, with a 4 in. embedment depth in a 5/8-in. diameter drilled hole. The bond failure along A-S interface was not considered in this study, hence the adhesive anchor part consists of a solid steel rod with an equivalent area of 0.1419 $in.^2$ at the center and a ring of mixed steel-adhesive material with an inside diameter of 0.4244 in. and an outside diameter of 0.625 in. A 4×6×0.25 in. plate was placed at the ends of the quarter block to simulate the reaction in unconfined tension tests when tensile loads are applied to the anchor. The reaction plate was 2.5×2.5×0.25 in. with a 1.0-in. diameter center hole, placed next to the anchor on the quarter block in the confined tension test. Finally, longitudinal crack-controlling bars and stirrups were modeled using 3D wires located at the center of the bars.

Element selection

General purpose brick elements (Type C3D8R) were used for all parts in the model. The element size was roughly controlled with a smallest edge length of 0.25 in. near the anchor and 2 in. away from the anchor. The interface between the top and bottom block was modeled using a tied constraint available in ABAQUS. The interface between the reaction plates and the top block was also modeled using a tied constraint. The interface between the concrete and the adhesive is critical to the FE analyses because bond failure along the A-C interface was the focus of this study. Pullout failure is only possible when relative displacement is allowed at the A-C interface; hence, the interface was modeled using two techniques in two directions: normal to the interface, frictionless, hard contact was used and separation of the elements representing two materials was prevented in the normal direction. Meanwhile, parallel to the interface along the anchor, a total of eight layers of three nonlinear springs were used to model the A-C interface bond. Separation of the elements representing two materials was allowed to simulate the pullout failure. The frictionless contact constraint allowed rotation of the anchor in the circumferential direction; hence, the rotation motion was prevented by the applied displacement boundary condition at the top of the anchor: only Z-direction motion was allowed such that the rigid-body rotation was prevented. This combined interface model was shown to be critical to the FE analyses because using discrete springs to model interface bond created unreasonable concentrated tensile forces on the nodes of the concrete elements with a damage plasticity material model, which could cause significant convergence issues. The inseparable hard contact constraint between complex concrete elements and elastic adhesive elements effectively released the impact of the concentrated forces.

Along the perimeter eight elements were used for the concrete block and sixteen elements were used for the concrete anchors, leading to eight coincident points along the perimeter, where nonlinear springs were specified. A total of eight layers of solid elements were used for the concrete and anchor within the embedded length; hence, eight layers of springs (with three springs each layer due to symmetry) were used as illustrated in Figure 5.12. Therefore, a total of twenty-four nonlinear springs are used in the quarter model to simulate the interaction on adhesive-concrete interface. Details of the nonlinear spring elements can be found elsewhere (Liu, 2020).

Material properties

A damage plasticity model as described in Lee and Fenves (1998) was used for concrete elements. The Young's modulus was 4488.2 ksi based on a measured concrete compressive strength of 6200 psi (ACI 318-19). The Poisson' s ratio was 0.17 as suggested by McCormac and Brown (2014). The damage plasticity model requires a uniaxial stress-strain curve in both tension and compression. A modified model based on that in Popovic (1970) was used for concrete in compression. Details of the model equation can be found in Liu (2020). A bilinear curve was used to model the tensile behavior of concrete. The tensile strength was taken as $0.1f_c'$. The descending part of the concrete model in tension was not considered in this study because the focus of this study was on the pullout failure of adhesive anchors controlled by the bond on A-C interfaces. The use of nonlinear springs caused unreasonable tensile stress concentration on concrete and including the post-peak behavior caused convergence problems.

An elastoplastic model was used for the steel anchor. The Young's modulus of anchor was 29000 ksi and he Poisson' s ratio was 0.25. The yield strength was 112 ksi and the ultimate stress was 129 ksi at a plastic strain of 0.054 in./in. (Liu 2020). The adhesive was modeled as an elastic material again because the focus of this study was on the pullout failure of adhesive anchors

controlled by the bond on A-C interfaces. The modulus of Elasticity for the adhesive was 315.4 ksi and the Poisson's ratio was 0.38 from the material tests (Fig. 3.6); however, a randomly increased value (3150 ksi) was used in the model to consider the steel threads in the adhesive layer. Again, a more realistic element mesh nor a nonlinear material model was deemed unnecessary for the adhesive layer in this comparison study because the focus was on the A-C interface failure. This is different from all previous numerical studies as reviewed in Section 5.2 because the experimental tests in Chapter 3 indicated that shear failure in the adhesive was scarce.

For the simulation of the bond failure of adhesive anchors, surface-to-surface frictionless, hard contact was used normal to the adhesive-concrete interface. Nonlinear springs were used to simulate the bond behavior on adhesive-concrete interface. Nonlinear spring with a predefined bond-slip law have been used to model the interaction between concrete and reinforcement (Molina et al. 2015). Hence, this was deemed suitable for modeling bond failure of adhesive anchors during pullout tests. As mentioned in Chapter 4, adhesive flow into the micro-indents on concrete surfaces would form spikes and the adhesive spikes provide mechanical interlock after hardening. Pullout failure occurs when these hardened adhesive spikes are sheared off. Subsequently, the bond strength is maintained through friction on the adhesive-concrete interface. This procedure is similar to the pullout of a deformed bars from concrete; hence, a bond-slip relationship similar to that proposed by Eligehausen et al. (1983) was chosen to simulate the bond failure adhesive anchors.

Figure 5.13 shows the proposed bond-slip relationship: The ascending branch was assumed linear up to a maximum bond stress (τ_{max}) at a slip of s_1. The τ_{max} is 2000 psi obtained from the average bond stress of unconfined pullout tests used in specimen design in Chapter 3. The maximum bond stress is maintained till the slip reaches at s_2, beyond which, the bond stress reduces to a bond stress mainly from friction τ_3. The lowest bond stress is the friction in the proposed model. τ_3 was taken as 1000 psi, which is the average bond stress from unconfined pullout tests of anchors in partly clean holes (Liu 2020). The characteristic slips s_1 and s_2 were estimated from the observation of hardened adhesive spikes: s_1 being the minimum spike width and s_2 the maximum width, respectively. Six spikes shown in red arrows were randomly selected on the Figure 6.8 and the observation indicates that s_1=0.02 in. and s_2=0.08 in. The slope of descending part of the bond slip is controlled by s_3, which was randomly selected as 0.5 in. This slip value coincides with the element size in Z-direction. The bond-slip model must be converted into a load-displacement for the nonlinear springs. While the displacement was automatically calculated as the difference of displacement of the nodes that define the springs in Z-direction, the spring forces are calculated from the total bond force with a ½-in. height. For example, corresponding to the peak bond stress (at a slip of 0.02 in.), the spring force should be $(\pi \times 0.625" \times 0.5") \times 2000psi/12 = 0.16kips$.

FE analysis results

Figure 5.14 shows a comparison between three tests of Specimen UC-0.5-4.0 and the FE analysis in terms of load vs. displacement behavior. The test was repeated four times, out of which the first test was controlled by pullout (#1) and two tests controlled by combined breakout-pullout (#2 and #3). The FE analysis is able to reasonably capture the pullout failure observed in Test #1. The 4-in. specimen was not subjected to a confined tension test because the predicted capacity exceeded the full steel capacity of the anchor.

The calculated bond stress distribution shown in Figure 5.15 is quite uniform along the whole anchor at all load levels, which is a bit different from the results of the elastoplastic analyses in the

literature. This uniform bond distribution was deem reasonable because the adhesive in reality has a very small Young's modulus (about 315 ksi) comparted with steel (29000 ksi) and concrete (4488 ksi); hence the differential displacement between the steel anchor and the surrounding concrete is expected to be uniformly applied to the A-C interface. The reduced spring forces (bond stresses) near the top is the result of large deformation in concrete, which was modeled as an elastoplastic material in tension. Meanwhile, the nonlinear springs, representing the A-C interface bond, had a rudimentary bond-slip relationship (Figure 5.13); hence, the predicted bond stress distribution should be viewed with caution. Specifically, concrete cracked at the top in Test #1 as shown in the inserted picture in Figure 5.14. The splitting crack after the loading was about 0.0008 in. (0.2 mm) while the cracks were at least twice the width near the peak load. It was hypothesized that the splitting crack would disengage the concrete from hardened adhesive, leading to greatly reduced bond resistance, as shown by the intact adhesive surface near the top in the inserted picture in Figure 5.14. Such complex bond behavior was not included in the constitutive model of the nonlinear springs. Therefore, the spring force distribution shows negligible difference between the simulation results of the confined and unconfined tension tests (Figure 5.15).

The analyses indicated that the closely placed reaction does cause additional lateral confining pressure to the adhesive or the A-C interface. The Mises stresses developed in concrete are very different as shown in Figure 5.16, indicating the expected impact of reaction locations on concrete. Figure 5.17 shows the pressure on the contact interface between the adhesive elements and surrounding concrete. With the identical contour scale (from 0 to 3 ksi positive pressure), the adhesive from 0.5 down to 2.0 in. in confined tension tests experienced a bit more pressure as indicated by the wider red colored ranges. The blue-colored strip with lower contact interface pressure in the middle of the quarter adhesive layer was caused by the tension from the nonlinear bond springs. A mesh sensitivity analysis should be conducted to quantify the (unrealistic) influential range of the chosen modeling technique. Again, the nonlinear spring model should consider the impact of pressure on bond capacities in order to quantify the impact of closely placed reaction.

The stresses (Figure 5.18) and strains (Figures 5.19 and 5.20) developed in concrete confirmed that closely placed reaction restrains tensile splitting of concrete, which was responsible for higher observed bond strength in confined tension tests. Specifically, the maximum principal tensile stresses in Figure 5.18 indicated that concrete may develop splitting cracks in both transverse and longitudinal directions in unconfined tension tests, which was observed in many tests shown in Appendix I. The strains in concrete in both the longitudinal direction (Figure 5.19) and the transverse direction (Figure 5.20) indicated that the splitting crack may be as deep as 2.5 in., as marked by a tensile strain of 0.00022, which is calculated as $\frac{12\sqrt{f_c}}{E_c} = 0.00021$. The large tensile strains in Figure 5.19 and 5.20 were localized to the anchor due to the softening of concrete material using a plasticity-based model.

5.4 Summary

In summary, the finite element analyses in this chapter indicates that concrete surrounding adhesive anchors in tension may develop splitting in unconfined tension tests. The splitting cracks may be localized near the test anchor or through entire concrete specimen. In addition, the splitting cracks may occur at the top portion of concrete, leading to partial disengagement of adhesive and

concrete and reduced bond resistance. Such splitting cracks are not permitted in confined tension tests. This is clearly shown in Figure 5.19 for ¾-in. anchors with an embedment depth of 4.5 in.: the adhesive was engaged through hardened adhesive in micro-indents, randomly generated in concrete, along the entire embedded depth in confined tension test while the top portion of the anchor/adhesive in unconfined tension tests was partly disengaged. Pullout failure in both tests occurred when the hardened adhesive in the micro-indents got crushed as shown by the white powdered quartz fillers in Figure 5.21. This is similar to the observation by Barnat and Bajer (2011) as shown in Figure 5.22

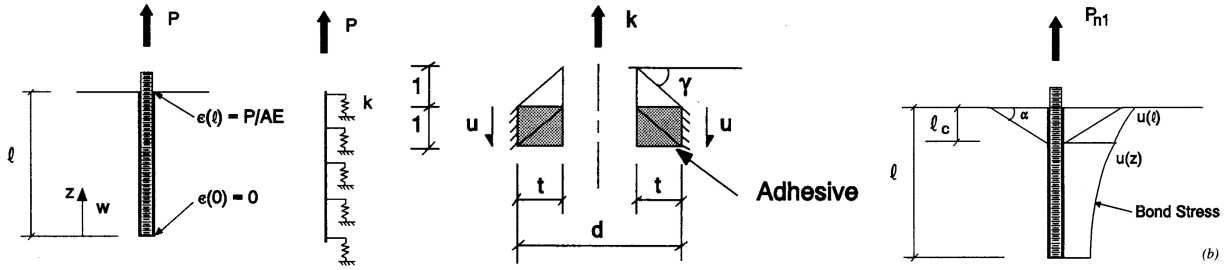

Figure 5.1 Load transfer model in adhesive anchors by Cook et al. (1993)

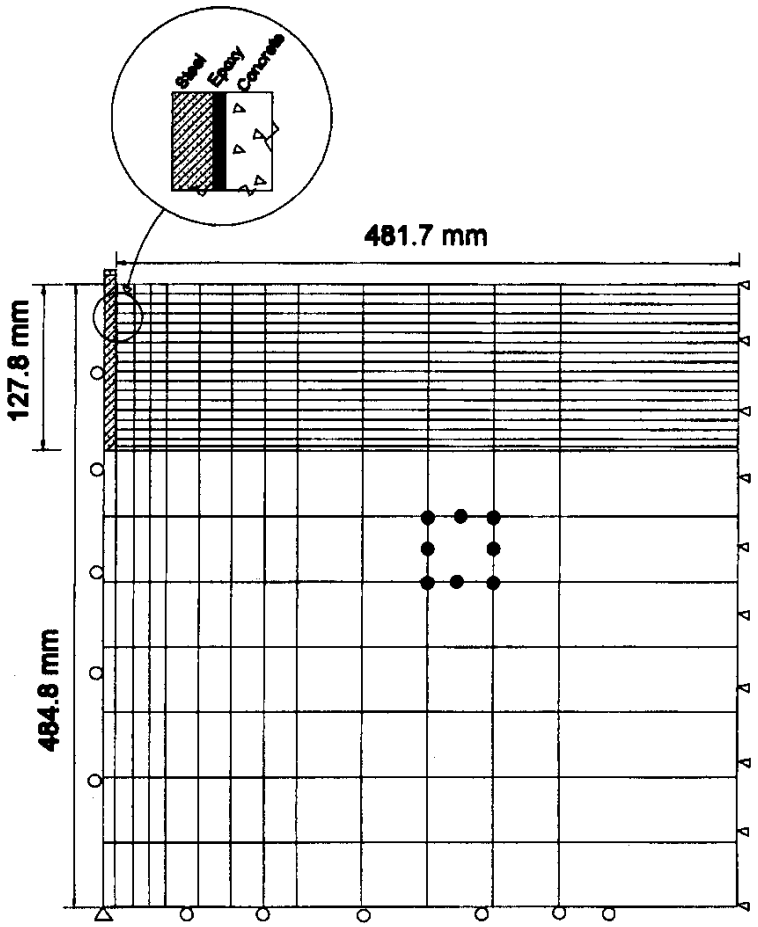

Figure 5.2 Finite element model for anchor bolt pullout simulation (Fig. 6 from McVay et al. (1996))

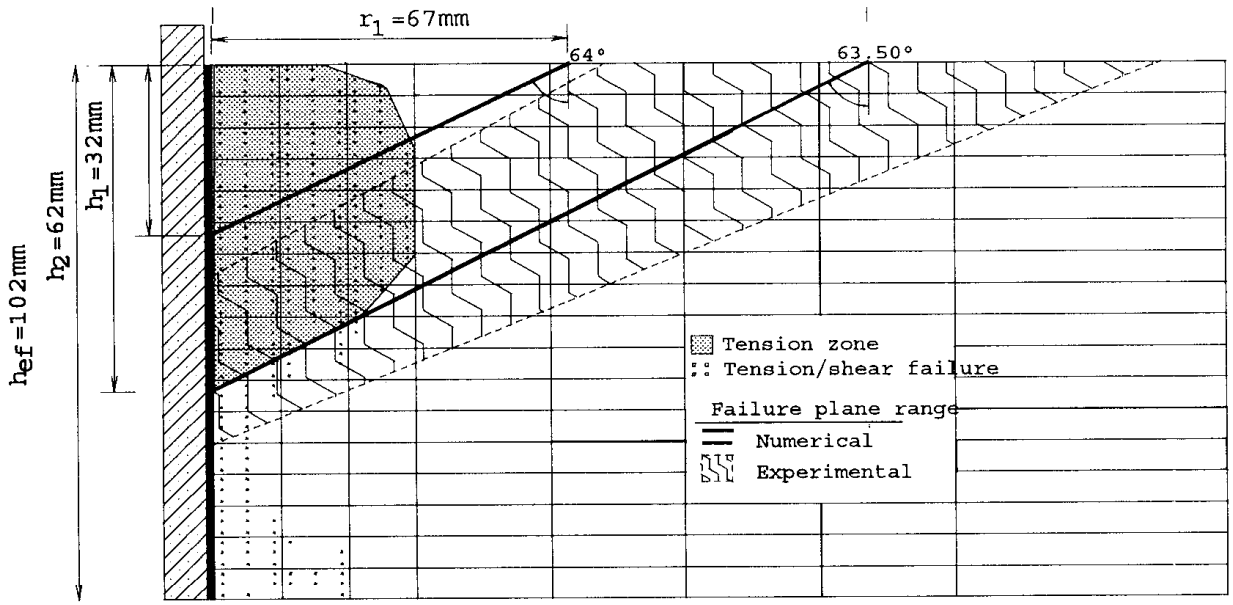

Figure 5.3 Simulated breakout-pullout failure of a 4-in. anchor (Fig. 8c from McVay et al. (1996))

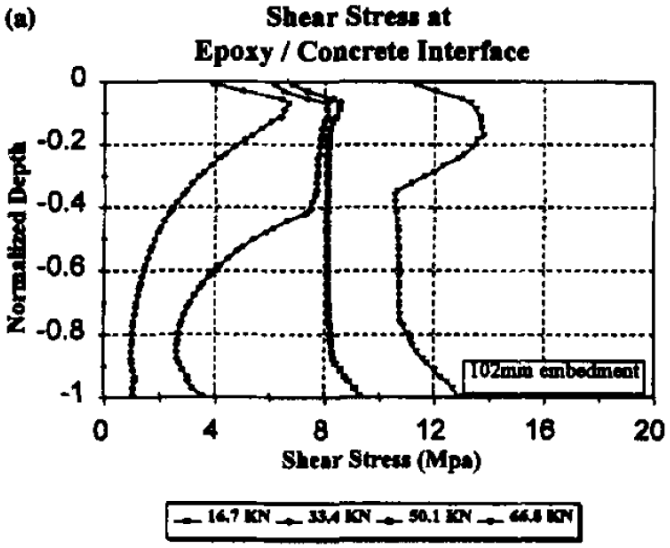

Figure 5.4 Shear (bond) stresses along concrete-adhesive layer interface in McVay et al. (1996)

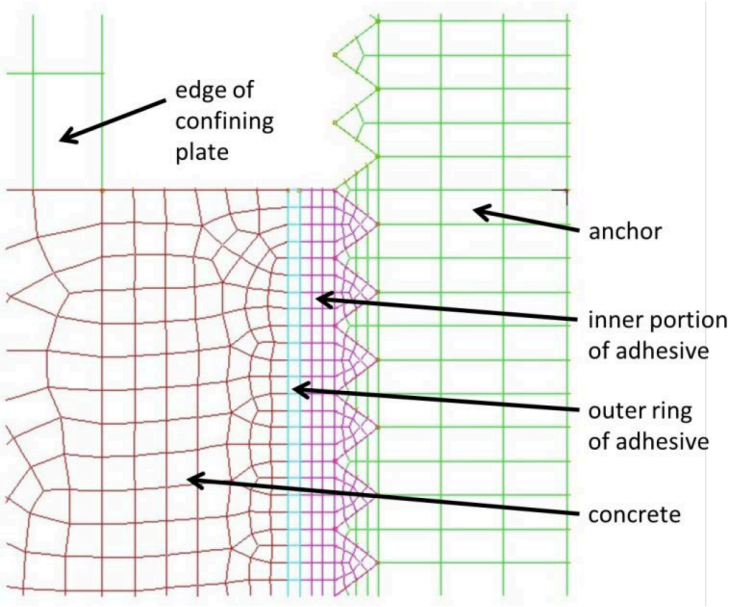

Figure 5.5 2D finite element model of adhesive anchors (Figure 7-4 in Davis (2012))

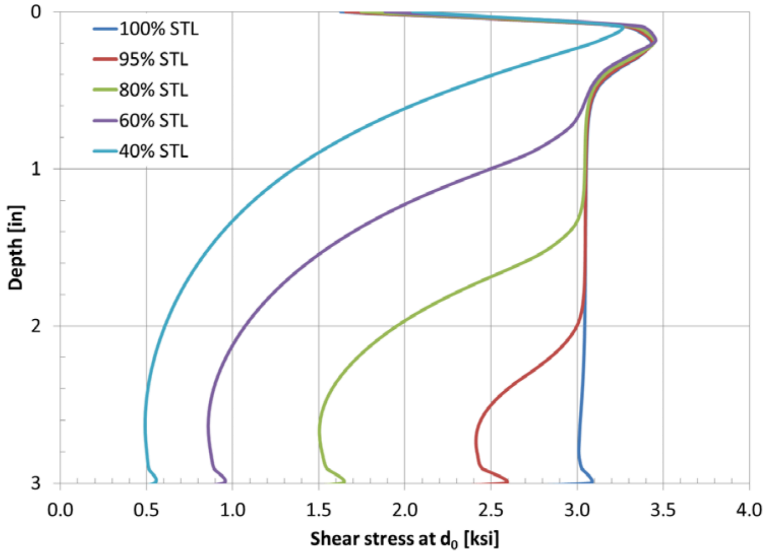

Figure 5.6 shear stress at interface at various load levels (Figure 7-5 in Davis (2012))

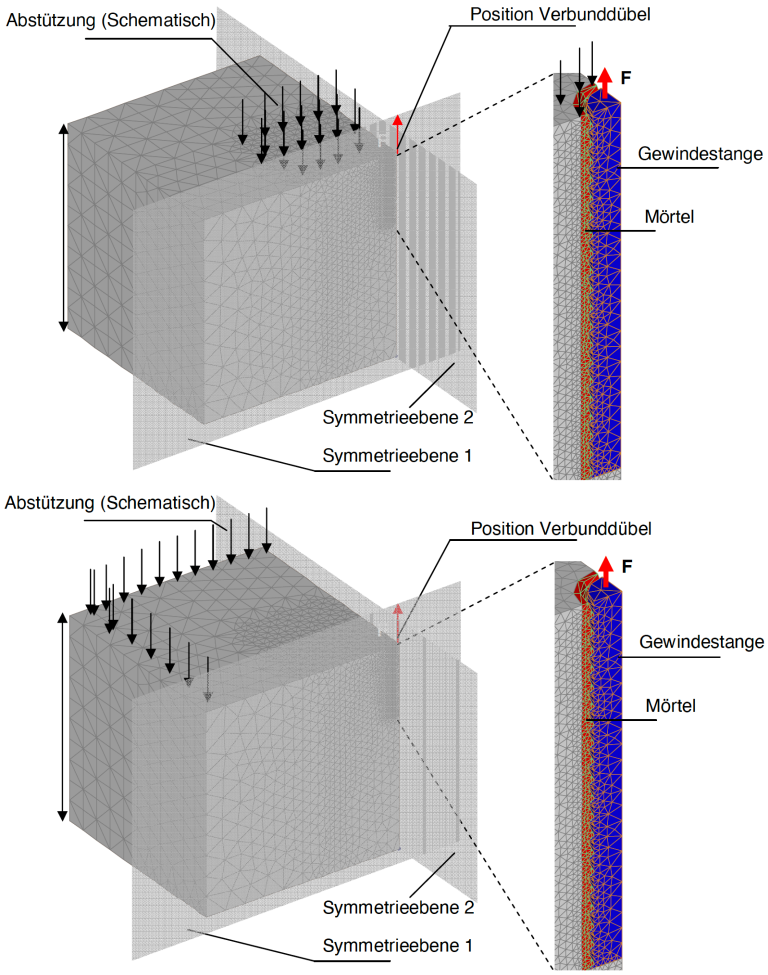

Figure 5.7 Finite element model in FEMAP by Appl (2009)

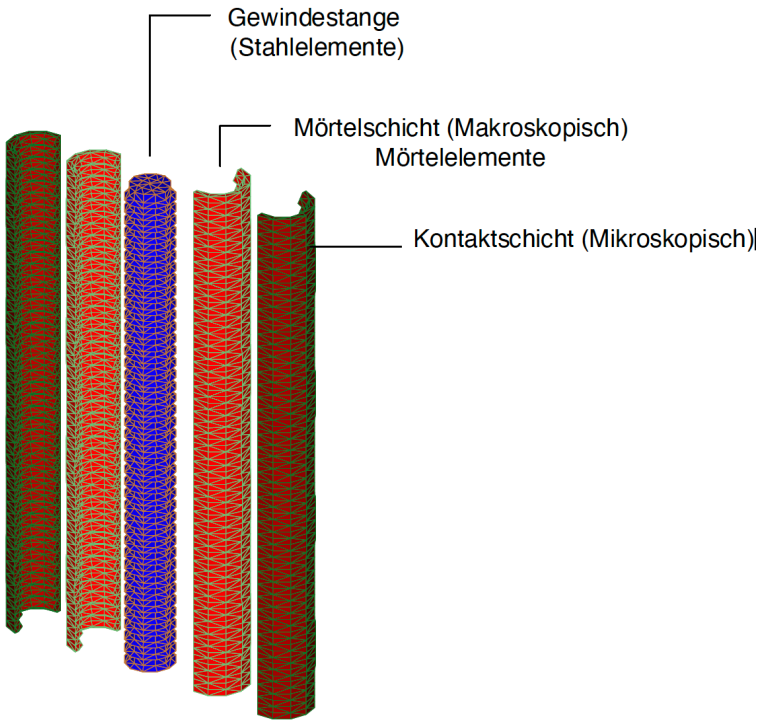

Figure 5.8 Anchor-adhesive-concrete interface in Appl (2009)

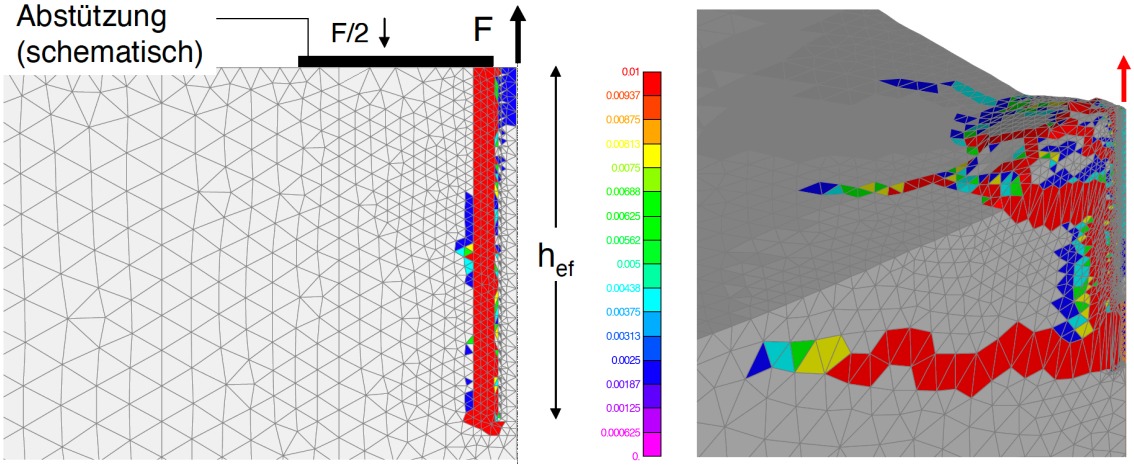

a) confined tension test; b) unconfined tesion test

Figure 5.9 Principal tensile strains in concrete (M12, h_{ef}/d = 10, fcc = 25 MPa, Adhesive C)

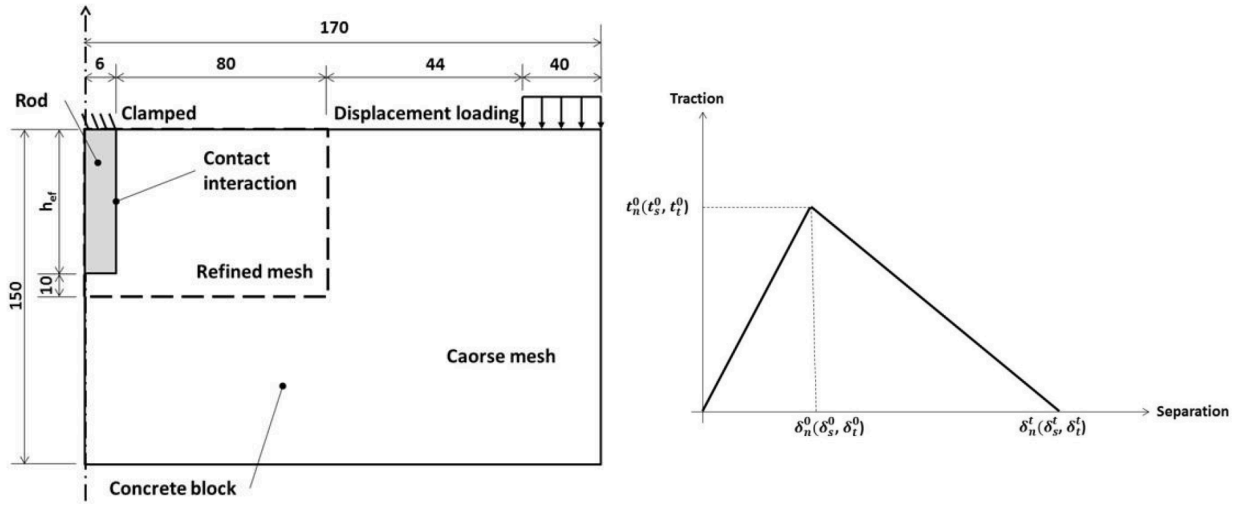

Figure 5.10 Axisymmetric model and anchor-concrete interface model by Delhomme and Brun (2018)

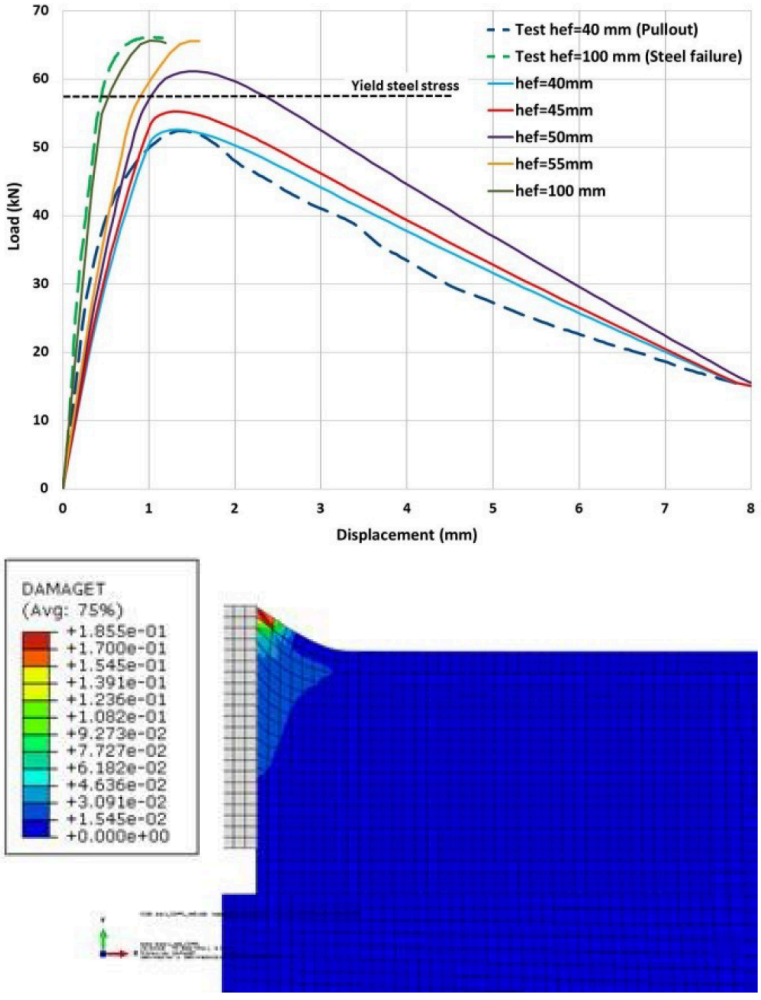

Figure 5.11 Analysis results by Delhomme and Brun (2018)

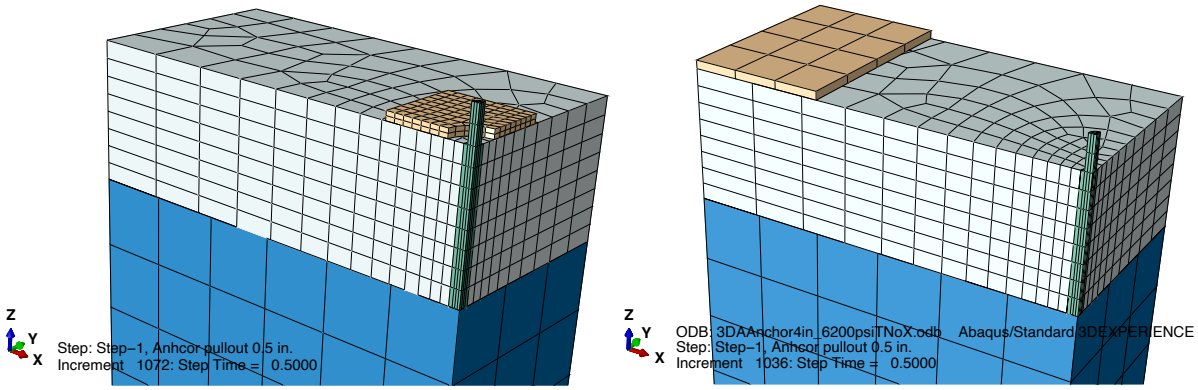

a) in confined tension test; b) in unconfined tension test

Figure 5.12 Finite element model of Specimen UC-0.5-4.0.

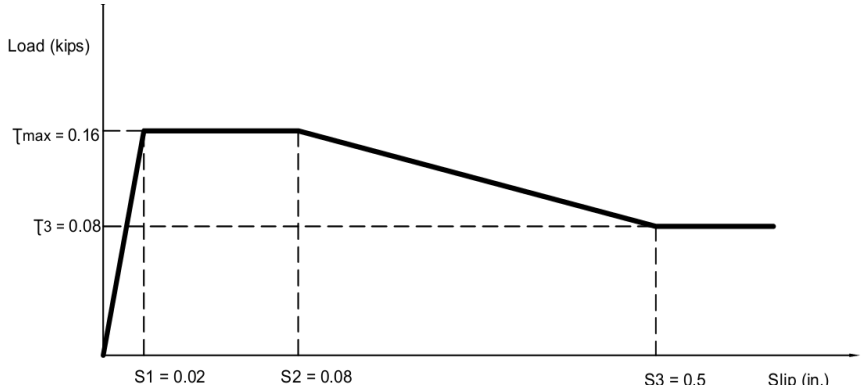

Figure 5.13 Material model for nonlinear springs representing A-C interface bond.

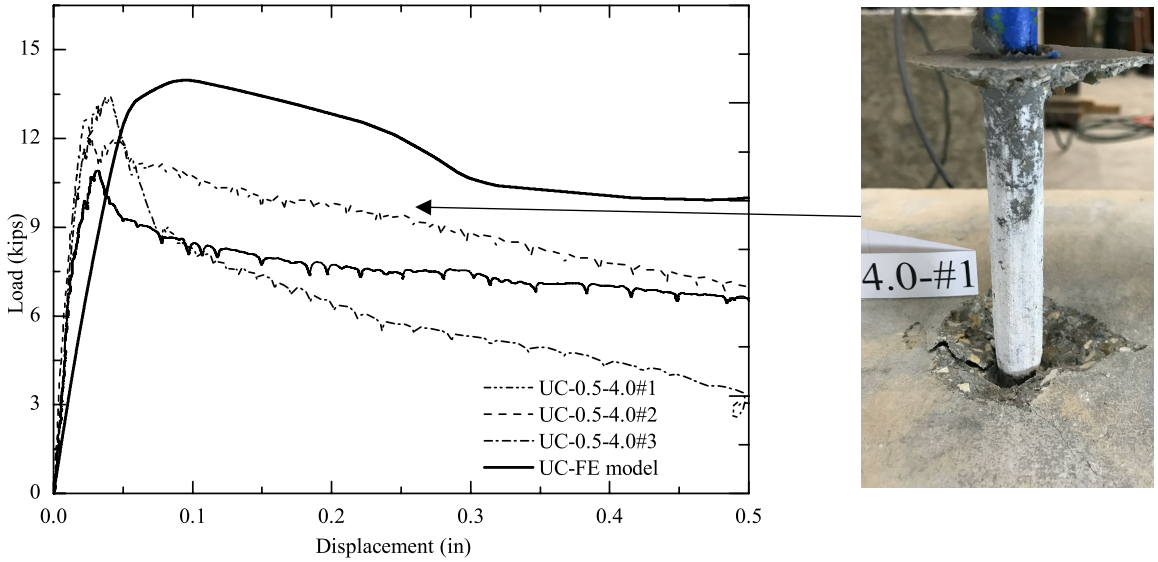

Figure 5.14 Comparison of FE analysis with tests of Specimens UC-0.5-4.0.

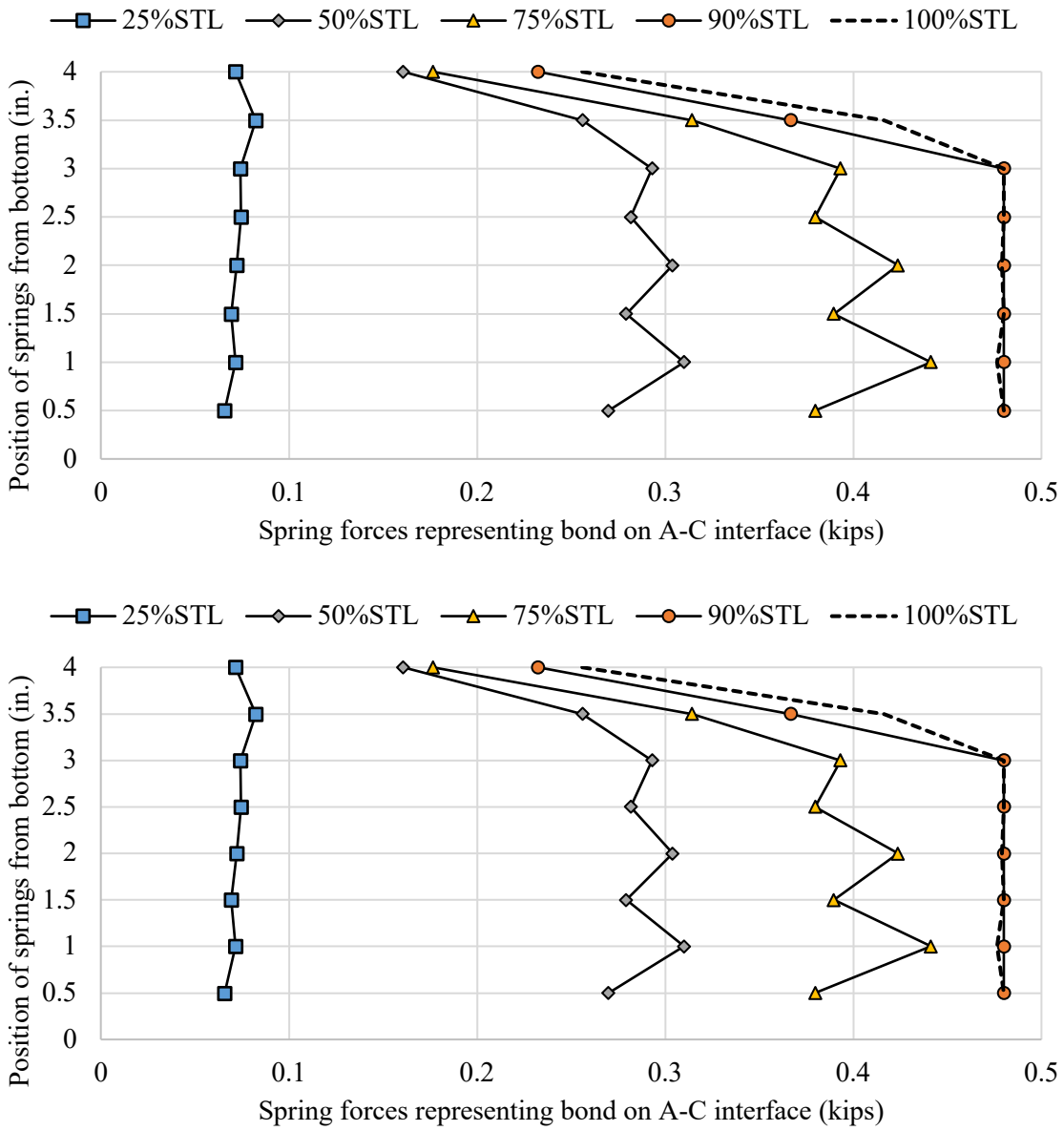

Figure 5.15 Comparison of spring forces in Specimens UC-0.5-4.0. a) in confined tension test; and b) in unconfined tension test

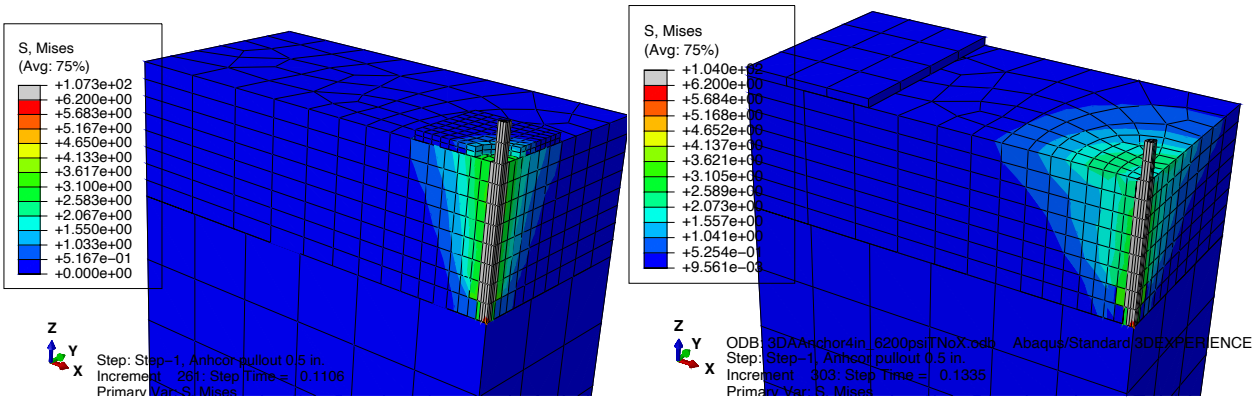

Figure 5.16 Misses stresses in concrete developed in Specimen UC-0.5-4.0 at peak loads.

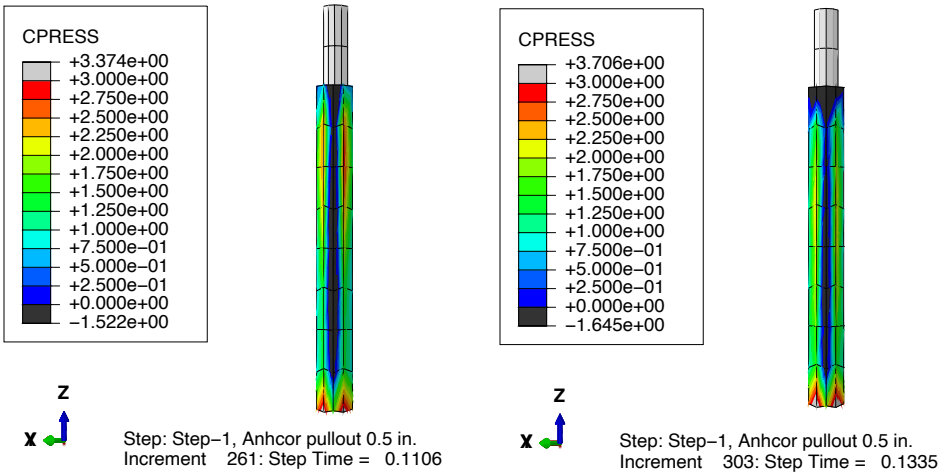

a) in confined tension test; b) in unconfined tension test

Figure 5.17 Pressure generated on adhesive-concrete interface in Specimen UC-0.5-4.0 at peak loads.

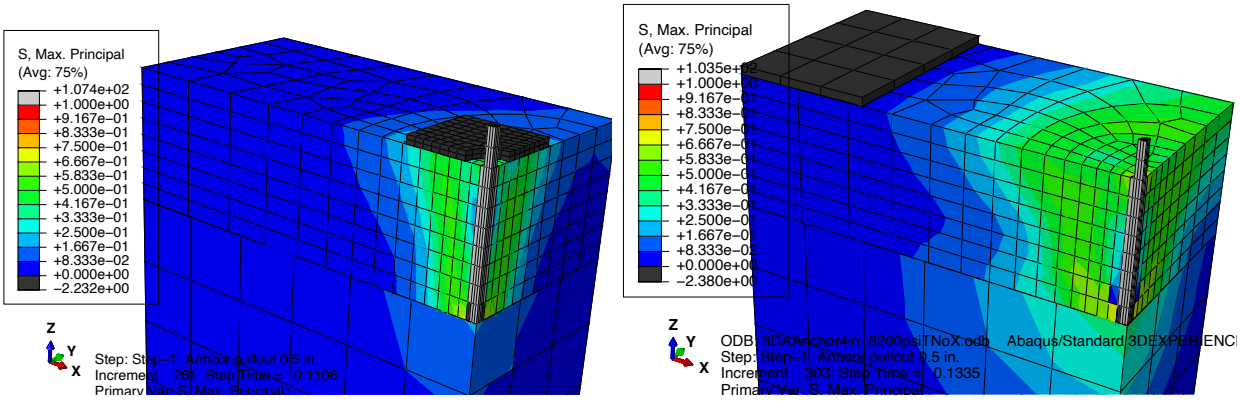

Figure 5.18 Comparison of the maximum principal stress in concrete in Specimen UC-0.5-4.0 at peak loads.

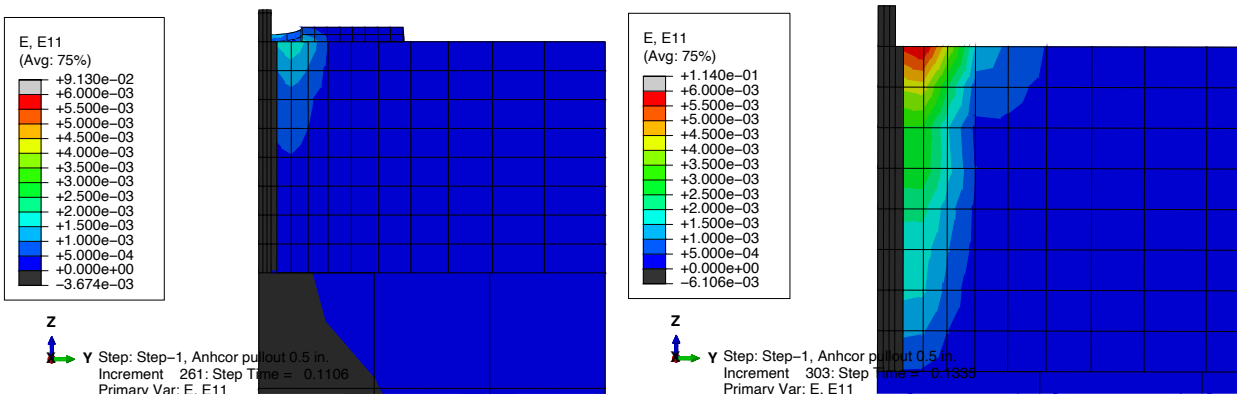

Figure 5.19 Comparison of the X-direction strain in concrete in Specimen UC-0.5-4.0 at peak loads.

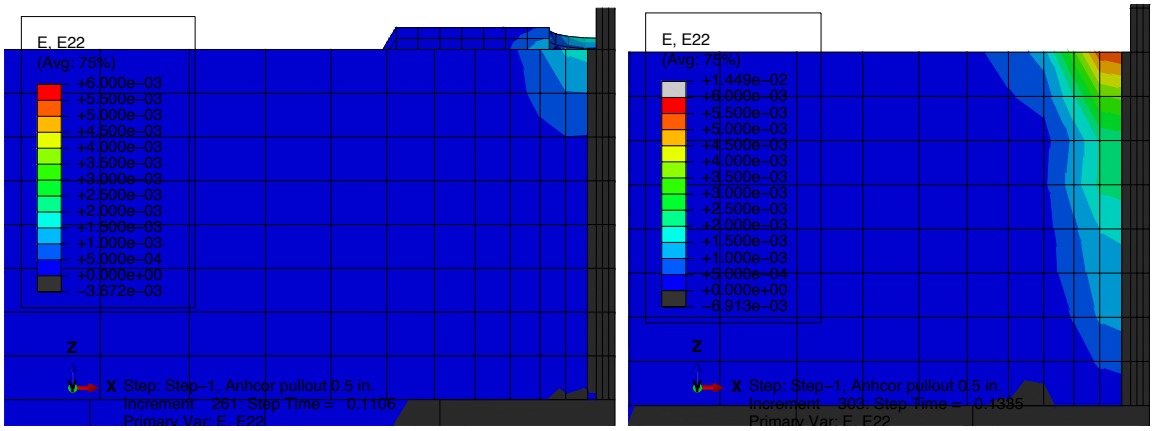

Figure 5.20 Comparison of the Y-direction strain in concrete in Specimen UC-0.5-4.0 at peak loads.

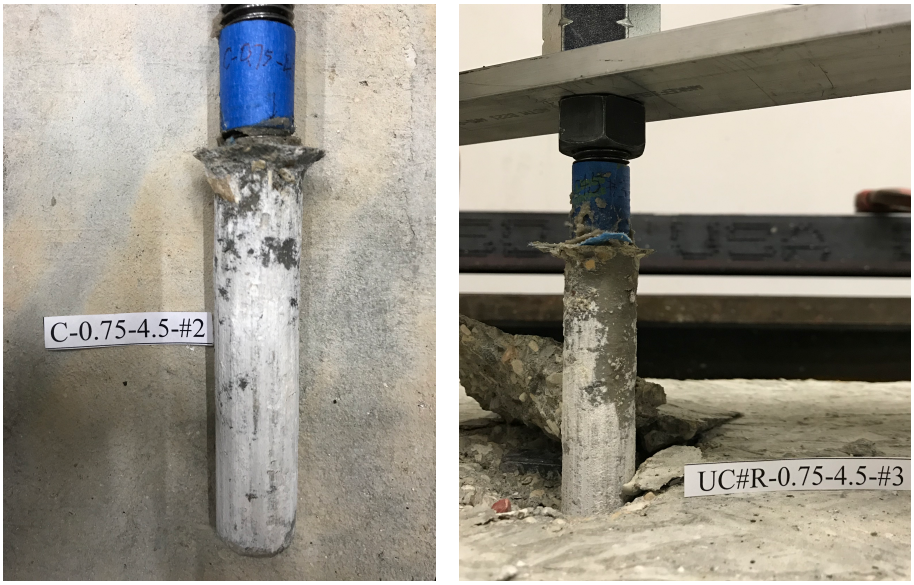

a) in confined tension test; b) in unconfined tension test

Figure 5.21 Comparison of bond failure at A-C interface.

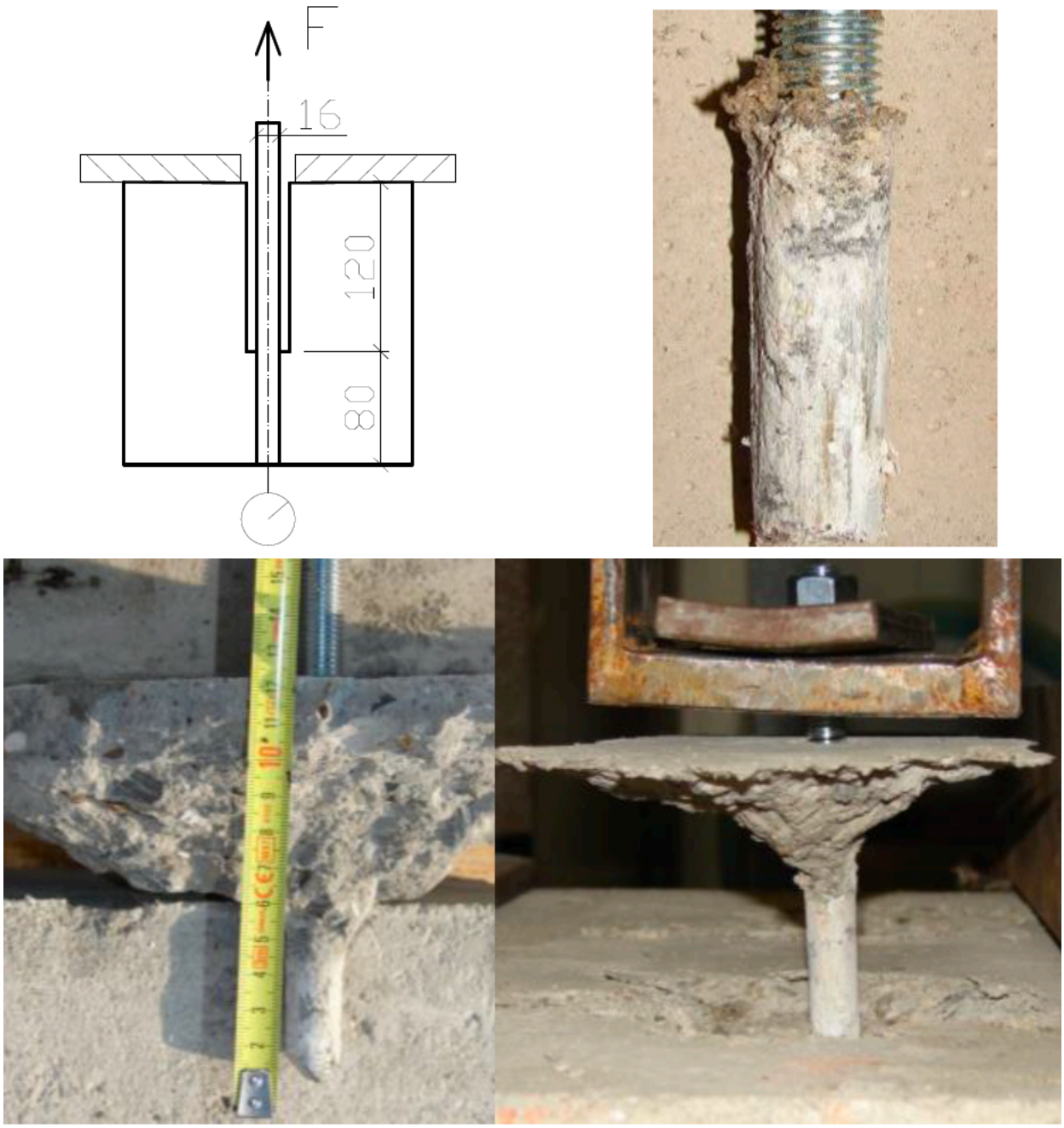

Figure 5.22 Bond failure observed by Barnat and Bajer (2011)

Chapter 6. Summary

6.1 Summary of Research Activities

This report describes a study of adhesive anchors in tension focusing on the behavioral difference of the anchors in confined and unconfined tension tests. Confined tension (CT) tests are widely used to evaluate the bond strength of adhesive. The reaction in CT setup is placed very close to the test anchors, leading to convenient and material-saving tests. However, the closely placed reaction may create undesirable and unrealistic confining conditions to the specimen. Therefore, bond strengths obtained from confined tension tests must be reduced. Unconfined tension (UCT) tests are then needed to evaluate the tensile capacity of adhesive anchors designed using the bond strength obtained from the CT tests. The capacity of anchors in UCT tests is expected to small that those in CT tests; hence, Section 10.4.5.1 of ACI 355.4-11 stipulates a reduction factor of 0.75. Based on the tests by Davis (2012), Cook (2018) suggested that the reduction factor should be taken as 0.5 instead of 0.75. Committee 355 discussion in 2018 indicated that this is a critical issue for the committee, and a task group (TG9) was formed in 2019 to investigate the reduction factor.

In this study, we attempted to explore the impact of test setup on behavior of adhesive anchors. One adhesive and one concrete strength (6200 psi) were used while multiple anchor diameters (that is 1/2, 5/8, and 3/4 in.) and multiple embedment depths were used. Bond failure, especially along the adhesive-concrete interface was the targeted failure mode following the suggestion by Wall (2109). Test design indicated that concrete breakout may be a controlling failure mode; hence specimens were included, in which anchor reinforcement was used to force bond failure. A standard installation procedure was strictly followed to ensure the quality of the data.

A total of 28 confined tension tests and 44 unconfined tension tests were conducted as part of this study. Based on the observation made during the laboratory tests, we envisioned the following difference between confined and unconfined tension tests:

- Closely placed reaction may cause lateral pressure on adhesive-concrete interface in confined tension tests, leading to increased bond strength.
- Closely placed reaction may also change the stress field in concrete such that splitting cracks is restrained in confined tension tests while such restrain does not exist in unconfined tension tests. The splitting cracks, though not through the entire embedment depth, may disengage the microscopic interlock between hardened adhesive and concrete, leading to reduced bond strength, especially near the concrete surface.
- Closely placed reaction prohibits the formation of concrete breakout cones, which often occurs in unconfined tension tests along with bond failure. The mixed failure mode may occur under a lower tensile load than the individual failure modes.

Nonlinear finite element analyses were conducted to explore the impact of these factors. We believe the bond along adhesive-concrete (A-C) interface is established through hardened adhesive in micro-indents, randomly generated in concrete during hole drilling and proper hole cleaning, along the entire embedded depth; hence nonlinear interface models were created in this study.

6.2 Conclusions

The measured capacities in both confined and unconfined tension tests were reasonably proportional to the embedment depths though more than half of the specimens in unconfined

tension tests were controlled by combined breakout-pullout failure, indicating that the current uniform bond stress model in ACI 318-19 is reasonable. The tests also indicated that a reduction factor of 0.75 is unconservative if bond strength is determined as the average measured bond from confined tension tests and a reduction factor of 0.5 seems reasonable; however, the 0.75 reduction factor is appropriate if bond strength is determined as the 5%-fractile of measured bond from confined tension tests.

The FE analyses indicated that 1) the impact of lateral confining pressure from closely placed reaction is reasonably negligible; 2) the concrete surrounding adhesive anchors in unconfined tension tests may develop splitting in unconfined tension tests, especially near the top portion of concrete, leading to partial disengagement of adhesive and concrete and reduced bond resistance. Such splitting cracks are not permitted in confined tension tests; hence, we believe the main difference of the two tests and the reason for the reduction factor is that closely placed reaction in confined tension tests restrains tensile strain/splitting near concrete top, which disengage top part of A-C interface. Meanwhile, concrete breakout may occur at top simultaneously with bond failure. This widely observed behavior only in unconfined tension tests may also be responsible for the reduction factor.

6.3 Suggested Future Studies

The adhesive used in this study had a low-medium bond strength (the measured average bond strength from confined tension tests with ½-in. diameter threaded rods was about 2800 psi). The reduction factor from test setup is expected to be lower than the current code recommendation (that is 0.75) mainly for adhesives with relatively high bond strength; therefore, the tests should be repeated using a different adhesive, such as a high-strength epoxy.

With the same adhesive, confined tension tests with larger-size anchors showed a lower average bond strength (the measured average bond strength from confined tension tests with 3/4-in. diameter threaded rods was about 1800 psi). This may have been attributed to poor hole cleaning even with the same standard procedure. The tests should be repeated for large size anchors with properly cleaned holes.

The finite element analyses used a simple interface model. Specifically, the constitutive model for the nonlinear springs should consider the stresses normal to the adhesive-concrete interface. This is needed in order to quantify the impact of closely placed reaction.

Finally, in an unrelated attempt, anchor reinforcement designed following ACI 318 requirements, was used in two group of specimens. The reinforcement was able to delay concrete breakout such that the anchors in reinforced concrete were controlled by pullout or combined breakout-pullout failure. However, it is recommended that impact of supplementary reinforcement should be further studied because the reinforcement was not able to greatly increase the tensile capacity of adhesive anchors.

References

1. American Concrete Institute (2019). Building Code Requirements for Structural Concrete. ACI 318-19. Farmington Hills, MI.
2. ACI 355.4-11 (2011). Qualification of Post-Installed Adhesive Anchors, American Concrete International, Farmington Hills, MI.
3. AASHTO (2013). LRFD Bridge Design Specifications. AASHTO, Washington, D.C.
4. Appl, J.J. (2009). Tragverhalten von Verbunddübeln unter Zugbelastung (Load-bearing behavior of bonded anchors under tensile load) PhD Dissertation, University of Stuttgart, Germany. In German
5. ASTM A193 (2012). Standard Specification for Alloy-Steel and Stainless Steel Bolting for High Temperature or High Pressure Service and Other Special Purpose Applications, American Society for Testing and Materials, West Conshohocken, PA.
6. ASTM E488 (2003). Standard Test Methods for Strength of Anchors in Concrete and Masonry Elements, American Society for Testing and Materials, West Conshohocken, PA.
7. Barnat, J. and Bajer, M., (2011). "Analysis of bonded anchor in combined concrete-bond failure mode." In *Proceedings of the 4th WSEAS international conference on Energy and development-environment-biomedicine* (pp. 364-367). World Scientific and Engineering Academy and Society (WSEAS).
8. Cook, R.A., Doerr, G.T., and Klingner, R.E. (1993). "Bond Stress Model for Design of Adhesive Anchors," *ACI Structural Journal*, 90(5), pp. 514-524.
9. Cook, R.A., Eligehausen, R. and Appl, J.J., (2007). "Overview: behavior of adhesive bonded anchors." *Beton-und Stahlbetonbau*, 102(S1), pp.16-21.
10. Cook, R.A., Kunz, J., Fuchs, W., and Konz, R.C. (1998). "Behavior and Design of Single Adhesive Anchors Under Tensile Load in Uncracked Concrete." *ACI Structural Journal*, 95(1), pp. 9-26.
11. Davis, T. (2012) Sustained Load Performance of Adhesive Anchor Systems in Concrete. PhD Dissertation, University of Florida, Gainesville, FL.
12. Delhomme, F. and Brun, M. (2018). Pullout simulation of post installed chemically bonded anchors in UHPFRC. *MATEC Web of Conferences*. Vol. 199, p. 11007. EDP Sciences.
13. Eligehausen, R., Popov, E.P. & Bertero, V.V. (1983). Local bond stress-slip relationships of deformed bars under generalized excitations, Report No. UCB/EERC-83/23. Berkeley: University of California.
14. Eligehausen, R., Cook, R.A., and Appl, J. (2006). "Behavior and Design of Adhesive Bonded Anchors." *ACI Structural Journal*, 103(6), pp. 822-31.
15. Eligehausen, R., Mallée, R., & Silva, J. (2006). Anchorage in concrete construction (Vol. 10). John Wiley & Sons.
16. Epackachi, S., Esmaili, O., Mirghaderi, S. and Behbahani, A., (2015). "Behavior of adhesive bonded anchors under tension and shear loads." *Journal of Constructional Steel Research*, Vol. 114, pp.269-280.
17. Forbes, C., Evans, M., N. Hastings, and B. Peacock. (2011). Statistical Distributions. 4th ed. New York: J. Wiley.
18. Lee J. and Fenves G.L. (1998). Plastic-damage model for cyclic loading of concrete structure. ASCE J. Eng. Mech. Vol. 124, pp. 892-900.
19. Liu, H. (2020). Novel adhesive anchoring systems through engineered adhesive-concrete interface. PhD Dissertation, University of Wisconsin, Milwaukee, WI.
20. McCormac, J. and Brown, R. (2015). Design of reinforced concrete. John Wiley & Sons.

21. McVay, M., Cook, R.A., Krishnamurthy, K. (1996). “Pullout Simulation of Postinstalled Chemically Bonded Anchors.” *Journal of Structural Engineering*, ASCE, 122(9), 1016-1024.
22. Meszaros, J. (2002). “Tragverhalten von Verbunddübeln im ungerissenen und gerissenen Beton” (Load-bearing behavior of bonded anchors in uncracked and cracked concrete). Doctoral thesis, University of Stuttgart, Germany. In German
23. Luna Molina, F. J., Fernández Ruiz, M. A., Hernández Montes, E., and Alonso Alonso, M. C. (2015). Bond strength of galvanized steel: experimental and numerical study based on pull-out tests. 3rd International Conference on Mechanical Models in Structural Engineering, 143-158. Sevilla, España: CMMoST 2015. Víctor Compán Cardiel [etc.].
24. Popovics, S., (1970), March. A review of stress-strain relationships for concrete. ACI Journal Proceedings. Vol. 67, No. 3, pp. 243-248.
25. Petersen, D., Lin, Z., and Zhao, J. (2018) “Design of Anchor Reinforcement for Seismic Tension Loads,” *Engineering Structures*, Vol 164, pp. 109-118.
26. Wollmershauser, R. (1997). “Anchor Performance and the 5% Fractile,” Hilti Technical Services Bulletin, Hilti, Inc., Tulsa, OK. 5 pp.

Appendix I: Summary of specimen preparation and tests

Table I.1 Summary of specimen preparation

No.	Specimen name	Block	Face†	d_a (in.)	Drilling date	Testing date	Hole depth (in.)	Measured h_{ef} (in.)	Drilling time (s)	Vacuum time (s)	Brush time (s) per time*	Dispense time (s)	Installation time (s)	Num. of Injection strokes	Time
1	UC-0.5-2.0-#1	B1	1	0.5	25-Sep	27-Sep	2	2.03	15	10	3.5	10	95	1	Drilling 2:22 pm~15:46pm. Dispensing epoxy and installing anchor 15:55pm~16:46pm
2	UC-0.5-3.0-#1	B2	1	0.5	25-Sep	27-Sep	3.125	3	24	18	3.9	20	82	1.5	
3	UC-0.5-4.0-#1	BR9	1	0.5	25-Sep	27-Sep	3.9375	3.95	26	27	5.8	25	160	2	
4	UC#R-0.5-4.0-#1	BR7	1	0.5	25-Sep	27-Sep	3.875	3.78	25	15	4.5	32	89	2	
5	UC#R-0.5-5.0-#1	BR20	1	0.5	25-Sep	27-Sep	4.625	4.66	28	22	4.8	35	121	2.5	
6	UC#R-0.75-6.0-#1	BR22	1	0.75	25-Sep	30-Sep	5.875	5.61	67	25	4.6	56	73	5	
7	UC-0.625-2.5-#1	B3	1	0.625	26-Sep	28-Sep	2.625	2.63	23	20	3.6	25	60	1.25	Drilling 10:35 am~11:45am. Dispensing epoxy and installing anchor 1:30pm~2:15pm
8	UC-0.625-3.75-#1	B4	1	0.625	26-Sep	28-Sep	3.75	3.73	36	41	3.8	22	61	2	
9	UC-0.625-5.0-#1	B17	1	0.625	26-Sep	28-Sep	5.25	4.87	47	32	4.1	26	60	2.5	
10	UC#R-0.625-5.0-#1	BR21	1	0.625	26-Sep	28-Sep	5	4.72	45	17	4.1	27	60	2.5	
11	UC-0.75-3.0-#1	B5	1	0.75	26-Sep	30-Sep	2.938	2.91	45	21	2.8	22	60	2.5	
12	UC#R-0.75-4.5-#1	BR18	1	0.75	26-Sep	28-Sep	4.5	4.42	70	28	4.2	30	60	3.5	
13	C-0.5-2.0-#1	BR7	1	0.5	1-Oct	2-Oct	2	2.027	13	11	2.8	11	51	N/A	Drilling 10:35 am~11:45am. Dispensing epoxy and installing anchor 3:56 pm~4:14 pm
14	C-0.5-2.5-#1	BR9	1	0.5	1-Oct	2-Oct	2.378	2.436	19	18	3.4	13	42	N/A	
15	C-0.5-3.0-#1	BR7	1	0.5	1-Oct	2-Oct	2.875	2.825	21	23	3.4	13	54	N/A	
16	C-0.625-2.0-#1	BR20	1	0.625	1-Oct	2-Oct	2	1.976	24	17	1.9	14	33	N/A	
17	C-0.625-2.5-#1	B3	1	0.625	1-Oct	2-Oct	2.5	2.418	32	30	3.5	16	29	N/A	
18	C-0.625-3.0-#1	B4	1	0.625	1-Oct	2-Oct	3	2.937	31	20	4.1	19	43	N/A	
19	C-0.75-2.0-#1	BR20	1	0.75	1-Oct	2-Oct	2	1.879	37	16	2.4	19	32	N/A	
20	C-0.75-2.5-#1	BR20	1	0.75	1-Oct	2-Oct	2.4375	2.314	43	30	2.6	21	41	N/A	
21	C-0.75-3.0-#1	BR20	1	0.75	1-Oct	2-Oct	3	3.006	47	22	2.8	36	26	N/A	
22	C-0.5-2.0-#2	BR20	1	0.5	3-Oct	4-Oct	2.0625	2.055	15	12	2.3	6	30	N/A	Drilling 14:53 pm~16:31 pm. Dispensing epoxy and installing
23	C-0.5-2.5-#2	BR20	1	0.5	3-Oct	4-Oct	2.5	2.585	17	18	3.7	10	45	N/A	
24	C-0.5-3.0-#2	BR20	1	0.5	3-Oct	4-Oct	3.125	3.063	19	13	2.8	16	53	N/A	
25	C-0.625-2.5-#2	BR22	1	0.625	3-Oct	4-Oct	2.4375	2.458	25	16	3.8	22	35	N/A	

26	C-0.625-3.0-#2	BR22	1	0.625	3-Oct	4-Oct	3.0625	3.051	31	22	3	23	33	N/A	anchor 17:00 pm~17:18 pm
27	C-0.625-3.75-#2	BR22	1	0.625	3-Oct	4-Oct	3.8125	3.683	39	21	3.8	38	42	N/A	
28	C-0.75-2.5-#2	B3	1	0.75	3-Oct	4-Oct	2.5625	2.493	49	25	4.1	27	34	N/A	
29	C-0.75-3.0-#2	BR9	1	0.75	3-Oct	4-Oct	3	2.89	50	20	3.2	32	30	N/A	
30	C-0.75-4.5-#2	BR22	1	0.75	3-Oct	4-Oct	4.3125	4.286	66	20	6.4	51	58	N/A	
31	UC-0.5-3.75-#2	B1	2	0.5	6-Oct	7-Oct	3.75	3.707	22	18	3.5	21	46	2	Drilling 14:00 pm~15:15 pm. Dispensing epoxy and installing anchor 15:27 pm~15:40 pm
32	UC-0.5-3.0-#2	B2	2	0.5	6-Oct	7-Oct	N/A	N/A	N/A	N/A	N/A	N/A	N/A	N/A	
33	UC-0.5-4.0-#2	BR9	2	0.5	6-Oct	7-Oct	4	3.976	27	17	3.5	25	50	2	
34	UC#R-0.5-4.0-#2	BR7	2	0.5	6-Oct	7-Oct	4.0625	4.07	29	22	3.32	21	53	2	
35	UC#R-0.5-5.0-#2	BR20	2	0.5	6-Oct	7-Oct	5.125	4.885	31	21	4.3	23	65	2.5	
36	UC#R-0.75-6.0-#2	BR22	2	0.75	6-Oct	8-Oct	6.25	5.864	83	34	5.4	40	69	5	
37	UC-0.625-2.5-#2	B3	2	0.625	5-Oct	8-Oct	2.5	2.543	30	22	2.8	27	29	1.5	Drilling 16:40 pm~17:58 pm. Dispensing epoxy and installing anchor 20:18 pm~20:40 pm
38	UC-0.625-3.75-#2	B4	2	0.625	5-Oct	8-Oct	3.75	3.716	37	38	4.1	28	42	2	
39	UC-0.625-5.0-#2	B17	2	0.625	5-Oct	8-Oct	5	4.835	50	42	4.3	29	45	2.5	
40	UC#R-0.625-5.0-#2	BR21	2	0.625	5-Oct	8-Oct	5.0625	4.881	46+5	26+10	3.5	30	46	2.5	
41	UC-0.75-3.0-#2	B5	2	0.75	5-Oct	8-Oct	2.9375	2.854	44	21	3.4	29	46	2.5	
42	UC#R-0.75-4.5-#2	BR18	2	0.75	5-Oct	8-Oct	4.5	4.581	65	35	4.3	32	60	3.5	
43	C-0.5-2.0-#3	B20	2	0.5	11-Oct	12-Oct	1.9375	1.979	13	17	2.5	9.9	49	1	Drilling 11:29 am~14:30 pm. Dispensing epoxy and installing anchor 15:24 pm~15:43 pm
44	C-0.5-2.5-#3	BR9	2	0.5	11-Oct	12-Oct	2.625	2.695	18	16	3.4	13	43	1.25	
45	C-0.5-3.0-#3	BR9	2	0.5	11-Oct	12-Oct	3	2.982	21	20	3.4	18	36	1.25	
46	C-0.625-2.5-#3	B5	2	0.625	11-Oct	12-Oct	2.75	2.694	33	13	2.5	25	36	1.5	
47	C-0.625-3.0-#3	B3	2	0.625	11-Oct	12-Oct	2.875	2.829	37	34	3.2	23	25	1.75	
48	C-0.625-3.75-#3	B3	2	0.625	11-Oct	12-Oct	3.5625	3.508	45	27	4.3	26	34	2	
49	C-0.75-2.5-#3	BR20	2	0.75	11-Oct	12-Oct	2.375	2.312	39	28	2.4	24	33	2	
50	C-0.75-3.0-#3	BR20	2	0.75	11-Oct	12-Oct	3	2.886	48	30	3.8	37	23	2.25	
51	C-0.75-4.5-#3	BR20	2	0.75	11-Oct	12-Oct	4.375	4.27	67	24	4.3	46	32	3.5	
52	UC-0.5-2.5-#3	B1	3	0.5	13-Oct	14-Oct	2.625	2.714	20	33	4.4	8	33	1	Drilling 11:30 am~12:22 pm. Dispensing epoxy and installing
53	UC-0.5-3.0-#3	B2	3	0.5	N/A	N/A	N/A	N/A	N/A	N/A	N/A	N/A	N/A	N/A	
54	UC-0.5-4.0-#3	BR7	3	0.5	13-Oct	14-Oct	4	4.028	30	30	4.8	22	33	2	
55	UC#R-0.5-4.0-#3	BR9	3	0.5	13-Oct	14-Oct	4	4.165	28	44	4.7	17	32	2	

56	UC#R-0.5-4.5-#3	BR20	3	0.5	13-Oct	14-Oct	4.4375	4.438	4+45	26	5	24	40	2.25	anchor 13:48 pm~14:05 pm
57	UC#R-0.75-6.0-#3	BR22	3	0.75	13-Oct	14-Oct	6	5.754	84	30	5.1	30	46	4.5	
58	C-0.75-6.0-#4	BR22	3	0.75	13-Oct	14-Oct	5.9375	5.826	84	30	5.1	25	56	4.5	
59	UC-0.625-2.5-#3	B3	3	0.625	14-Oct	16-Oct	2.5	2.377	25	18	3.5	14	20	1.5	Drilling 12:20 pm~13:48 pm, 15:08 pm ~ 15:43 pm. Dispensing epoxy and installing anchor 16:04 pm~16:18 pm.
60	UC-0.625-3.75-#3	B4	3	0.625	14-Oct	15-Oct	3.6875	3.725	33	19	3.4	15	27	2	
61	UC-0.625-5.0-#3	B17	3	0.625	14-Oct	15-Oct	5	4.808	51	30	4.9	20	45	3	
62	UC#R-0.625-5.0-#3	BR21	3	0.625	14-Oct	16-Oct	5	4.867	48	30	5.4	15	36	3	
63	UC-0.75-3.0-#3	B5	3	0.75	14-Oct	16-Oct	3	3.032	48	36	3.3	15	30	2.25	
64	UC#R-0.75-4.5-#3	BR18	3	0.75	14-Oct	16-Oct	4.375	4.422	67	33	4.9	23	54	3.5	
65	UC-0.5-2.0-#4	B1	4	0.5	21-Nov	22-Nov	2	2.029	19	8	1.2	9	20	1	Drilling 11:15 am~14:58 pm. Dispensing epoxy and installing anchor 15:10 pm~15:35pm.
66	UC-0.5-3.0-#4	B2	4	0.5	N/A	N/A	N/A	N/A	N/A	N/A	N/A	N/A	N/A	N/A	
67	UC-0.5-4.0-#4	BR7	4	0.5	21-Nov	22-Nov	4	3.916	34	8	1.4	N/A	N/A	2	
68	UC#R-0.5-4.0-#4	BR9	4	0.5	21-Nov	22-Nov	4	3.939	34	10	1.3	N/A	N/A	2	
69	UC#R-0.5-3.0-#4	BR20	4	0.5	21-Nov	22-Nov	3	2.934	24	9	1.5	N/A	N/A	1.5	
70	UC#R-0.75-6.0-#4	BR22	4	0.75	21-Nov	22-Nov	5.625	5.616	106	23	1.7	N/A	N/A	5	
71	UC-0.625-2.5-#4	B3	4	0.625	N/A	N/A	N/A	N/A	N/A	N/A	N/A	N/A	N/A	N/A	
72	UC-0.625-3.75-#4	B4	4	0.625	21-Nov	25-Nov	3.6875	3.744	53	13	2	N/A	N/A	2	
73	UC-0.625-5.0-#4	B17	4	0.625	21-Nov	25-Nov	5	4.92	59	15	2.2	N/A	N/A	3	
74	UC#R-0.625-5.0-#4	BR21	4	0.625	21-Nov	25-Nov	4.9375	4.885	63	17	2	N/A	N/A	3	
75	UC-0.75-3.0-#4	B5	4	0.75	21-Nov	25-Nov	2.875	2.764	30	13	1.4	N/A	N/A	2.5	
76	UC#R-0.75-4.5-#4	BR18	4	0.75	21-Nov	25-Nov	4.25	4.268	80	19	1.5	N/A	N/A	3.5	

†Face 1: top face; Face 2: bottom face; Face 3: east or north face; and Face 4: west or south face as shown in Figure I.1.

*: Hole brushing process included a total of four times of brushing.

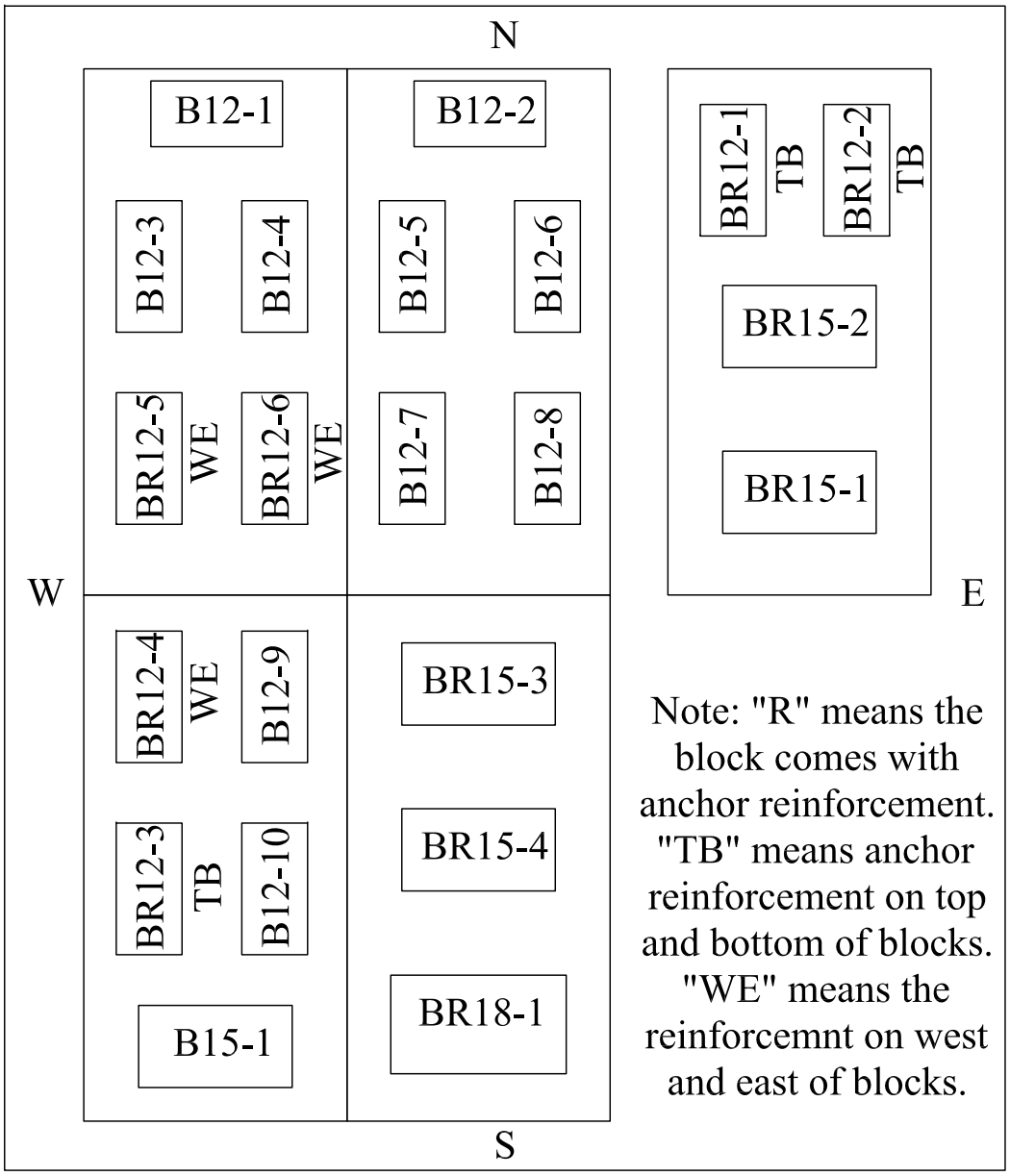

Figure I.1 Casting position of concrete blocks

Table I.2 Summary of test results

No.	Specimen name	d_a (in.)	h_{ef} (in.) (Measured)	Peak Load (v)	Peak load (kips)	Failure mode	Length of A-C bond failure (in)	Bond strength (psi)
1	UC-0.5-2.0-#1	0.5	2.03	1.24	6.66	Breakout	N/A	2089
2	UC-0.5-3.0-#1	0.5	3	2.25	12.03	Breakout	N/A	2553
3	UC-0.5-4.0-#1	0.5	3.95	2.04	10.91	Pullout	3.5	1760
4	UC#R-0.5-4.0-#1	0.5	3.78	2.37	12.69	Pullout+Breakout	N/A	2138
5	UC#R-0.5-5.0-#1	0.5	4.66	3.07	16.42	Steel failure	N/A	2244
6	UC#R-0.75-6.0-#1	0.75	5.61	4.81	25.73	Pullout+Breakout	N/A	1947
7	UC-0.625-2.5-#1	0.625	2.63	1.20	6.42	Pullout+Breakout	N/A	1243
8	UC-0.625-3.75-#1	0.625	3.73	2.10	11.25	Pullout+Breakout	N/A	1536
9	UC-0.625-5.0-#1	0.625	4.87	3.10	16.57	Breakout	N/A	1733
10	UC#R-0.625-5.0-#1	0.625	4.72	3.17	16.97	Pullout+Breakout	N/A	1832
11	UC-0.75-3.0-#1	0.75	2.91	2.07	11.06	Breakout	N/A	1614
12	UC#R-0.75-4.5-#1	0.75	4.42	3.72	19.90	Pullout+Breakout	N/A	1911
13	C-0.5-2.0-#1	0.5	2.027	1.76	9.43	AC	N/A	2964
14	C-0.5-2.5-#1	0.5	2.436	2.58	13.82	AC+AS	N/A	3614
15	C-0.5-3.0-#1	0.5	2.825	2.66	14.21	AC+AS	N/A	3205
16	C-0.625-2.0-#1	0.625	1.976	1.27	6.81	AC	N/A	1756
17	C-0.625-2.5-#1	0.625	2.418	2.50	13.38	AC+AS	N/A	2820
18	C-0.625-3.0-#1	0.625	2.937	2.16	11.57	AC	N/A	2008
19	C-0.75-2.0-#1	0.75	1.879	1.50	8.02	AC	N/A	1812
20	C-0.75-2.5-#1	0.75	2.314	1.46	7.79	AC	N/A	1430
21	C-0.75-3.0-#1	0.75	3.006	2.50	13.38	AC	N/A	1890
22	C-0.5-2.0-#2	0.5	2.055	1.48	7.92	AC	N/A	2455
23	C-0.5-2.5-#2	0.5	2.585	2.53	13.55	AC+AS	N/A	3338
24	C-0.5-3.0-#2	0.5	3.063	2.47	13.22	AC+AS	N/A	2749
25	C-0.625-2.5-#2	0.625	2.458	1.61	8.62	AC	N/A	1787
26	C-0.625-3.0-#2	0.625	3.051	2.64	14.14	AC	N/A	2361
27	C-0.625-3.75-#2	0.625	3.683	2.85	15.24	AC+AS	N/A	2108

28	C-0.75-2.5-#2	0.75	2.493	2.51	13.42	AC	N/A	2286
29	C-0.75-3.0-#2	0.75	2.89	1.99	10.65	AC	N/A	1565
30	C-0.75-4.5-#2	0.75	4.286	3.52	18.86	AC	N/A	1868
31	UC-0.5-3.75-#2	0.5	3.707	1.63	8.71	Pullout+Breakout	2.5	1497
32	UC-0.5-3.0-#2	0.5	N/A	N/A	N/A	N/A	N/A	N/A
33	UC-0.5-4.0-#2	0.5	3.976	2.37	12.69	Pullout+Breakout	3.25	2032
34	UC#R-0.5-4.0-#2	0.5	4.07	2.37	12.65	Pullout+Breakout	2.75	1980
35	UC#R-0.5-5.0-#2	0.5	4.885	3.25	17.39	Steel failure	N/A	2268
36	UC#R-0.75-6.0-#2	0.75	5.864	4.89	26.14	Pullout+Breakout		1893
37	UC-0.625-2.5-#2	0.625	2.543	1.08	5.76	Pullout	2.0	1154
38	UC-0.625-3.75-#2	0.625	3.716	2.15	11.53	Pullout	3.25	1581
39	UC-0.625-5.0-#2	0.625	4.835	3.45	18.46	Breakout	N/A	1945
40	UC#R-0.625-5.0-#2	0.625	4.881	3.21	17.20	Pullout+Breakout	2.625	1795
41	UC-0.75-3.0-#2	0.75	2.854	1.66	8.89	Pullout	N/A	1323
42	UC#R-0.75-4.5-#2	0.75	4.581	2.91	15.56	Pullout+Breakout	N/A	1443
43	C-0.5-2.0-#3	0.5	1.979	1.29	6.90	AC	N/A	2220
44	C-0.5-2.5-#3	0.5	2.695	2.20	11.78	AC	N/A	2783
45	C-0.5-3.0-#3	0.5	2.982	1.81	9.66	AC+AS	N/A	2063
46	C-0.625-2.5-#3	0.625	2.694	1.87	9.99	AC	N/A	1890
47	C-0.625-3.0-#3	0.625	2.829	2.19	11.70	AC	N/A	2108
48	C-0.625-3.75-#3	0.625	3.508	1.63	8.71	AC	N/A	1266
49	C-0.75-2.5-#3	0.75	2.312	1.40	7.50	AC	N/A	1378
50	C-0.75-3.0-#3	0.75	2.886	1.82	9.72	AC	N/A	1430
51	C-0.75-4.5-#3	0.75	4.27	3.63	19.40	AC	N/A	1929
52	UC-0.5-2.5-#3	0.5	2.714	1.61	8.59	Breakout	N/A	2017
53	UC-0.5-3.0-#3	0.5	N/A	N/A	N/A	N/A	N/A	N/A
54	UC-0.5-4.0-#3	0.5	4.028	2.50	13.40	Pullout+Breakout	2.25	2119
55	UC#R-0.5-4.0-#3	0.5	4.165	2.85	15.22	Pullout+Breakout	N/A	2328
56	UC#R-0.5-4.5-#3	0.5	4.438	3.50	18.74	Steel failure	N/A	2690
57	UC#R-0.75-6.0-#3	0.75	5.754	4.86	26.02	Pullout+Breakout	3.25	1920

58	C-0.75-6.0-#4	0.75	5.826	5.30	28.35	AC	N/A	2066
59	UC-0.625-2.5-#3	0.625	2.377	1.85	9.89	Breakout	N/A	2119
60	UC-0.625-3.75-#3	0.625	3.725	1.84	9.86	Pullout+Breakout	N/A	1349
61	UC-0.625-5.0-#3	0.625	4.808	2.39	12.76	Breakout	N/A	1353
62	UC#R-0.625-5.0-#3	0.625	4.867	3.35	17.95	Pullout+Breakout	N/A	1879
63	UC-0.75-3.0-#3	0.75	3.032	1.80	9.64	Pullout+Breakout	N/A	1350
64	UC#R-0.75-4.5-#3	0.75	4.422	3.15	16.86	Pullout+Breakout	N/A	1619
65	UC-0.5-2.0-#4	0.5	2.029	1.21	6.49	Breakout	N/A	2038
66	UC-0.5-3.0-#4	0.5	N/A	N/A	N/A	N/A	N/A	N/A
67	UC-0.5-4.0-#4	0.5	3.916	2.11	11.27	Breakout	N/A	1833
68	UC#R-0.5-4.0-#4	0.5	3.939	2.41	12.87	Pullout+Breakout	2.25	2082
69	UC#R-0.5-3.0-#4	0.5	2.934	2.32	12.40	Pullout+Breakout	1.5	2693
70	UC#R-0.75-6.0-#4	0.75	5.616	4.33	23.15	Pullout	N/A	1750
71	UC-0.625-2.5-#4	N/A	N/A	N/A	N/A	N/A	N/A	N/A
72	UC-0.625-3.75-#4	0.625	3.744	1.86	9.96	Pullout+Breakout	2.25	1355
73	UC-0.625-5.0-#4	0.625	4.92	1.99	10.63	Pullout	4	1101
74	UC#R-0.625-5.0-#4	0.625	4.885	3.31	17.69	Pullout	N/A	1846
75	UC-0.75-3.0-#4	0.75	2.764	1.74	9.32	Pullout+Breakout	N/A	1431
76	UC#R-0.75-4.5-#4	0.75	4.268	3.60	19.26	Pullout+Breakout	N/A	1916

Appendix II: Details of confined tension tests

1. C-0.5-2.0-#1

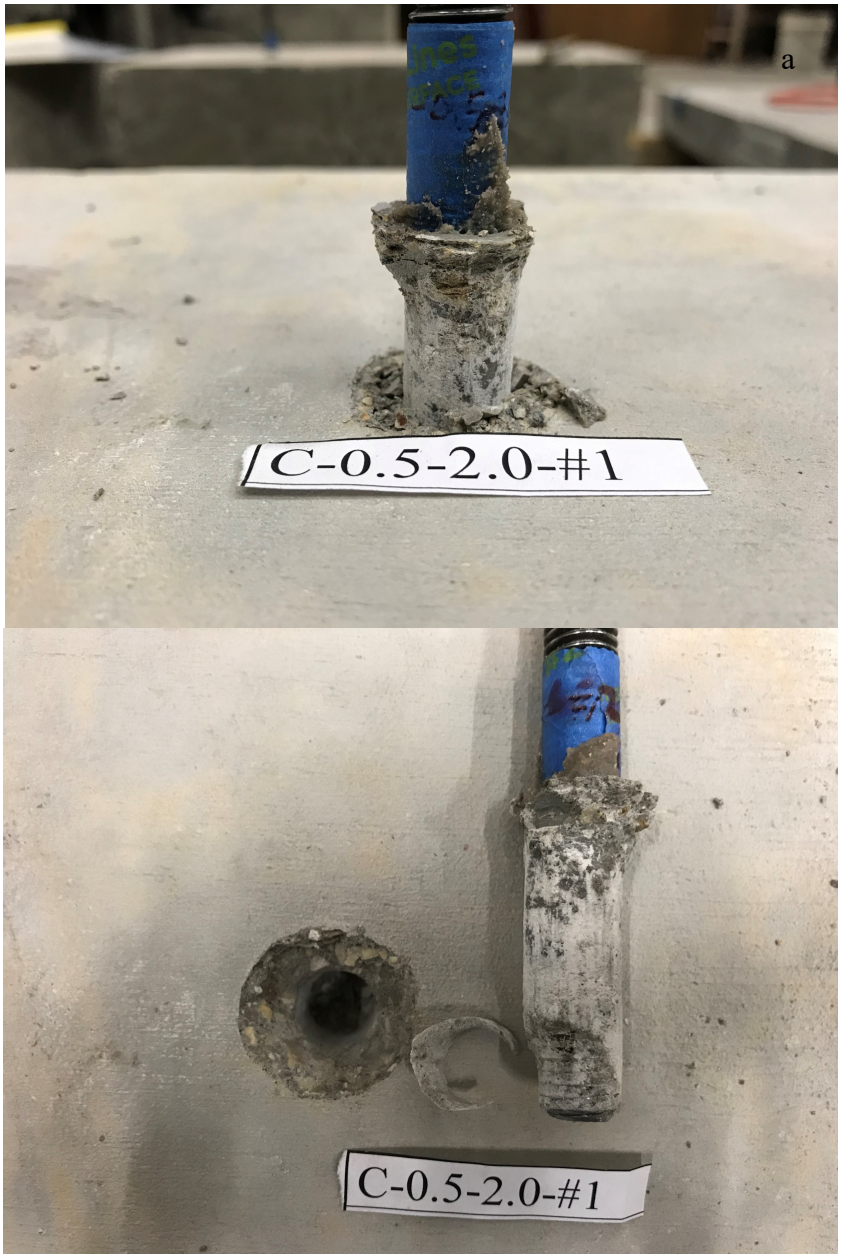

Adhesive-concrete interface (AC) bond failure.

Figure II.1. Observed behavior of Specimen C-0.5-2.0-#1

2. C-0.5-2.0-#2



Adhesive-concrete interface (AC) bond failure.

Figure II.2. Observed behavior of Specimen C-0.5-2.0-#2

3. C-0.5-2.0-#3

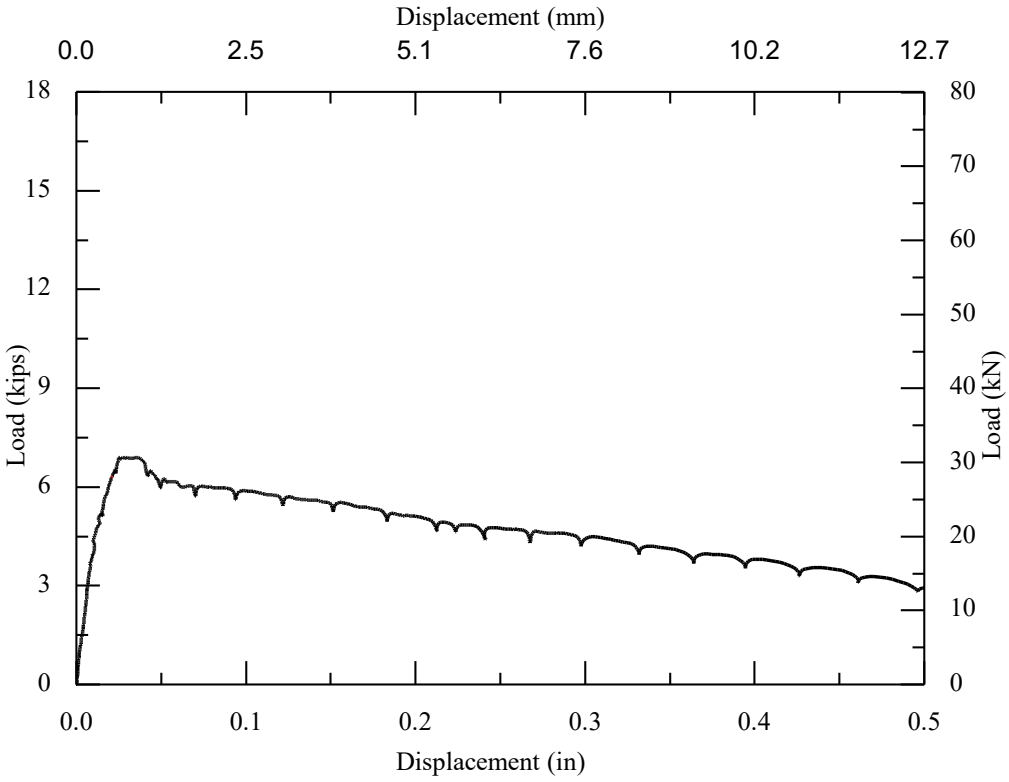

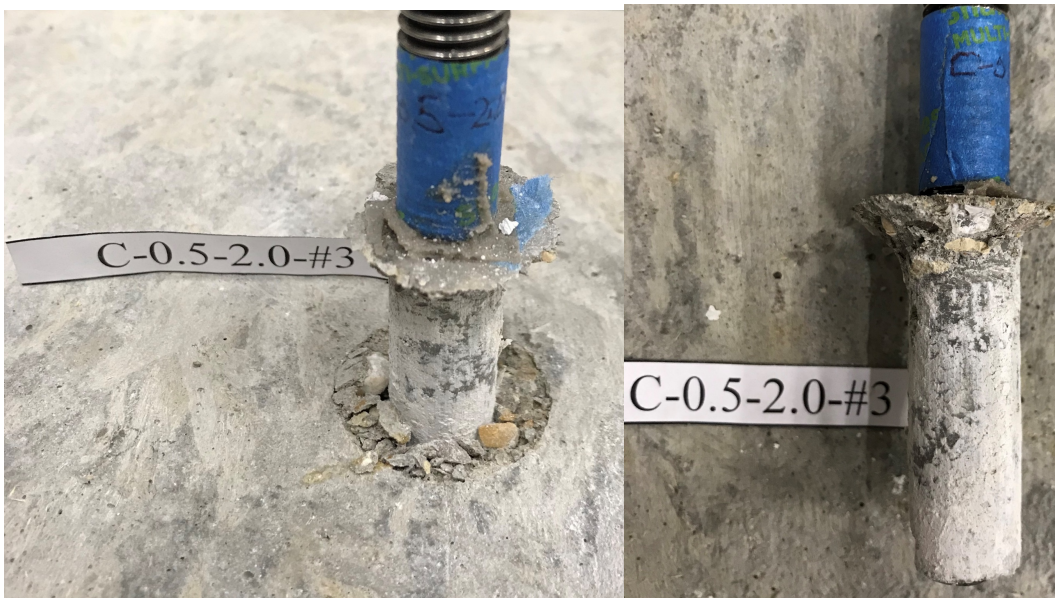

Adhesive-concrete interface (AC) bond failure.

Figure II.3. Observed behavior of Specimen C-0.5-2.0-#3

4. C-0.5-2.5-#1

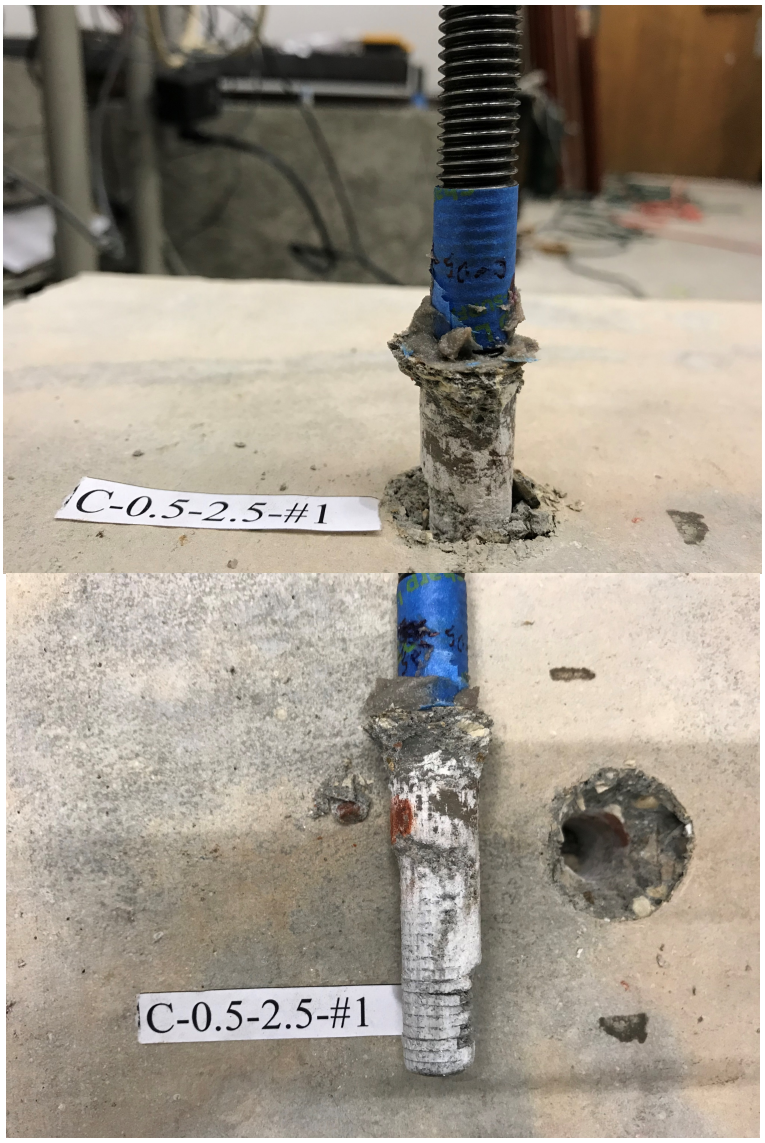

Adhesive-concrete and Adhesive-steel interface (AC+AS) bond failure.

Figure II.4. Observed behavior of Specimen C-0.5-2.5-#1

5. C-0.5-2.5-#2

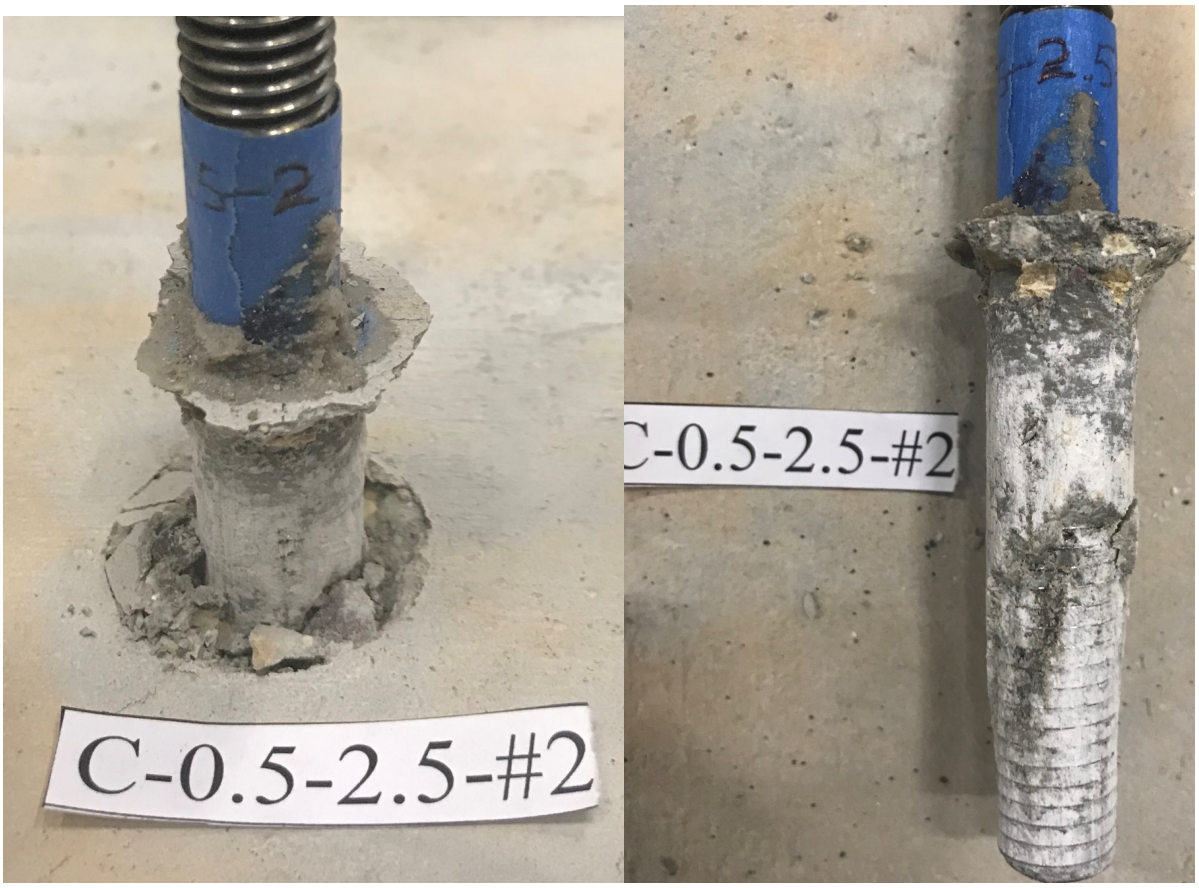

Adhesive-concrete and Adhesive-steel interface (AC+AS) bond failure.

Figure II.5. Observed behavior of Specimen C-0.5-2.5-#2

6. C-0.5-2.5-#3

Drill frame was shaking due to the concrete surface was not flat.

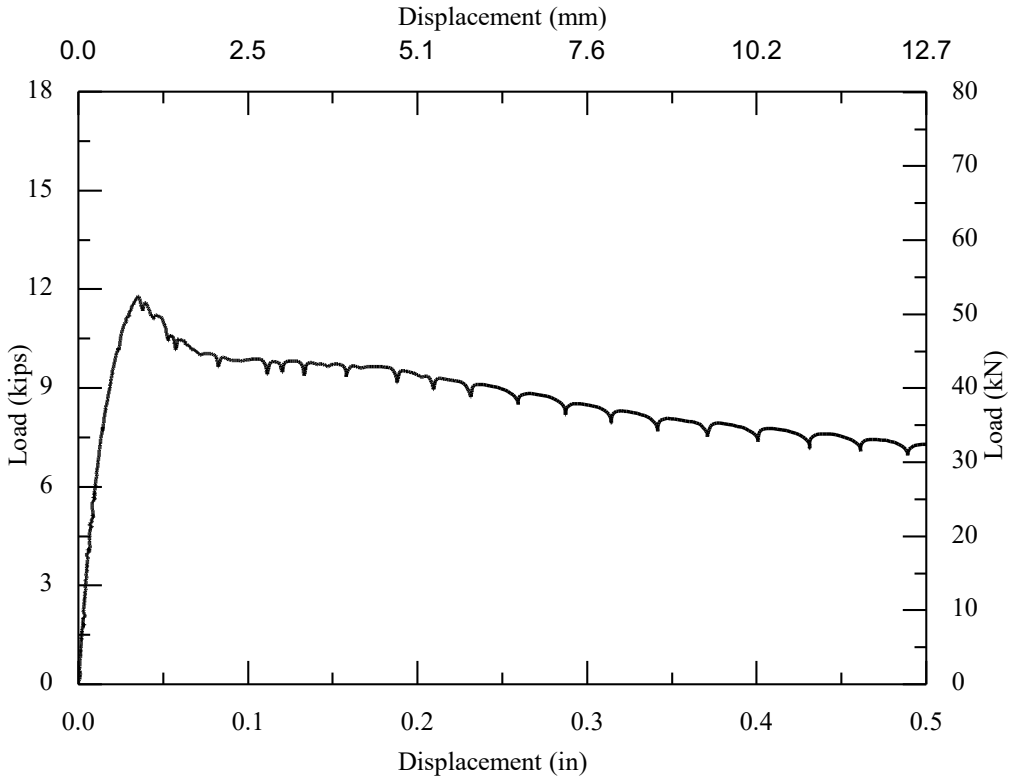

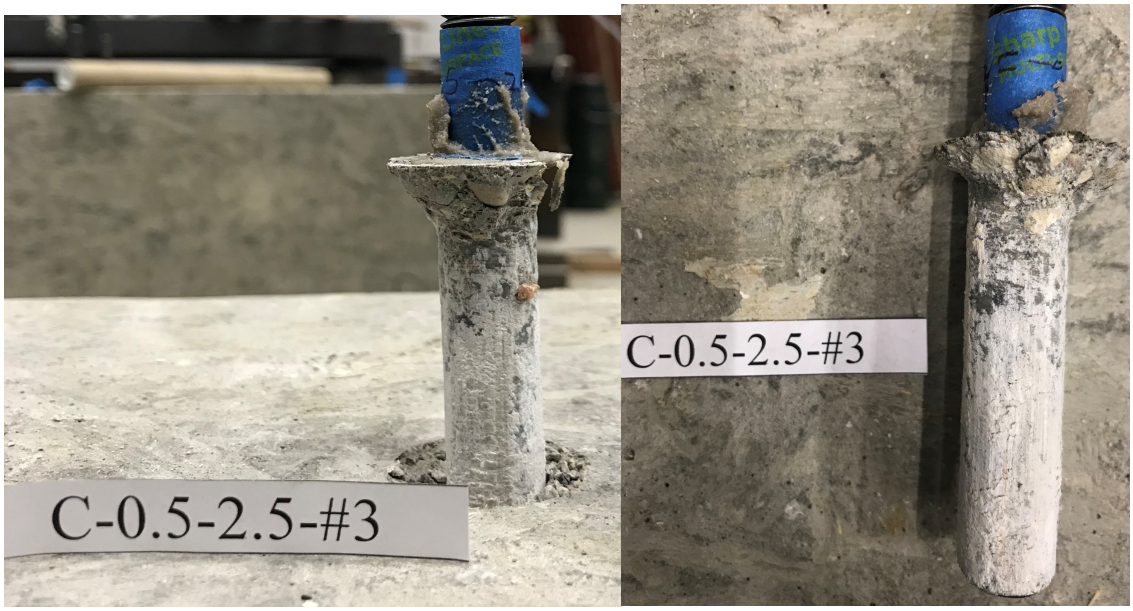

Adhesive-concrete interface (AC) bond failure.

Figure II.6. Observed behavior of Specimen C-0.5-2.5-#3

7. C-0.5-3.0-#1



Adhesive-concrete and Adhesive-steel interface (AC+AS) bond failure.

Figure II.7. Observed behavior of Specimen C-0.5-3.0-#1

8. C-0.5-3.0-#2

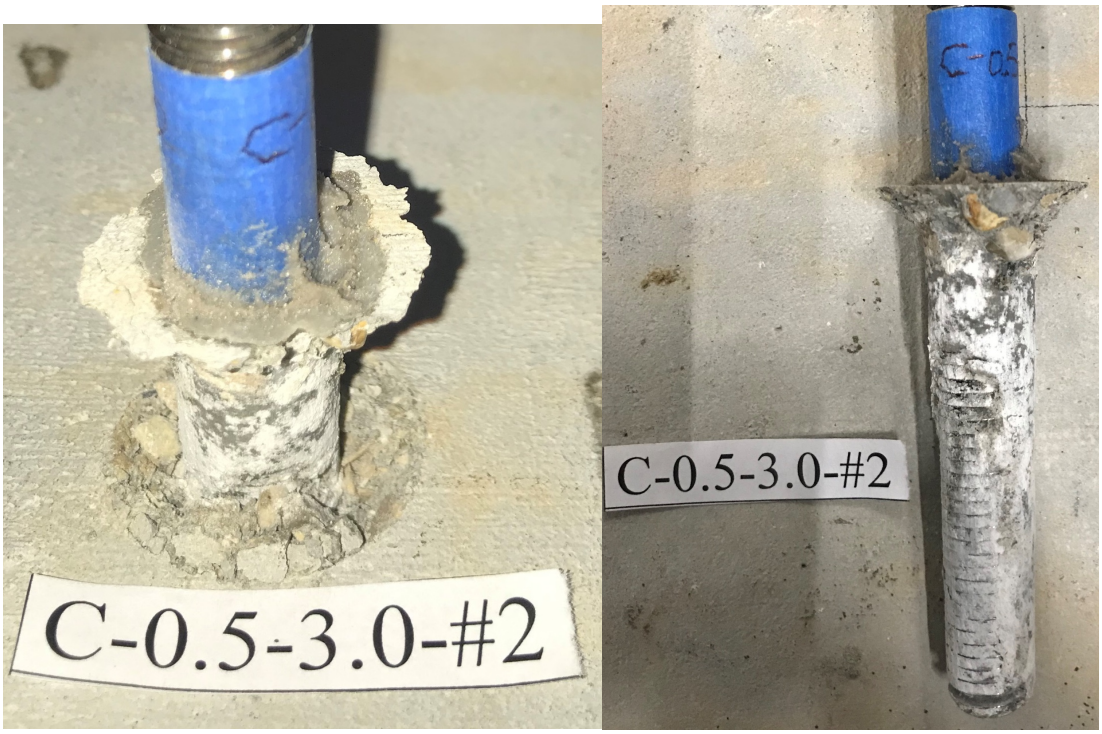

Adhesive-concrete and Adhesive-steel interface (AC+AS) bond failure.

Figure II.8. Observed behavior of Specimen C-0.5-3.0-#2

9. C-0.5-3.0-#3

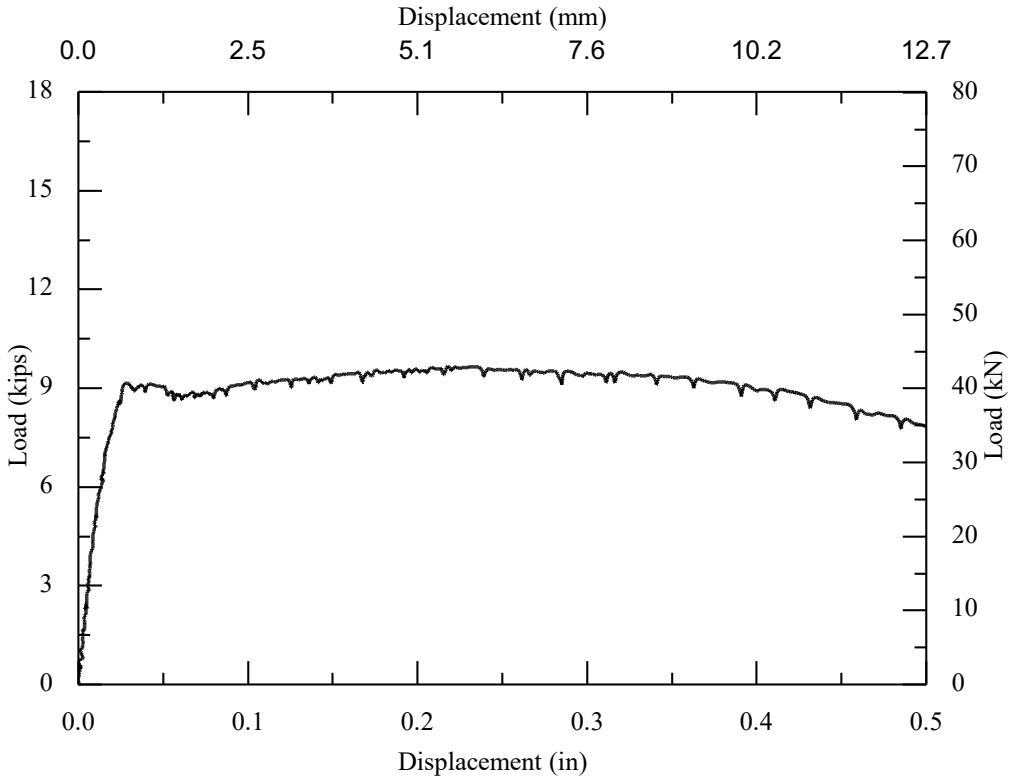

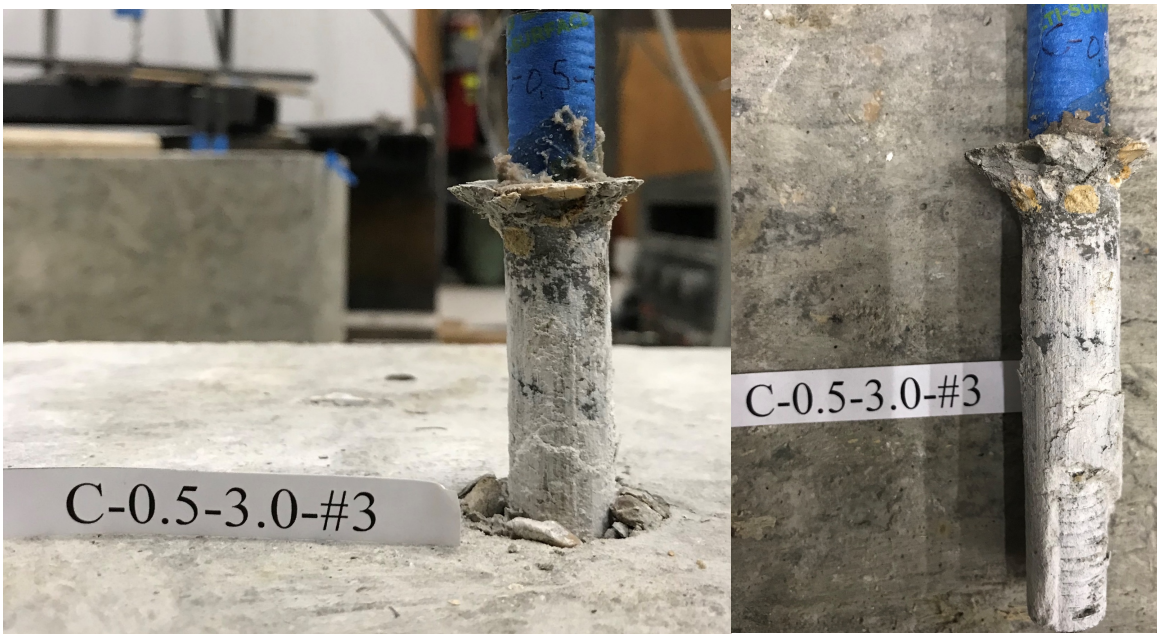

Adhesive-concrete and Adhesive-steel interface (AC+AS) bond failure.

Figure II.9. Observed behavior of Specimen C-0.5-3.0-#3

10. C-0.625-2.0-#1

Small concrete pieces left at the bottom of the hole. A 0.3 in. diameter hole on wall was seen at the bottom of the hole, which may have been the reason for the partial A-S failure shown below.





Adhesive-concrete interface (AC) bond failure.

Figure II.10. Observed behavior of Specimen C-0.625-2.0-#1

11. C-0.625-2.5-#1

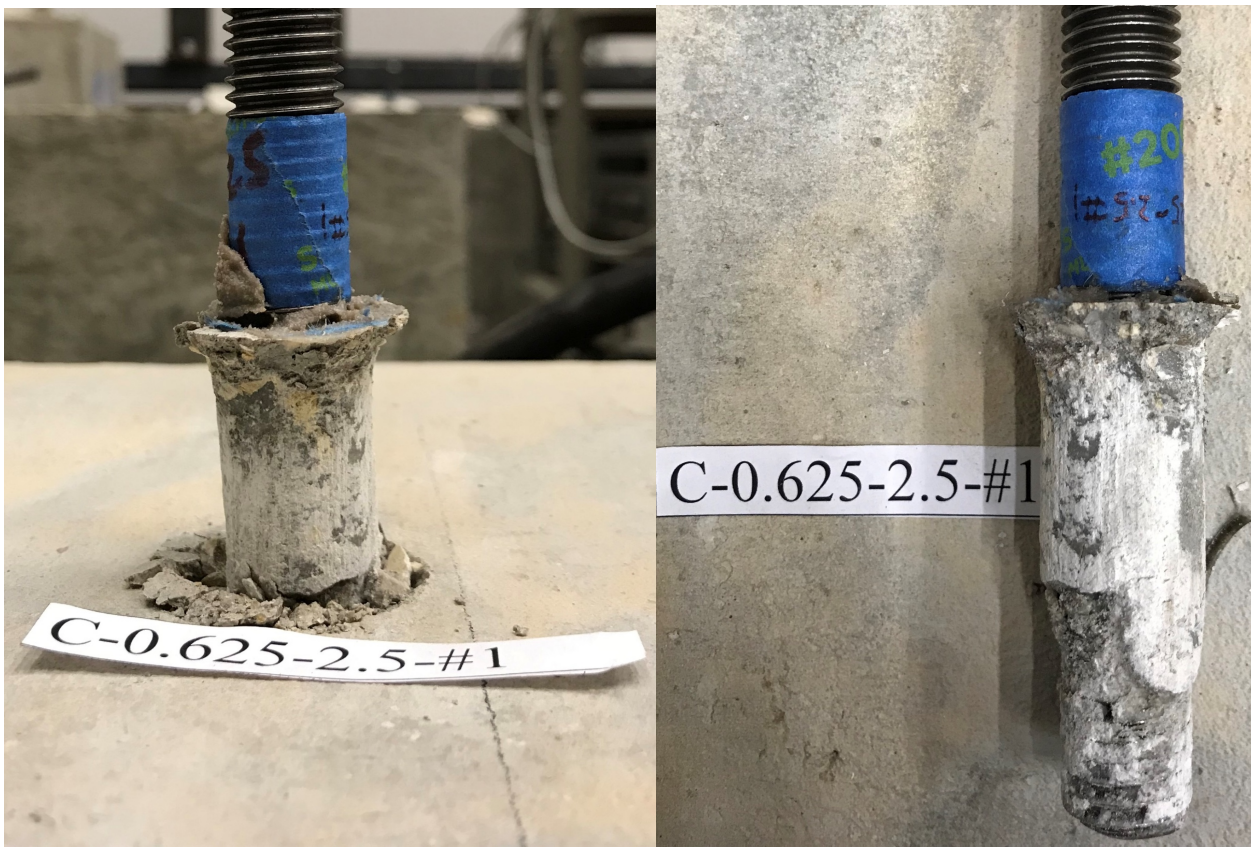

Adhesive-concrete and Adhesive-steel interface (AC+AS) bond failure.

Figure II.11. Observed behavior of Specimen C-0.625-2.5-#1

12. C-0.625-2.5-#2

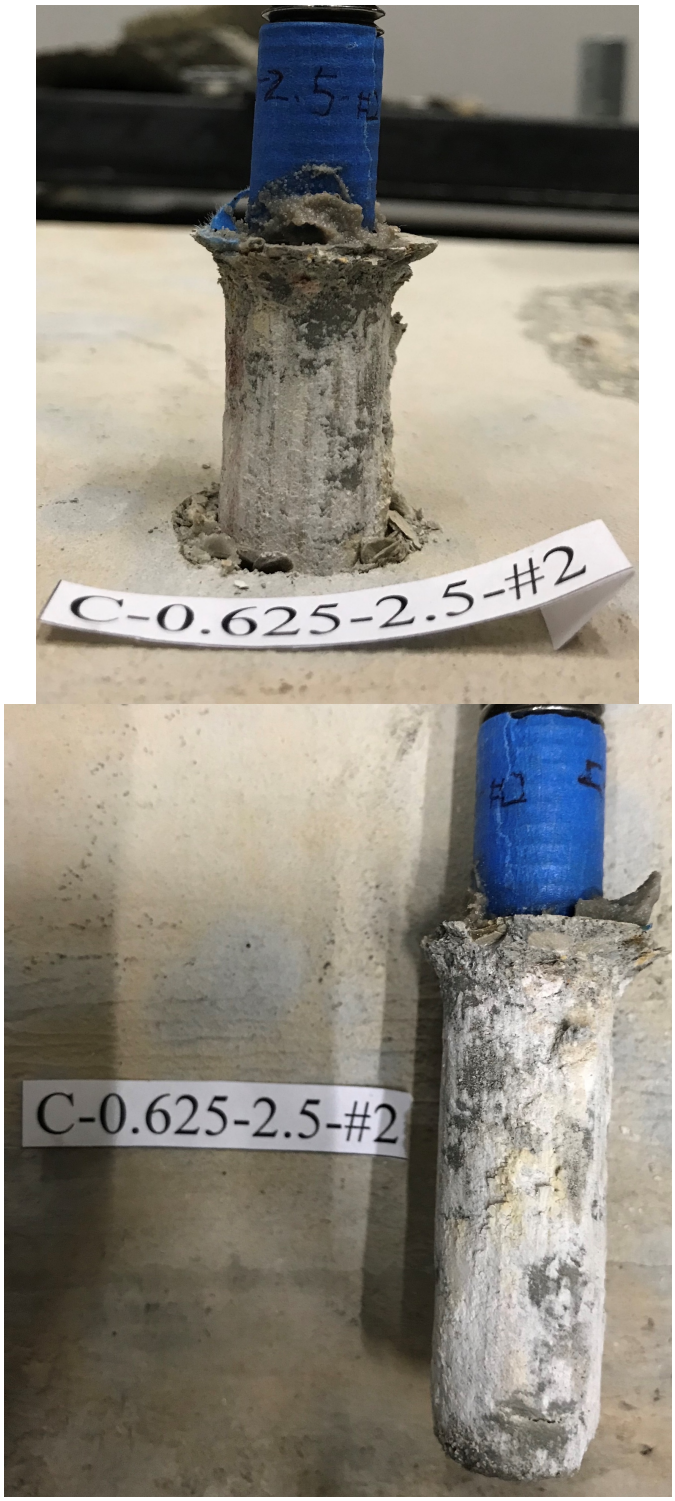

Adhesive-concrete interface (AC) bond failure.

Figure II.12. Observed behavior of Specimen C-0.625-2.5-#2

13. C-0.625-2.5-#3

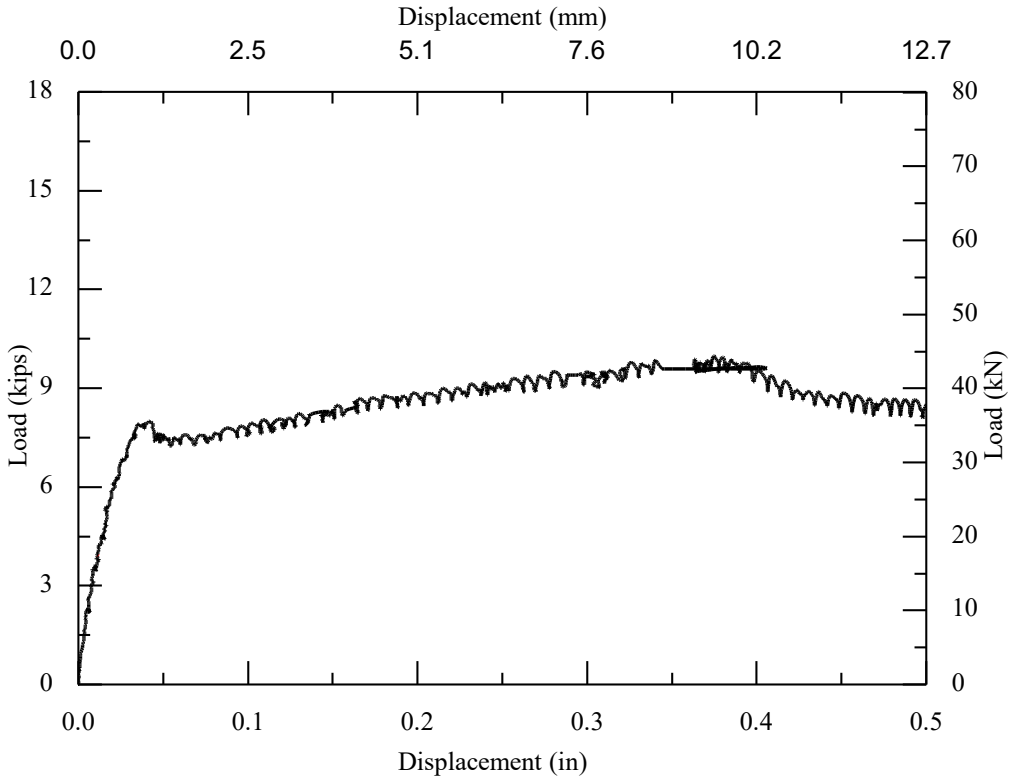

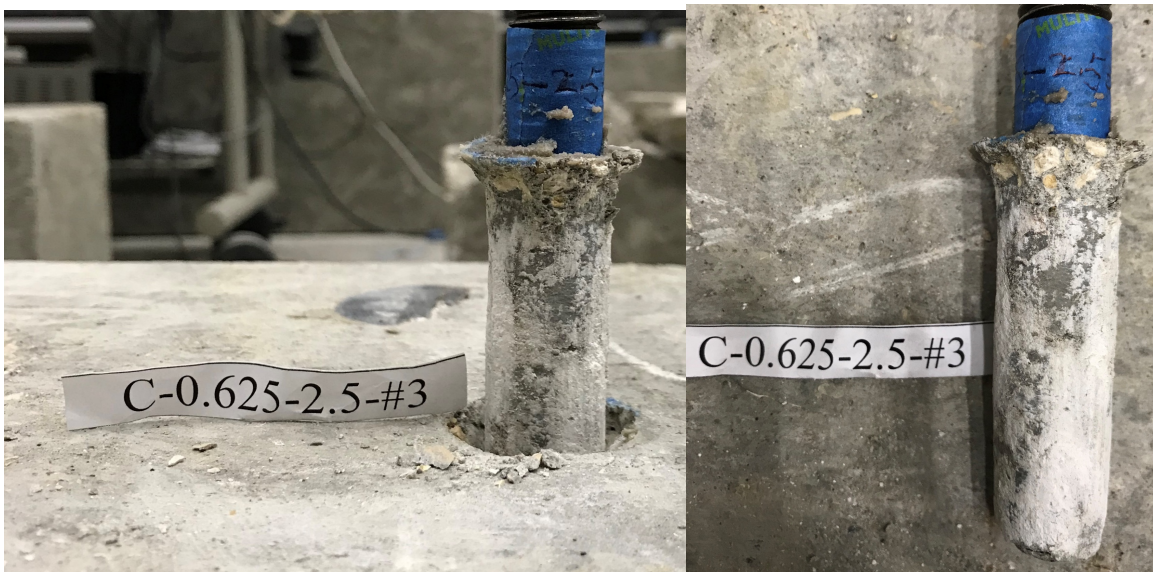

Adhesive-concrete interface (AC) bond failure.

Figure II.13. Observed behavior of Specimen C-0.625-2.5-#3

14. C-0.625-3.0-#1

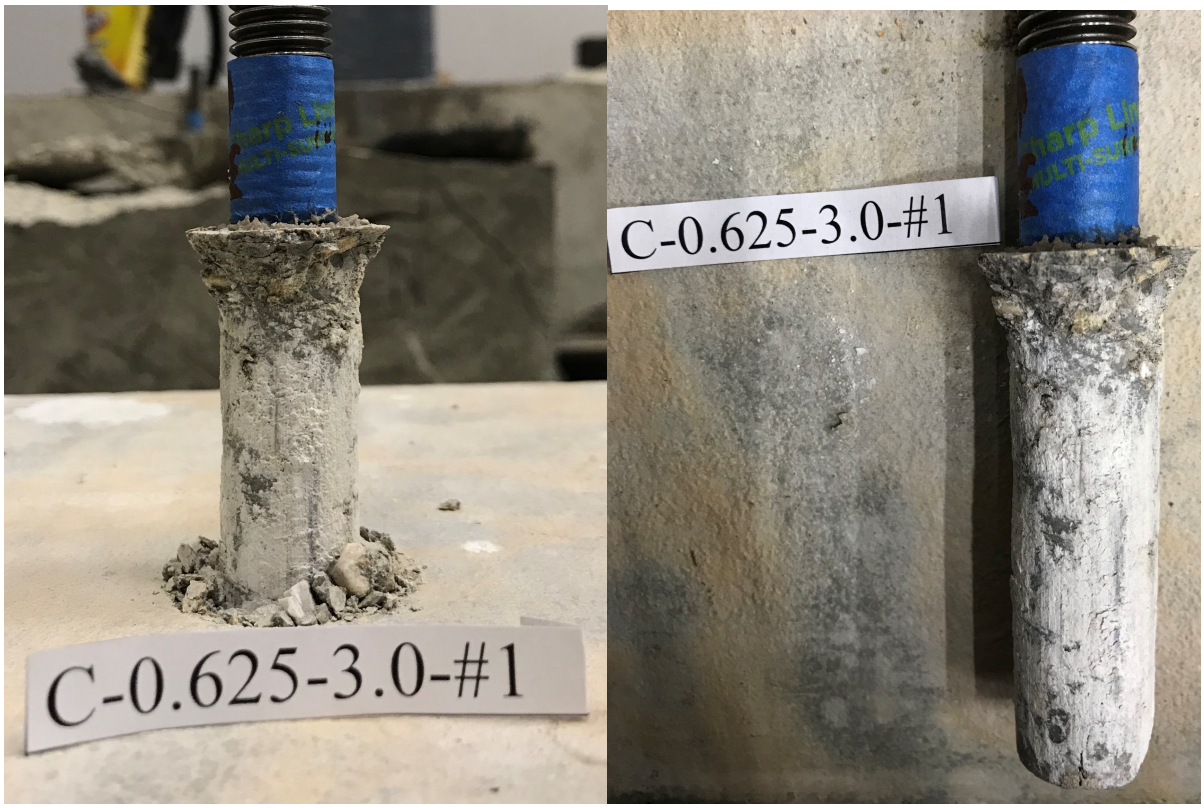

Adhesive-concrete interface (AC) bond failure.

Figure II.14. Observed behavior of Specimen C-0.625-3.0-#1

15. C-0.625-3.0-#2

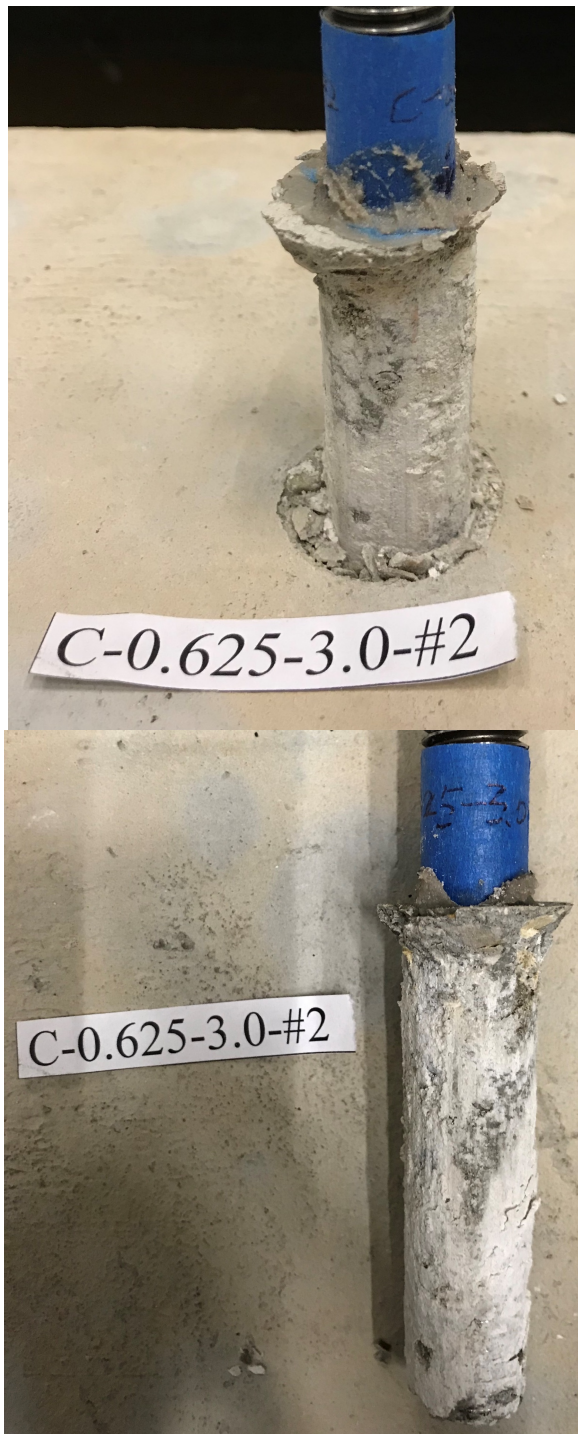

Adhesive-concrete interface (AC) bond failure.

Figure II.15. Observed behavior of Specimen C-0.625-3.0-#2

16. C-0.625-3.0-#3

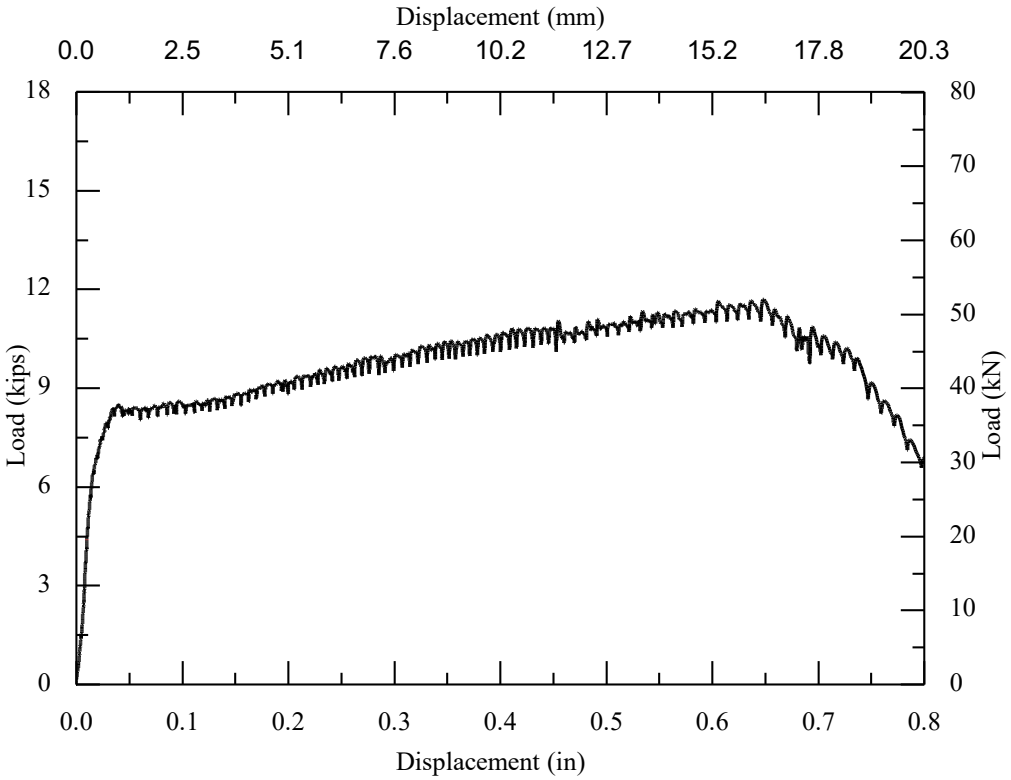

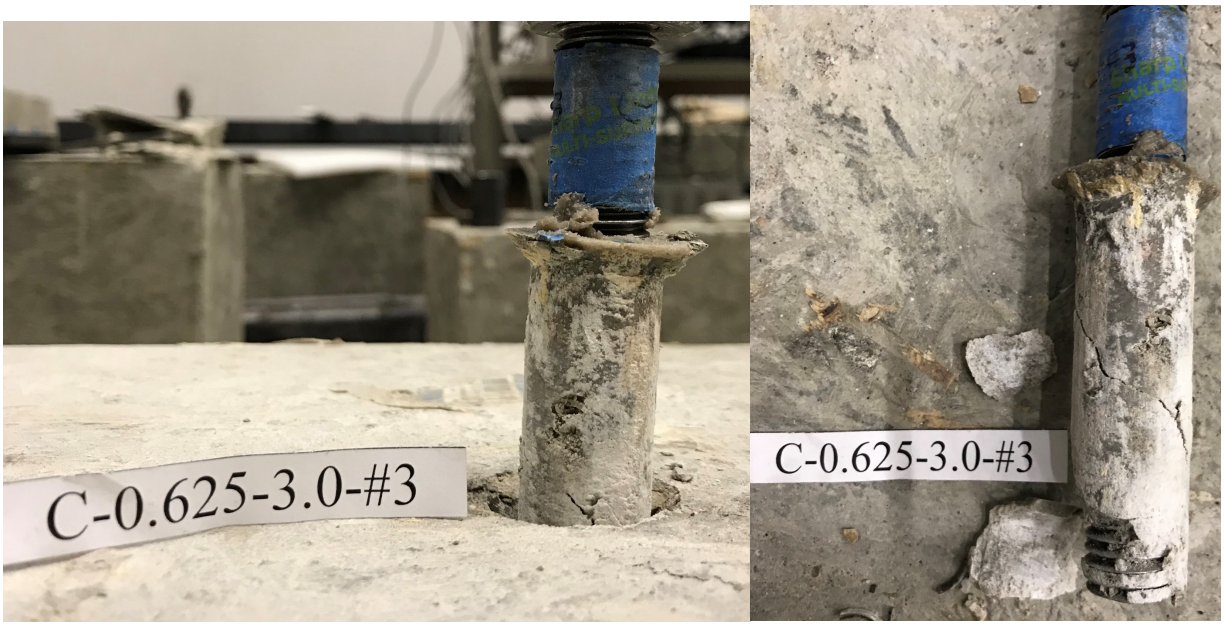

Adhesive-concrete interface (AC) bond failure.

Figure II.16. Observed behavior of Specimen C-0.625-3.0-#3

17. C-0.625-3.75-#2



Adhesive-concrete and adhesive-steel interface (AC+AS) bond failure.

Figure II.17. Observed behavior of Specimen C-0.625-3.75-#2

18. C-0.625-3.75-#3

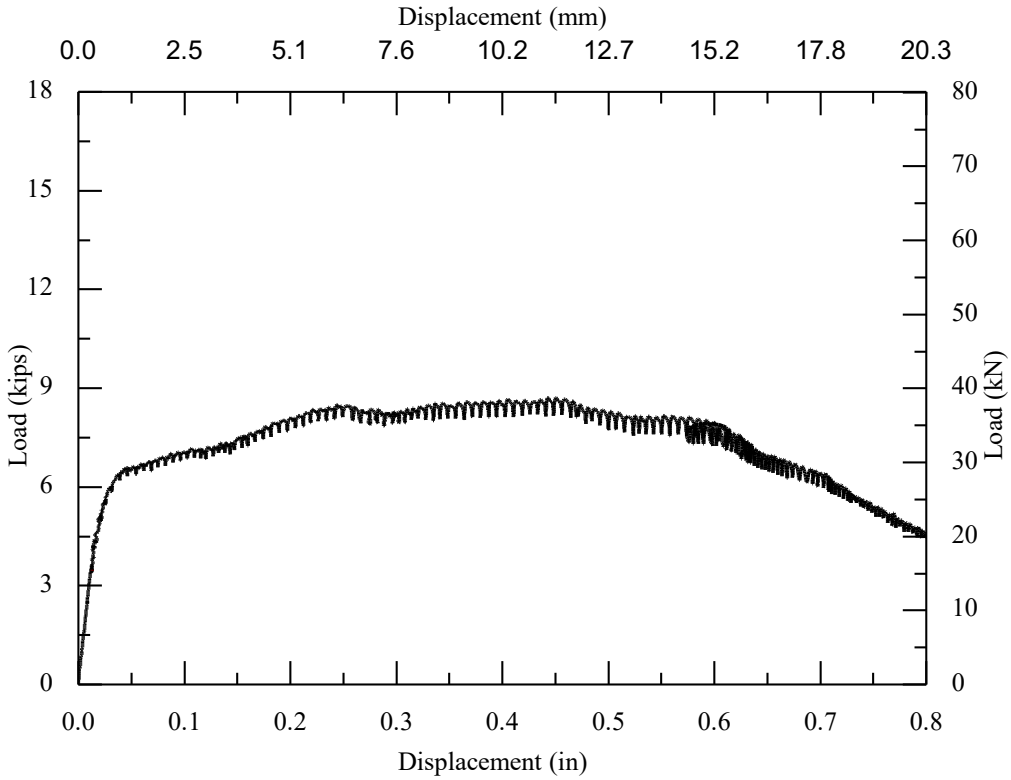



Adhesive-concrete and adhesive-steel interface (AC+AS) bond failure.

Figure II.18. Observed behavior of Specimen C-0.625-3.75-#3

19. C-0.75-2.0-#1



Adhesive-concrete interface (AC) bond failure.

Figure II.19. Observed behavior of Specimen C-0.75-2.0-#1

20. C-0.75-2.5-#1

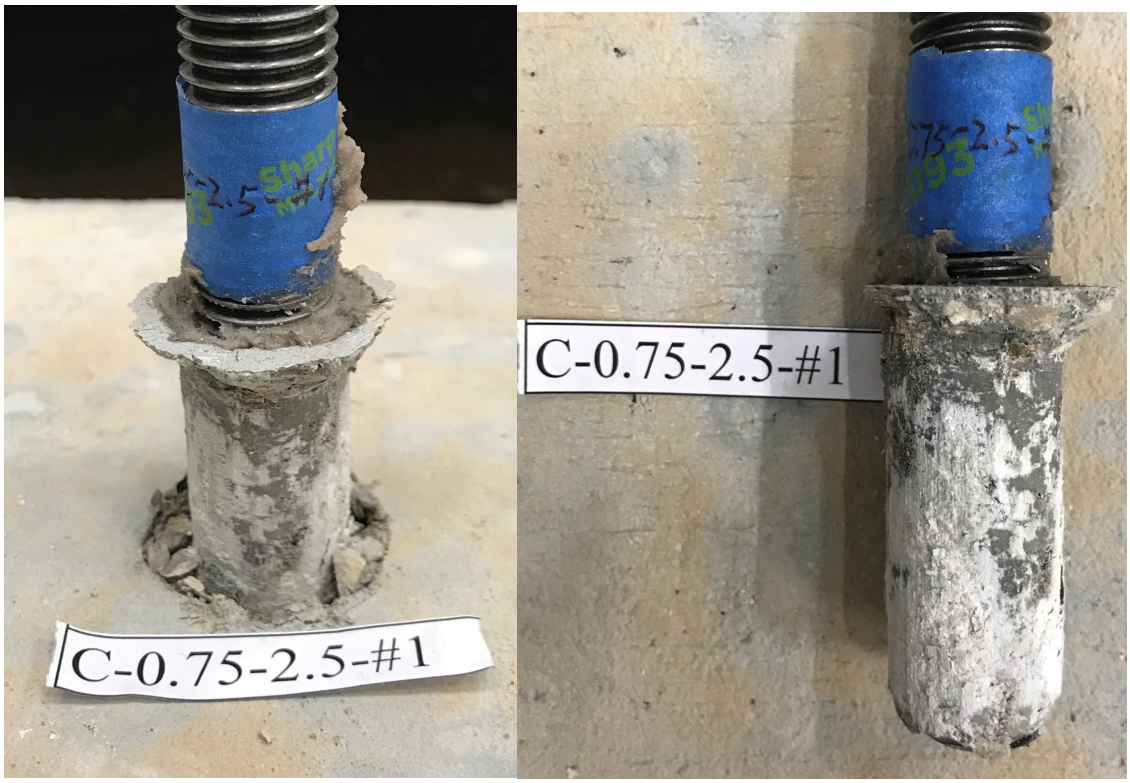

Adhesive-concrete interface (AC) bond failure.

Figure II.20. Observed behavior of Specimen C-0.75-2.5-#1

21. C-0.75-2.5-#2

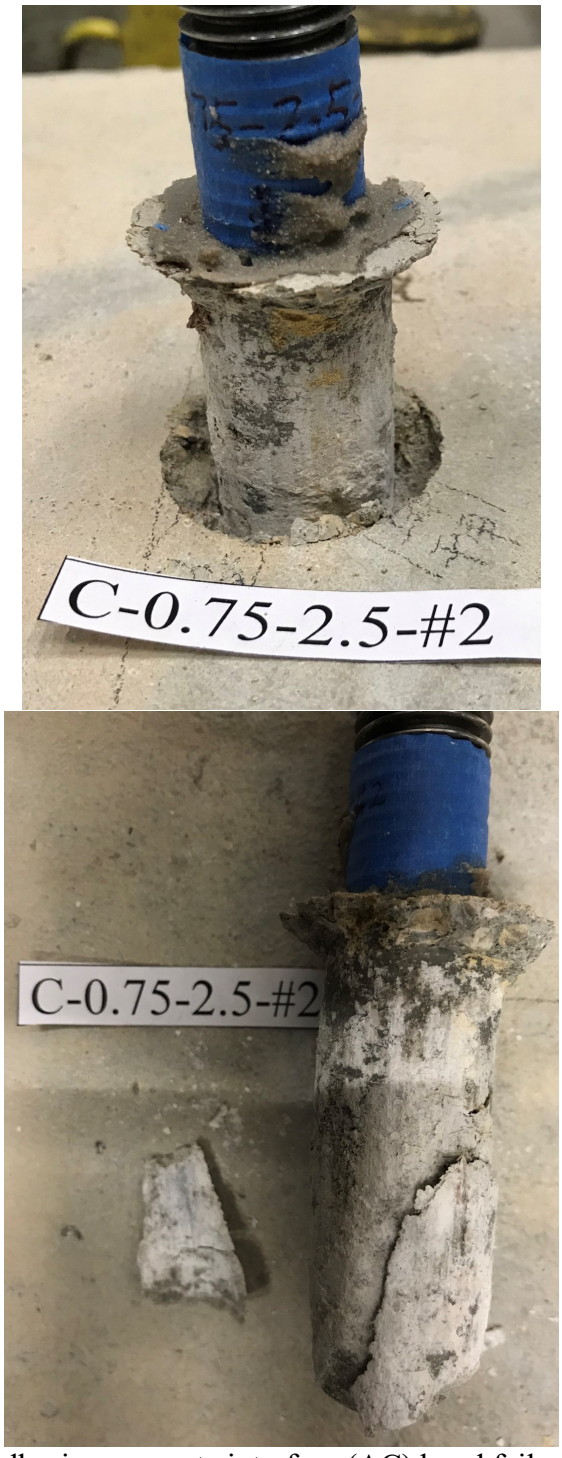

Adhesive-concrete interface (AC) bond failure.

Figure II.21. Observed behavior of Specimen C-0.75-2.5-#2

22. C-0.75-2.5-#3

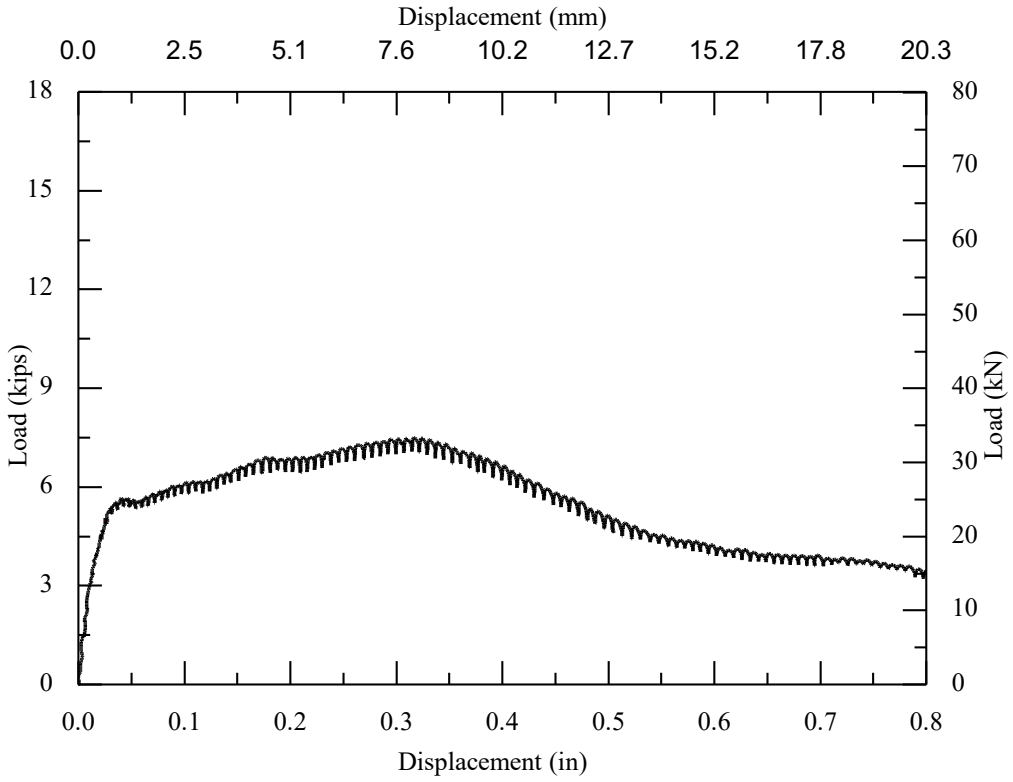



Adhesive-concrete interface (AC) bond failure.

Figure II.22. Observed behavior of Specimen C-0.75-2.5-#3

23. C-0.75-3.0-#1

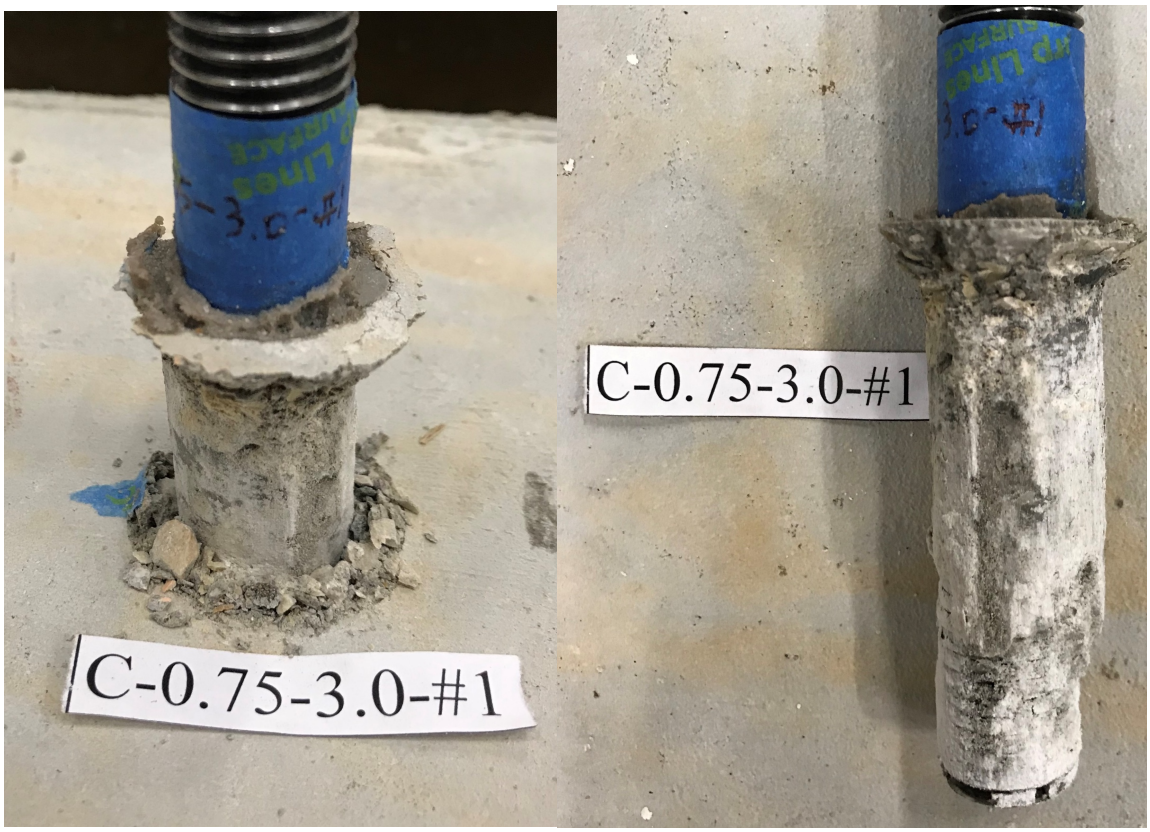

Adhesive-concrete interface (AC) bond failure.

Figure II.23. Observed behavior of Specimen C-0.75-3.0-#1

24. C-0.75-3.0-#2

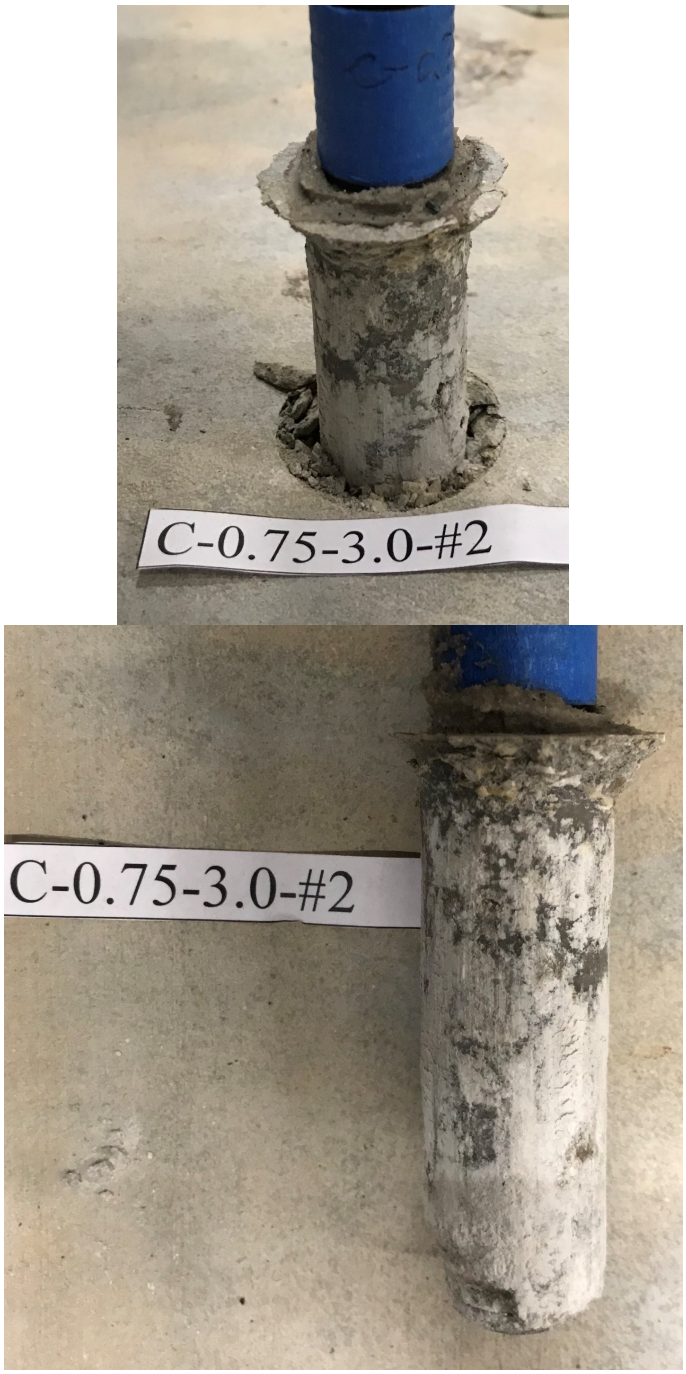

Adhesive-concrete interface (AC) bond failure.

Figure II.24. Observed behavior of Specimen C-0.75-3.0-#2

25. C-0.75-3.0-#3

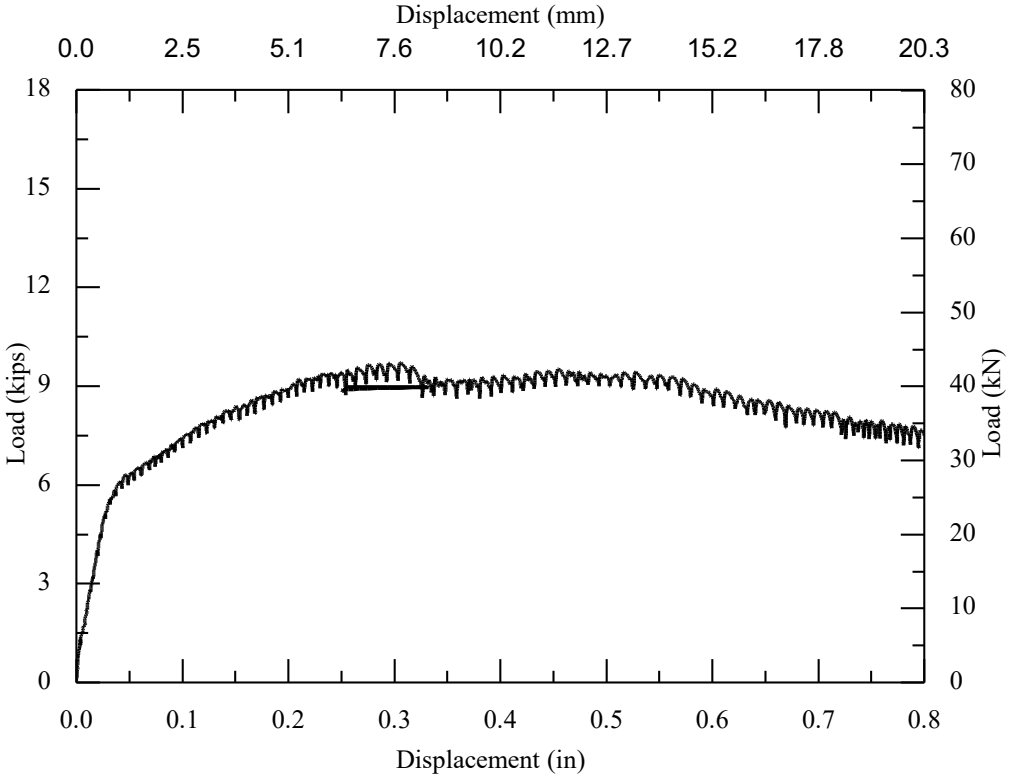

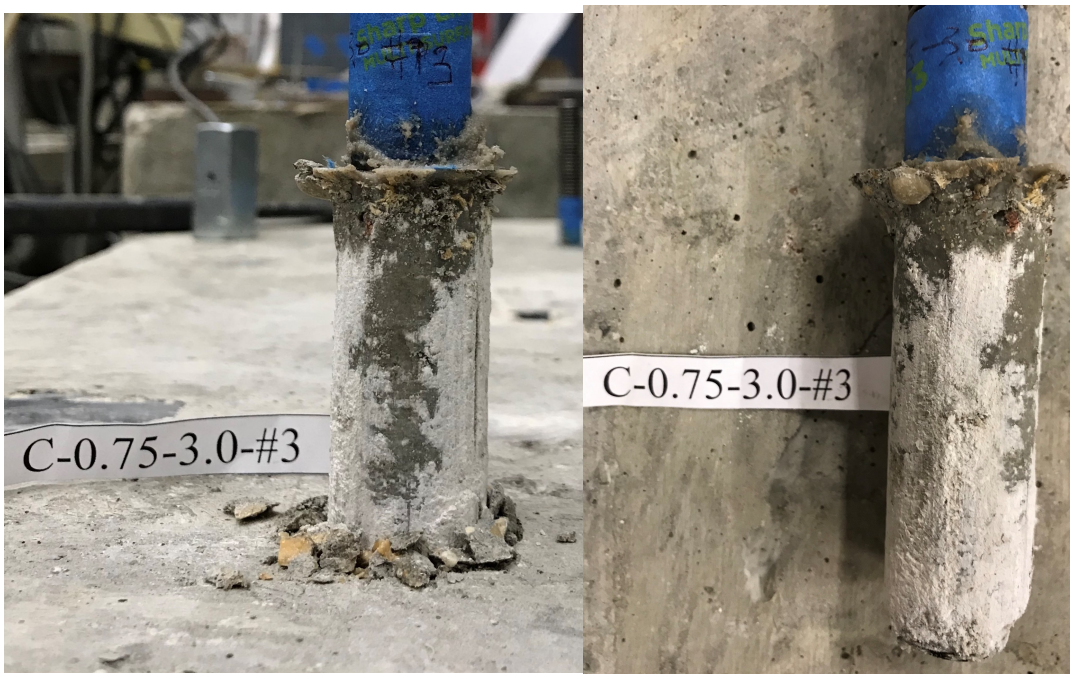

Adhesive-concrete interface (AC) bond failure.

Figure II.25. Observed behavior of Specimen C-0.75-3.0-#3

26. C-0.75-4.5-#2

The steel plate was shaking during drilling process.

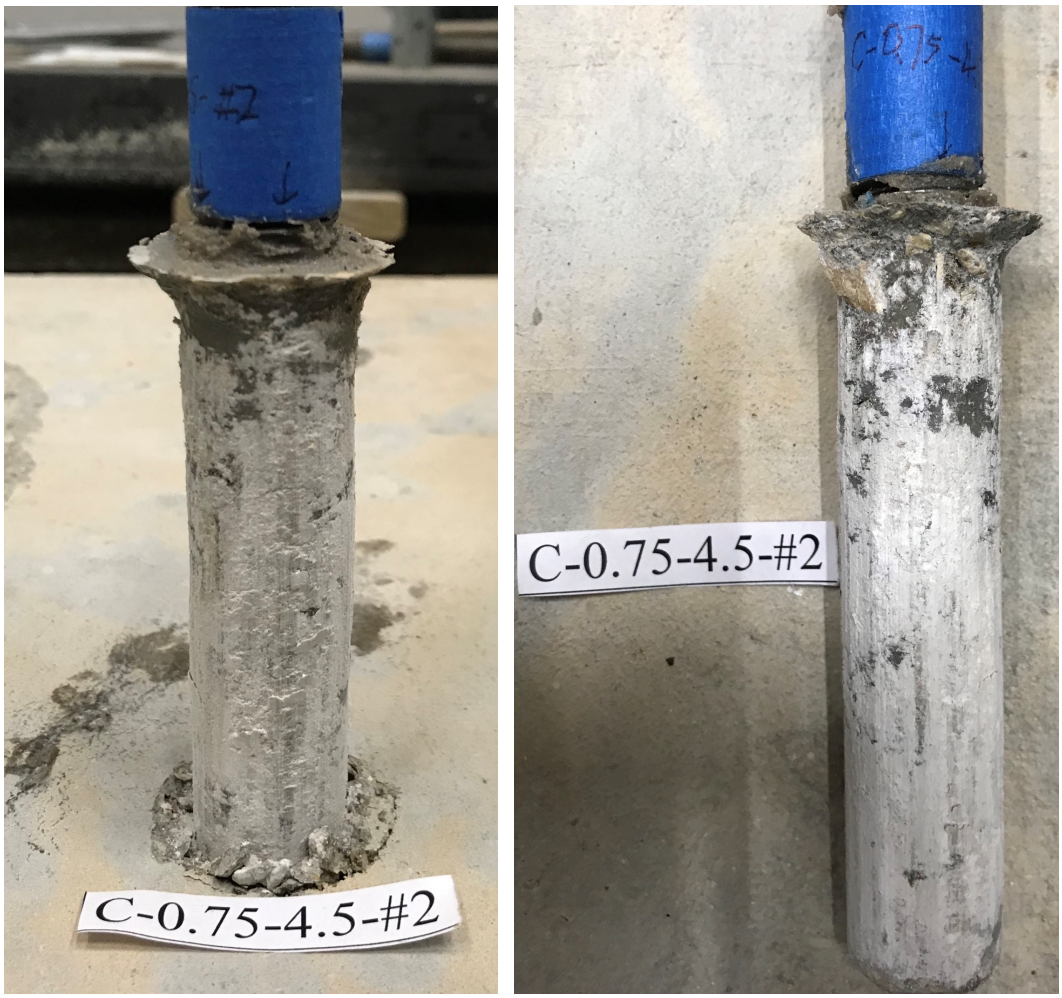

Adhesive-concrete interface (AC) bond failure.

Figure II.26. Observed behavior of Specimen C-0.75-4.5-#2

27. C-0.75-4.5-#3

The adhesive was wetter than before and the adhesive might have poor quality for this tube.

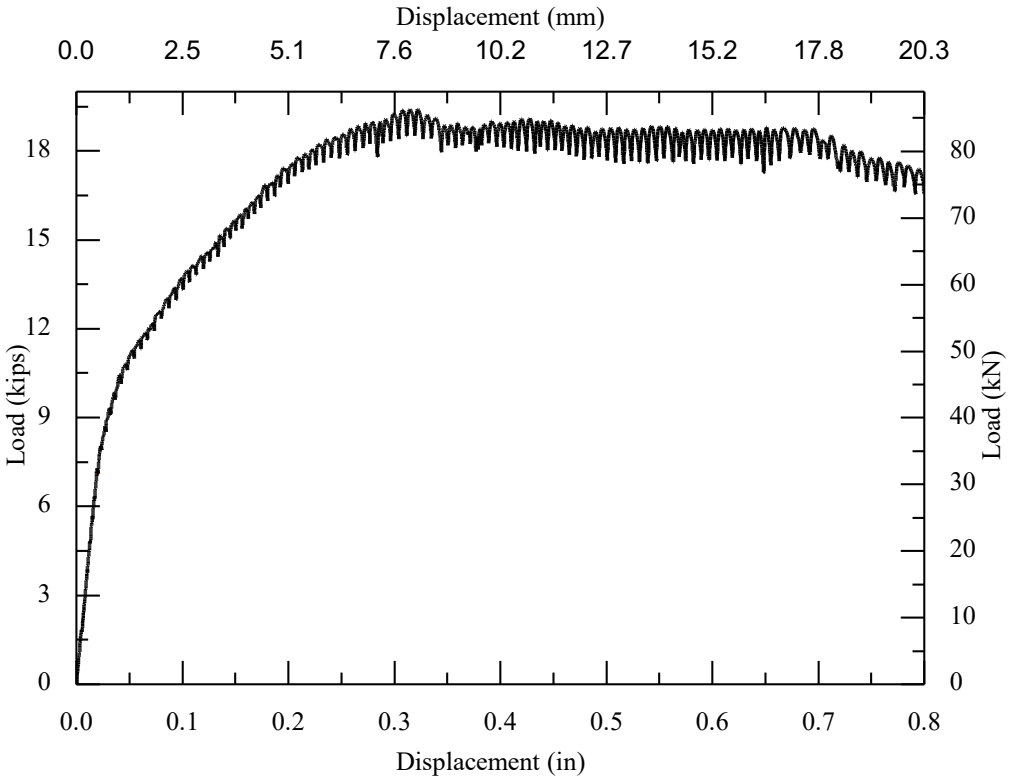

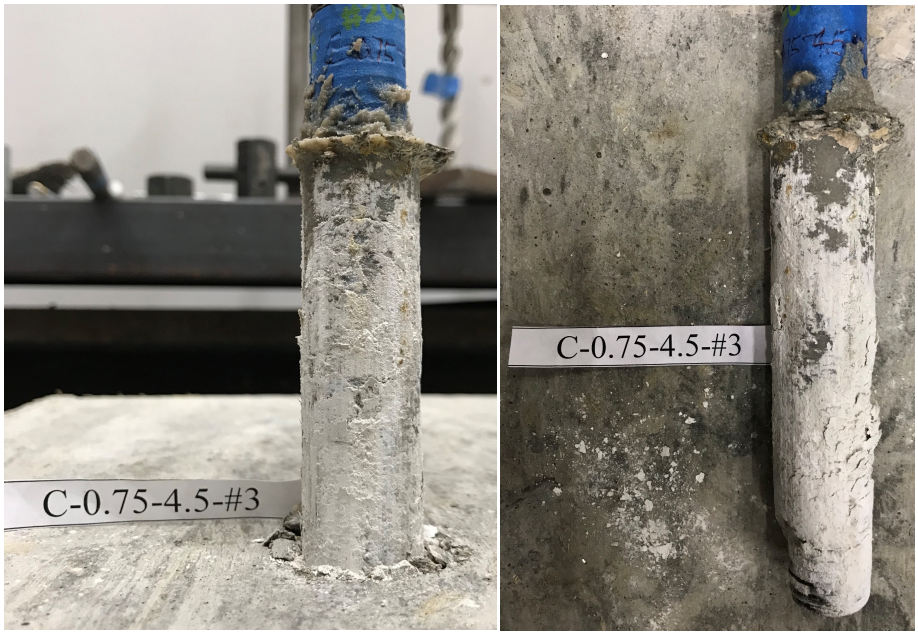

Adhesive-concrete interface (AC) bond failure.

Figure II.27. Observed behavior of Specimen C-0.75-4.5-#3

28. C-0.75-6.0-#4

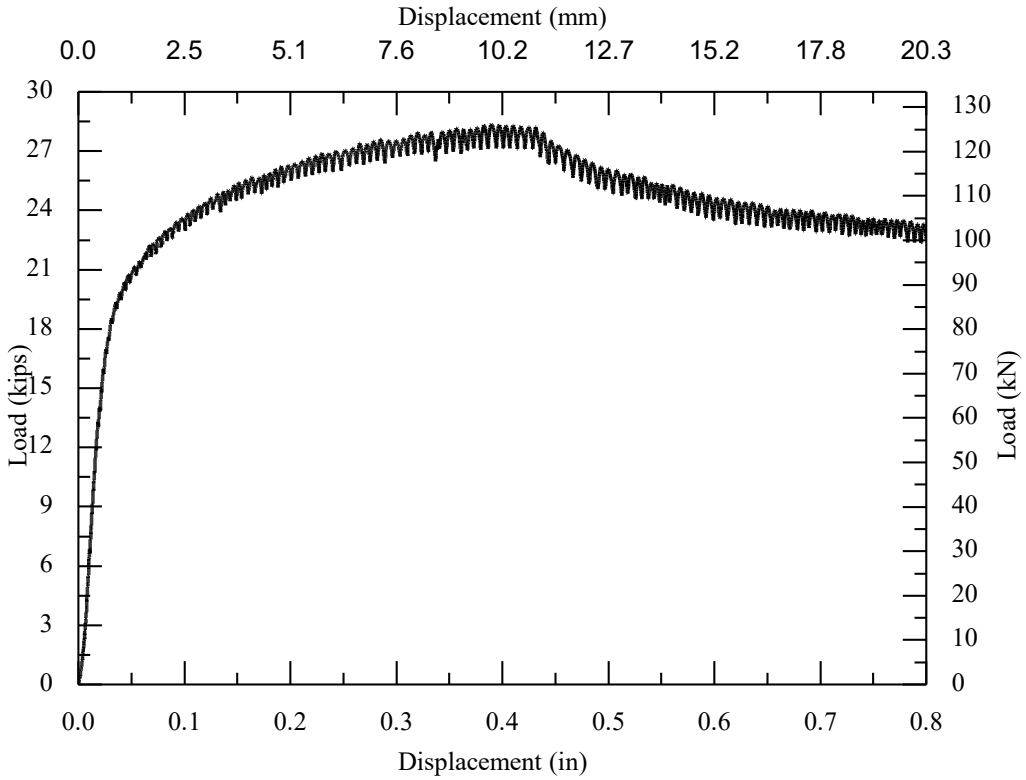



Adhesive-concrete interface (AC) bond failure.

Figure II.28. Observed behavior of Specimen C-0.75-6.0-#4

Appendix III: Details of unconfined tension tests

1. UC-0.5-2.0-#1

There was a slight noise when the load reached 4.3 kips. With a load of 6.7 kips, the top surface of the concrete suddenly formed four major cracks that developed toward the long side and the support side respectively and expanded rapidly. Subsequently, the bearing capacity was gradually reduced to 3.4 kips, and the corresponding displacement was increased to 0.094 in., The measured ultimate load is at 6.7 kips at a displacement of 0.020 in. After passing the ultimate load, the load dropped slowly as the displacement increased and the anchor was pulled out. As shown in figure 1b and 1c the concrete around the anchor was basically broken out. White powder could not be observed at the failure interface of anchor rod, which indicated that before the adhesive-concrete failure, the concrete has cracked and separated from the perimeter of the bolt, then only a small portion of adhesive-concrete interface could still provide bearing capacity after the concrete cracks appearing, and then the friction between the concrete and disengagement concrete was the main part of the bearing capacity after peak load.

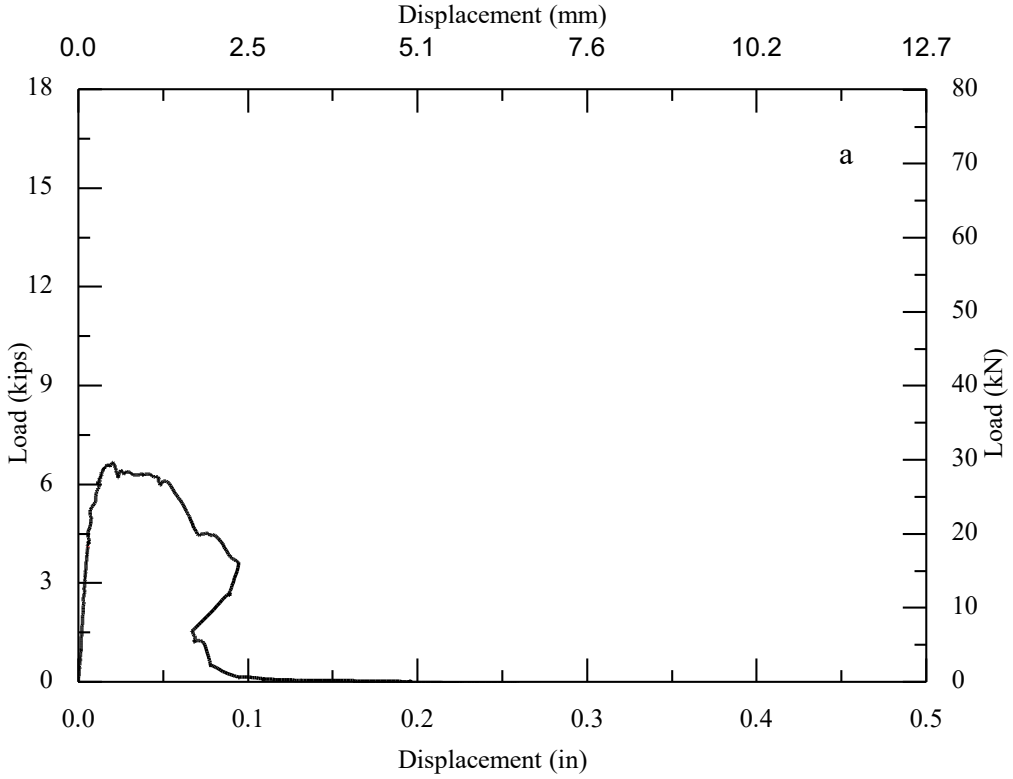



a) load-displacement behavior; b) cracked surface; c) breakout failure.

Figure III.1. Observed behavior of Specimen UC-0.5-2.0-#1

2. UC-0.5-2.0-#4

Breakout crack in longitudinal direction from testing specimen #1, breakout failure reduced edge distance by 0.25 in. A 5/8 in. diameter hole was around 1 in. away from the top of the drilled hole. The measured ultimate load is at 6.5 kips at a displacement of 0.0167 in. Breakout crack in longitudinal direction from testing specimen #1, breakout failure reduced edge distance by 0.25 in. A 5/8 in. diameter hole was around 1 in away from the top of the drilled hole; A circular crack was formed when the load reached 6.42 kips; After passing the ultimate load, the load dropped quickly as the displacement increased. The anchor was pulled out with a concrete cone due to concrete breakout failure shown in Figure 2c and 2b.

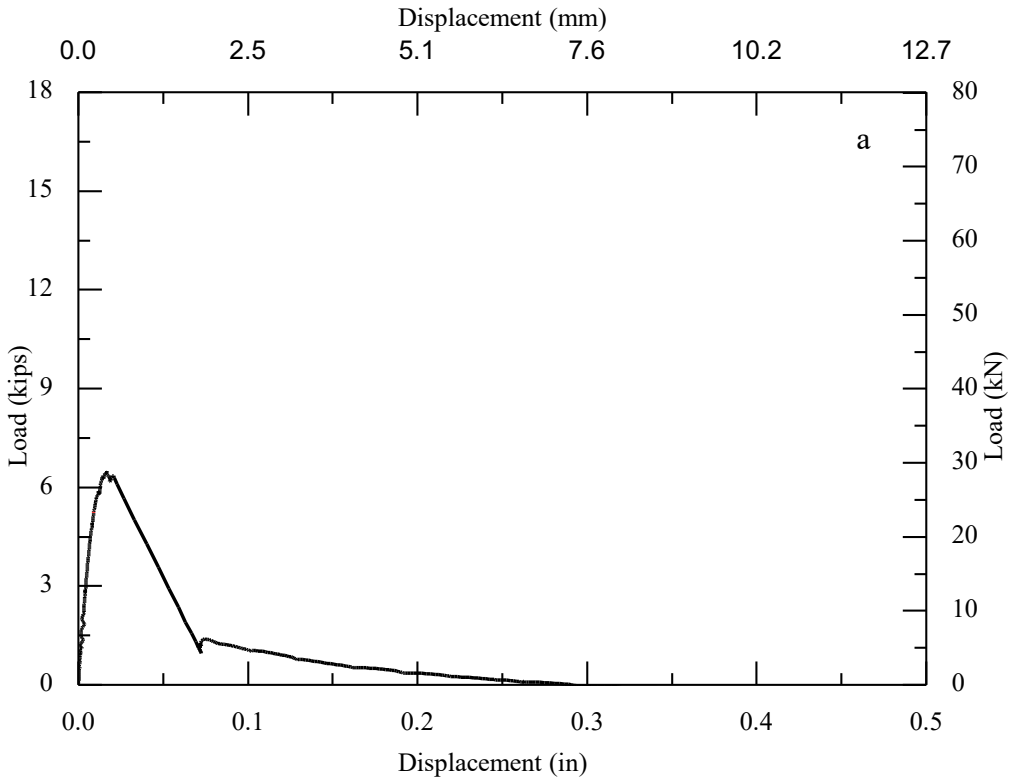



a) load-displacement behavior; b) cracked surface; c) breakout failure.

Figure III.2. Observed behavior of Specimen UC-0.5-2.0-#4

3. UC-0.5-2.5-#3

The anchor location was offset 0.5 in. in the transverse direction and 2.25 in. in the longitudinal direction. Transverse splitting crack from testing specimen #1, crack tip 4 in away from the test anchor. The measured ultimate load is at 8.59 kips at a displacement of 0.0276 in. Initial transverse splitting crack was from testing specimen #1, crack tip 4 in away from the test anchor. A crack represented splitting and passing the anchor in the diagonal direction when the load reached 8.59 kips. A larger cracking sound and a circular crack was formed when the load dropped to 8.24 kips. The anchor was pulled out with a concrete cone due to concrete breakout failure shown in Figure 3b and 3c. A splitting crack (with a width about 0.008 in.) in the transverse direction can be seen in Figure 3b.

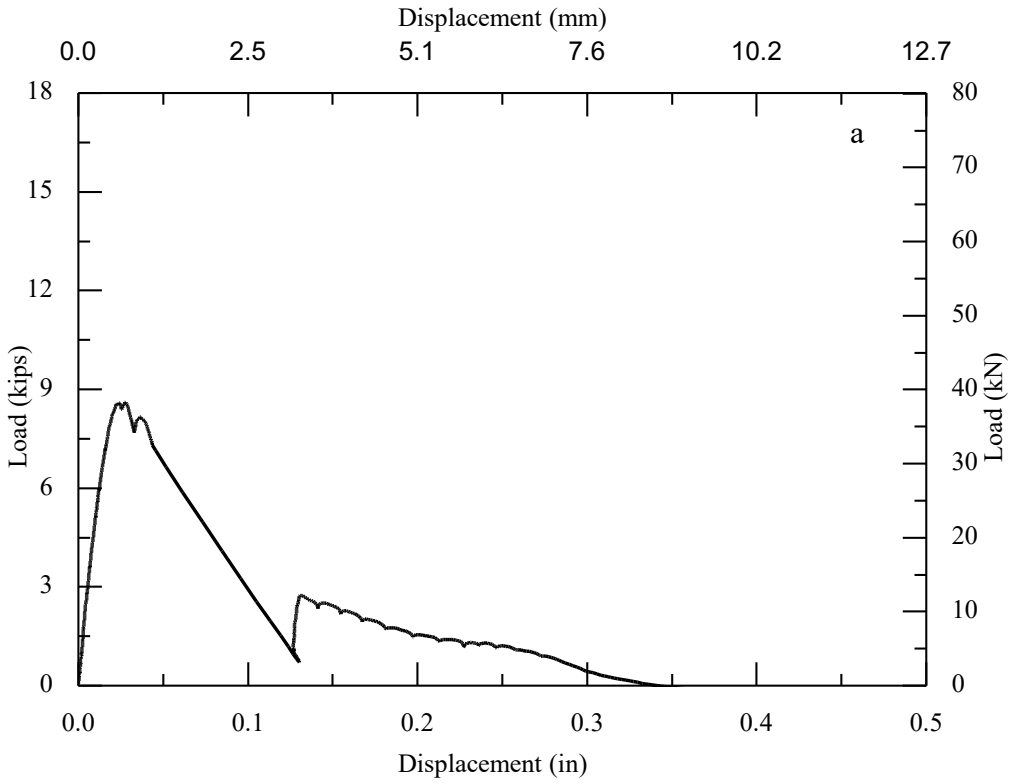

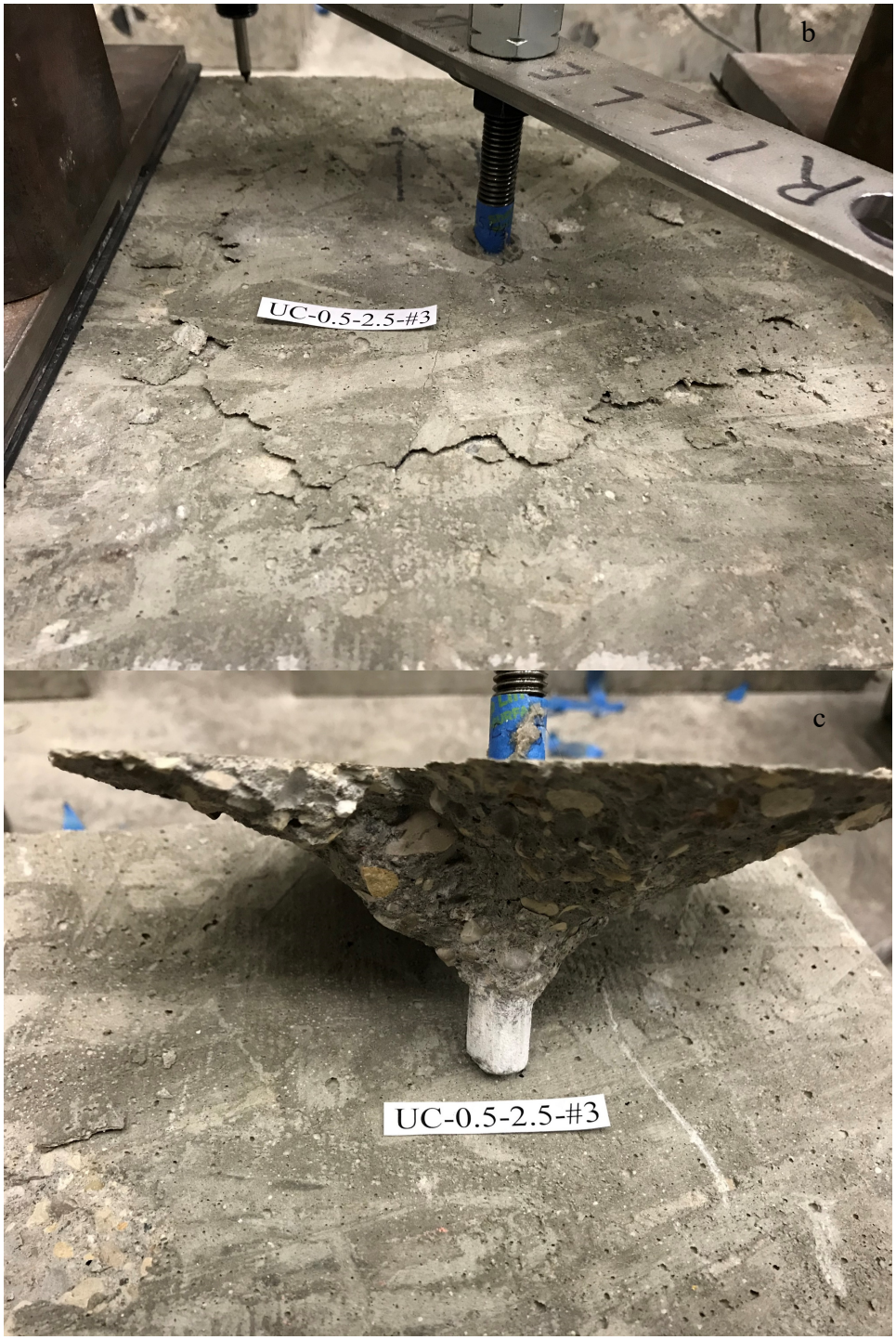

a) load-displacement behavior; b) cracked surface; c) breakout failure.

Figure III.3. Observed behavior of Specimen UC-0.5-2.5-#3

4. UC-0.5-3.0-#1

No record is available. The measured ultimate load is at 12 kips at a displacement of 0.0216 in.

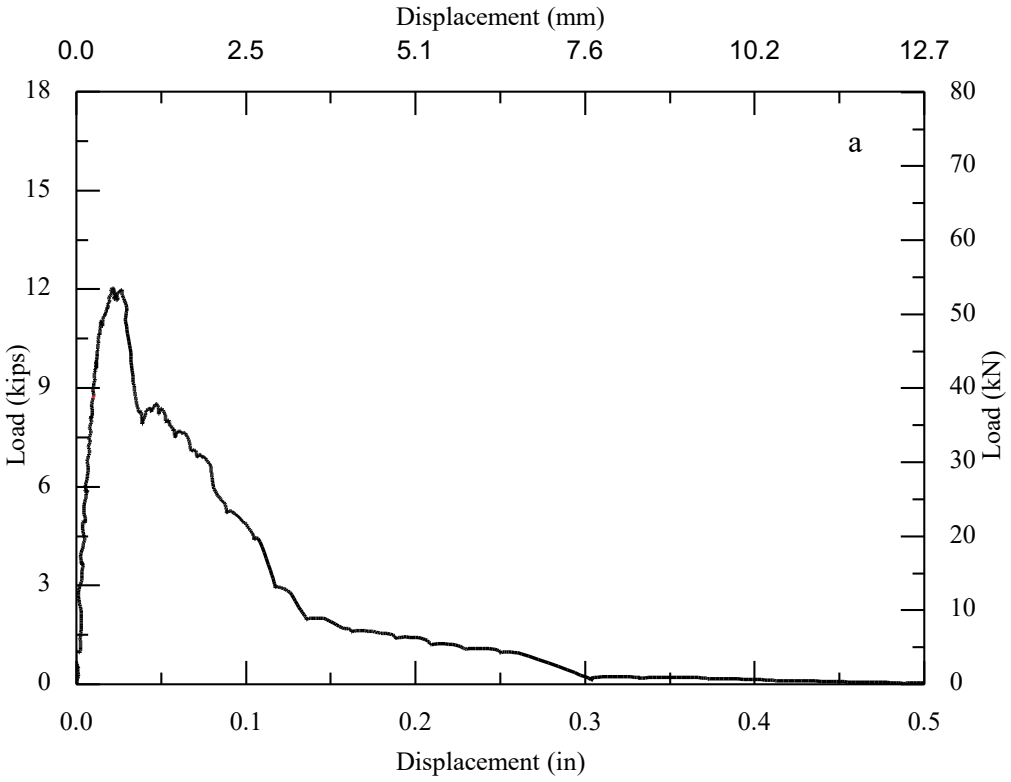

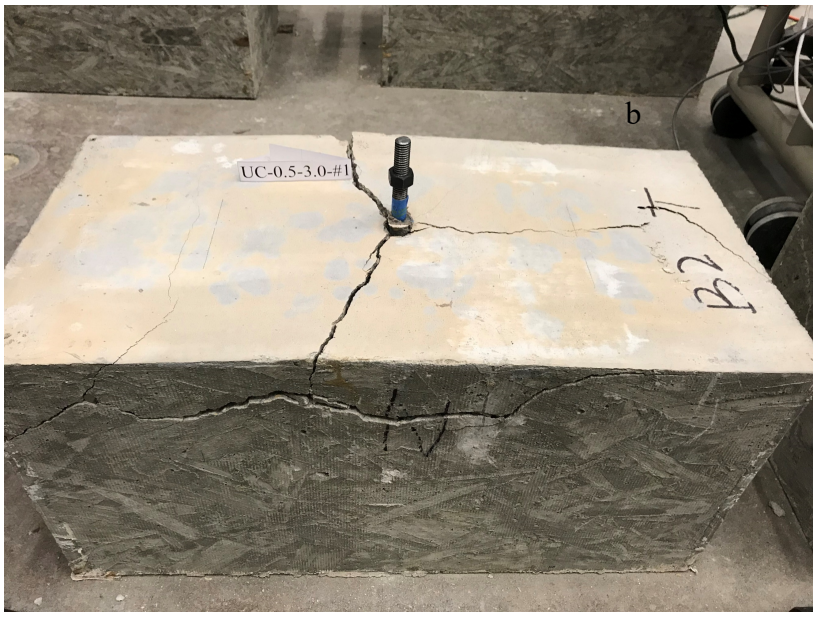

a) load-displacement behavior; b) breakout failure.

Figure III.4. Observed behavior of Specimen UC-0.5-3.0-#1

5. UC-0.5-3.0-#2

The concrete face was damaged. The test was not conducted because it was not viable to conduct test due to the significantly reduced concrete side face shown in Figure III.4.

6. UC-0.5-3.0-#3

The test was not conducted because it was not viable to conduct test due to the significantly reduced concrete side face as indicated by Figure III.4.

7. UC-0.5-3.0-#4

The test was not conducted because it was not viable to conduct test due to the significantly damaged concrete top face such that when flipped, the specimen could not provide a leveled position. A test for the ½ in. anchors with an embedment depth of 3 in. was conducted in a reinforced concrete block, and the specimen was named UC#R-0.5-3.0-#4 below.

8. UC#R-0.5-3.0-#4

The measured ultimate load is at 12.4 kips at a displacement of 0.0393 in. When the load reached 12.31 kips, a large crack was formed, and a large cracking sound occurred; Then, the load dropped quickly. The anchor was pulled out with a concrete cone due to pullout and breakout failure shown in Figure 8b and 8c. No transverse splitting crack was observed

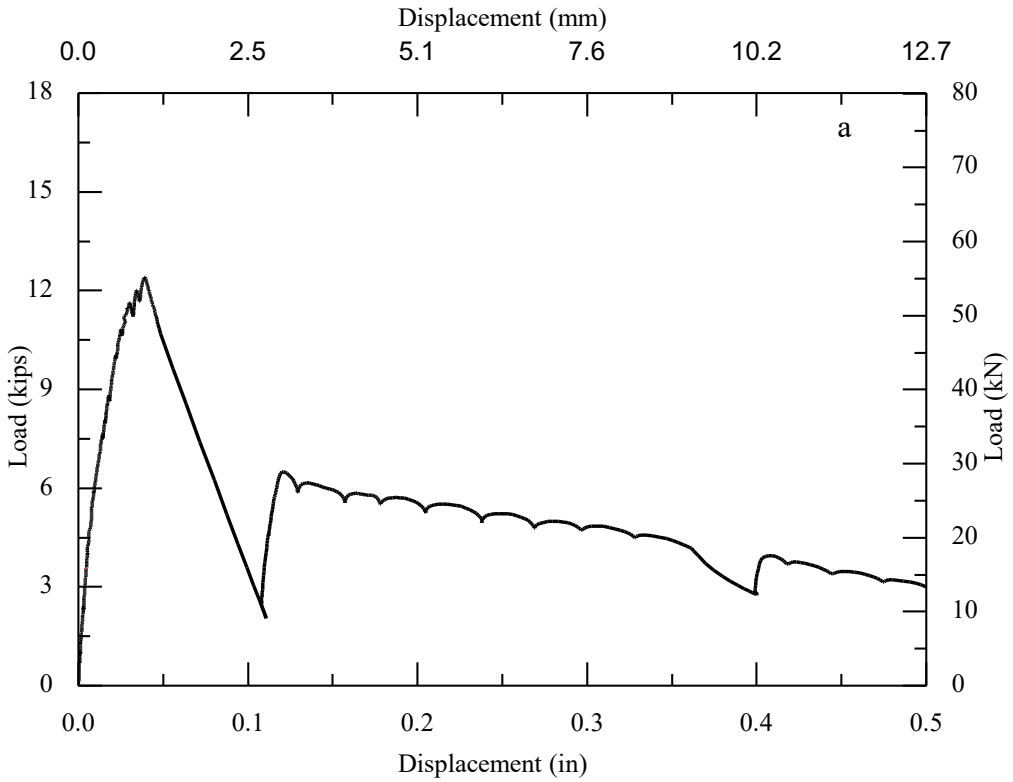



a) load-displacement behavior; b) cracked surface; c) partial cone bond failure.

Figure III.8. Observed behavior of Specimen UC#R-0.5-3.0-#4

9. UC-0.5-3.75-#2

The measured ultimate load is at 8.7 kips at a displacement of 0.0476 in. A cracking sound occurred when the load reached 8.7 kips; Then, the load dropped; When the load dropped to 7.17 kips, a large cracking sound occurred; When the load dropped to 5.67 kips, a large cracking sound occurred. The anchor was pulled out with a concrete cone due to pullout and breakout failure shown in Figure 9b and 9c.

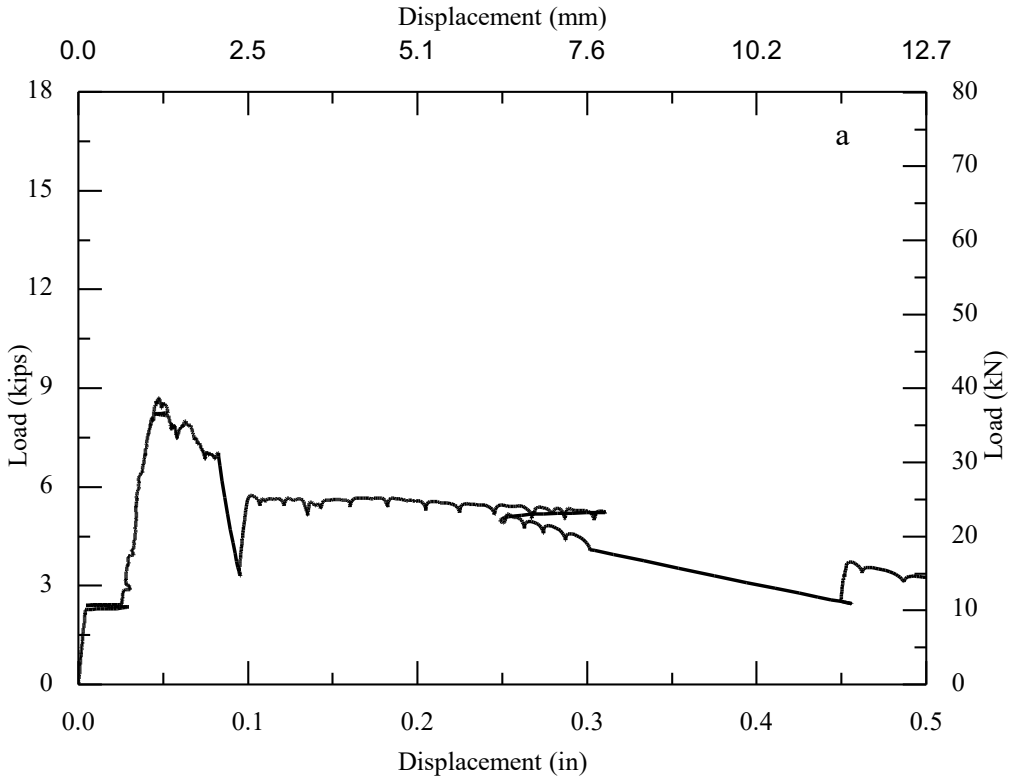



a) load-displacement behavior; b) cracked surface; c) partial cone bond failure.

Figure III.9. Observed behavior of Specimen UC-0.5-3.75-#2

10. UC-0.5-4.0-#1

The measured ultimate load is at 10.9 kips at a displacement of 0.031 in. One crack represented splitting and passing the anchor in the transverse direction when the load reached 10.91 kips. The predicted capacity measuring a negligible 0.44-in. deep breakout simultaneously with a 3.5-in deep bond failure (11.54 kips). The anchor was controlled adhesive-concrete interface failure as shown in Figure III.10c. Figure III.10.b shows splitting cracks about 0.0008 in. wide in both transverse and longitudinal directions. The adhesive-concrete bond within about 1.0 in. from the top was disengaged during loading as shown in Figure III.10.c

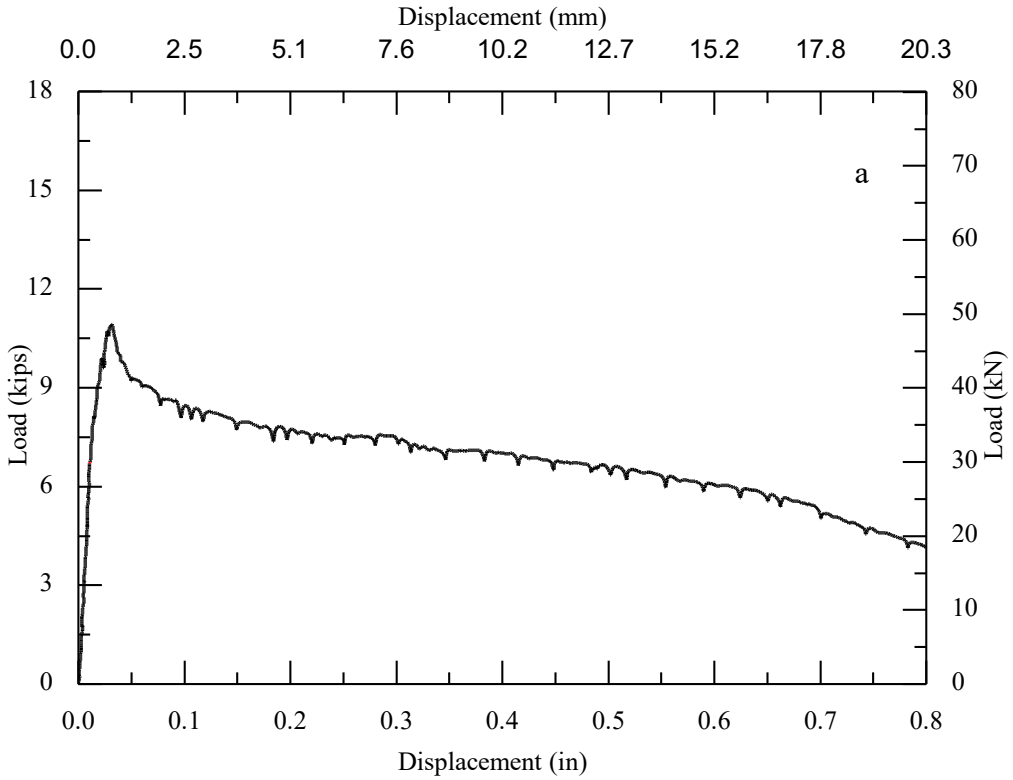

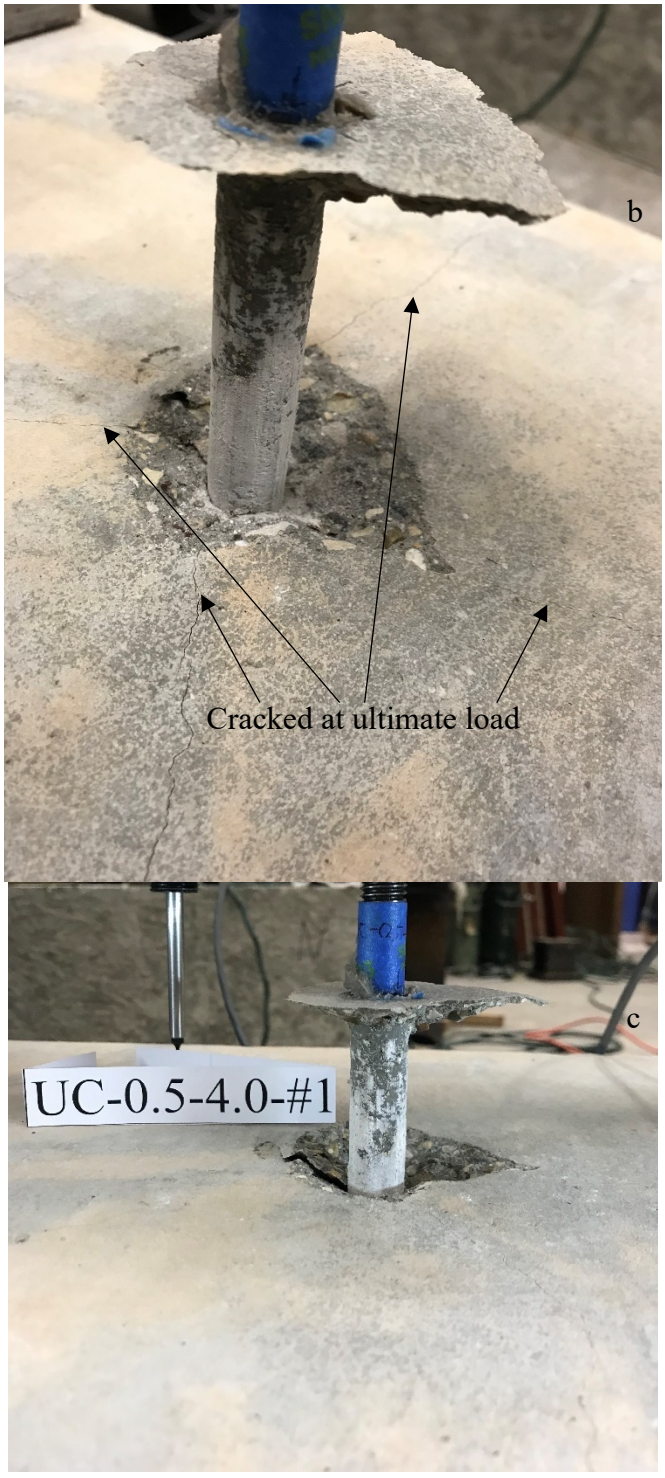

a) load-displacement behavior; b) cracked surface; c) pullout failure

Figure III.10. Observed behavior of Specimen UC-0.5-4.0-#1

11. UC-0.5-4.0-#2

Dusts stuck on the wall that it was around 1 in. from the bottom of the hole. The measured ultimate load is at 12.69 kips at a displacement of 0.023 in. One crack represented splitting and passing the anchor in the transverse direction and crack depth was 2 in when the load reached 12.69 kips. The predicted capacity measuring a 0.73-in. deep breakout simultaneously with a 3.25-in. deep bond failure (11.37 kips). The anchor was pulled out due to pullout and concrete breakout failure shown in Figure III.11c though the breakout depth is fairly small.

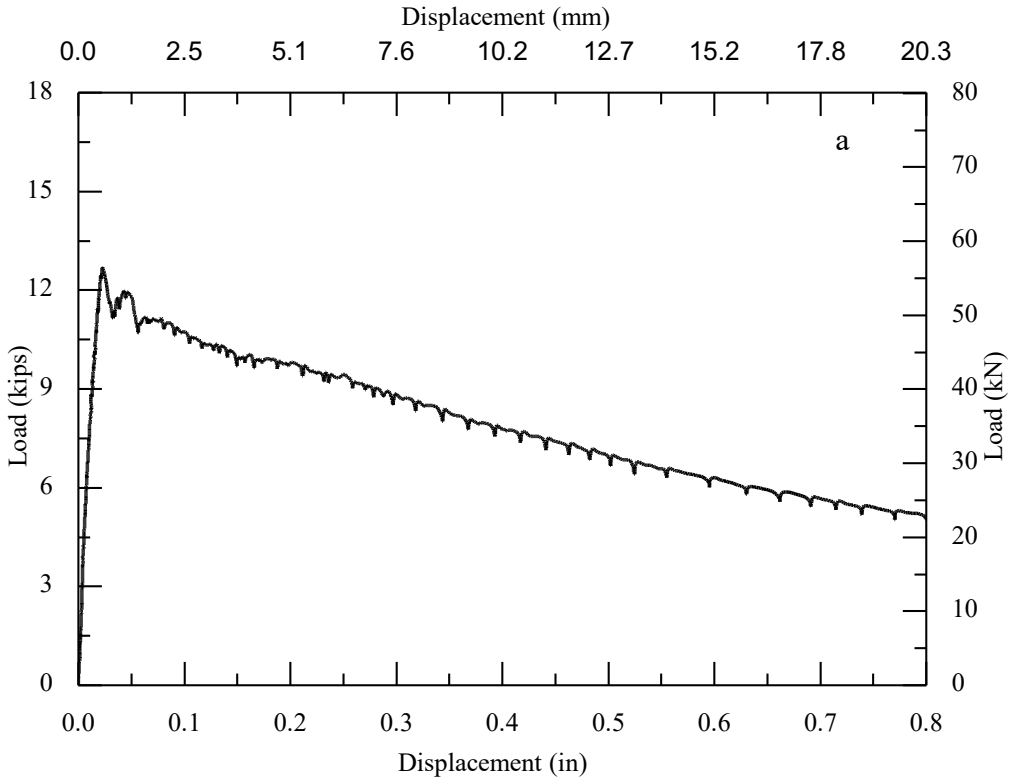



a) load-displacement behavior; b) cracked surface; c) partial cone bond failure

Figure III.11. Observed behavior of Specimen UC-0.5-4.0-#2

12. UC-0.5-4.0-#3

Transverse splitting crack from testing Repeat #2, crack tip 4 in away from the test anchor. The measured ultimate load is at 13.40 kips at a displacement of 0.041 in. An initial crack caused by the previous test represented splitting in the transverse direction at the bottom edge as shown in Figure III.12b. One crack represented splitting and passing the anchor in the transverse direction and the crack width enlarged to 0.004 in. when the load reached 10.22 kips. One crack represented splitting and passing the anchor in the diagonal direction when the load reached 13.38 kips. The predicted capacity in cracked concrete measuring a 1.75-in. deep breakout simultaneously with a 2.25-in. deep bond failure (10.16 kips). The anchor was pulled out with a concrete cone due to pullout and concrete breakout failure shown in Figure III.12d.

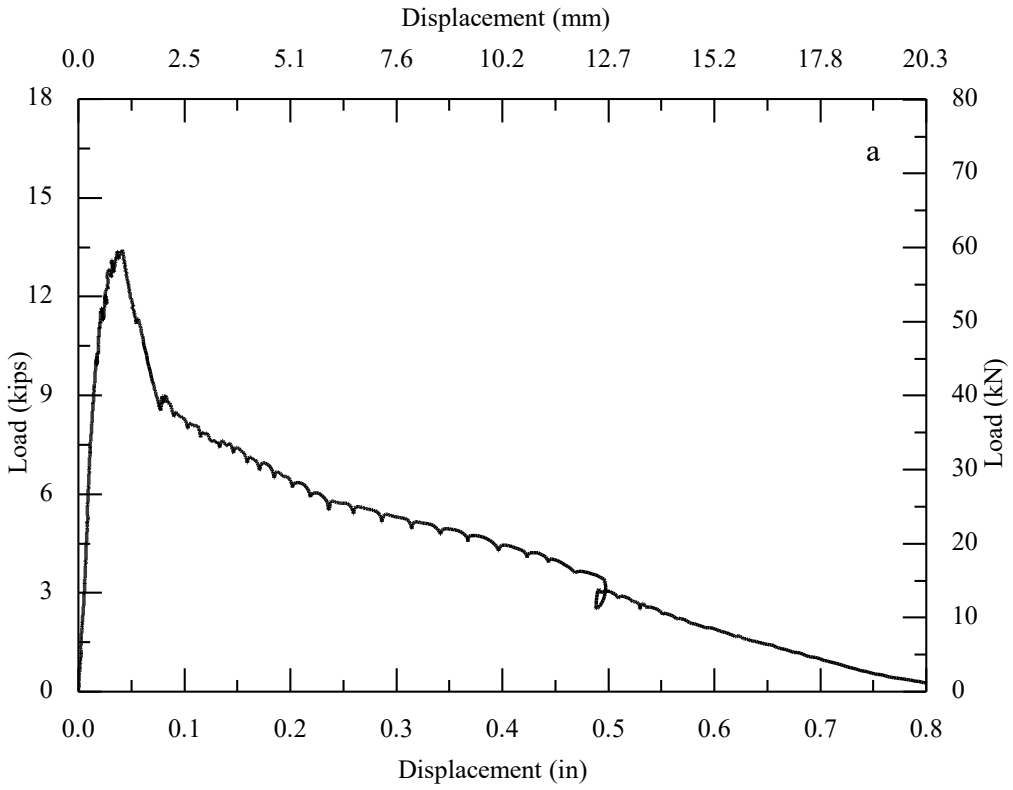



a) load-displacement behavior; b) initial cracked surface; c) cracked surface; d) partial breakout cone

Figure III.12. Observed behavior of Specimen UC-0.5-4.0-#3

13. UC-0.5-4.0-#4

The measured ultimate load is at 11.27 kips at a displacement of 0.045 in. As shown in Figure III.13b, one crack represented splitting in the transverse direction and the crack depth was 1.5 in. at the load of 6.58 kips; one represented splitting in the longitudinal direction at the load of 11.23 kips and two represented splitting in the diagonal direction at the load of 11.23 kips. The predicted capacity measuring a 2.67-in. deep breakout simultaneously with a 1.25-in. deep bond failure (12.15 kips). The anchor was pulled out due to concrete breakout failure shown in Figure III.13c. Crack lines of the concrete cone bypassed stirrups, indicating that such reinforcement cannot be assumed effective as anchor reinforcement (it was not intended to be anchor reinforcement either). The specimen was controlled by concrete breakout rather than pullout failure, which may have been attributed to the fact that hardened adhesive occupied a relatively large pocket in concrete, as shown in Figure III.13d, forming a macro-interlock.

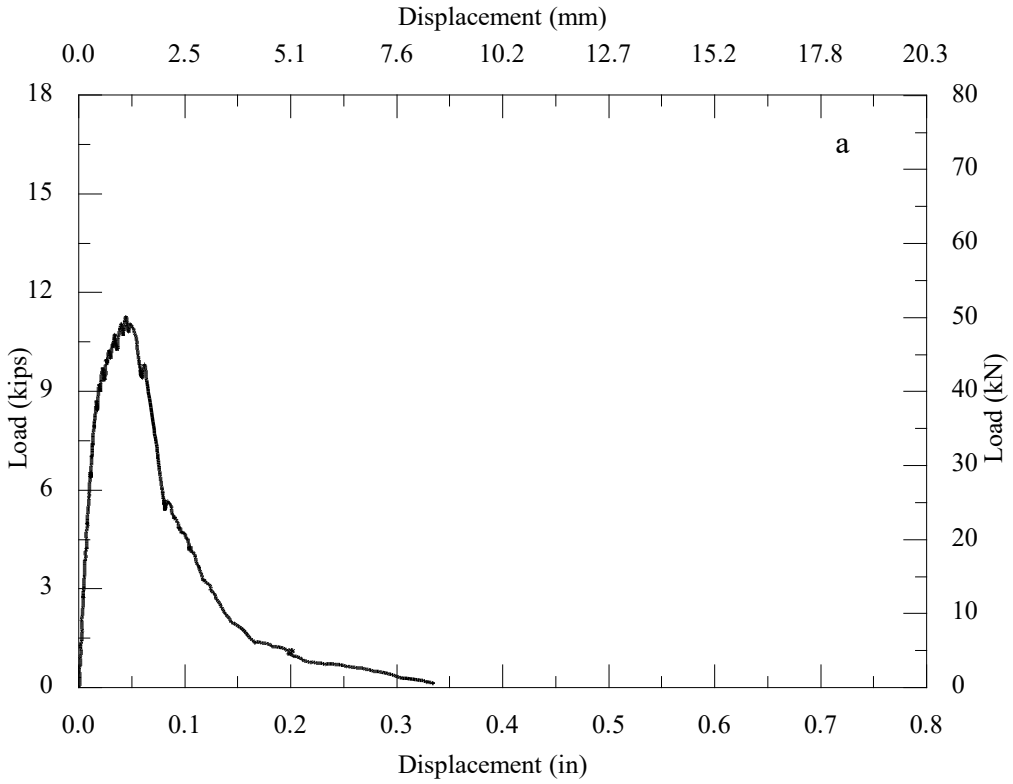

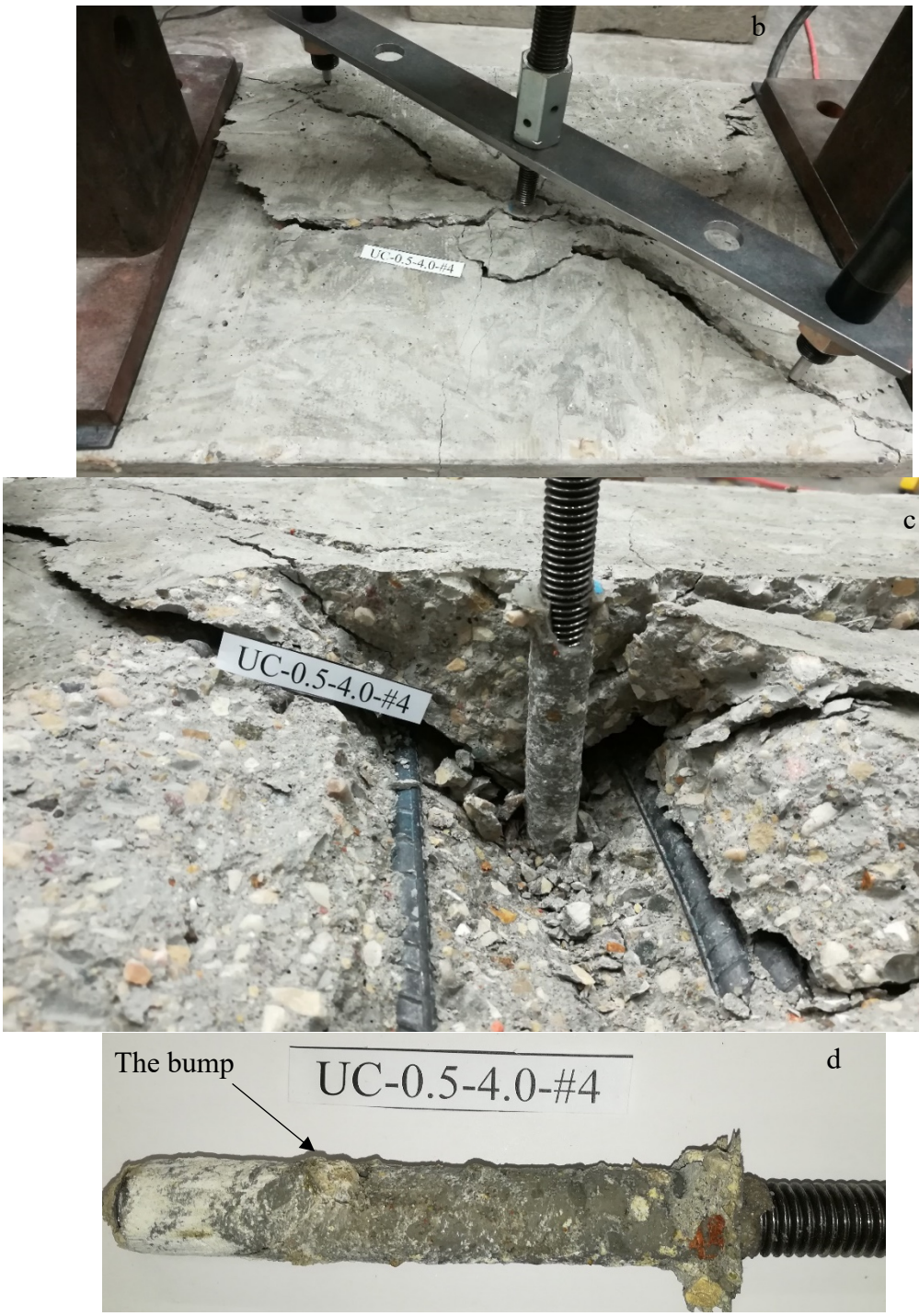

a) load-displacement behavior; b) cracked surface; c) concrete breakout cone in block; d) anchor with adhesive

Figure III.13. Observed behavior of Specimen UC-0.5-4.0-#4

14. UC#R-0.5-4.0-#1

The measured ultimate load is at 12.69 kips at a displacement of 0.0281 in. One crack representing splitting and passing the anchor in the transverse direction when the load reached 12.68 kips. The anchor was pulled out due to pullout and concrete breakout failure shown in Figure III.14b and 14c)

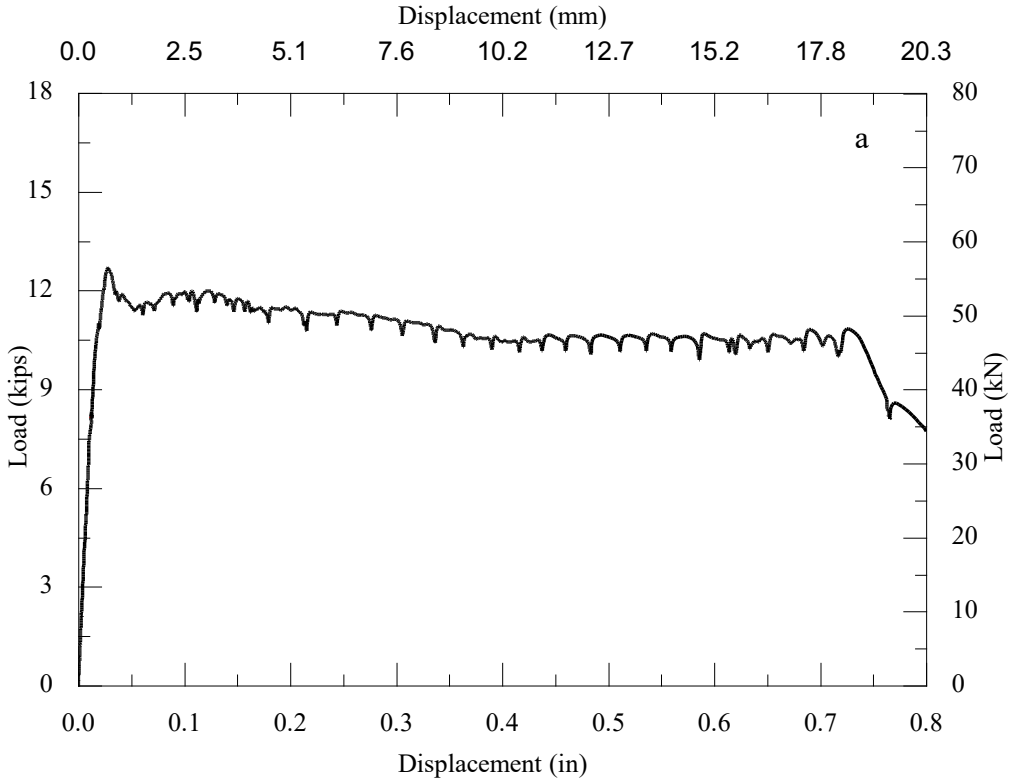

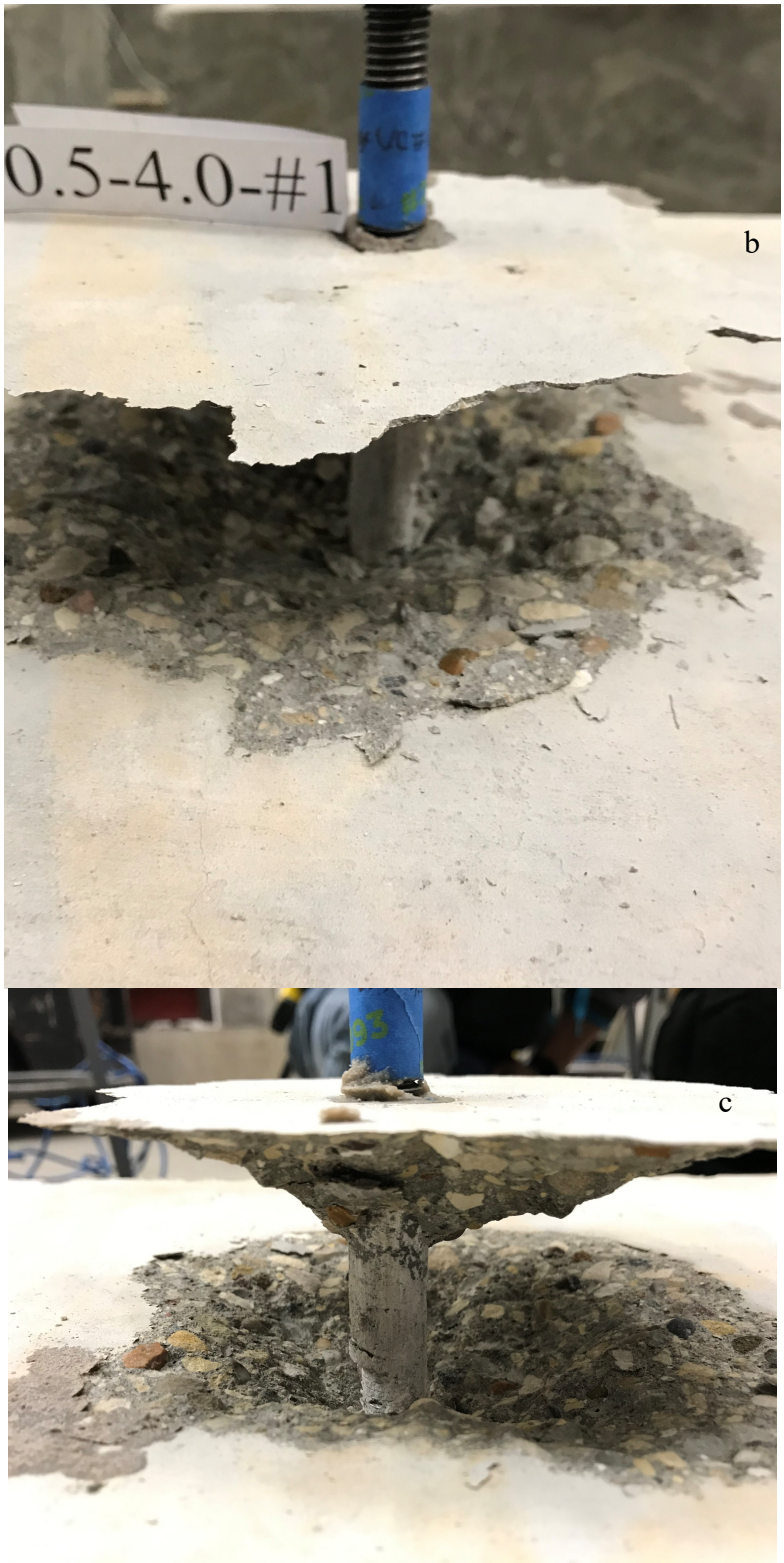

a) load-displacement behavior; b) cracked surface; c) partial breakout cone

Figure III.14. Observed behavior of Specimen UC#R-0.5-4.0-#1

15. UC#R-0.5-4.0-#2

Dusts stuck on the wall that it was around 1 in. from the bottom of the hole. The measured ultimate load is at 12.65 kips at a displacement of 0.0313 in. One crack represented splitting and passing the anchor in the transverse direction and crack depth was 3 in and a circular crack was formed when the load reached 12.65. The anchor was pulled out with a concrete cone due to pullout and concrete breakout failure shown in Figure III.15b and 15c.

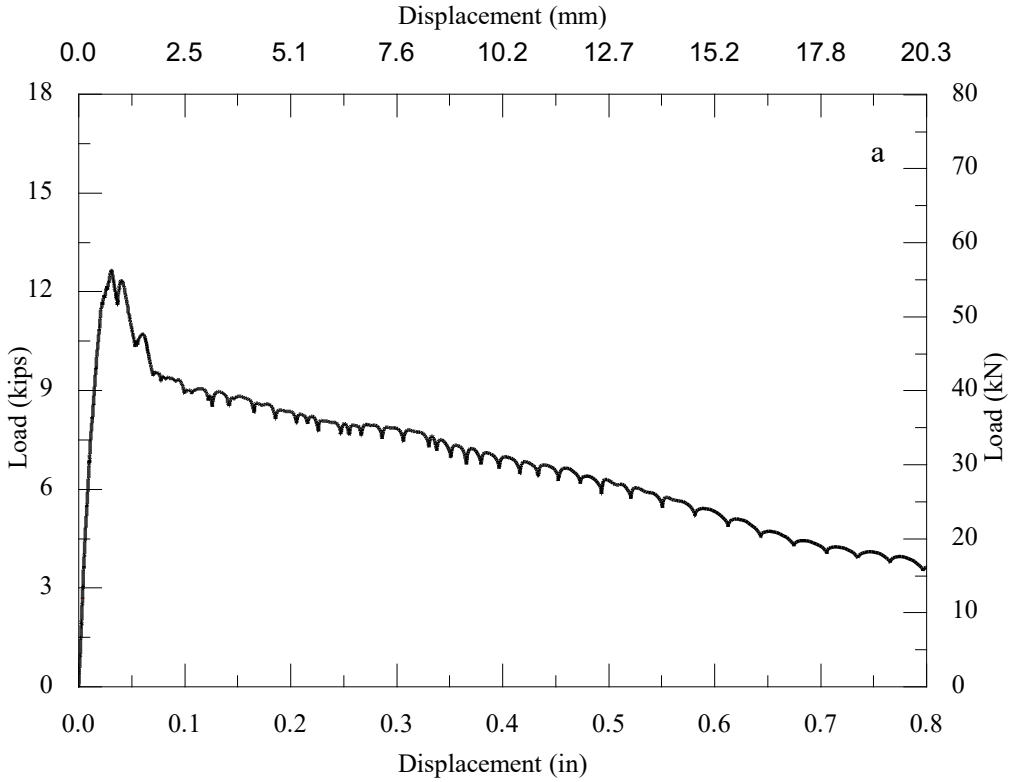



a) load-displacement behavior; b) cracked surface; c) partial breakout cone

Figure III.15. Observed behavior of Specimen UC#R-0.5-4.0-#2

16. UC#R-0.5-4.0-#3

Transverse splitting crack through the whole block width from testing specimen #1 and #2, crack passed test anchor. The measured ultimate load is at 15.22 kips at a displacement of 0.0522 in. Initial transverse splitting crack through the whole block width from testing specimen #1 and #2, crack passed test anchor. Two cracks represented splitting and passing the anchor in the diagonal direction when the load reached 14.82 kips; When the load dropped to 14.98 kips, a large cracking sound occurred. The anchor was pulled out with a concrete cone due to pullout and concrete breakout failure shown in Figure III.16b and 16c.

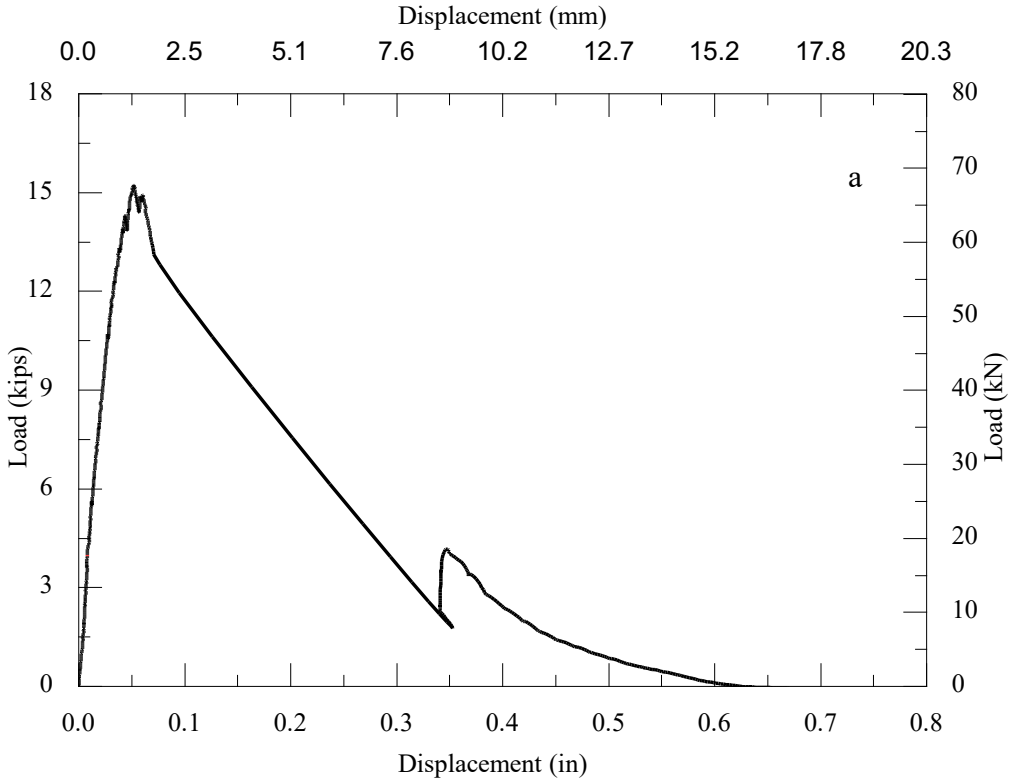



a) load-displacement behavior; b) initial cracked surface; c) cracked surface; d) partial breakout cone

Figure III.16. Observed behavior of Specimen UC#R-0.5-4.0-#3

17. UC#R-0.5-4.0-#4

A ½-in. diameter hole was around 1.5 in. away from the top of the drilled hole. Transverse splitting crack through the whole block width from testing Specimen #1 and #2, crack was 1 and 7/8 in. away from test anchor. The measured ultimate load is at 12.87 kips at a displacement of 0.0461 in. Initial transverse splitting crack through the whole block width from testing specimen #1 and #2, crack was 1 7/8 in. away from test anchor. Two cracks represented splitting and passing the anchor in the diagonal direction when the load reached 11.24 kips; one crack represented splitting and passing the anchor in the transverse direction when the load reached 12.84 kips and a large cracking sound occurred. Then, the load dropped. Two cracking sounds occurred at load of 4.3 kips and 2.1 kips respectively. The anchor was pulled out with a concrete cone due to pullout and concrete breakout failure shown in Figure III.17b and 17c.

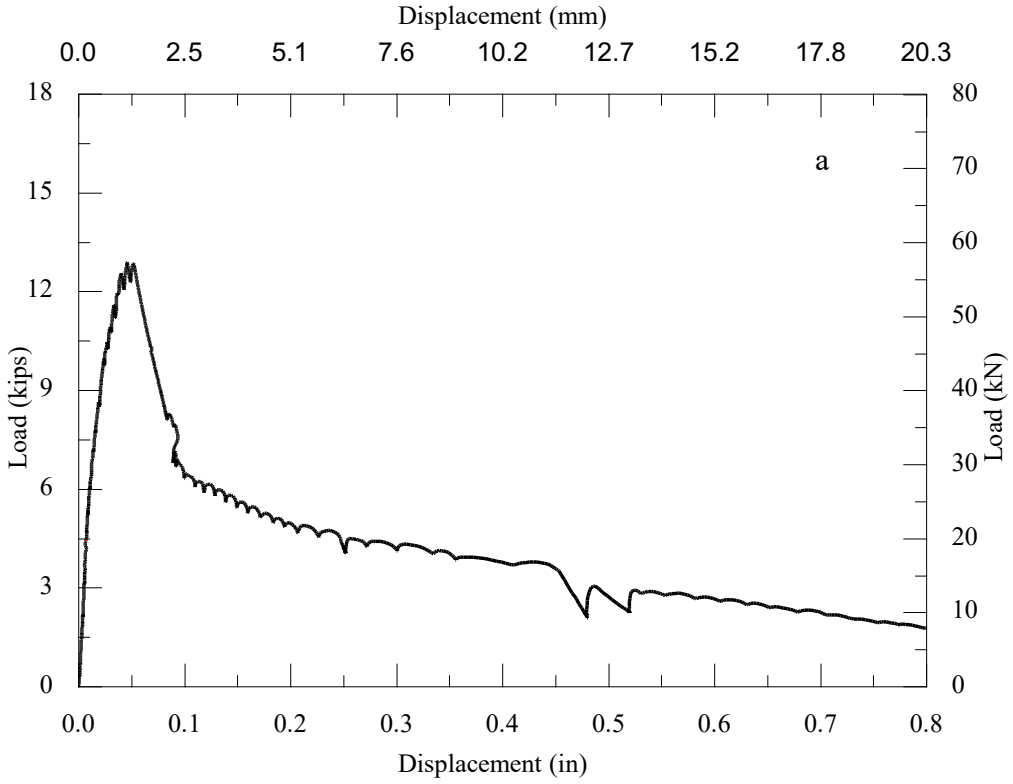



a) load-displacement behavior; b) cracked surface; c), d) partial breakout cone

Figure III.17. Observed behavior of Specimen UC#R-0.5-4.0-#4

18. UC#R-0.5-4.5-#3

The measured ultimate load is at 18.74 kips at a displacement of 0.2051 in. The anchor was failed due steel failure shown in Figure III.18b.

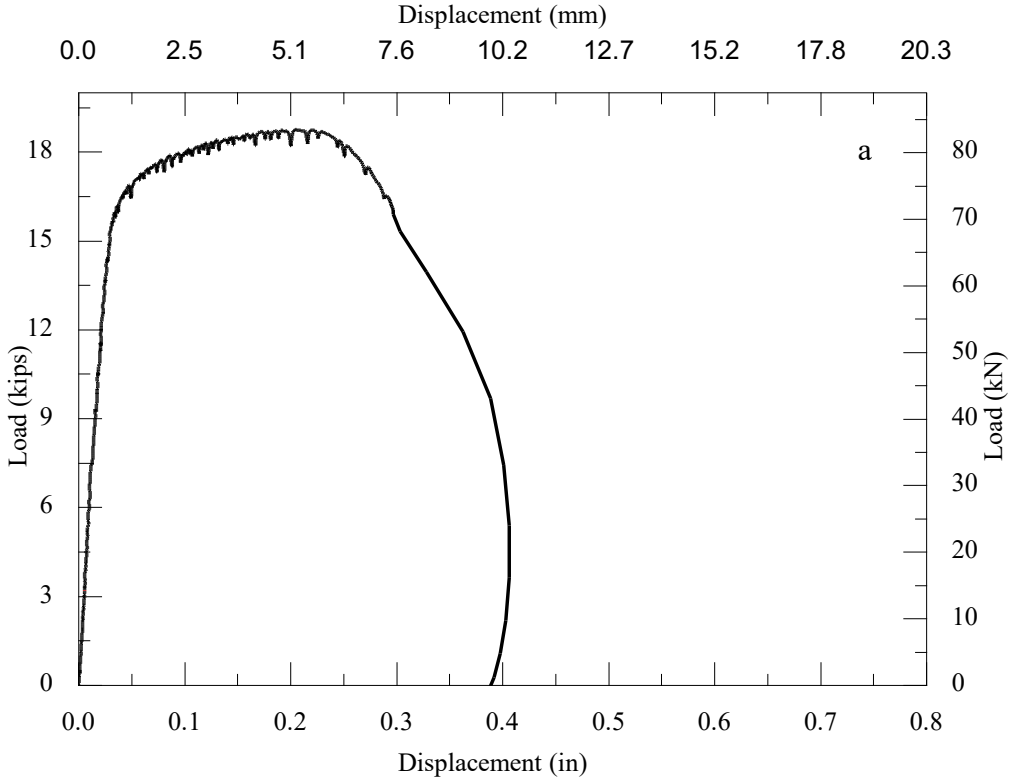



a) load-displacement behavior; b) steel failure

Figure III.18. Observed behavior of Specimen UC#R-0.5-4.5-#3

19. UC#R-0.5-5.0-#1

The hammer drill restarted at 1 in. away from the top of the hole during retraction due to the bit was stuck in the beginning. The measured ultimate load is at 16.42 kips at a displacement of 0.1897 in. The anchor was failed due steel failure shown in Figure III.19b. The ultimate load is within 15.6 kips (f_{uta}=110 ksi) and 17.73 kips (f_{uta}=125 ksi).

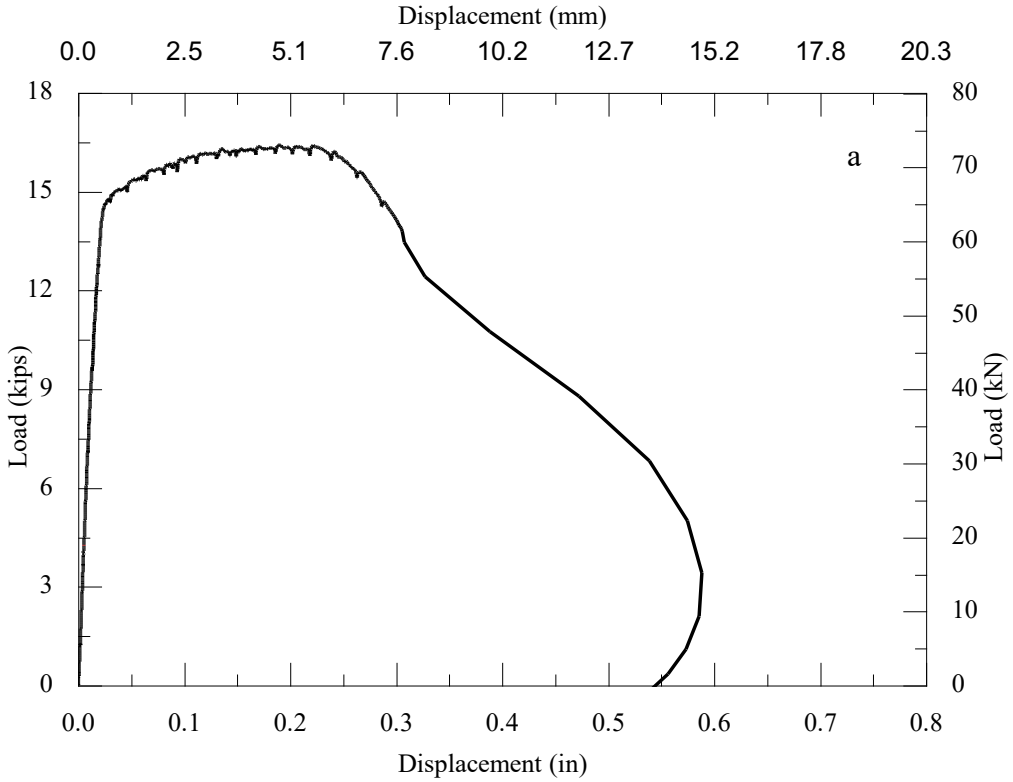



a) load-displacement behavior; b) steel failure

Figure III.19. Observed behavior of Specimen UC#R-0.5-5.0-#1

20. UC#R-0.5-5.0-#2

The measured ultimate load is at 17.4 kips at a displacement of 0.2281 in. The anchor was failed due steel failure shown in Figure III.20b.

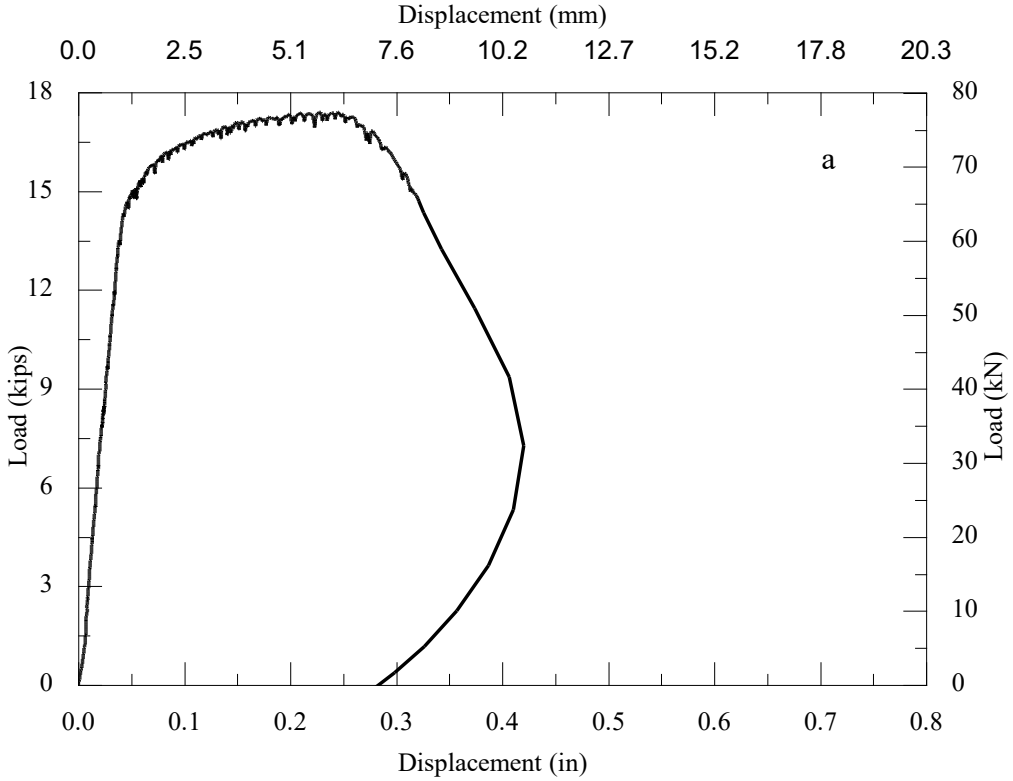



a) load-displacement behavior; b) steel failure

Figure III.20. Observed behavior of Specimen UC#R-0.5-5.0-#2

21. UC-0.625-2.5-#1

The anchor was tilted (0.7 degrees) in longitudinal direction. The measured ultimate load is at 6.42 kips at a displacement of 0.0190 in. A circular crack was form when the load reached 6.4 kips. Then, the load dropped. The anchor was pulled out with a concrete cone due to pullout and concrete breakout failure shown in Figure III.21b and 21c.

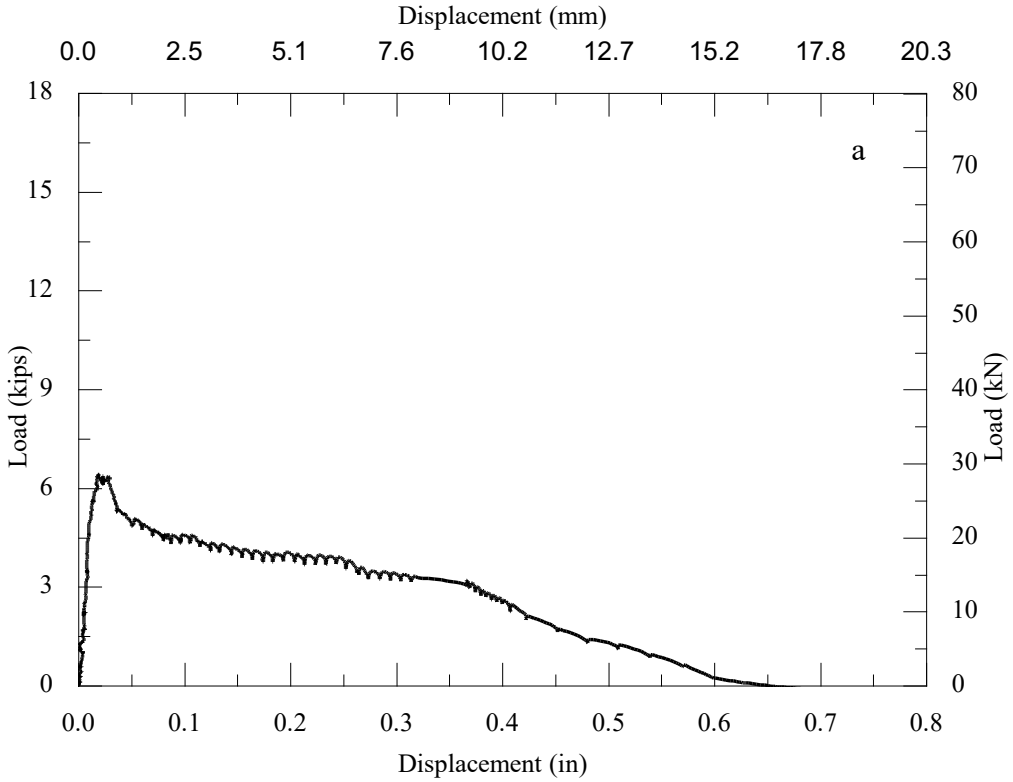

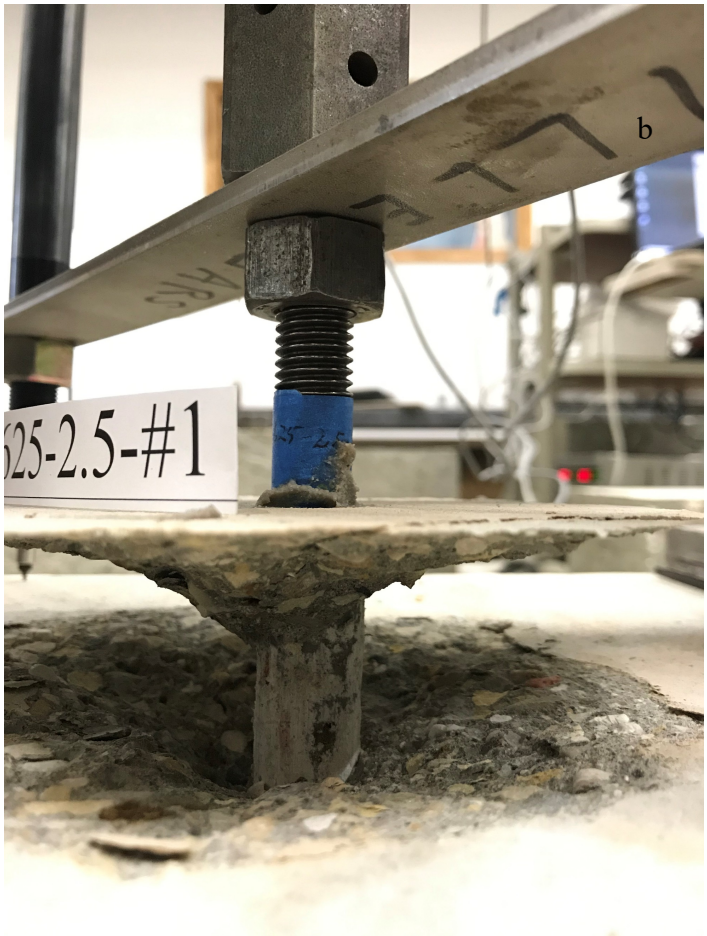



a) load-displacement behavior; b), c) partial breakout cone

Figure III.21. Observed behavior of Specimen UC -0.625-2.5-#1

22. UC-0.625-2.5-#2

The measured ultimate load is at 5.8 kips at a displacement of 0.0524 in. A circular crack was form when the load reached 5.8 kips. Then, the load dropped. The anchor was pulled out with a concrete cone due to adhesive-concrete interface failure shown in Figure III.22b and 22c.

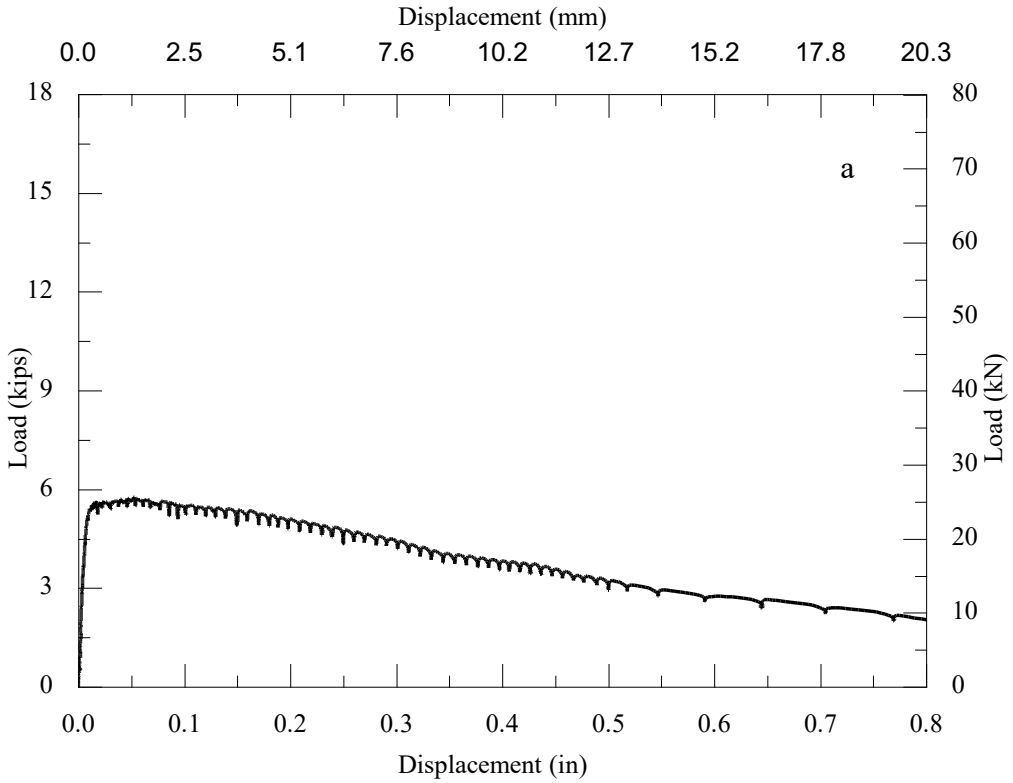

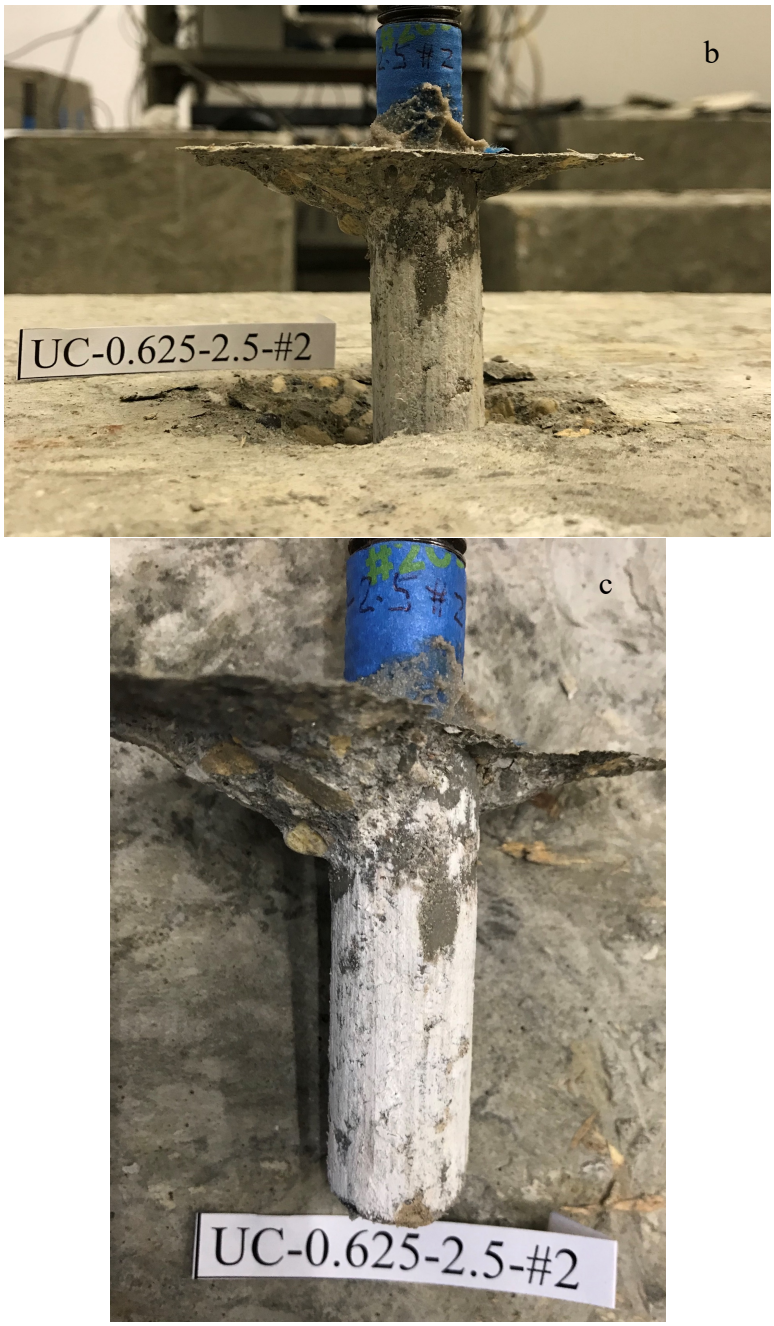

a) load-displacement behavior; b), c) partial breakout cone

Figure III.22. Observed behavior of Specimen UC -0.625-2.5-#2

23. UC-0.625-2.5-#3

The measured ultimate load is at 9.9 kips at a displacement of 0.0241 in. No record is available. The anchor was pulled out with a concrete cone due to concrete breakout failure shown in Figure III.23b.

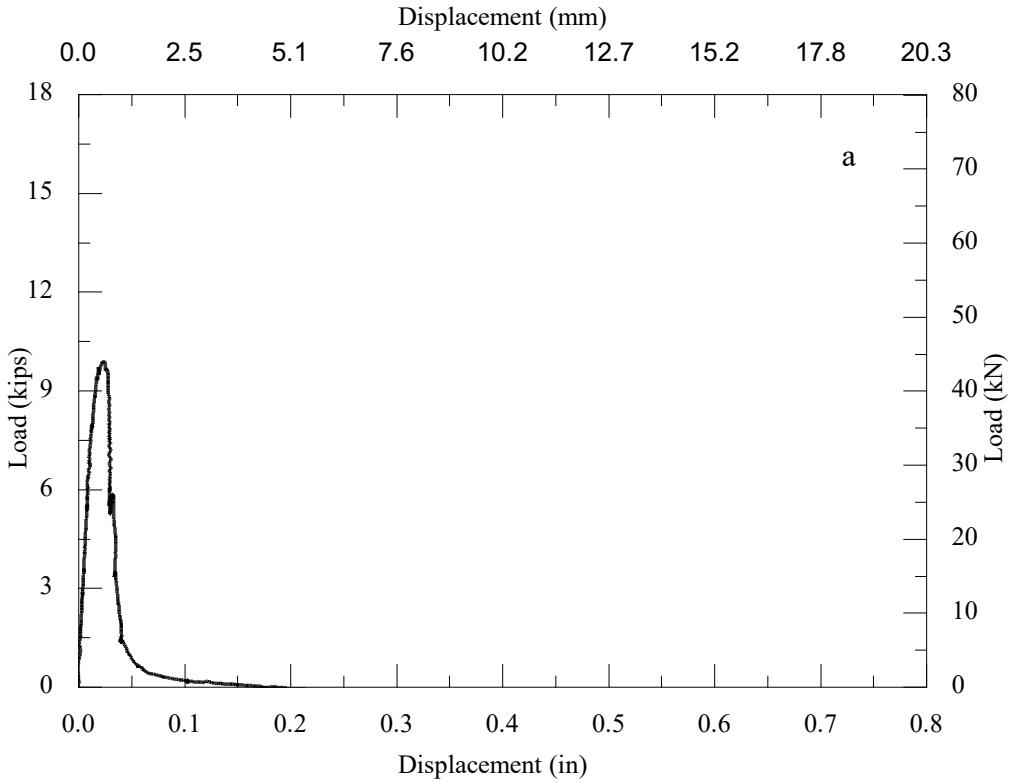



a) load-displacement behavior; b) breakout cone

Figure III.23. Observed behavior of Specimen UC -0.625-2.5-#3

24. UC-0.625-2.5-#4

It is not able to test due to the concrete face was damaged.

25. UC-0.625-3.75-#1

The measured ultimate load is at 11.2 kips at a displacement of 0.0378 in. A cracking sound occurred when the load reached 9.1 kips. One crack represented splitting and passing the anchor in the transverse direction when the load reached 10.75 kips. The anchor was pulled out with a concrete cone due to pullout and concrete breakout failure shown in Figure III.25b and 25c.

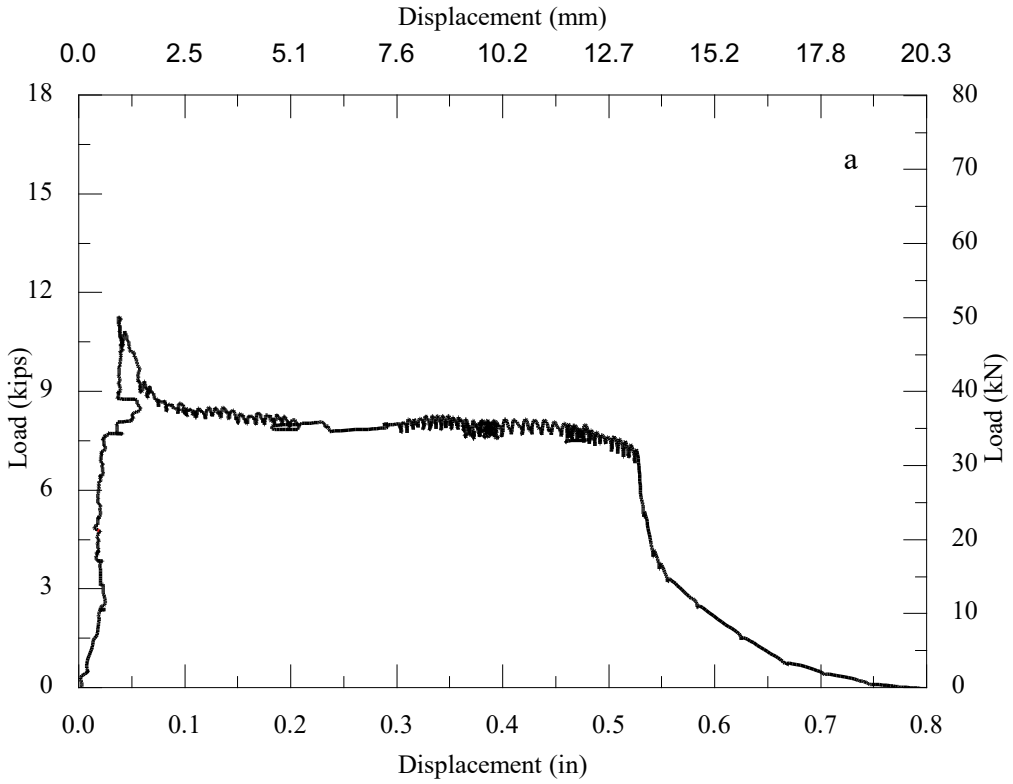

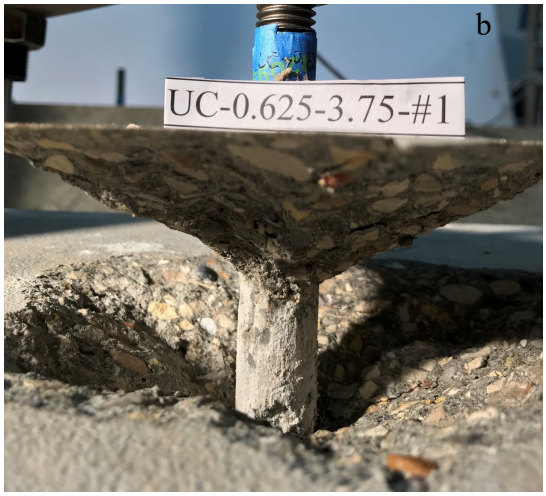

a) load-displacement behavior; b) partial breakout cone

Figure III.25. Observed behavior of Specimen UC -0.625-3.75-#1

26. UC-0.625-3.75-#2

The measured ultimate load is at 11.5 kips at a displacement of 0.0193 in. A circular crack occurred when the load reached 11.5 kips. Then the load dropped. A cracking sound occurred when the load dropped to 9.63 kips. One crack represented splitting and passing the anchor in the transverse direction and crack width was less than 0.0004 in. and crack depth was 3 in. when the load dropped to 9.63 kips. The crack width was enlarged to 0.01 in. and the crack depth was enlarged to 9 in. The anchor was pulled out with a concrete cone due to adhesive-concrete interface failure shown in Figure III.26b and 26c.

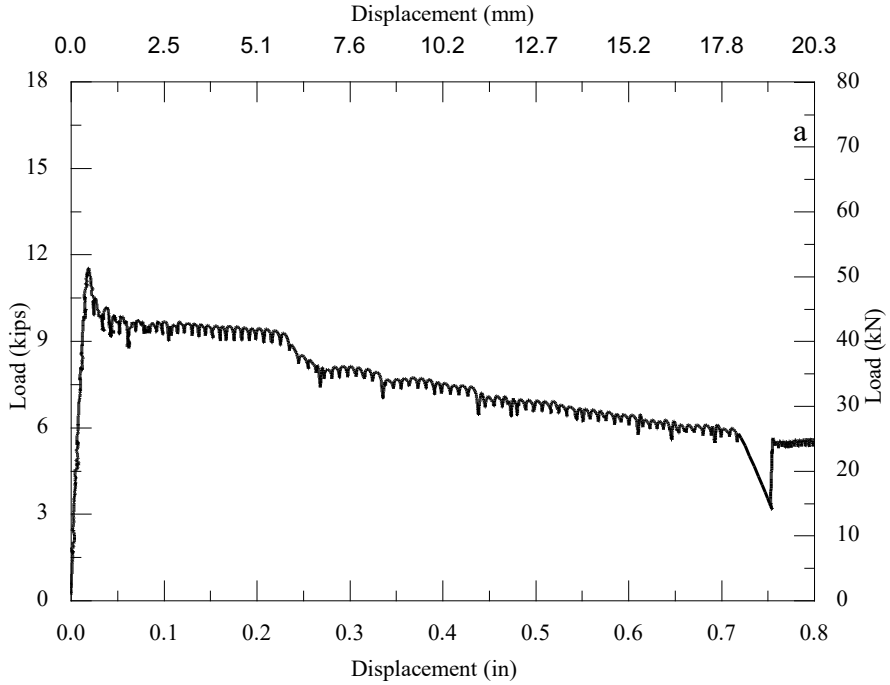

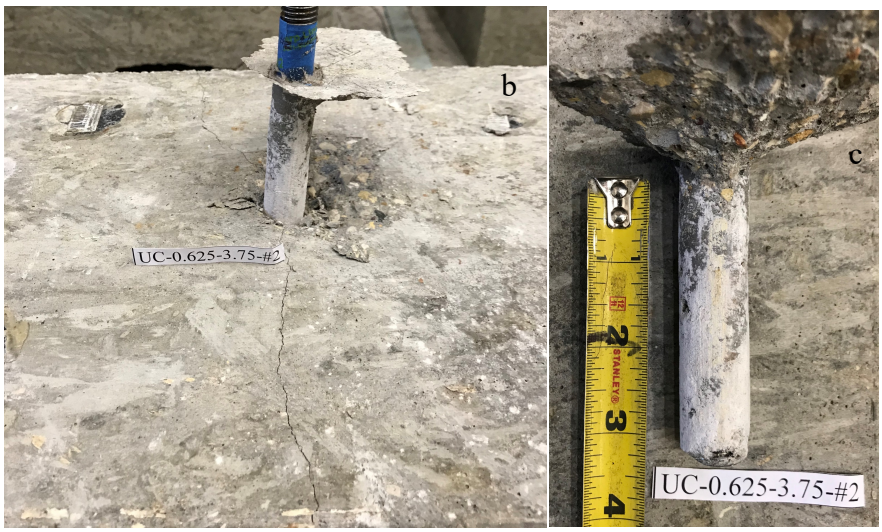

a) load-displacement behavior; b) crack surface; c) partial breakout cone

Figure III.26. Observed behavior of Specimen UC -0.625-3.75-#2

27. UC-0.625-3.75-#3

Transverse splitting crack through the whole block width from testing specimen #1 and #2, crack passed test anchor. The measured ultimate load is at 9.9 kips at a displacement of 0.35 in. Initial transverse splitting crack through the whole block width from testing specimen #1 and #2, crack passed test anchor. A circular crack occurred when the load reached 9.36 kips. Then the load kept constant. The anchor was pulled out with a concrete cone due to pullout and concrete breakout failure shown in Figure III.27b and 27c.

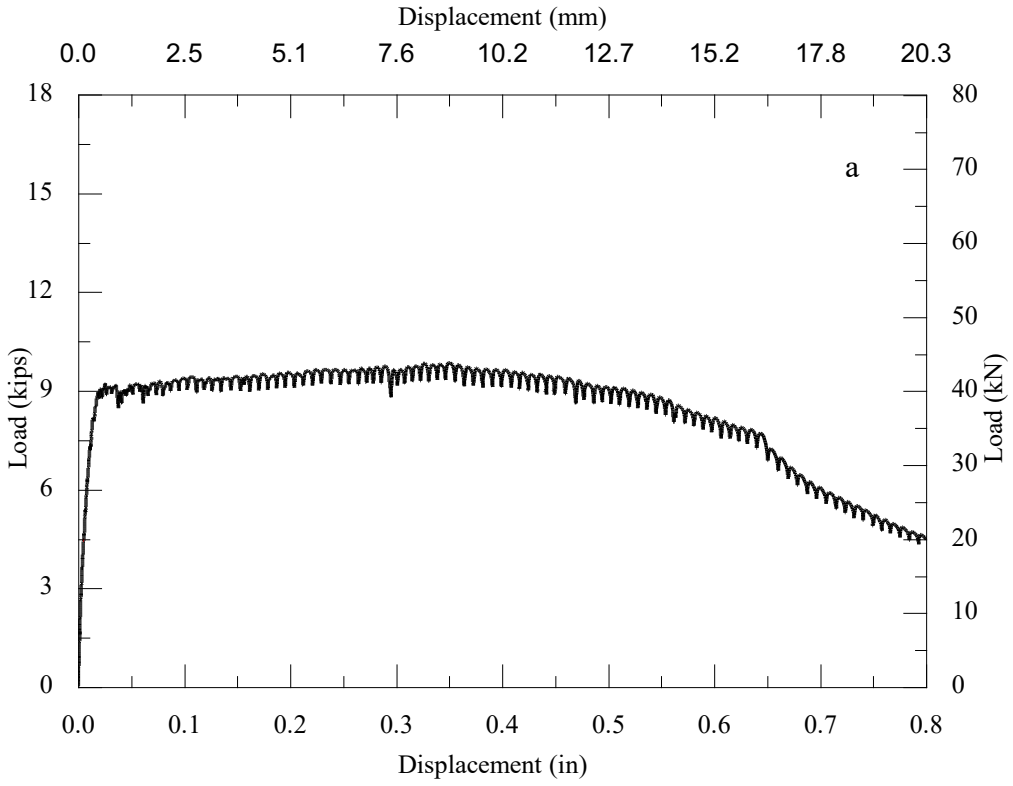



a) load-displacement behavior; b) crack surface; c) partial breakout cone

Figure III.27. Observed behavior of Specimen UC -0.625-3.75-#3

28. UC-0.625-3.75-#4

Dusts stuck on wall of the drilled hole. Transverse splitting crack through the whole block width from testing Specimen #1 and #2, crack was 5/8 in. away from test anchor. The measured ultimate load is at 9.96 kips at a displacement of 0.0382 in. Initial transverse splitting crack through the whole block width from testing specimen #1 and #2, crack was 5/8 in. away from test anchor and crack depth was 1 in. A circular crack occurred when the load reached 8.56 kips. Then the load dropped. The anchor was pulled out with a concrete cone due to pullout and concrete breakout failure shown in Figure III.28b and 28c.

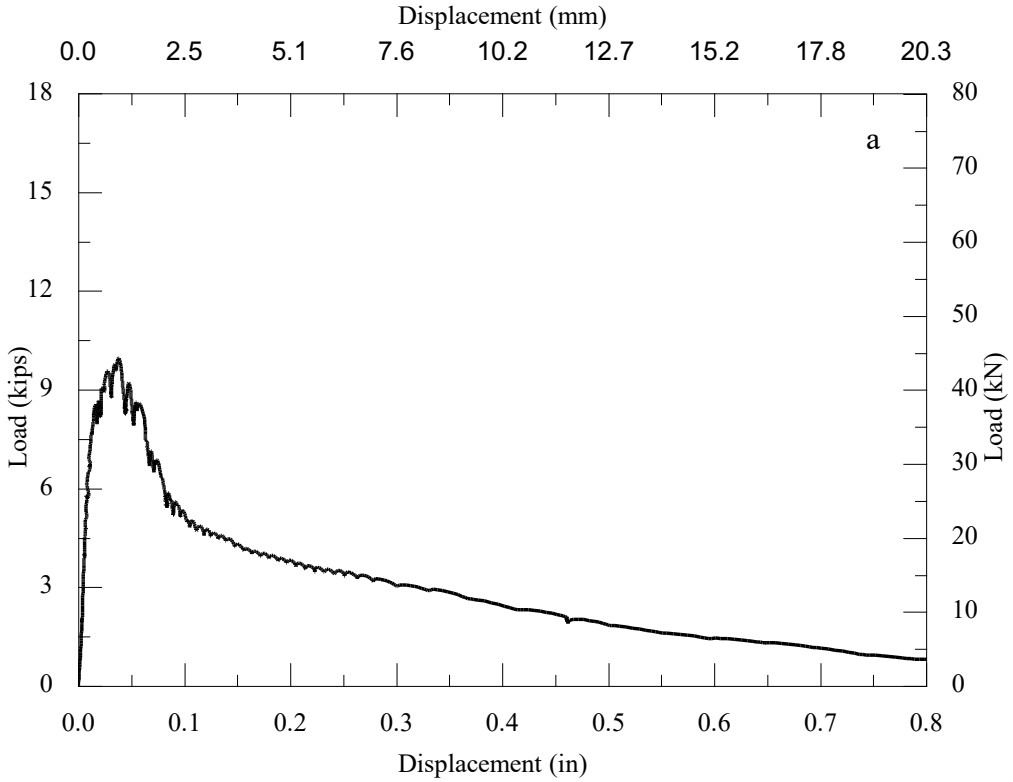





a) load-displacement behavior; b) crack surface; c) partial breakout cone

Figure III.28. Observed behavior of Specimen UC -0.625-3.75-#4

29. UC-0.625-5.0-#1

The measured ultimate load is at 16.57 kips at a displacement of 0.018 in. As shown in Figure III.29b, one crack represented splitting and passing the anchor in the transverse direction at the load of 16.57 kips with 1.5 in. crack depth; one represented splitting in the transverse direction at the load of 16.57 kips with 1.5 in, which was about 2.5 in. away from the left side of the anchor. The predicted capacity measuring a 2.87-in. deep breakout simultaneously with a 2 -in. deep bond failure (16.25 kips). The anchor was pulled out with a concrete cone due to concrete breakout failure shown in Figure III.29c.

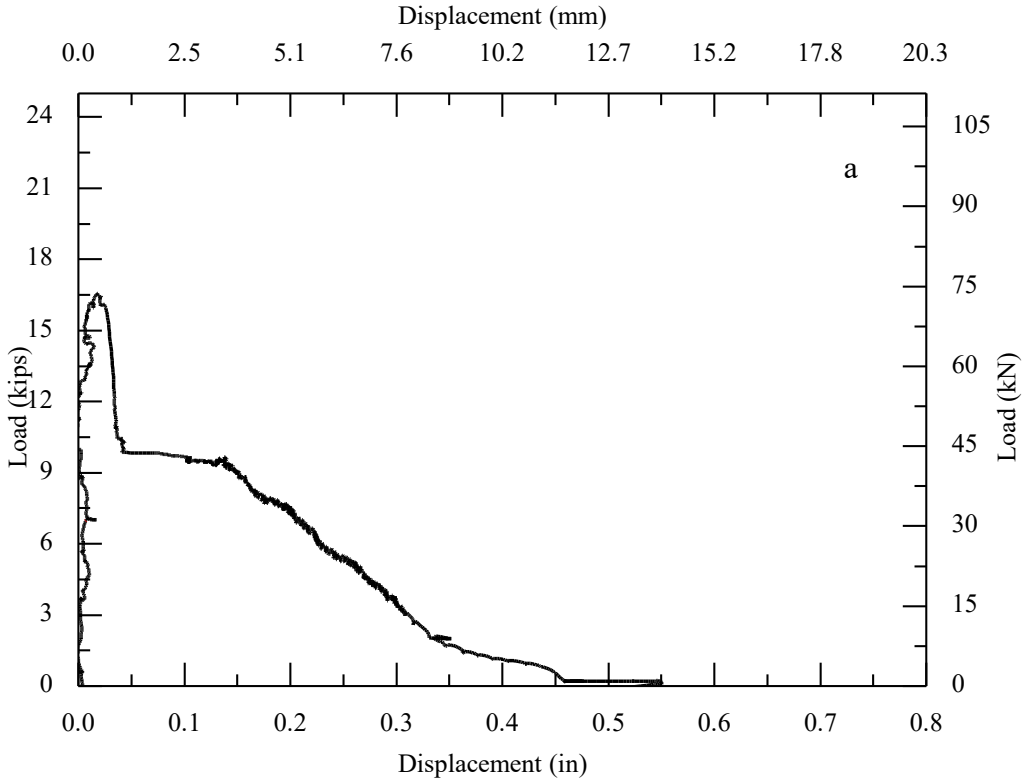

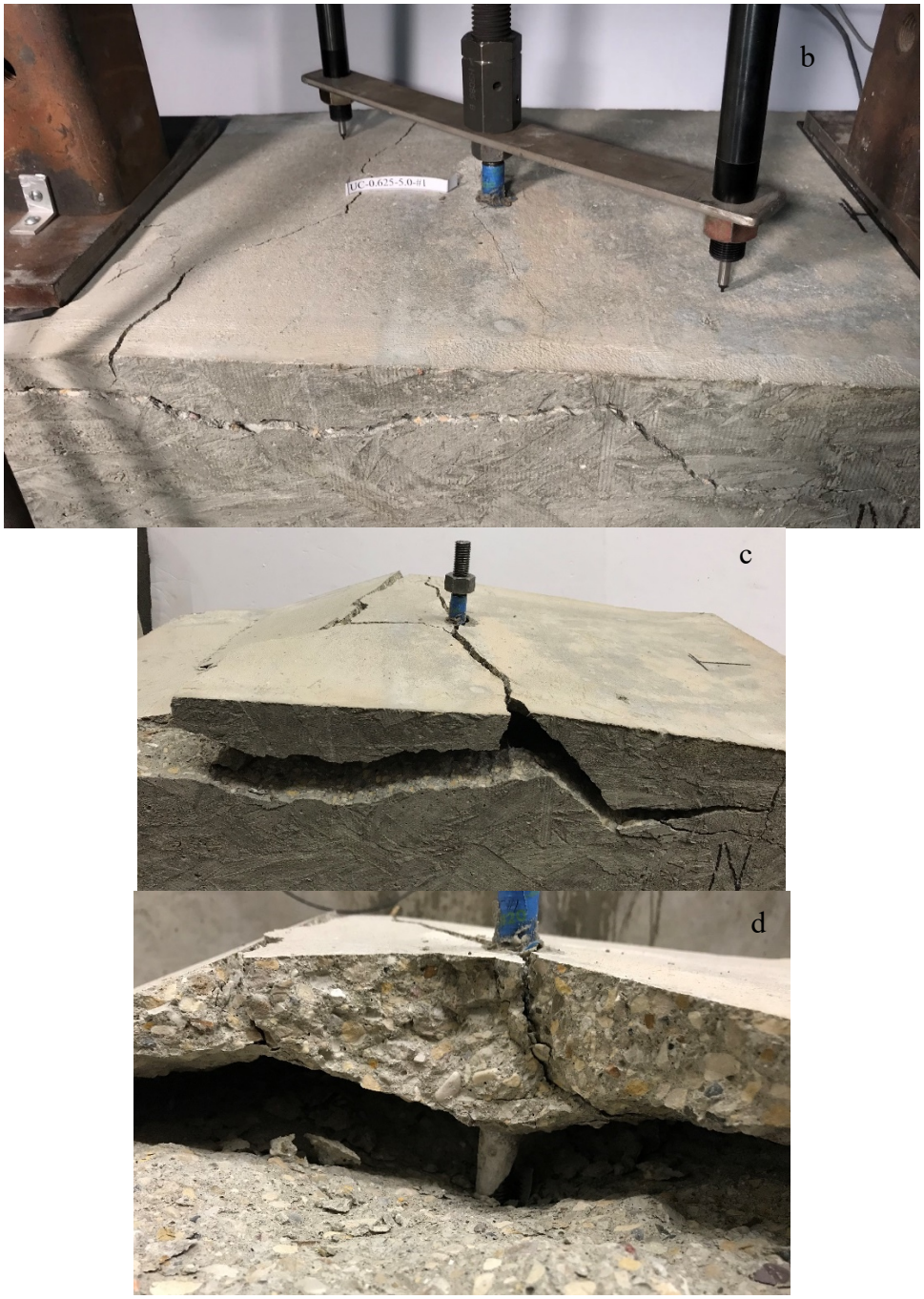

a) load-displacement behavior; b) cracked surface; c) d) concrete breakout failure.

Figure III.29. Observed behavior of Specimen UC-0.625-5.0-#1

30. UC-0.625-5.0-#2

The measured ultimate load is at 18.46 kips at a displacement of 0.0207 in. A circular crack was formed at the load of 15.52 kips. One crack represented splitting and passing the anchor in the transverse direction and crack width was less than 0.02 in. at the load of 18.46 kips; one cracks represented splitting and passing the anchor in the longitudinal direction and crack width was less than 0.08 in when the load dropped to 10.17 kips. The predicted capacity measuring a 4.09-in. deep breakout simultaneously with a 0.75 -in. deep bond failure (18.25 kips). The anchor was pulled out with a concrete cone due to concrete breakout failure shown in Figure III.30c.

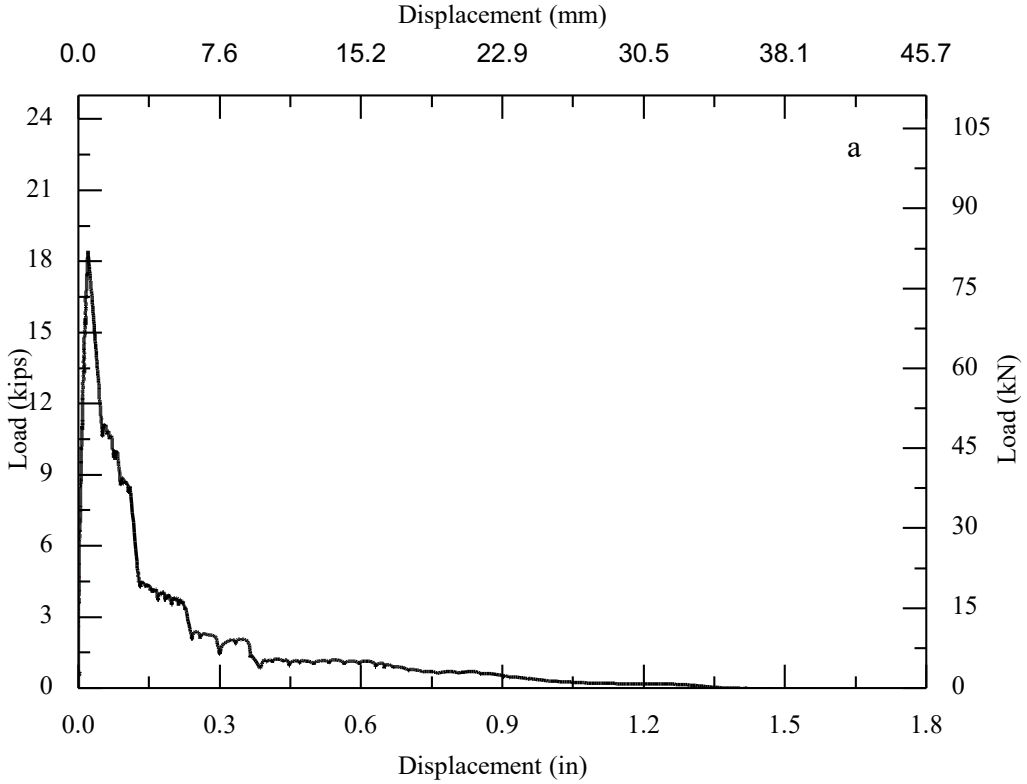



a) load-displacement behavior; b) c) cracked surface; d) concrete breakout failure.

Figure III.30. Observed behavior of Specimen UC-0.625-5.0-#2

31. UC-0.625-5.0-#3

Transverse splitting crack through the whole block width from testing Repeats #1 and #2, crack passed test anchor. Breakout crack in longitudinal direction from testing Repeat #2, breakout failure reduced edge distance by 1.5 in. The measured ultimate load is at 12.76 kips at a displacement of 0.034 in. Initial transverse splitting crack through the whole block width from testing specimen #1 and #2, crack passed test anchor. Breakout crack in longitudinal direction from testing specimen#2, breakout failure reduced edge distance by 1.5 in. One crack represented splitting and passing the anchor in the transverse direction at the load of 12.76 kips with 1.5 in. of crack depth. The predicted capacity in cracked concrete measuring a 1.06-in. deep breakout simultaneously with a 3.75 -in. deep bond failure (14.7 kips). The anchor was pulled out with a concrete cone due to concrete breakout failure shown in Figure III.31c and I.31d.

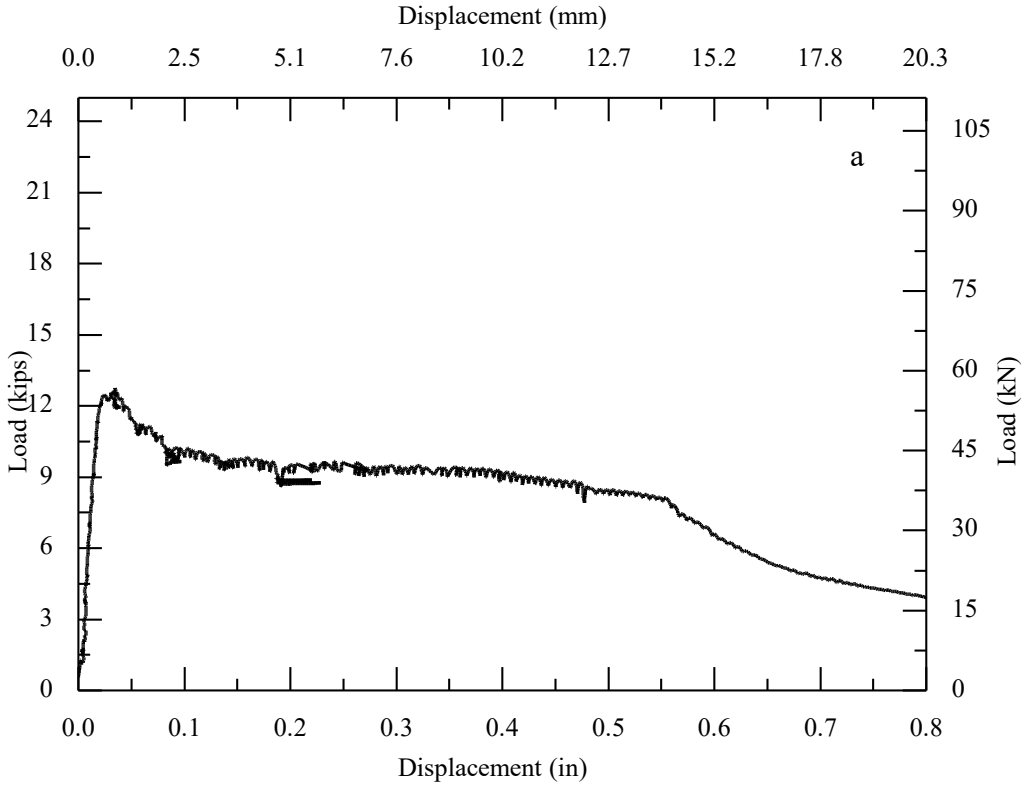



a) load-displacement behavior; b) cracked surface; c) d) concrete breakout failure.

Figure III.31. Observed behavior of Specimen UC-0.625-5.0-#3

32. UC-0.625-5.0-#4

Transverse splitting crack through the whole block width from testing Specimen #1 and #2, crack passed test anchor. Breakout crack in longitudinal direction from testing specimen #1 and #2, breakout failure reduced edge distances by 1 and 3 in. The measured ultimate load is at 10.63 kips at a displacement of 0.746 in. Initial transverse splitting crack through the whole block width from testing specimen #1 and #2, crack passed test anchor. Breakout crack in longitudinal direction from testing specimen #1 and #2, breakout failure reduced edge distance by 1 and 3 in. A circular crack was formed at the load of 16.05 kips. One crack represented splitting and passing the anchor in the transverse direction and the crack depth was 0.5 in. when the load reached 16.37 kips. The predicted capacity in cracked concrete measuring a 0.92-in. deep breakout simultaneously with a 4 -in. deep bond failure (15.31 kips). The anchor was pulled out with a concrete cone due to adhesive-concrete interface failure shown in Figure III.32c.

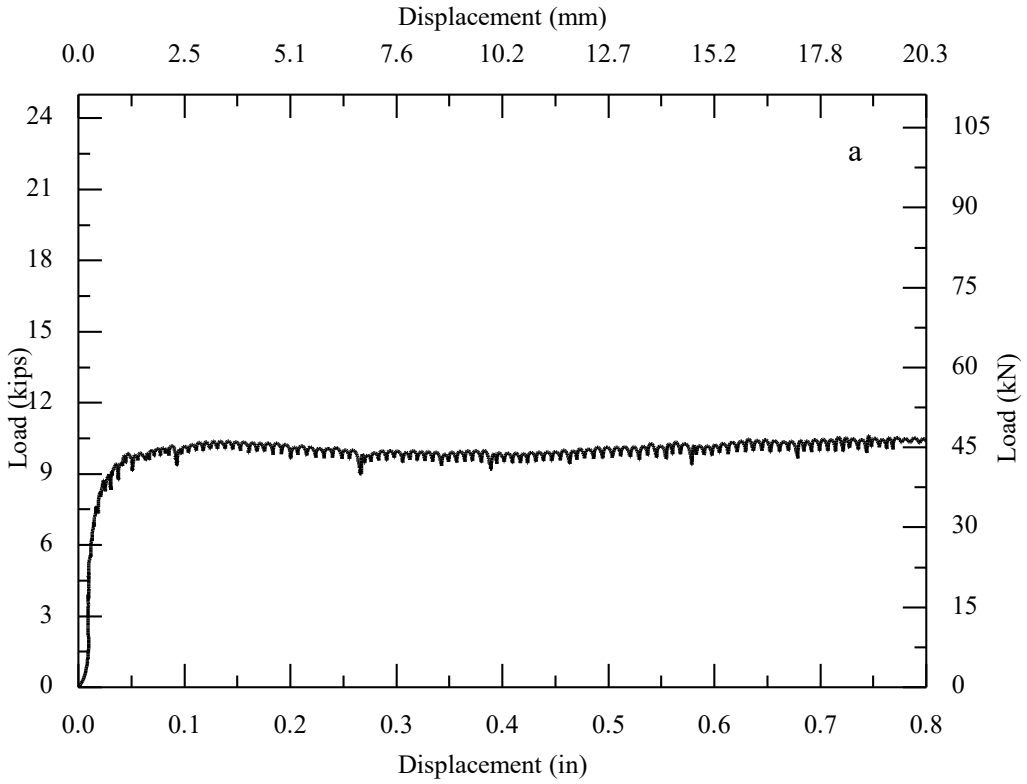



a) load-displacement behavior; b) cracked surface; c) partial cone bond failure.

Figure III.32. Observed behavior of Specimen UC-0.625-5.0-#4

33. UC#R-0.625-5.0-#1

The measured ultimate load is at 16.97 kips at a displacement of 0.379 in. A cracking sound occurred, and a circular crack was formed when the load reached 12.31 kips. One crack represented splitting and passing the anchor in the transverse direction and crack depth was 3 in. when the load reached 16.05 kips. The anchor was pulled out with a concrete cone due to pullout and breakout failure shown in Figure III.33b and 33c.

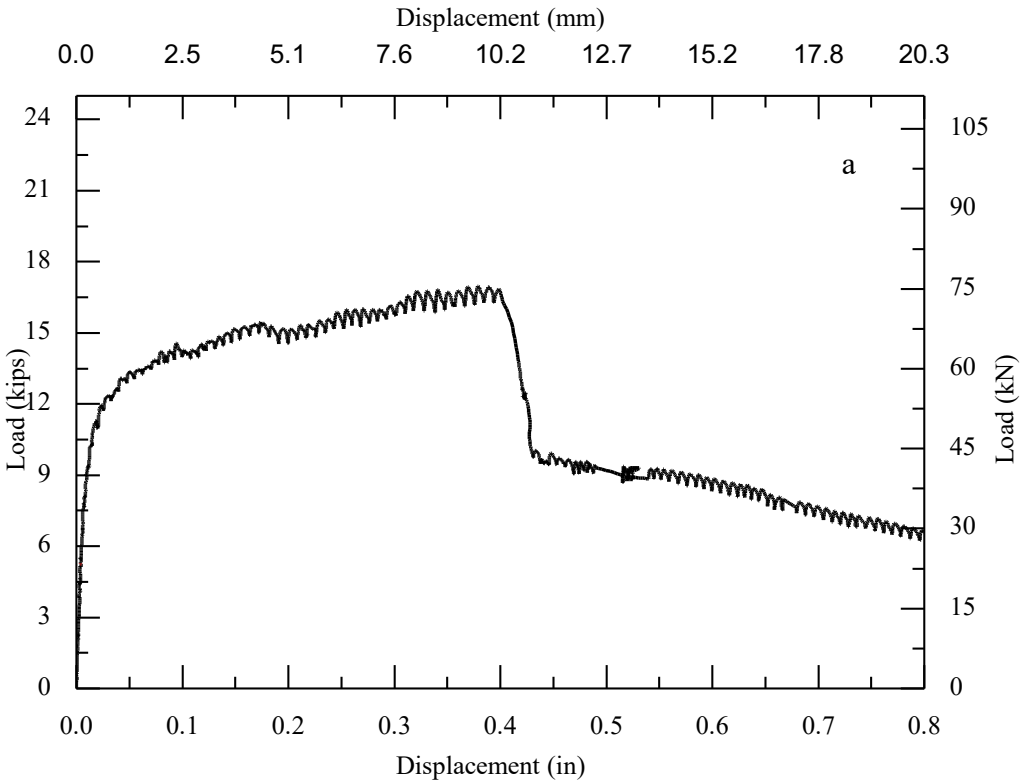

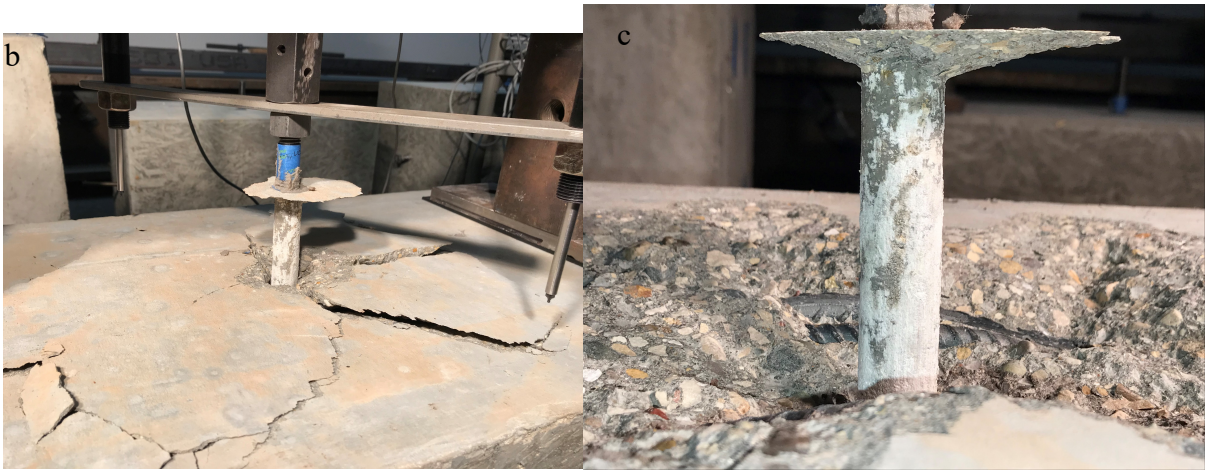

a) load-displacement behavior; b) cracked surface; c) partial cone bond failure.

Figure III.33. Observed behavior of Specimen UC#R-0.625-5.0-#1

34. UC#R-0.625-5.0-#2

The measured ultimate load is at 17.2 kips at a displacement of 0.0291 in. One crack represented splitting and passing the anchor in the transverse direction and crack width was 0.001 in. when the load reached 17.2 kips. Then, the load dropped to 15.51 kips and a circular crack was formed; A large cracking sound occurred when the load reached 10.86 kips. The anchor was pulled out with a concrete cone due to adhesive-concrete interface failure shown in Figure III.34c and 34d.

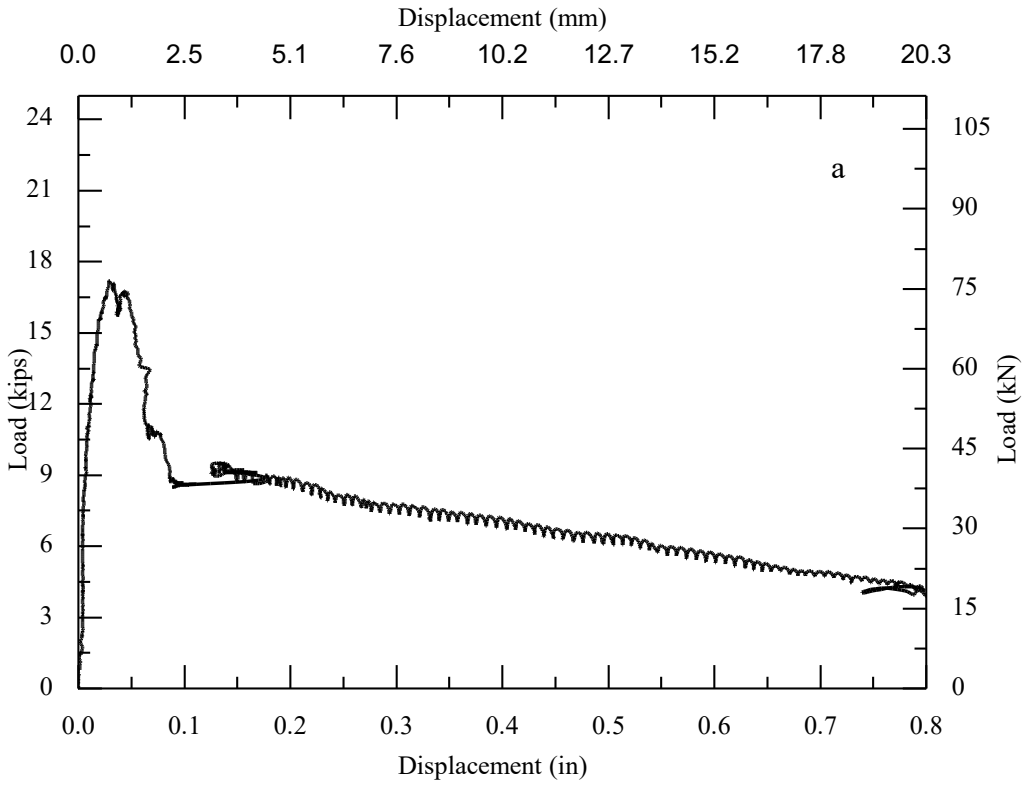



a) load-displacement behavior; b) cracked surface; c), d) partial cone bond failure.

Figure III.34. Observed behavior of Specimen UC#R-0.625-5.0-#2

35. UC#R-0.625-5.0-#3

The measured ultimate load is at 17.95 kips at a displacement of 0.0484 in. Initial transverse splitting crack from testing specimen #1 and #2, crack tip 1 in. away from the test anchor. A circular was formed when the load reached 14.28 kips. One crack represented splitting and passing the anchor in the diagonal direction when the load reached 17.66 kips. The anchor was pulled out with a concrete cone due to pullout and breakout failure shown in Figure III.35b and 35c.

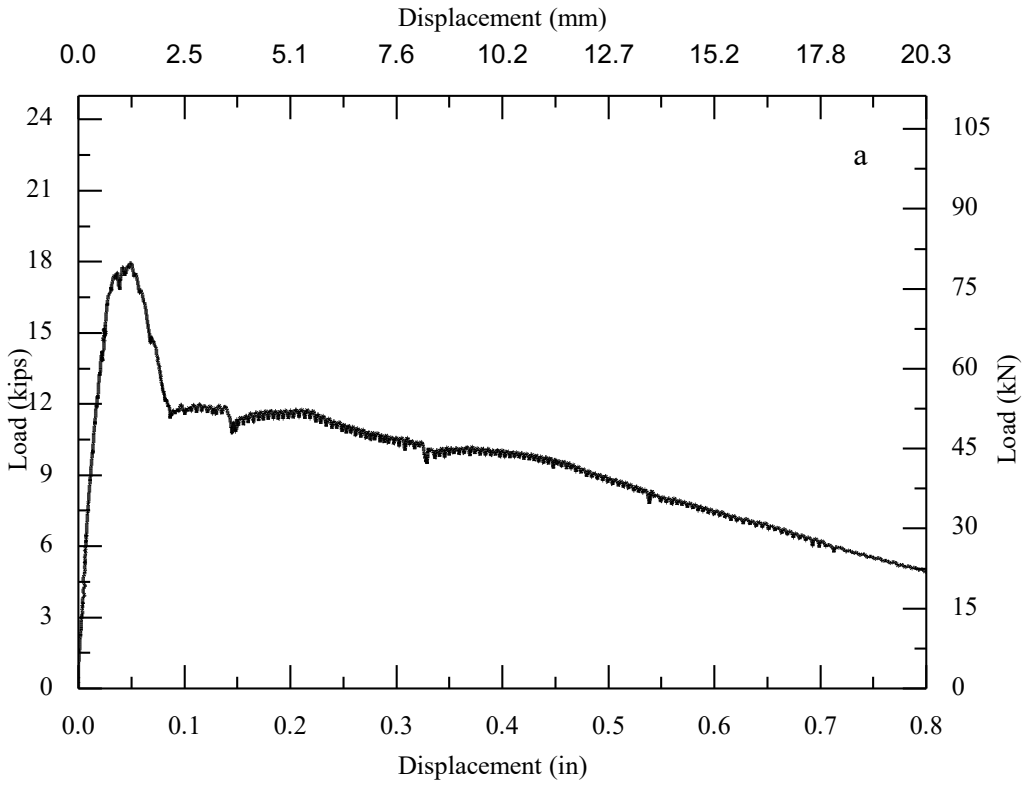

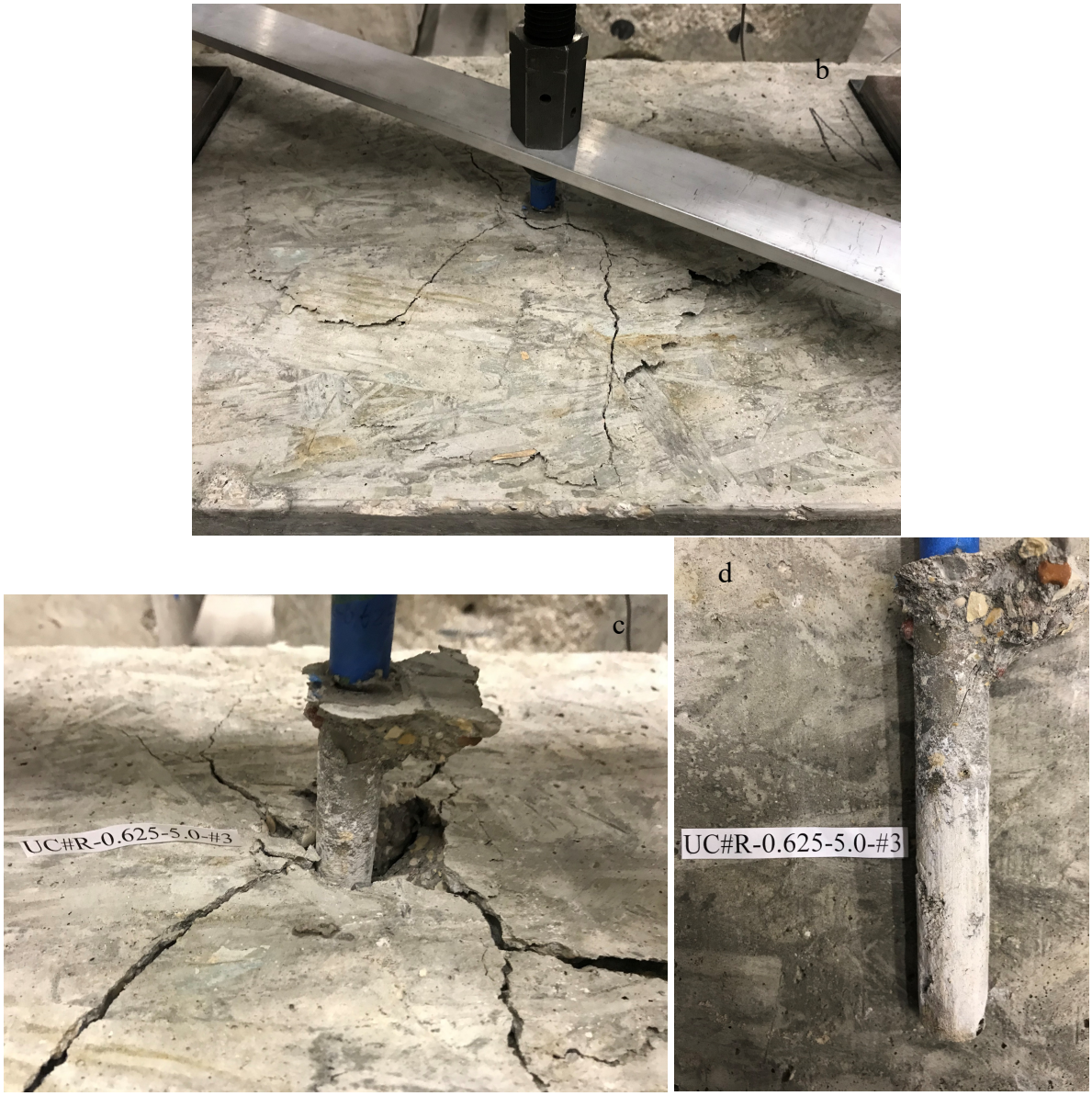

a) load-displacement behavior; b) cracked surface; c), d) partial cone bond failure.

Figure VI.36. Observed behavior of Specimen UC#R-0.625-5.0-#3

36. UC#R-0.625-5.0-#4

Transverse splitting crack from testing specimen #1, crack tip 4 in away from the test anchor. The measured ultimate load is at 17.69 kips at a displacement of 0.3893 in. An initial transverse splitting crack from testing specimen #1, crack tip 4 in. away from the test anchor. A circular was formed when the load reached 16.05 kips. One crack represented splitting and passing the anchor in the transverse direction and the crack depth was 0.5 in. when the load reached 16.37 kips. Then, the load kept constant. The anchor was pulled out with a concrete cone due to adhesive-concrete interface failure shown in Figure III.36b and 36c.

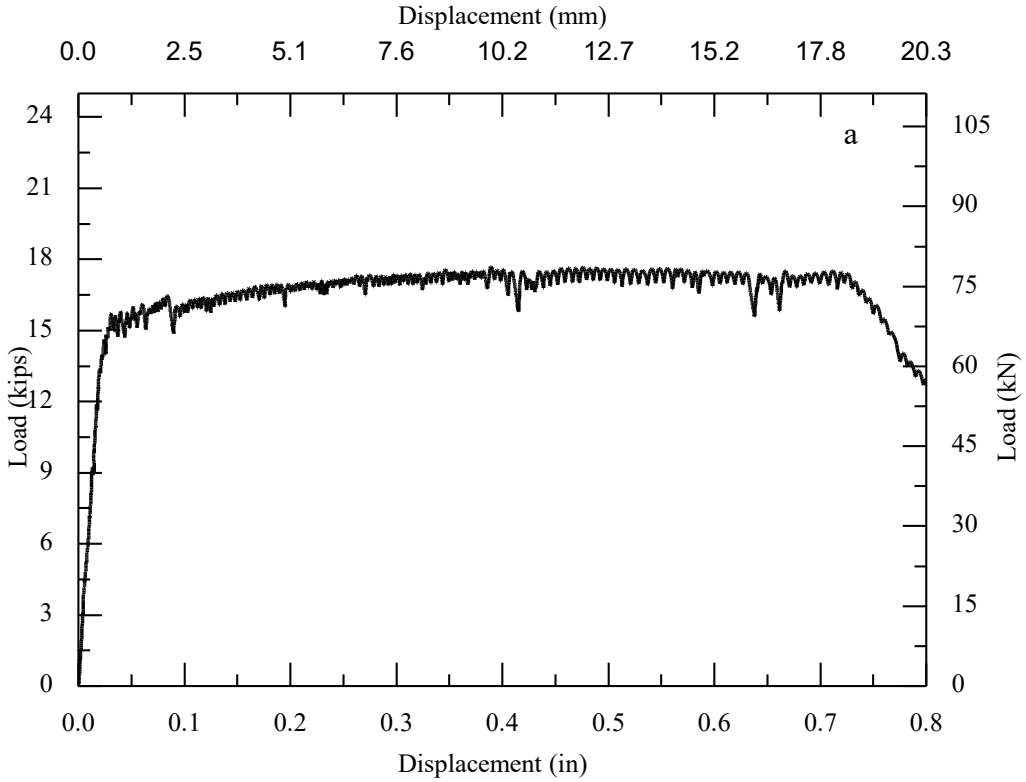



a) load-displacement behavior; b) cracked surface; c), d) partial cone bond failure.

Figure III.36. Observed behavior of Specimen UC#R-0.625-5.0-#4

37. UC-0.75-3.0-#1

The measured ultimate load is at 11.06 kips at a displacement of 0.0209 in. A circular crack was formed when the load reached 11.06 kips. The anchor was pulled out with a concrete cone due to concrete breakout failure shown in Figure III.37b.

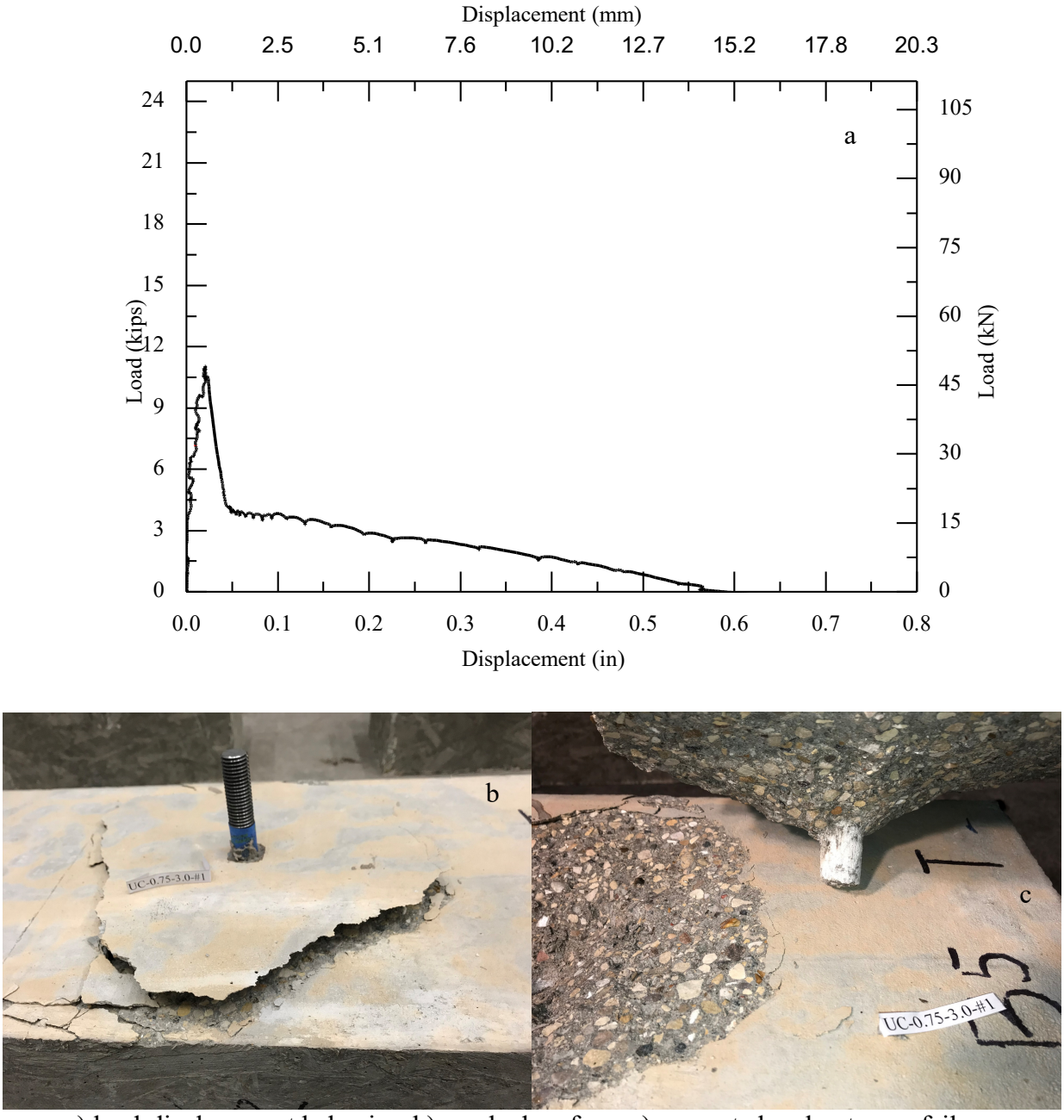

a) load-displacement behavior; b) cracked surface; c) concrete breakout cone failure.

Figure III.37. Observed behavior of Specimen UC-0.75-3.0-#1

38. UC-0.75-3.0-#2

The measured ultimate load is at 8.89 kips at a displacement of 0.3379 in. A circular crack was formed when the load reached 5.62 kips. The anchor was pulled out with a concrete cone due to adhesive-concrete interface bond failure shown in Figure III.38c.

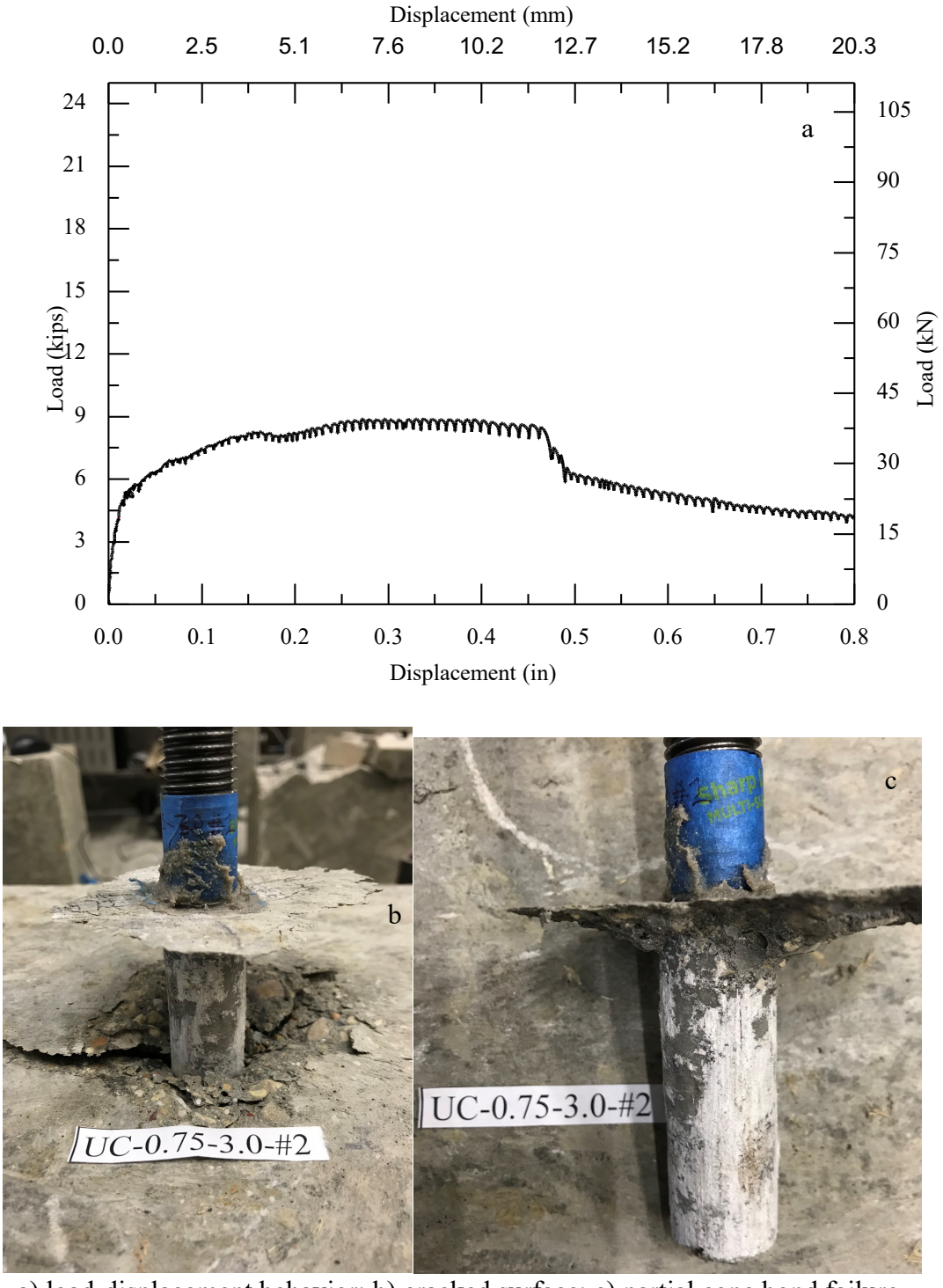

a) load-displacement behavior; b) cracked surface; c) partial cone bond failure.

Figure III.38. Observed behavior of Specimen UC-0.75-3.0-#2

39. UC-0.75-3.0-#3

The measured ultimate load is at 9.64 kips at a displacement of 0.0266 in. A circular crack was formed when the load reached 7.49 kips. One crack represented splitting and passing the anchor in diagonal direction when the load reached 8.77 kips. One crack represented splitting and passing the anchor in the transverse direction when the load reached 9.64 kips. The anchor was pulled out with a concrete cone due to pullout and breakout failure shown in Figure III.39c.

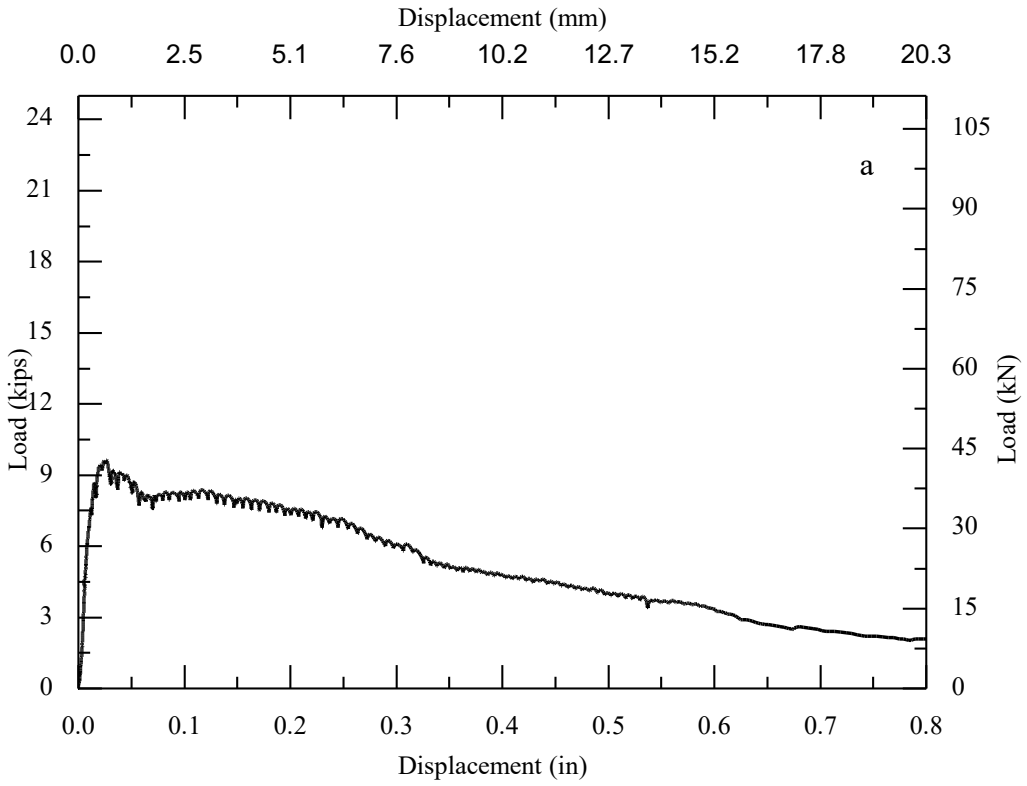

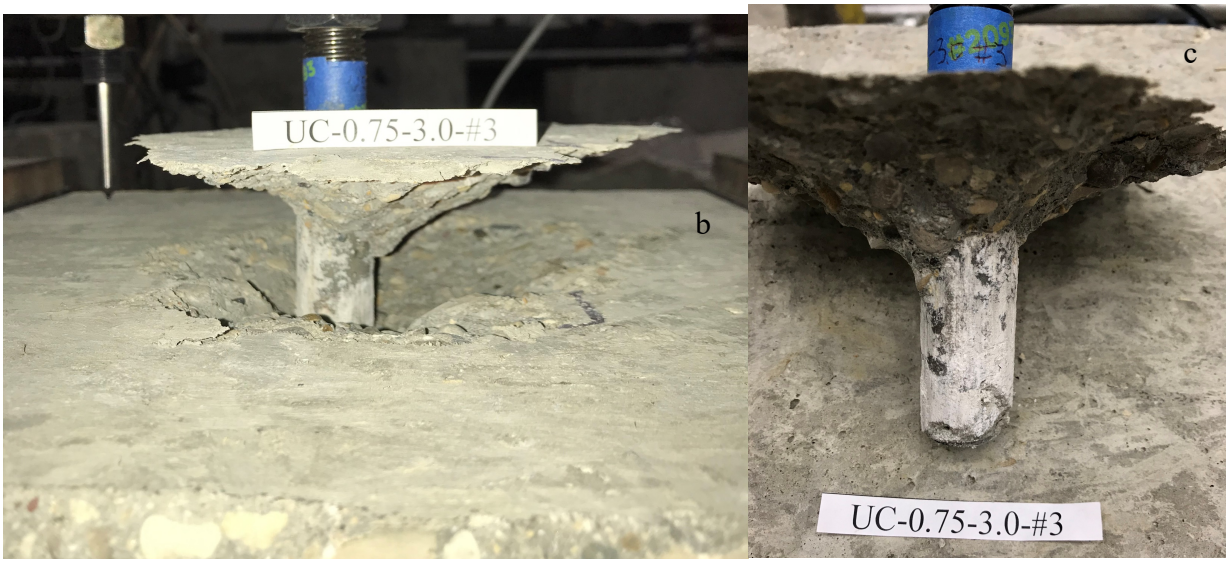

a) load-displacement behavior; b) cracked surface; c) partial cone bond failure.

Figure III.39. Observed behavior of Specimen UC-0.75-3.0-#3

40. UC-0.75-3.0-#4

Dusts stuck on wall that it was around 1 in. away from the bottom of the drilled hole. The measured ultimate load is at 9.32 kips at a displacement of 0.1317 in. A circular crack was formed when the load reached 8.56 kips. The anchor was pulled out with a concrete cone due to pullout and breakout failure shown in Figure III.40c.

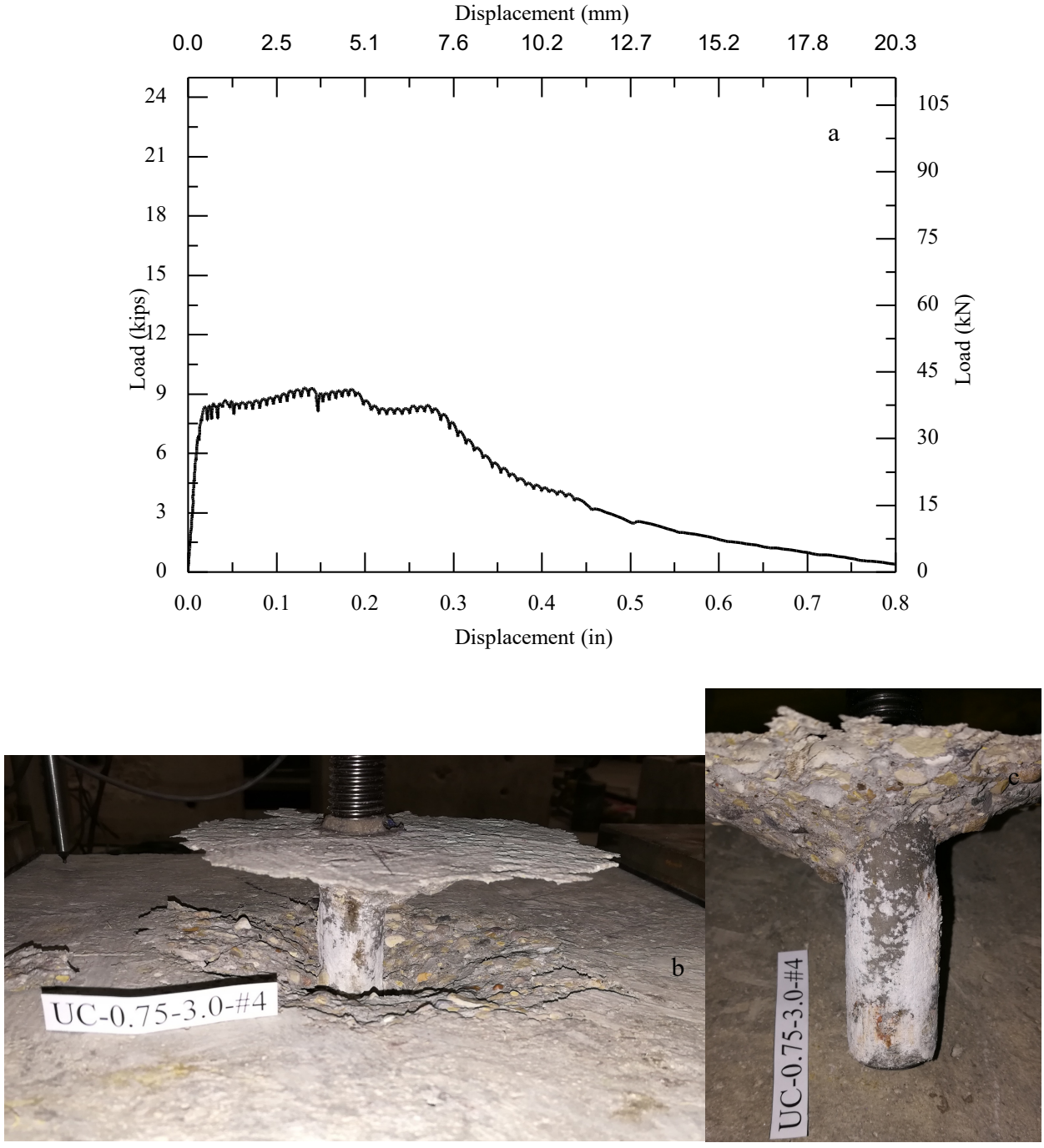

a) load-displacement behavior; b) cracked surface; c) partial cone bond failure.

Figure III.40. Observed behavior of Specimen UC-0.75-3.0-#4

41. UC#R-0.75-4.5-#1

The measured ultimate load is at 19.9 kips at a displacement of 0.1560 in. A cracking sound occurred, and a circular crack was formed when the load reached 11.77 kips. One crack represented splitting and passing the anchor in diagonal direction when the load reached 18.73 kips. The anchor was pulled out with a concrete cone due to pullout and breakout failure shown in Figure III.41c.

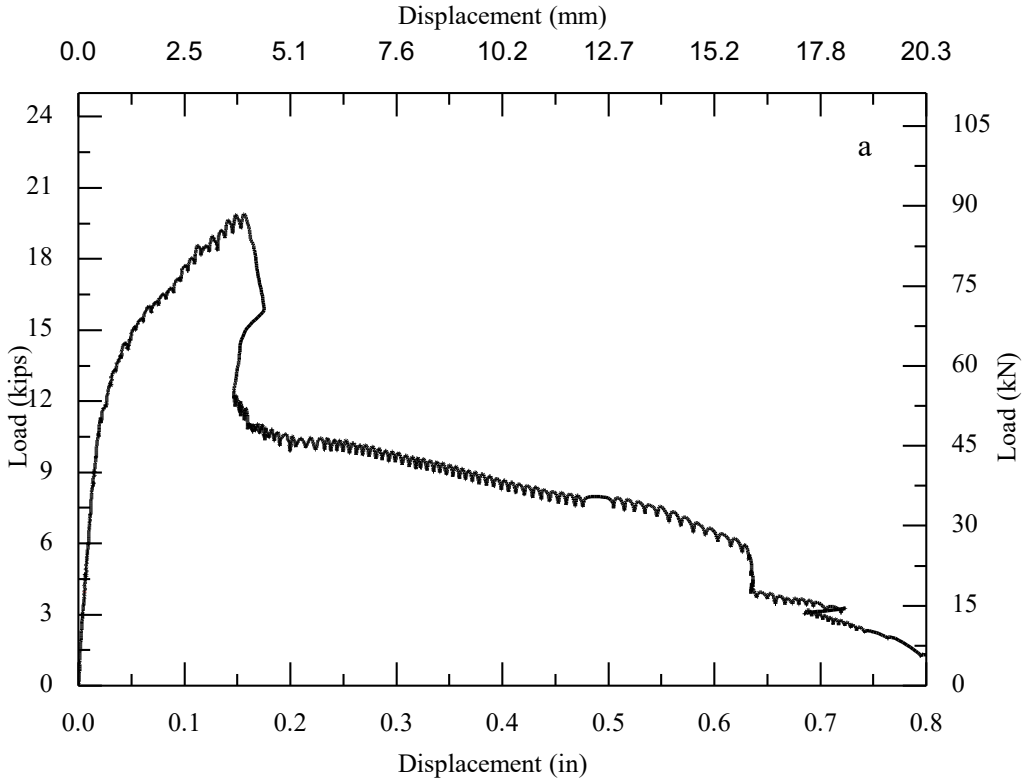



a) load-displacement behavior; b) cracked surface; c), d) partial cone bond failure.

Figure III.41. Observed behavior of Specimen UC#R-0.75-4.5-#1

42. UC#R-0.75-4.5-#2

The measured ultimate load is at 15.56 kips at a displacement of 0.2327 in. A circular crack was formed when the load reached 8.03 kips. Two cracks represented splitting and passing the anchor in diagonal direction when the load reached 14.45 kips and 14.98 respectively. The anchor was pulled out with a concrete cone due to pullout and breakout failure shown in Figure III.42c.

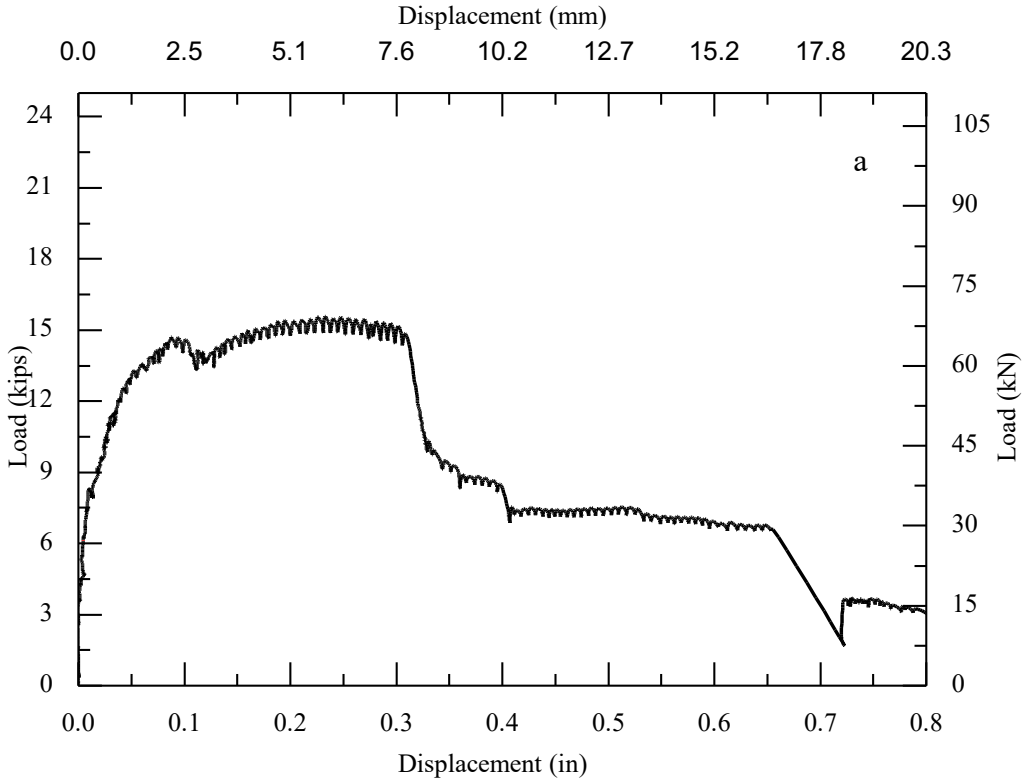

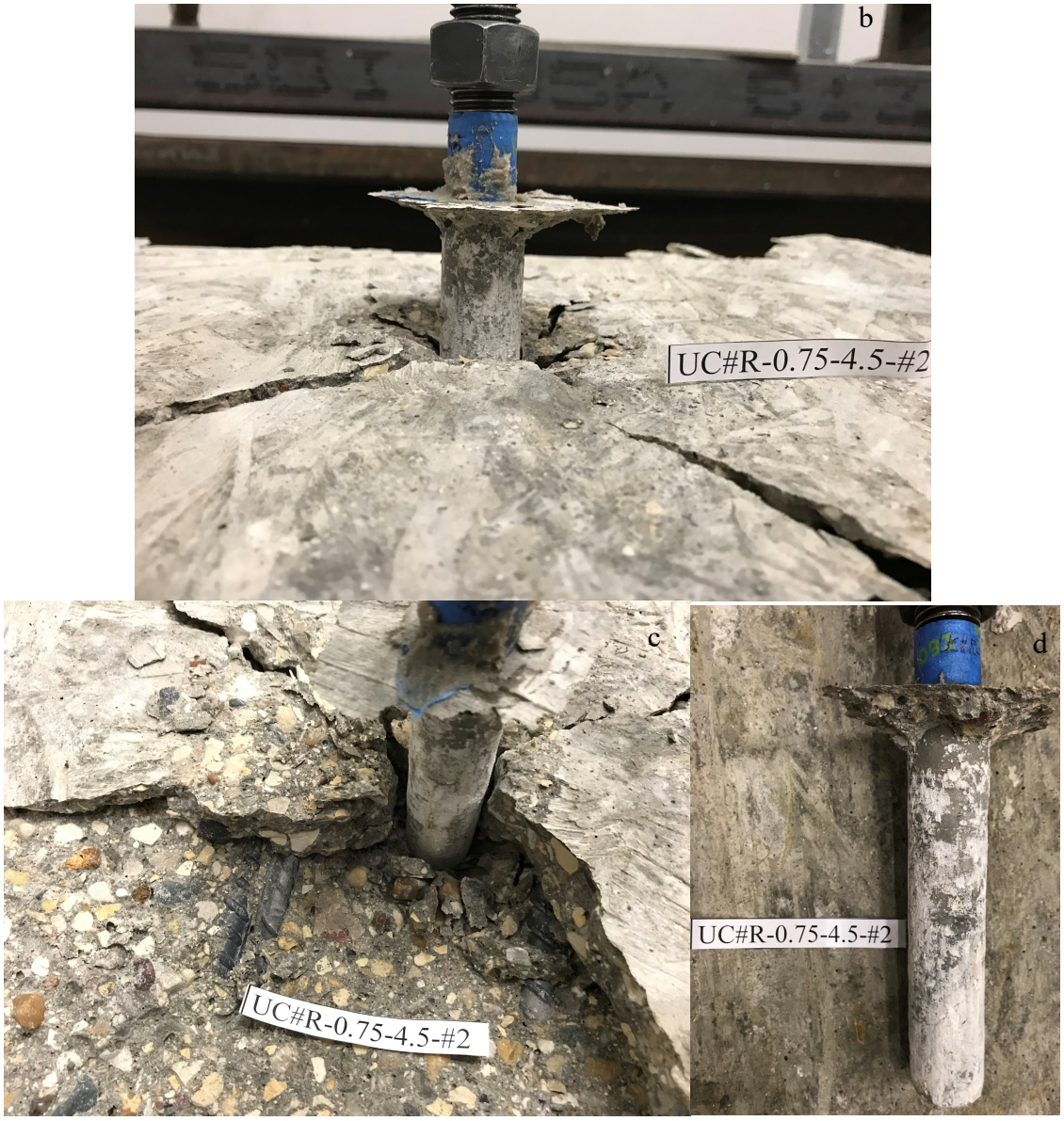

a) load-displacement behavior; b) cracked surface; c), d) partial cone bond failure.

Figure III.42. Observed behavior of Specimen UC#R-0.75-4.5-#2

43. UC#R-0.75-4.5-#3

The measured ultimate load is at 16.86 kips at a displacement of 0.2554 in. A circular crack was formed when the load reached 13.38 kips. The load dropped to 14.12 kips and a large cracking sound occurred. The anchor was pulled out with a concrete cone due to pullout and breakout failure shown in Figure III.43c.

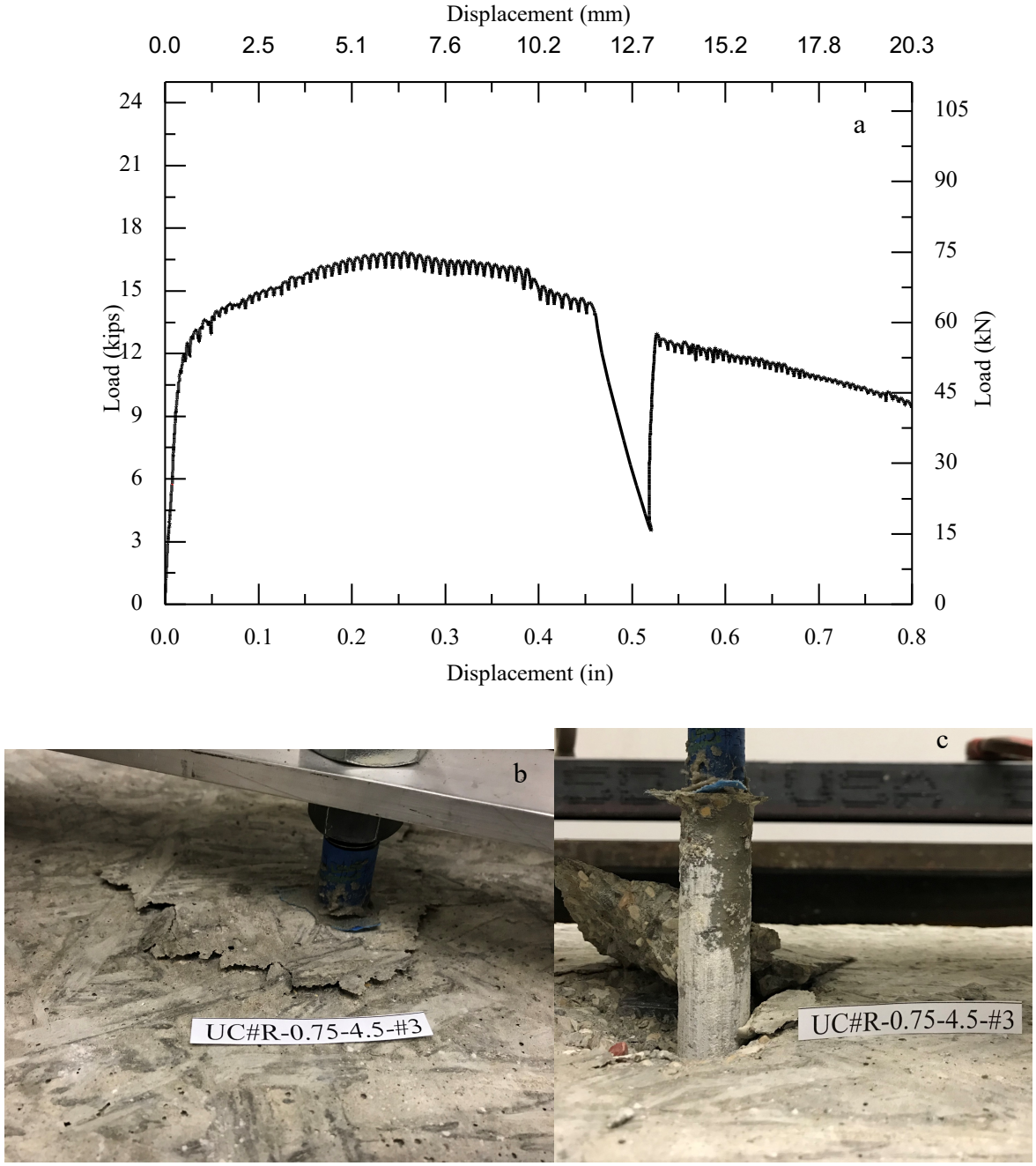

a) load-displacement behavior; b) cracked surface; c) partial cone bond failure.

Figure III.43. Observed behavior of Specimen UC#R-0.75-4.5-#3

44. UC#R-0.75-4.5-#4

The measured ultimate load is at 19.26 kips at a displacement of 0.1249 in. An initial crack represented splitting and passing the anchor in the transverse direction and crack depth was 1 in. A circular crack was formed when the load reached 14.98 kips. A cracking sound occurred at the load of 16.05 kips. The anchor was pulled out with a concrete cone due to pullout and breakout failure shown in Figure III.44c.

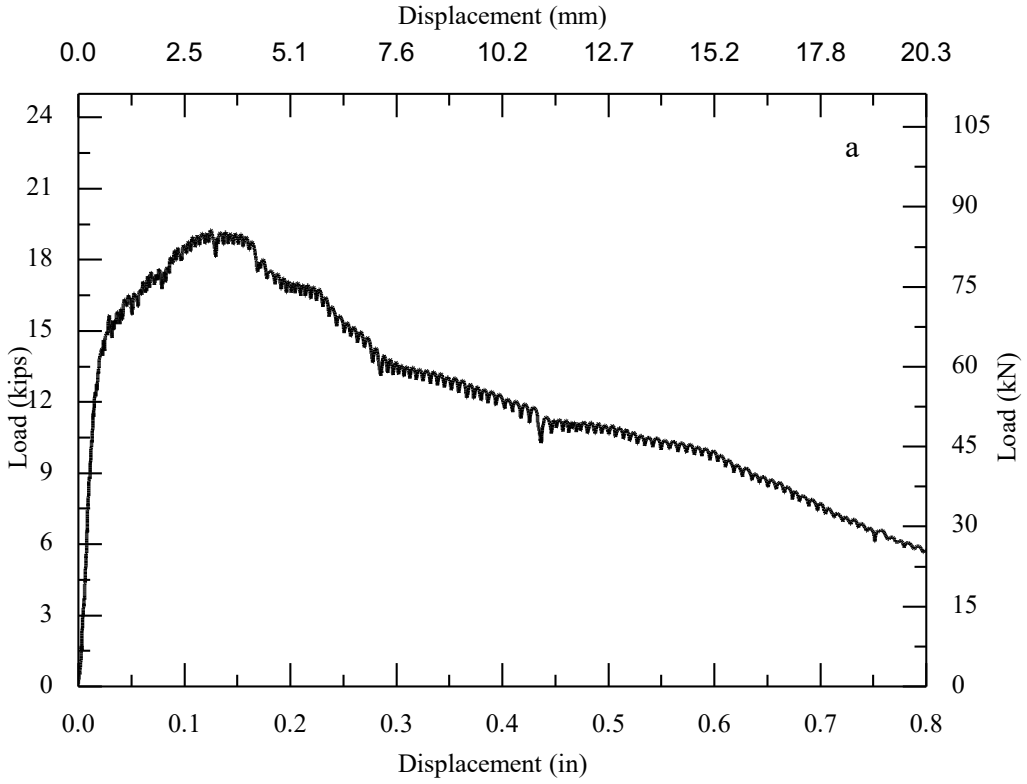

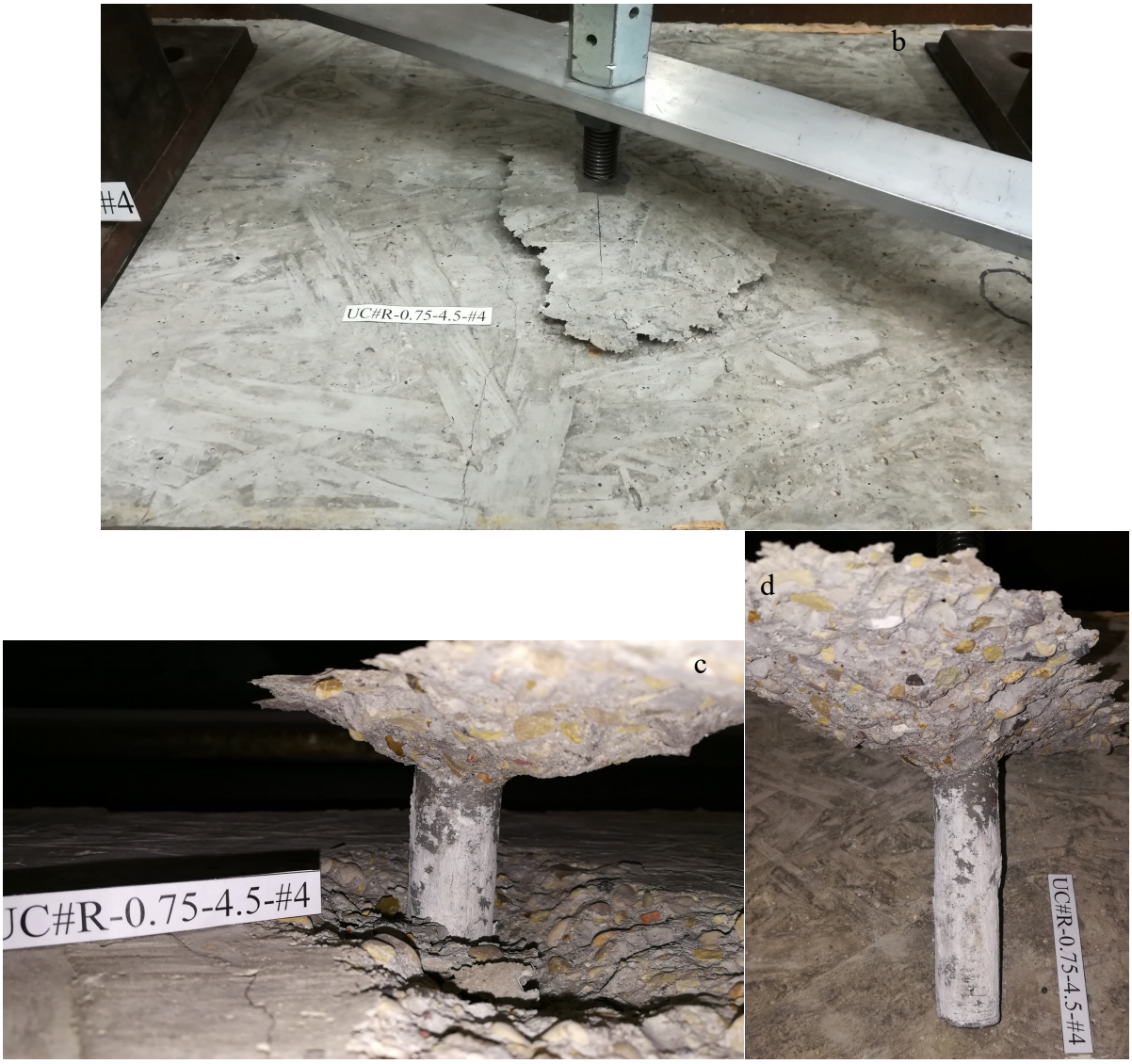

a) load-displacement behavior; b) cracked surface; c), d) partial cone bond failure.

Figure III.44. Observed behavior of Specimen UC#R-0.75-4.5-#4

45. UC#R-0.75-6.0-#1

The first drilling stopped at 67 seconds; The second drilling lasted 6 seconds due to the first drill did not reach desired depth. 5 blows including one incomplete blow. The measured ultimate load is at 25.73 kips at a displacement of 0.0478 in. One crack represented splitting and passing the anchor in the transverse direction and crack width was 0.004 in. when the load reached 22.47 kips. The load reached 25.73 kips and then dropped after a large cracking sound occurred. The anchor was pulled out with a concrete cone due to pullout and breakout failure shown in Figure III.45c

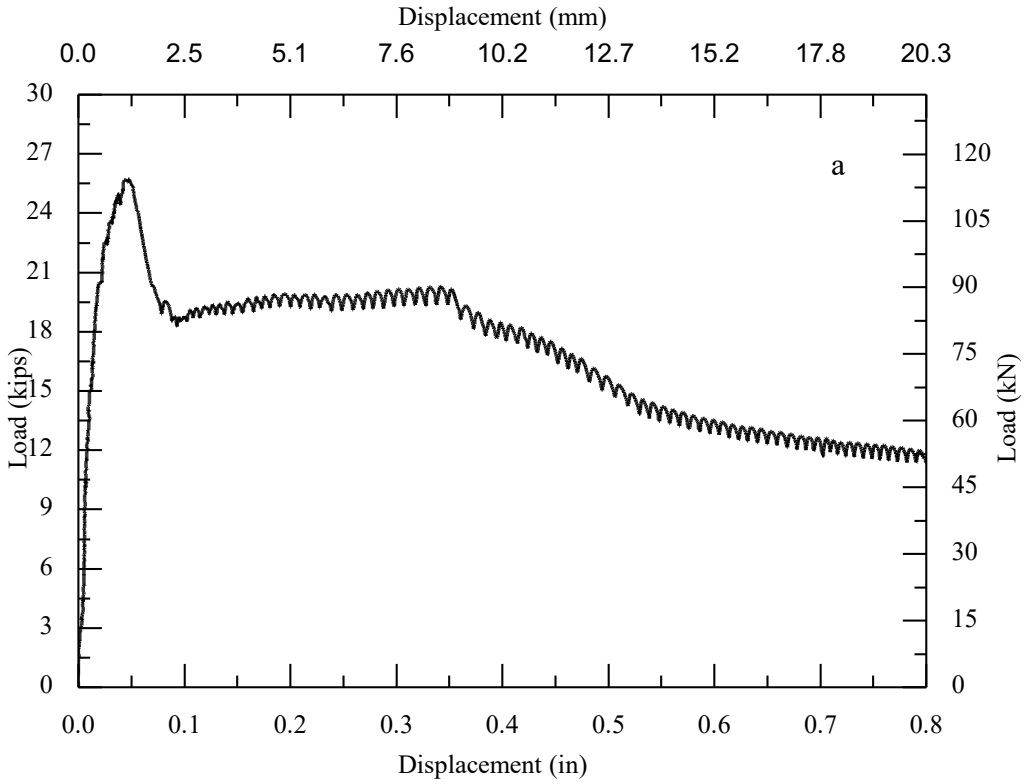

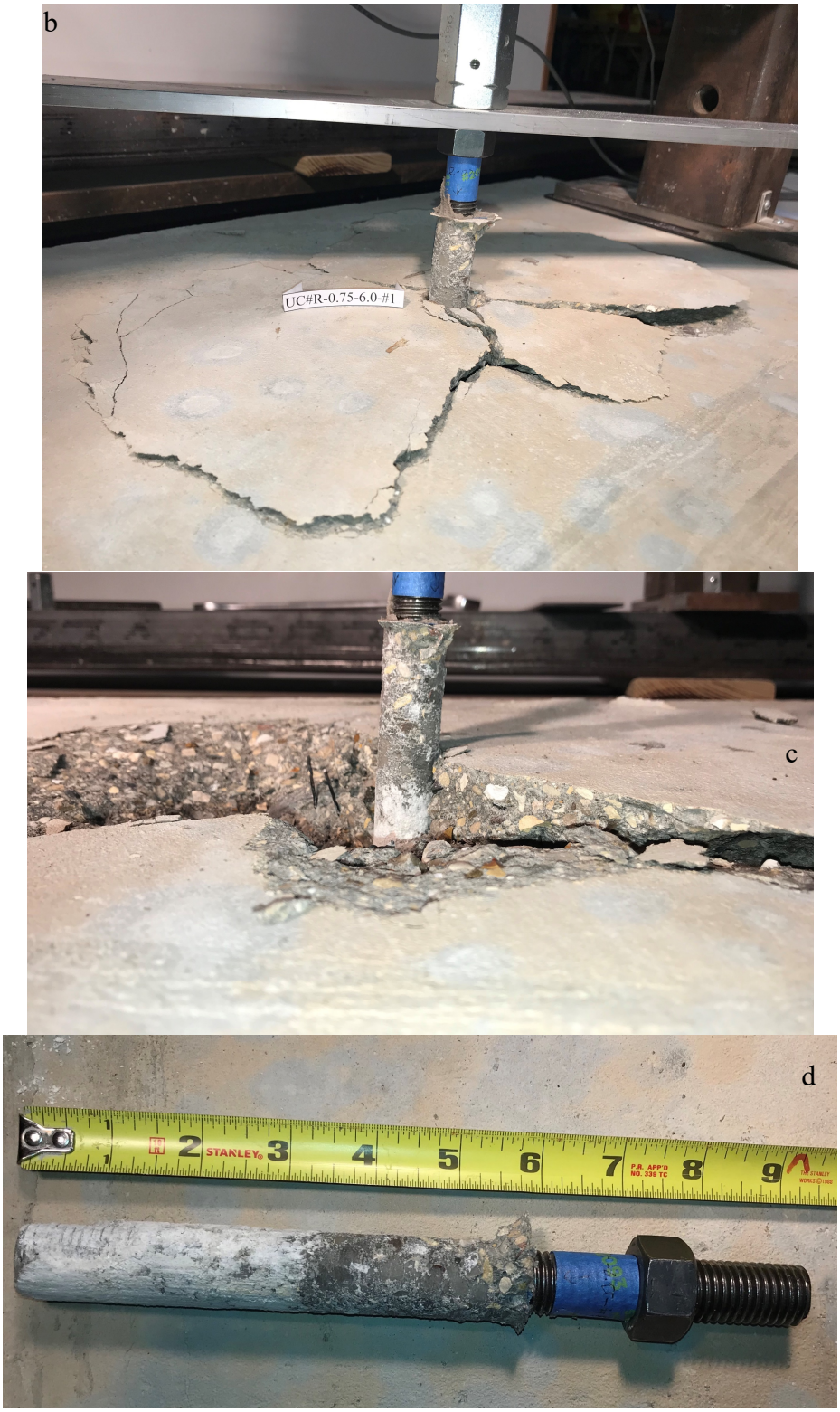

a) load-displacement behavior; b) cracked surface; c), d) partial cone bond failure

Figure III.45. Observed behavior of Specimen UC#R-0.75-6.0-#1

46. UC#R-0.75-6.0-#2

Dusts left at the bottom of the drilled hole and dusts stuck on walls of the drilled hole. The measured ultimate load is at 26.14 kips at a displacement of 0.3208 in. A circular crack was formed when the load reached 15.52 kips. One crack represented splitting and passing the anchor in the transverse direction when the load reached 25.15 kips. The load dropped to 23.01 kips and a large cracking sound occurred. The anchor was pulled out with a concrete cone due to pullout and breakout failure shown in Figure III.46c.

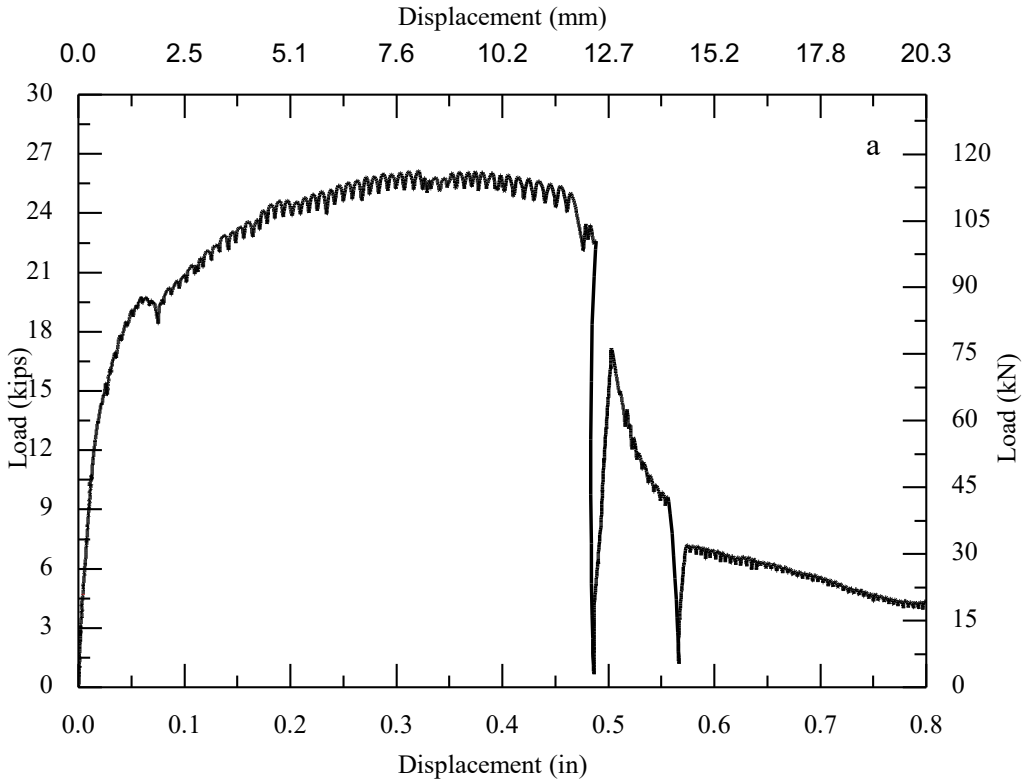

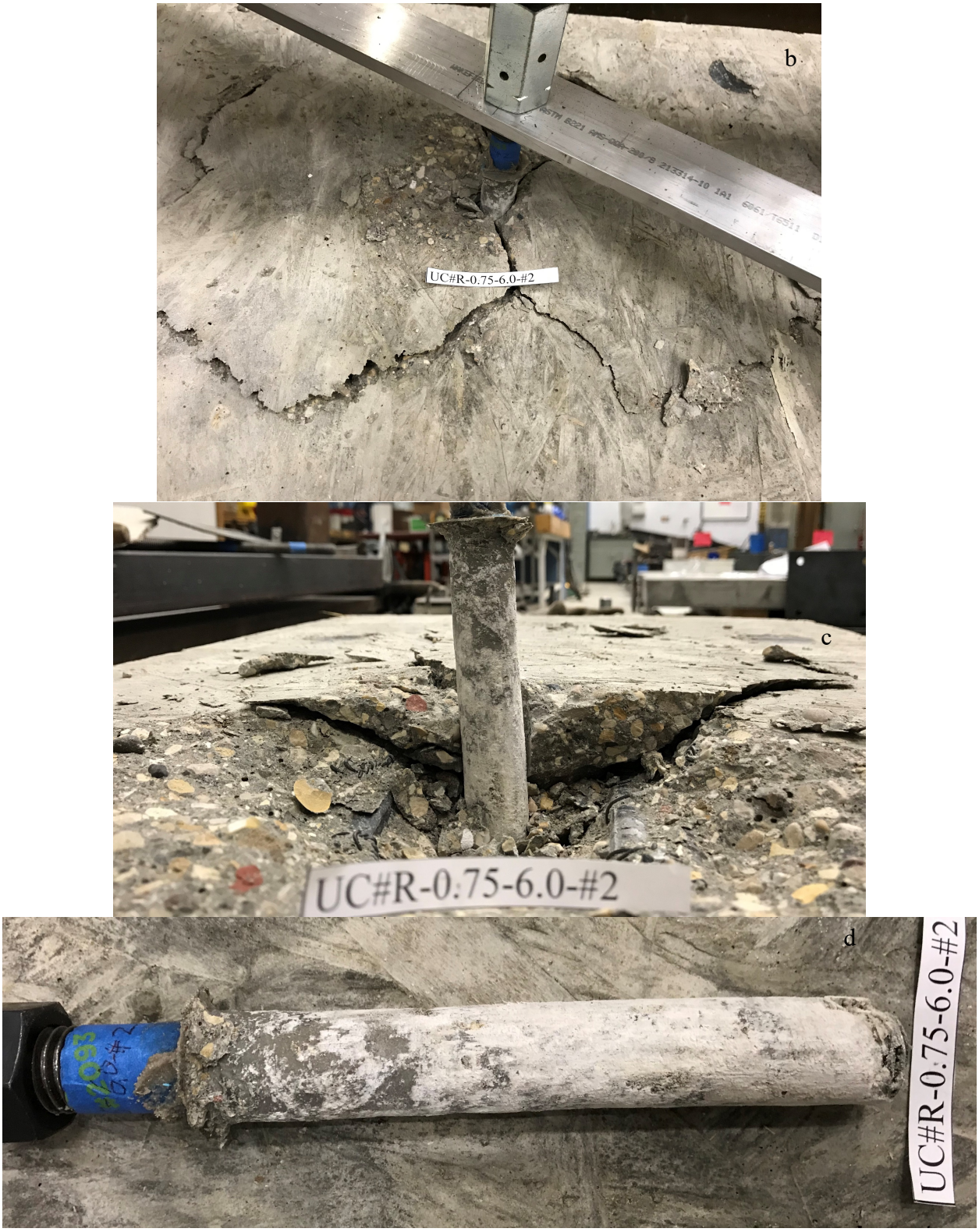

a) load-displacement behavior; b) cracked surface; c), d) partial cone bond failure

Figure III.46. Observed behavior of Specimen UC#R-0.75-6.0-#2

47. UC#R-0.75-6.0-#3

Transverse splitting crack through the whole block width from testing Repeats #1 and #2, crack was 2 in away from test anchor. The measured ultimate load is at 28.35 kips at a displacement of 0.3894 in. An initial transverse splitting crack through the whole block width from testing specimen #1 and #2, crack was 2 in away from test anchor. A circular crack was formed and one crack represented splitting and passing the anchor in the diagonal direction when the load reached 25.68 kips. The anchor was pulled out with a concrete cone due to pullout and breakout failure shown in Figure III.47c.

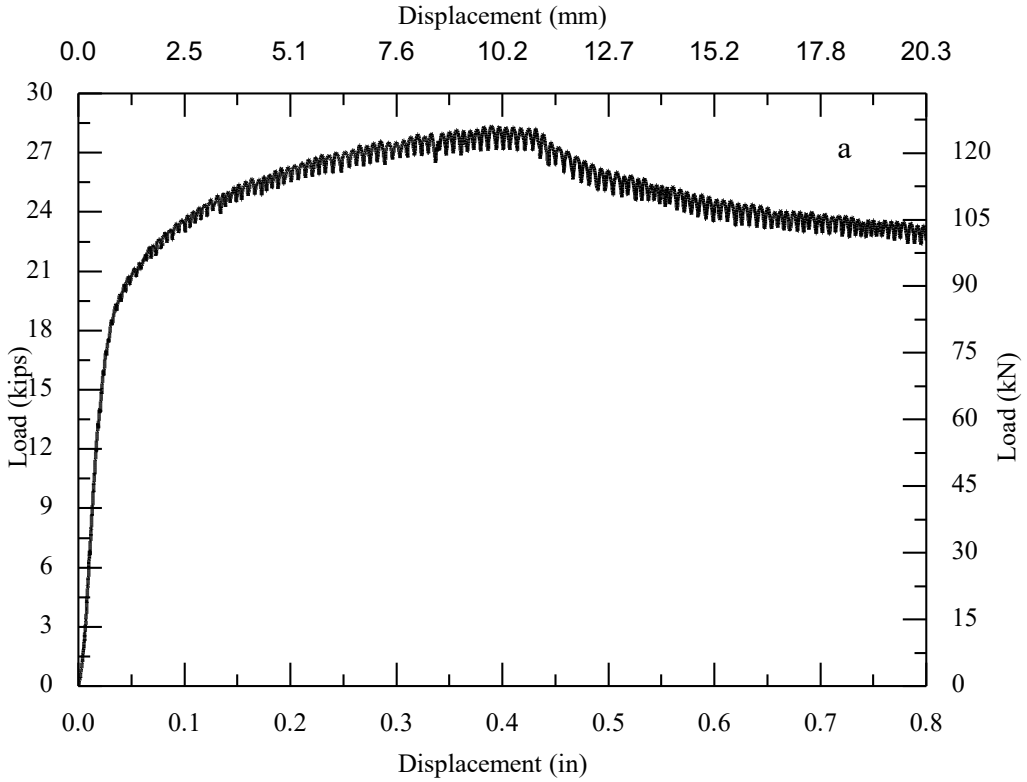



a) load-displacement behavior; b) cracked surface; c), d) partial cone bond failure

Figure III.47. Observed behavior of Specimen UC#R-0.75-6.0-#3

48. UC#R-0.75-6.0-#4

The measured ultimate load is at 23.17 kips at a displacement of 0.1312 in. An initial crack represented splitting and passing the anchor in the transverse direction. One crack represented splitting and passing the anchor in the transverse direction and the crack depth was 2 in. when the load reached 19.80 kips. The anchor was pulled out with a concrete cone due to adhesive-concrete interface bond failure shown in Figure III.48c.

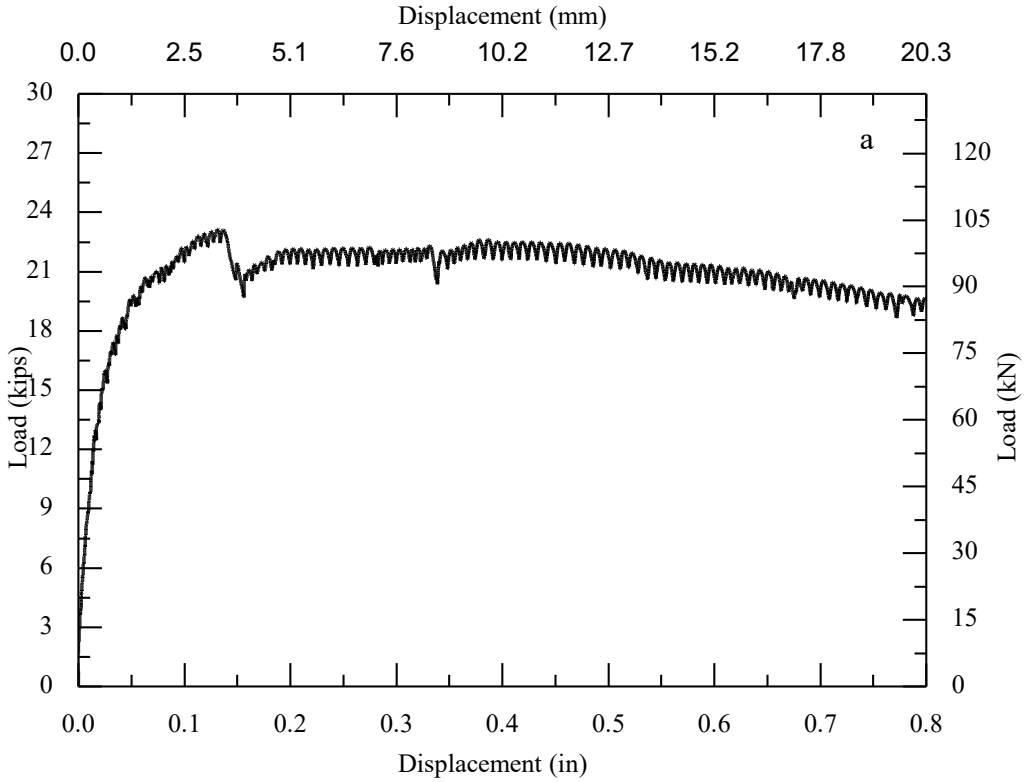



a) load-displacement behavior; b) cracked surface; c) partial cone bond failure

Figure III.48. Observed behavior of Specimen UC#R-0.75-6.0-#4

Appendix IV: Percentiles of the Student's t Distribution

n	$(1-\alpha)$ upper-tail area of the distribution for n degrees of freedom						
	0.400	0.250	0.100	0.050	0.025	0.010	0.005
1	0.325	1.000	3.078	6.314	12.706	31.821	63.657
2	0.289	0.816	1.886	2.920	4.303	6.965	9.925
3	0.277	0.765	1.638	2.353	3.182	4.541	5.841
4	0.271	0.741	1.533	2.132	2.776	3.747	4.604
5	0.267	0.727	1.476	2.015	2.571	3.365	4.032
6	0.265	0.718	1.440	1.943	2.447	3.143	3.707
7	0.263	0.711	1.415	1.895	2.365	2.998	3.499
8	0.262	0.706	1.397	1.860	2.306	2.896	3.355
9	0.261	0.703	1.383	1.833	2.262	2.821	3.250
10	0.260	0.700	1.372	1.812	2.228	2.764	3.169
11	0.260	0.697	1.363	1.796	2.201	2.718	3.106
12	0.259	0.695	1.356	1.782	2.179	2.681	3.055
13	0.259	0.694	1.350	1.771	2.160	2.650	3.012
14	0.258	0.692	1.345	1.761	2.145	2.624	2.977
15	0.258	0.691	1.341	1.753	2.131	2.602	2.947
16	0.258	0.690	1.337	1.746	2.120	2.583	2.921
17	0.257	0.689	1.333	1.740	2.110	2.567	2.898
18	0.257	0.688	1.330	1.734	2.101	2.552	2.878
19	0.257	0.688	1.328	1.729	2.093	2.539	2.861
20	0.257	0.687	1.325	1.725	2.086	2.528	2.845
21	0.257	0.686	1.323	1.721	2.080	2.518	2.831
22	0.256	0.686	1.321	1.717	2.074	2.508	2.819
23	0.256	0.685	1.319	1.714	2.069	2.500	2.807
24	0.256	0.685	1.318	1.711	2.064	2.492	2.797
25	0.256	0.684	1.316	1.708	2.060	2.485	2.787
26	0.256	0.684	1.315	1.706	2.056	2.479	2.779
27	0.256	0.684	1.314	1.703	2.052	2.473	2.771
28	0.256	0.683	1.313	1.701	2.048	2.467	2.763
29	0.256	0.683	1.311	1.699	2.045	2.462	2.756
30	0.256	0.683	1.310	1.697	2.042	2.457	2.750
40	0.255	0.681	1.303	1.684	2.021	2.423	2.704
60	0.254	0.679	1.296	1.671	2.000	2.390	2.660
120	0.254	0.677	1.289	1.658	1.980	2.358	2.617
∞	0.253	0.674	1.282	1.645	1.960	2.326	2.576

Note: Table adapted from Table 48.4 of Forbes et al. (2011)